Government of Western Australia

Department of
Mines and Petroleum

REPORT 125

REGIONAL-SCALE TARGETING FOR GOLD IN THE YILGARN CRATON: PART 1 OF THE YILGARN GOLD EXPLORATION TARGETING ATLAS

by WK Witt, A Ford, B Hanrahan, and A Mamuse

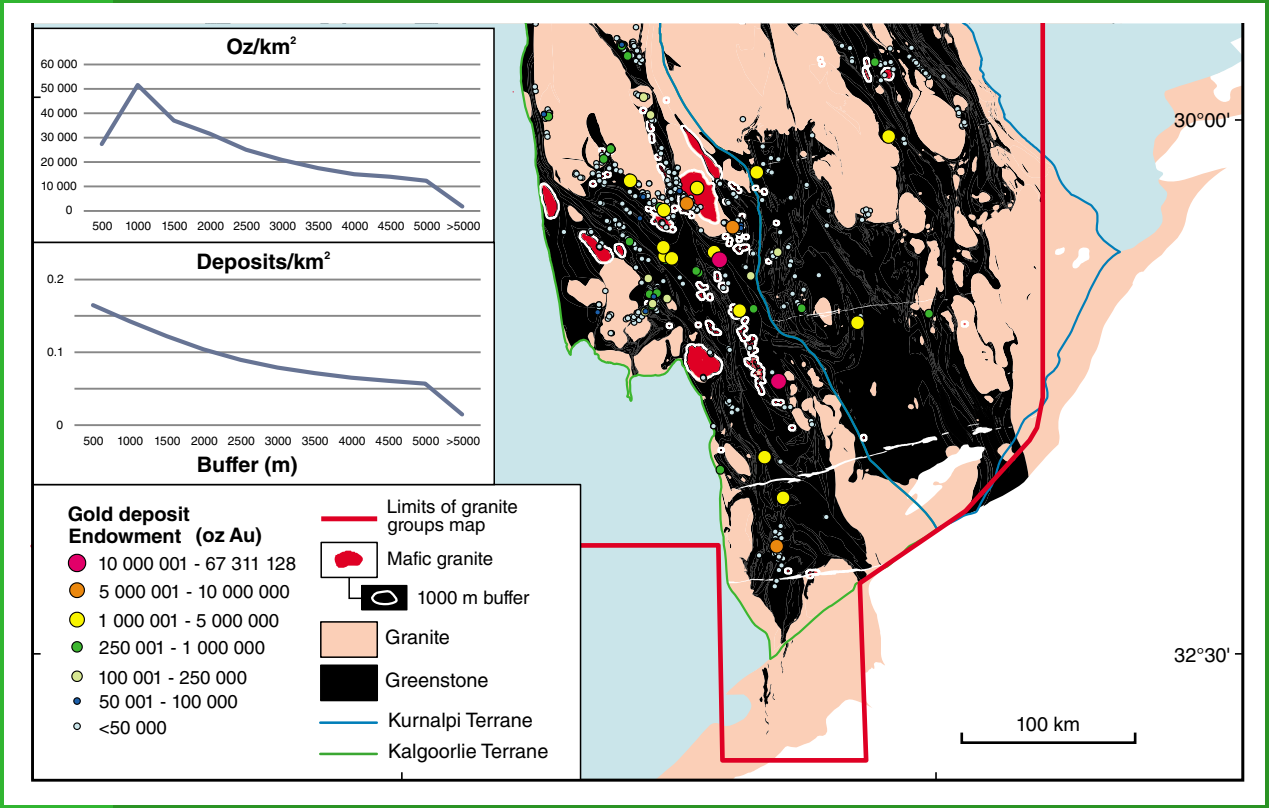

Geological Survey of Western Australia

REGIONAL-SCALE TARGETING FOR GOLD IN THE YILGARN CRATON: PART 1 OF THE YILGARN GOLD EXPLORATION TARGETING ATLAS

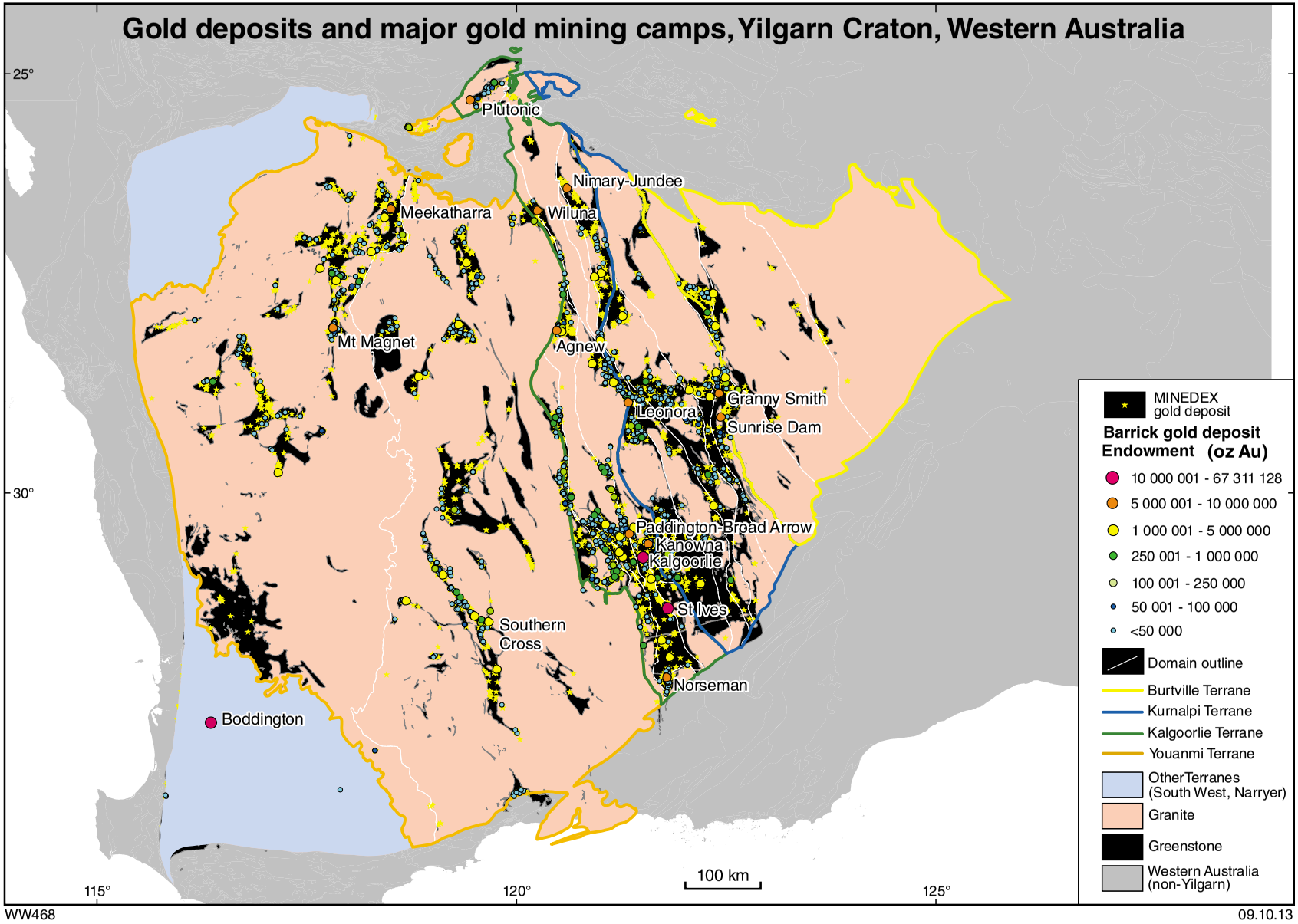
Gold deposits and major gold mining camps, Yilgarn Craton, Western Australia
25°
30°
115°
120°
125°
Plutonic
Nimary-Jundee
Meekatharra
Wiluna
Mt Magnet
Agnew
Granny Smith
Leonora
Sunrise Dam
Paddington-Broad Arrow
Kanowna
Kalgoorlie
St Ives
Southern Cross
Norseman
Boddington
100 km
MINEDEX gold deposit
Barrick gold deposit Endowment (oz Au)
10 000 001 - 67 311 128
5 000 001 - 10 000 000
1 000 001 - 5 000 000
250 001 - 1 000 000
100 001 - 250 000
50 001 - 100 000
<50 000
Domain outline
Burtville Terrane
Kurnalpi Terrane
Kalgoorlie Terrane
Youanmi Terrane
OtherTerranes (South West, Narryer)
Granite
Greenstone
Western Australia (non-Yilgarn)
WW468
09.10.13

Government of **Western Australia**
Department of **Mines and Petroleum**

REPORT 125

REGIONAL-SCALE TARGETING FOR GOLD IN THE YILGARN CRATON: PART 1 OF THE YILGARN GOLD EXPLORATION TARGETING ATLAS

by
WK Witt[1], A Ford[1], B Hanrahan, and A Mamuse[2]

1 **Centre for Exploration Targeting, University of Western Australia, Nedlands, Western Australia 6009**

2 **Centre for Exploration Targeting, Department of Mineral and Energy Economics, Curtin University, Bentley, Western Australia 6102**

Perth 2013

Geological Survey of Western Australia

MINISTER FOR MINES AND PETROLEUM
Hon. Bill Marmion MLA

DIRECTOR GENERAL, DEPARTMENT OF MINES AND PETROLEUM
Richard Sellers

EXECUTIVE DIRECTOR, GEOLOGICAL SURVEY OF WESTERN AUSTRALIA
Rick Rogerson

REFERENCE
The recommended reference for this publication is:
Witt, WK, Ford, A, Hanrahan, B, and Mamuse, A, 2013, Regional-scale targeting for gold in the Yilgarn Craton: Part 1 of the Yilgarn Gold Exploration Targeting Atlas: Geological Survey of Western Australia, Report 125, 130p.

National Library of Australia Cataloguing-in-Publication entry:

Author:	Witt, W. K., author.
Title:	Regional-scale targeting for gold in the Yilgarn Craton. Part 1 of the Yilgarn Gold Exploration Targeting Atlas / WK Witt, A Ford, B Hanrahan, and A Mamuse.
ISBN:	9781741685237 (ebook)
Subjects:	Gold ores--Western Australia--Yilgarn Craton. Gold mines and mining--Western Australia--Yilgarn Craton. Geology--Western Australia--Yilgarn Craton. Yilgarn Craton (W.A.)
Other Authors/Contributors:	Ford, A., author. Hanrahan, B., author. Mamuse, A., author. Geological Survey of Western Australia, issuing body.
Dewey Decimal Classification:	553.41099416

ISSN 1834–2280

Grid references in this publication refer to the Geocentric Datum of Australia 1994 (GDA94). Locations mentioned in the text are referenced using Map Grid Australia (MGA) coordinates, Zones 49–52. All locations are quoted to at least the nearest 100 m.

Copy editor: A Forbes
Cartography: J Peng
Desktop publishing: RL Hitchings

Published 2013 by Geological Survey of Western Australia
This Report is published in digital format (PDF), as part of a digital dataset on USB, and is available online at <www.dmp.wa.gov.au/GSWApublications>.

Further details of geological publications and maps produced by the Geological Survey of Western Australia are available from:
Information Centre
Department of Mines and Petroleum
100 Plain Street
EAST PERTH WESTERN AUSTRALIA 6004
Telephone: +61 8 9222 3459 Facsimile: +61 8 9222 3444
www.dmp.wa.gov.au/GSWApublications

Cover image: Map of part of Eastern Goldfields Superterrane showing results of GIS proximity analysis relating gold endowment to Mafic Group granite intrusions

Frontispiece: Map of Yilgarn Craton showing major tectonic divisions and gold deposits

Contents

Figures

Tables

Regional-scale targeting for gold in the Yilgarn Craton: Part 1 of the Yilgarn Gold Exploration Targeting Atlas

by

WK Witt[1], A Ford[1], B Hanrahan, and A Mamuse[2]

Abstract

The Yilgarn Craton of Western Australia is well known for its gold endowment (more than 324 Moz, or 9730 t), including the giant Golden Mile deposit at Kalgoorlie (67.3 Moz, or more than 2000 t). Despite considerable success in the identification of near-surface gold during the periods 1890–1910 and 1985–2005, the discovery rate for gold in the Yilgarn has since slowed, a situation that is commonly attributed to exhaustion of economic near-surface resources. This view has led to a greater focus on exploration for 'blind' orebodies with tonnages and grades in excess of modern near-surface resources. Exploration for blind orebodies relies on identification of a geophysical expression of subsurface ore, a geochemical expression of the ore in overlying transported sediments or sedimentary rock, or a conceptual approach that predicts the presence of ore on the basis of the geological controls of known near-surface mineralization. Although each approach has both advantages and limitations, this Atlas focuses on the conceptual approach. Eighteen targeting criteria for gold exploration at regional scale are addressed in the Atlas, with individual criteria ranging from well-established geological controls such as intersecting faults to more recent suggestions (e.g. proximity to late-stage basins). Each criterion (and sub-criteria, in some cases) is examined in relation to gold distribution, at scales ranging from craton to domain, using a GIS platform. The results of the spatial analyses are summarized in the form of maps, and histograms (containment analyses) or curves (proximity analyses) showing ounces per square kilometre and deposits per square kilometre. Full results of the spatial analyses are presented in the Appendix.

The results of this study suggest that the four most effective targeting criteria for gold in the Yilgarn Craton are proximity to intrusions of Mafic Group granites, elevated fault density, proximity to regional fault bends, and the well-known preference for gold to be found in greenstone belts rather than in intervening areas of granite. A fuzzy logic approach has been used to combine and weight the results of spatial analyses for these four criteria to produce spatial arrays of prospectivity values that have then been used to produce regional prospectivity maps for gold in the Yilgarn Craton and in the Eastern Goldfields Superterrane. Correlation coefficients relating gold endowment to prospectivity values range from 0.38 to 0.78, depending on the parameter used to measure endowment. The results for the Yilgarn Craton as a whole are better than those for the Eastern Goldfields Superterrane, and results expressed in terms of deposit density are better than those expressed as ounces per square kilometre. Although spatial analyses for domes (containment) and late-stage basins (proximity) suggest a relationship to gold mineralization, prospectivity maps produced after their addition to the previous fuzzy logic analysis compromised the correlation between gold endowment and prospectivity value.

This report forms the first part of a three-part Atlas. Parts two and three deal with district-scale and deposit-scale targeting, respectively.

KEYWORDS: exploration, fuzzy logic, geochemical interpretation, gold, resource development, spatial analysis

Introduction

The concept of the Yilgarn Exploration Targeting Atlas (YETA) Project for gold was conceived in 2009. At that time, a wealth of pre-competitive geological, geochemical, and geophysical data had become available to explorers through government agencies, especially the Geological Survey of Western Australia (GSWA), Geoscience Australia, and the Commonwealth Scientific and Industrial Research Organisation (CSIRO). A major research effort (known as the Predictive Mineral Discovery Cooperative Research Centre, or pmd*CRC) on the geology and mineralization of the Yilgarn Craton, co-funded by government and industry, had also been recently completed. This was also a time when several new exploration targeting strategies were proposed, adding to those already established through scientific publications or time-honoured practical application. With some exceptions, these proposed exploration targeting criteria were based on work carried out for a particular gold deposit, camp, or district and purported to have possible applications in regions beyond the specific study area. Moreover, in most cases, the suggested exploration criteria were only briefly proposed towards the end of a publication, as an outcome of a larger body of work.

1 Centre for Exploration Targeting, University of Western Australia, Nedlands, Western Australia 6009

2 Centre for Exploration Targeting, Department of Mineral and Energy Economics, Curtin University, Bentley, Western Australia 6102

The initial concept for the Atlas was to gather various exploration targeting criteria and techniques into one volume and to make them the main subject of the publication rather than an afterthought. Assessment of the targeting criteria would be restricted to depths below the base of weathering because the common conception was that the Yilgarn Craton is a mature exploration province and that significant new discoveries would almost invariably be made below the relatively thin near-surface intervals of transported cover and weathered basement. Studies by CSIRO during the 1980s and 1990s, summarized by Anand and Butt (2010), had already clearly laid out recommended exploration strategies for gold and other commodities in the regolith layer, but there was no comparable publication dealing with exploration in basement rocks below the regolith layer.

During the course of the YETA Project, Guj et al. (2011) published results of the application of Zipf's Law to the exploration maturity of the Yilgarn Craton. Guj et al. (2011) used the Barrick Gold Corporation gold deposit database in their analysis and this same database has been used in most of the regional- and district-scale analyses presented in the YETA Atlas. Guj et al. (2011) concluded that (in 2008) only 75% of the endowment of the Yilgarn Craton had been discovered. Based on a total Yilgarn Craton gold endowment of 324 375 897 oz (Barrick gold deposit database), the remaining undiscovered gold in the Yilgarn Craton is 108 125 299 oz. This undiscovered gold was predicted by Guj et al. (2011) to include two world-class deposits containing more gold than at St Ives (13 Moz Au) but less than that at Boddington (38.6 Moz Au).

The substantial remaining gold endowment for the Yilgarn Craton calculated by Guj et al. (2011), and the common consensus (Griffin, 2007) that remaining major discoveries will be found below transported cover and/or below the base of weathered bedrock ('blind' deposits) means that 'conceptual' exploration for gold (prediction rather than direct detection; Hronsky and Groves, 2008; McCuaig et al., 2010) will become increasingly important in the twenty-first century. It is therefore timely for publication of a volume that describes and assesses the effectiveness of a wide range of targeting criteria for gold in the Yilgarn Craton. This is the aim of the YETA Project.

From the outset, it was determined that the YETA Project would assess the effectiveness of targeting criteria based on undivided gold deposits, that is, regardless of deposit models. This means that VMS-hosted gold deposits, such as those at Golden Grove and Jaguar, have been grouped together with deposits such as Mount Charlotte, which is widely regarded as belonging to the orogenic class of gold deposits. It also groups gold deposits believed to have formed at different ages and under different geological circumstances (e.g. Czarnota et al., 2010b). The decision to assess all gold deposits as one group rather than subdivide the deposits based on genetic models reflects the ephemeral and controversial classification of many gold deposits in the Yilgarn Craton. Furthermore, recent years have seen a realisation that gold deposits belonging to several genetic models (e.g. orogenic, intrusion-related, Carlin-type) display common controls, particularly at global to regional scales (Hronsky et al., 2012; Witt et al., 2012a).

Terminology for subdivisions of the Yilgarn Craton

There have been several recent attempts to subdivide the Yilgarn Craton into component terranes and domains; the most commonly cited is that of Cassidy et al. (2006). The spatial extents of the datasets used to produce the maps presented with this Atlas were constrained by a more recent tectonic subdivision presented by pmd*CRC (Czarnota et al., 2010b), who followed the terrane and domain terminology of Cassidy et al. (2006), albeit with slightly different spatial extents. For the most part, these differences are minimal, except in the case of the South West Terrane, and the Murchison and Southern Cross domains. The differences in the extents of terranes and domains defined by pmd*CRC and Cassidy et al. (2006) are minimal for the Burtville, Kurnalpi, and Kalgoorlie Terranes. The broader divisions used by pmd*CRC refer to the eastern Yilgarn Craton (EYC), the central Yilgarn Craton (CYC), and the Murchison. Relative to the subdivisions of Cassidy et al. (2006), the EYC corresponds broadly to the combined Kalgoorlie, Kurnalpi, and Burtville Terranes (Eastern Goldfields Superterrane), the CYC to the Southern Cross domain, and the Murchison to the Murchison domain. For convenience and familiarity, references in this Atlas to these entities follow the terminology of Cassidy et al. (2006) (i.e. Eastern Goldfields Superterrane, Youanmi Terrane, and Murchison domain).

Structure of the Atlas

The Atlas comprises three parts reflecting the scale of exploration (Hronsky and Groves, 2008). Part 1 (this volume) examines regional-scale exploration targeting criteria at the craton to domain scale and addresses those criteria thought to be useful when selecting an exploration project area, the initial stage of gold exploration. Part 2 addresses district-scale targeting criteria for selecting a prospect for more detailed exploration within a project area. Part 3 addresses deposit-scale targeting criteria for identification of high-grade lodes within gold deposits. The three scale divisions are similar to three of the four proposed by Hronsky and Groves (2008), but their global-scale exploration (which addresses areas larger than the Yilgarn Craton) is omitted. Some preliminary results from the regional-scale analyses were presented by Witt et al. (2012b).

The explosion of freely available pre-competitive datasets has provided an opportunity for quantitative analysis of the relationships between gold mineralization and various proposed exploration targeting criteria in and beyond the areas where those criteria were initially proposed. In some respects, this approach is similar to that advocated by Barnett and Williams (2012), although in this Atlas, targeting criteria have been assessed individually and a fuzzy logic (rather than neural network) approach has been used to synthesize some of the results and generate gold prospectivity maps of the Yilgarn Craton and Eastern Goldfields Superterrane. To allow ranking and comparison of the relative effectiveness of exploration

targeting criteria, quantitative spatial analysis has been applied to those targeting criteria that have been mapped at regional to district scale. Where suitable spatial data for quantitative spatial analysis were not available, the relationships between gold and the targeting criteria have been determined qualitatively. Data availability is such that there is an emphasis on quantitative spatial analyses at regional scale (Part 1 of the Atlas), a mix of quantitative and qualitative analyses at district scale (Part 2), and dominantly qualitative analyses at deposit scale (Part 3). These scale-dependent differences reflect both the nature of publicly available datasets and the change of emphasis from prediction to direct detection as exploration changes from regional scale to deposit scale (Hronsky and Groves, 2008).

Both quantitative and qualitative analyses relating gold endowment to exploration targeting criteria require an accurate database of the locations and endowments of gold deposits. For regional-scale analyses, the Yilgarn component of the Barrick gold deposit database was used. The locational accuracy of the Barrick database was sufficient for regional-scale analyses, but at district scale, some deposits did not fall within the appropriate geological polygon, indicating that the database is near its limit of locational accuracy at district scale. For district-scale analyses, results based on the GSWA MINEDEX database (available from <www.dmp.wa.gov.au>) were compared to those derived from the Barrick database. The locational accuracy of the MINEDEX database is well-suited to analyses at district scale, but the database does not contain endowment data. Although endowment data from the Barrick database is sufficiently accurate to provide meaningful results, some short-comings have been identified. A common problem with Yilgarn gold deposit databases arises from the practice of attributing gold production to a treatment plant (mill) rather than to the deposits that contributed ore to that plant. Treatment plants are typically close to a large deposit and all mill production from such plants is attributed in the database to that large deposit. Gold from outlying, generally smaller satellite deposits is incorrectly attributed to the large deposit if its ore passes through the same treatment plant. This leads to overestimation of the endowment of the larger deposit and (more critically) underestimation of the endowments of smaller satellite deposits. As an extreme example, the large endowment for Granny Smith (8.0 Moz Au) compared to that of Wallaby (2.8 Moz Au) likely reflects attribution of some ore from Wallaby to Granny Smith because Wallaby ore was treated at the Granny Smith plant.

Quantitative spatial analyses: description and presentation

Two types of quantitative spatial analysis have been used in this Atlas. *Containment analyses* measure the gold contained in a polygon or set of polygons. An example of a containment analysis is the measurement of gold contained in the various terranes or domains of the Yilgarn Craton. Proximity analyses measure the gold content in a series of progressively larger buffers around a target element (geological features defined by polygons, lines, or points). The size and separation of buffer distances used were determined subjectively based on the size and extent of the target features, but in every case the largest buffer filled the entire analysis area. The *analysis area* was determined by the intersection of the Yilgarn Craton (or a subdivision of it) with the extent of the input file representing the target element. Consequently, the analysis area may vary from one analysis to another. A measure of the confidence in the relationship between gold and the target element can be achieved by plotting the amount of gold within each successive buffer against buffer distance. The amount of gold is expressed as endowment per unit area (oz/km^2) or deposit density (deposits/km^2). Curves that define steadily declining quantities of gold from a peak near the target element suggest a genuine positive relationship with the geological feature. A steadily increasing curve suggests a genuine negative relationship (negative targeting criteria). Erratic curves suggest the absence of a genuine geological relationship between gold mineralization and the target element.

The parameter %Endowment/%Area is used as a measure of the success of the targeting criteria. For example, a 500 m buffer around granitic domes in the Eastern Goldfields Superterrane captures 38.4% of the gold endowment (oz) in 15.9% of the analysis area, equivalent to a %Endowment/%Area ratio of 2.41. This can be interpreted to indicate that exploration within 500 m of a dome will increase the likelihood of gold discovery by a factor of almost two and a half relative to random exploration within the Eastern Goldfields Superterrane. This same buffer captures 47.1% of the deposits of the Eastern Goldfields Superterrane at a density of 0.032 deposits/km^2. Some other analyses produce favourable %Endowment/%Area ratios, but capture only small amounts of total gold. For example, the medium pressure, lower amphibolite facies M_2 metamorphic domains of Goscombe et al. (2009) have a %Endowment/%Area ratio of 5.22, but capture only 5.4% of the gold endowment and 7.3% of deposits. Although the %Endowment/%Area ratio appears to favour gold exploration, the amount of gold captured in these relatively small areas is limited. Therefore, it is advisable to consider the parameter %Endowment*(%Endowment/%Area), which normalizes the ratio using the proportion of total ounces captured.

Results of spatial analyses are presented as maps and spreadsheets. The basic quantitative data arising from the analyses are presented in the Appendix as spreadsheets (Tables A1.1 to A1.102) containing the following parameters: buffer distance (or polygon set), number of deposits, number of deposits (%), area (km^2), area (%), endowment (oz), endowment (%), endowment per unit area (oz/km^2), deposit density (deposits/km^2), %Endowment/%Area, %Endowment*(%Endowment/%Area), expected endowment (E), expected deposits (E), (O-E)/E (endowment), (O-E)^2/E (endowment), (O-E)/E (deposits), and average deposit size (oz). The term 'O' in the last three parameters refers to the observed (actual) endowment or number of deposits in a polygon. 'E' is the expected (calculated) endowment (or number of deposits)

in a target polygon. E values are calculated by multiplying the total endowment (or number of deposits) in the analysis space by the proportion of the area of the target polygon relative to the total area of the analysis space. That is, E values are based on the assumption that the endowment (or number of deposits) is evenly distributed over the total analysis space. Bar charts (for containment analyses) or gold versus buffer distance curves (for proximity analyses) derived from these data are embedded in the spreadsheets.

Maps illustrating the results are presented for each quantitative spatial analysis. Generally, these maps show the distribution of the target element within the analysis area over the basic geology (granites and greenstones). Also shown are the distribution of gold deposits and the most prospective buffers around the target element. Bar charts (for containment analyses) or gold versus buffer distance curves (for proximity analyses), extracted from the corresponding spreadsheets, have been embedded within the maps. These show gold as ounces per square kilometre and deposits per square kilometre in each polygon (buffers in the case of proximity analyses).

A summary of the input data files used in the regional-scale quantitative spatial analyses is presented in Table 1.1. Those files are provided in digital format with this publication.

Limitations and application of the methodology

Soon after embarking on the YETA Project, it became clear that the ambitious aim of the Project to comprehensively cover all of the targeting criteria used to explore for gold at regional, district, and deposit scales would not be realised. In particular, geophysical methods and criteria used in gold exploration are under-represented.

Some further cautionary notes are warranted, especially as regards the quantitative spatial analyses. Results of these analyses are heavily dependent on the quality of the input data. Limitations of the gold deposit databases used for the YETA Project, including undiscovered gold, have already been discussed. Further limitations arise from the geological maps that underpin the spatial analyses, principally because such maps are not strictly uniform in levels of detail. The variation in detail arises from a number of factors: mapping is more detailed in areas of good outcrop and complex geology, and to some extent in more easily accessed areas, some of which are close to known mineralization. The distribution of most of the regional-scale targeting elements are ultimately derived from 1:100 000-scale geological maps prepared and published by GSWA and, as such, are not consciously biased towards areas of known mineralization, except to the extent that such areas are readily accessible and, in some cases, may be better exposed. The sparse outcrop throughout the Yilgarn Craton means that many targeting criteria (e.g. regional faults) are interpreted largely from aeromagnetic data, but constrained by outcrop. Consequently, the bias in detail of input geological maps is perhaps not such a severe limitation as may be presumed.

Results of quantitative spatial analyses are potentially strongly influenced by exceptionally large deposits, such as the Golden Mile (67.3 Moz Au) in the Eastern Goldfields Superterrane. There is little that can be done about this problem, short of eliminating the deposit from the database (e.g. Barnett and Williams, 2012), a solution that tends to defeat the purpose of the analyses (to determine which criteria can usefully be employed to explore for large tonnage gold deposits). Two approaches have been employed here to counter the influence of the Golden Mile. Firstly, within the Eastern Goldfields Superterrane, results expressed as deposits per square kilometre (i.e. each deposit given equal weight) can be compared with results expressed as ounces per square kilometre. Secondly, results from the Eastern Goldfields Superterrane expressed as ounces per square kilometre or %Endowment/%Area can be compared with those from the Southern Cross and Murchison domains, where extreme outliers such as the Golden Mile do not exist. In assessing the effectiveness of a particular targeting criterion and the possible influence of the Golden Mile on these results, the reader should consider the results also in terms of deposits per square kilometre, and compare them to results from the Southern Cross and Murchison domains. In most cases, these comparisons support the veracity of the results (in ounces per square kilometre) from the Eastern Goldfields Superterrane.

The results presented here confirm the efficacy of most of the well-established targeting criteria and cast some shadows over some of the more recently proposed criteria. However, it is up to the reader of this Atlas to judge how meaningful and reliable the results of these analyses are, and whether to incorporate such results into their exploration for gold in the Yilgarn Craton or elsewhere. Despite the limitations described above, the Atlas addresses most of the commonly used targeting criteria and, as such, is a unique document in the geological literature related to the Yilgarn Craton. Although the results are specific to the Yilgarn Craton, it is very likely that they will have relevance and application for other Archean cratons, and possibly for younger regions of accretionary tectonics known to contain gold mineralization.

Table 1.1. Summary of digital files used in analyses of regional targeting criteria

Analysis	*Type of analysis*	*Analysis area*	*Analysis area defined*	*Source files*[(a)]	*Modification of source file*
Geological terranes and domains	Containment	Yilgarn Craton	Terranes and domains as defined by pmd*CRC (Y4 Project)	*prov_dis_terrane* and *prov_dis_domain*	None
Geological terranes and domains (greenstones only)	Containment	Yilgarn Craton	Terranes and domains as defined by pmd*CRC (Y4 Project), but only in greenstone areas as defined by GSWA 500k interpreted bedrock geology	*prov_dis_terrane* and *prov_dis_domain*	None
Tomographic breaks (Criterion 1.1)	Proximity	Yilgarn Craton	Boundaries of source map, clipped to limits of the Yilgarn Craton as defined by pmd*CRC (Y4 Project)	*Edges_s1_s9* shape file from pmd*CRC (Y4 Project)	None
Sm-Nd isotope basement terranes (Criterion 1.2)	Containment	Yilgarn Craton	Boundaries of source map, clipped to limits of the Yilgarn Craton as defined by pmd*CRC (Y4 Project)	*two-stage1.tif* derived from unpublished GSWA *Sm-Nd_point_data_all file*	None
	Proximity	Yilgarn Craton	Boundaries of source map, clipped to limits of the Yilgarn Craton as defined by pmd*CRC (Y4 Project)	*New rationalised gradients* shape file manually digitized by rationalizing gradient arrays generated from *two_stage1.tif* using Intrepid software *(arcshapeWorms.shp)* and the CET plug-in for Geosoft *(sm_nd_STD_PS_NMS_THIN)*	Steep gradients in data generated using edge detection software (Intrepid and CET Grid Analysis Plug-in for Geosoft)
Granite Groups (Criterion 1.3)	Proximity	Yilgarn Craton, Eastern Goldfields Superterrane, Murchison domain, Kurnalpi ± Kalgoorlie Terranes	Boundaries of source map, clipped to limits of the Yilgarn Craton or its subdivisions as defined by pmd*CRC (Y4 Project)	supplied by D Champion (Geoscience Australia)	Queries to isolate various granite groups and some combinations of granite groups
Gravity lineaments (Criterion 1.4)	Proximity	Eastern Goldfields Superterrane	Boundaries of source map, clipped to limits of the Eastern Yilgarn as defined by pmd*CRC (Y4 Project)	Shape files representing individual gravity worm sets generated by pmd*CRC (Y4 Project)	No processing, except for a single analysis where a specific subset of gravity worms was selected (see text for explanation)
		Southern Cross and Murchison domains	Boundaries of source map, clipped to limits of the Central Yilgarn and Murchison subdivisions as defined by pmd*CRC (Y4 Project)	Shape files representing individual gravity worm sets generated by GSWA from regional gravity dataset	None
Aeromagnetic discontinuities (Criterion 1.5)	Proximity	Eastern Goldfields Superterrane	Boundaries of source map, clipped to limits of the Eastern Yilgarn as defined by pmd*CRC (Y4 Project)	Shape files representing individual aeromagnetic worm sets generated by pmd*CRC (A1 Project)	None
		Southern Cross and Murchison domains	Boundaries of source map, clipped to limits of the Central Yilgarn and Murchison subdivisions as defined by pmd*CRC (Y4 Project)	Shape files representing individual aeromagnetic worm sets generated by GSWA from regional aeromagnetic dataset	None

Table 1.1. continued

Analysis	*Type of analysis*	*Analysis area*	*Analysis area defined*	*Source files*[(a)]	*Modification of source file*
Greenstone thickness (Criterion 1.6)	Containment	Eastern Goldfields Superterrane	Boundaries of source map, clipped to limits of the Eastern Yilgarn as defined by pmd*CRC (Y4 Project)	Series of shape files manually derived from 500 m spaced depth to base of greenstones contours estimated from seismic and gravity data by pmd*CRC (Y4 Project)	None
Greenstone thickness gradient (Criterion 1.6)	Proximity	Eastern Goldfields Superterrane	Boundaries of source map, clipped to limits of the Eastern Yilgarn as defined by pmd*CRC (Y4 Project)	Shape file *30 degrees* was derived from pmd*CRC depth to base of greenstones data	A Triangular Irregular Network was applied to the depth data to generate a DEM representing the base of the greenstone sequence. A slope map was generated from the DEM and values representing a gradient >30° were isolated and converted into vector format.
Regional faults and shear zones (Criterion1.7)	Proximity	Eastern Goldfields Superterrane	Boundaries of source map, clipped to limits of the Eastern Yilgarn as defined by pmd*CRC (Y4 Project)	*Projected fault system* from pmd*CRC (Y4 Project)	None
		Southern Cross and Murchison domains	Boundaries of the source map, clipped to limits of the Central Yilgarn and Murchison subdivisions as defined by pmd*CRC (Y4 Project)	GSWA *1:2 500k linear structure* file (geolin01)	None
Regional fault density (Criterion 1.8)	Containment	Eastern Goldfields Superterrane	Boundaries of source map, clipped to limits of the Eastern Yilgarn as defined by pmd*CRC (Y4 Project)	*Projected fault system* from pmd*CRC (Y4 Project)	Fault density calculated using the Density Tool in Spatial Analyst (ArcGIS)
		Southern Cross and Murchison domains	Boundaries of source map, clipped to limits of the Central Yilgarn and Murchison subdivisions as defined by pmd*CRC (Y4 Project)	GSWA *1:2 500k linear structure* file	Fault density calculated using the Density Tool in Spatial Analyst (ArcGIS)
Regional fault intersections (Criterion 1.9)	Proximity	Eastern Goldfields Superterrane	Boundaries of source map, clipped to limits of the Eastern Yilgarn as defined by pmd*CRC (Y4 Project)	*EYC_intersections* shape file generated manually from *Projected fault system* from pmd*CRC (Y4 Project) and GSWA *2_5m_geology98_EYC* shape file from Eastern Yilgarn GIS	Digital file *2_5m_geology98_EYC* queried to select faults and shear zones only. Intersections with *Projected fault system* <40° discarded to avoid fault splays and risk of duplication of structures in the two source files. Faults from both files propagated up to 5 km to generate intersections.

Table 1.1. continued

Analysis	*Type of analysis*	*Analysis area*	*Analysis area defined*	*Source files*[(a)]	*Modification of source file*
Criterion 1.9 (continued)	Proximity	Southern Cross and Murchison domains	Boundaries of source map, clipped to limits of the Central Yilgarn and Murchison subdivisions as defined by pmd*CRC (Y4 Project)	*CYC_intersections and Murchison_ intersections* point files generated manually from GSWA *1:2 500k linear structure* file and GSWA *500K_ interpstrucl* and *500k_interpgeol* shape files. For the southern Central Yilgarn analysis, the 1141 m aeromagnetic worm was used as a substitute for oblique faults	Digital file *500K_interpstrucl* queried to select only faults and shear zones, and aeromagnetic lineaments. For Central Yilgarn, digital file *500k_interpgeol* queried to select only Proterozoic dykes. For Murchison, digital file *500k_interpstrucl* queried to select only faults and shear zones; *500k_interpgeol* queried to select only Proterozoic dykes. Intersections with *1:2 500k linear structure* <40° discarded to avoid fault splays and risk of duplication of structures in the two source files. Faults from all files in both provinces propagated up to 5 km to generate intersections.
Regional fault bends (Criterion 1.10)	Proximity	Eastern Goldfields Superterrane	Boundaries of the source map, clipped to limits of the Eastern Yilgarn as defined by pmd*CRC (Y4 Project)	*Projected fault system*, sourced from pmd*CRC (Y4 Project)	Fault bends generated digitally from source file using Mapinfo Fault Bend tool (bend angle 5–30°; bend length 200–5000 m)
		Southern Cross and Murchison domains	Boundaries of source map, clipped to limits of the Central Yilgarn and Murchison subdivisions as defined by pmd*CRC (Y4 Project)	GSWA *1:2 500k linear structure* file	Fault bends generated digitally from source file using Mapinfo Fault Bend tool (bend angle 5–30°; bend length 200–5000 m)
Vergence anomalies (Criterion 1.11)	Containment	Eastern Goldfields Superterrane	Boundaries of source map, clipped to limits of the Eastern Yilgarn, as defined by pmd*CRC (Y4 Project)	*West-vergent fault domains* shape file	*West-vergent fault domains* digitized manually from pmd*CRC (Y4 Project) data indicating dip direction of regional faults, assisted by information from AngloGold Ashanti in Laverton region
	Proximity	Eastern Goldfields Superterrane	Boundaries of source map, clipped to limits of the Eastern Yilgarn, as defined by pmd*CRC (Y4 Project)	*West-dipping faults_projected* shape file	*West-dipping faults_projected* shape file derived from pmd*CRC regional fault system shape file using pmd*CRC (Y4 Project) data indicating dip direction of regional faults, assisted by information from AngloGold Ashanti in Laverton region
Structural convergence (constriction) zones (Criterion 1.12)	Containment	Combined Kalgoorlie and Kurnalpi Terranes	Boundaries of source map, clipped to limits of the Kalgoorlie and Kurnalpi Terranes, as defined by pmd*CRC (Y4 Project)	Manually digitized domains representing six constriction zones derived from GSWA *500k_geologyp08* digital shape file	None

Table 1.1. continued

Analysis	*Type of analysis*	*Analysis area*	*Analysis area defined*	*Source files*[(a)]	*Modification of source file*
Criterion 1.12 (continued)	Containment	Murchison domain	Boundaries of source map, clipped to limits of the Murchison Terrane, as defined by pmd*CRC (Y4 Project)	Manually digitized domains representing five constriction zones from GSWA *500k_geologyp08* digital shape file	None
Domes (Criterion 1.13)	Containment and proximity	Eastern Goldfields Superterrane	Boundaries of source map, clipped to limits of the Eastern Yilgarn, as defined by pmd*CRC (Y4 Project)	*Domes_clip* shape file from pmd*CRC (Y4 Project)	None
Granite–greenstone contacts (Criterion 1.14)	Proximity	Eastern Goldfields Superterrane, Southern Cross and Murchison domains	Boundaries of source map, clipped to limits of the Eastern Yilgarn, Central Yilgarn, and Murchison subdivisions as defined by pmd*CRC (Y4 Project)	*eyc_contacts_dissolve* shape file derived from *GSWA 500k_geologyp08* digital shape file	None
Metamorphic grade (Criterion 1.15)	Containment	Eastern Goldfields Superterrane	Boundaries of source map, clipped to limits of the Eastern Yilgarn, as defined by pmd*CRC (Y4 Project)	Goscombe et al. (2009) *peakmeta_poly_mostly M2, M3a_poly*, *locus_of_D3_meta_event* and *D3_upper_plate* shape files	None
Strain index (Criterion 1.15)	Containment	Eastern Goldfields Superterrane	Boundaries of source map, clipped to limits of the Eastern Yilgarn, as defined by pmd*CRC (Y4 Project)	Goscombe et al. (2009) *strain_poly* shape file	None
Strain partitioning at regional scale (Criterion 1.16)	Containment	Yilgarn Craton (four areas)	Limits of three contiguous geological domains (two high-strain domains bounding a central low-strain domain)	GSWA *500k_geologyp08* digital shape file	For each of the four areas, two high-strain domains and one low-strain polygonal shape files were manually derived from GSWA *500k_geologyp08* digital shape file with input from aeromagnetic imagery
Late-stage basins (Criterion 1.17)	Containment and proximity	Eastern Goldfields Superterrane	Boundaries of source map, clipped to limits of combined Kalgoorlie and Kurnalpi Terranes, as defined by pmd*CRC (Y4 Project)	Late-stage *basins_updated 1108* shape file	Shape file derived from GSWA *500k_geologyp08* digital shape file
Geological complexity (Criterion 1.18)	Not applicable	Eastern Goldfields Superterrane	Arbitrary limits set on the basis of geology and availability of geological data	*500k_geologyp08*, *500k_geolstrucl08*, *geostrucl* (East Yilgarn GIS)	*500k_geologyp08* converted to polyline file, then merged with *500k_geolstrucl08* and geostrucl
		Southern Cross domain	Arbitrary limits set on the basis of geology and availability of geological data	*500k_interpgeop*, *500k_interpgeol*, *500k_interpstrucl* (Central Yilgarn GIS)	*500k_interpgeop* converted to polyline file, then merged with *500k_interpgeol* and *500k_interpstrucl*
		Murchison domain	Arbitrary limits set on the basis of geology and availability of geological data	*500k_interpgeologyp08*, *500k_geostrucl* (Murchison GEP)	*500k_interpgeologyp08* converted to polyline file, then merged with *500k_geostrucl*

NOTES: (a) Digital shape files used for analyses are provided with this digital publication
Barrick gold deposit database was used to represent gold endowment of the Yilgarn Craton in all analyses

Terranes and domains: Gold endowment

The Yilgarn Craton has been divided into a number of geological terranes and domains (e.g. Myers 1995; Cassidy et al., 2006). These geological entities are bounded by faults and preserve geological characteristics or histories that differ from adjacent terranes and domains. In this analysis, the most recent subdivisions developed by the pmd*CRC Y4 Project (Czarnota et al., 2010b) have been used (Figs 1.1 and 1.2). Results of containment analyses of terranes and domains are presented in Tables A1.1 and A1.2; results of similar analyses, but confined to greenstone areas of the terranes and domains, are shown in Tables A1.3 and A1.4. Greenstones were delineated according to the GSWA 1:500 000-scale geology shape file (500k_geologyp08; Table 1.1).

The calculated average gold endowment for the Yilgarn Craton is approximately 476 oz/km^2, which compares favourably with 251 oz/km^2 for the Archean Superior Province in Canada (B Dubé and V Becu, 2011, Geological Survey of Canada, pers. comm., 11 February; updated after Gosselin and Dubé, 2005). The greenstone areas in the Yilgarn Craton are significantly better endowed than granite areas, containing 90% of the deposits and 93% of the gold. Considering greenstone areas only, the Yilgarn Craton has an endowment of 2842 oz/km^2. The average size of gold deposits in the Yilgarn Craton is 108 778 oz (112 273 oz in greenstone areas only). Table 1.2 provides a comparison of these data for terranes of the Yilgarn Craton and sub-provinces of the Superior Province, Canada.

Within the Yilgarn Craton, the superior gold endowment of the Eastern Goldfields Superterrane and the premier position of the Kalgoorlie Terrane within it are well established (Witt and Vanderhor, 1998; Hagemann and Cassidy, 2000; Robert et al., 2005; Table A1.1, Fig. 1.1). The Eastern Goldfields Superterrane contains 1007 oz/km^2, compared to 1698 oz/km^2 for the richly mineralized Abitibi sub-province of the Superior Province. The Kalgoorlie Terrane contains an average of 3034 oz/km^2, and 8054 oz/km^2 in greenstone areas only. The South West Terrane is the second-best endowed terrane (677 oz/km^2, and 5425 oz/km^2 for greenstones only) and has the largest average gold deposit size, but the average endowments are biased by the small number of deposits in this area, which includes the very large Boddington deposit (37 Moz). The average size of deposits in the Kalgoorlie Terrane (151 049 oz) is significantly larger than those of other terranes (South West Terrane excluded).

Within the Eastern Goldfields Superterrane, the Kambalda domain is clearly best endowed (Table A1.2, Fig. 1.2), containing 24 252 oz/km^2, including major gold deposits or camps at Kalgoorlie (Golden Mile and Mount Charlotte), St Ives, New Celebration, Higginsville, and Norseman. Kalgoorlie and St Ives are the only >10 Moz camps in the Eastern Goldfields Superterrane. Second-tier domains include Boorara, Jundee, Ora Banda, Depot, and Linden (1878 to 2739 oz/km^2), and most (Depot is the exception) contain one or two deposits or camps with endowments of 1 to 5 Moz. Interestingly, the Jundee domain emerges as the domain with the largest average deposit size (484 638 oz), slightly ahead of the Kambalda and Linden domains.

Robert et al. (2005) suggested a possible correlation between gold endowment and the ratio of greenstones to granite, based on data from selected districts or sub-provinces of the Superior and Yilgarn Cratons. The data from the Yilgarn Craton do not provide strong support for this proposition. Although there is a degree of correlation among the terranes, the greenstone-rich Kurnalpi Terrane is relatively poorly endowed, and there is little correlation between the percentage of greenstones and gold endowment among the domains of the Yilgarn Craton.

Possible explanations for the superior gold endowment of the Eastern Goldfields Superterrane are discussed in the following sections of this Atlas. Briefly, a range of geological, geochemical, geochronological, and geophysical evidence, particularly Sm-Nd isotope data from granitic intrusions, suggests that greenstones of the Kalgoorlie and Kurnalpi Terranes were deposited in some form of rift (on relatively young basement) on the eastern margin of the proto-Yilgarn Craton represented by older basement (Czarnota et al., 2010b). The bulk of the gold in this region was deposited during an accretion or re-accretion event at c. 2.67 to 2.62 Ga (Robert et al., 2005; Czarnota et al., 2010b). Within the Kalgoorlie and Kurnalpi Terranes of the Eastern Goldfields Superterrane, three subdivisions can be distinguished. Greenstones in the central subdivision overlie the youngest basement (<2.9 Ga; see Targeting Criterion 1.2), are relatively undeformed, and contain some east-striking trends and numerous internal granite intrusions, but few with a mantle source component (Fig. 1.3). The central subdivision contains few large gold deposits, and greenstones within it correspond broadly to the Kurnalpi Terrane, but with numerous mismatches if examined in detail. Relative to the central subdivision, those to the east (corresponding broadly to the Linden domain) and the west (corresponding broadly to the Kalgoorlie Terrane), contain numerous large gold deposits and appear to have been relatively high-strain zones during the gold-forming orogeny. In addition to numerous closely spaced faults, they also contain numerous intermediate to felsic intrusions with a mantle source component (Mafic Group intrusions of Cassidy et al., 2002), record widespread hydrothermal alteration throughout the periods of formation and deformation of the greenstones, and grade into high-grade, high-strain metamorphic rocks (the dynamic metamorphism of Binns et al., 1976) at their distal margins. These observations suggest strain partitioning and relatively high heat flow and fluid flux (magmas, hydrothermal fluids) into the rheologically weak and thermally softened margins of the rift that is underlain by the youngest (<2.9 Ga) basement crust. These are considered to be the main regional-scale factors responsible for concentration of gold in the Kalgoorlie Terrane and the Linden domain (the Laverton Tectonic Zone).

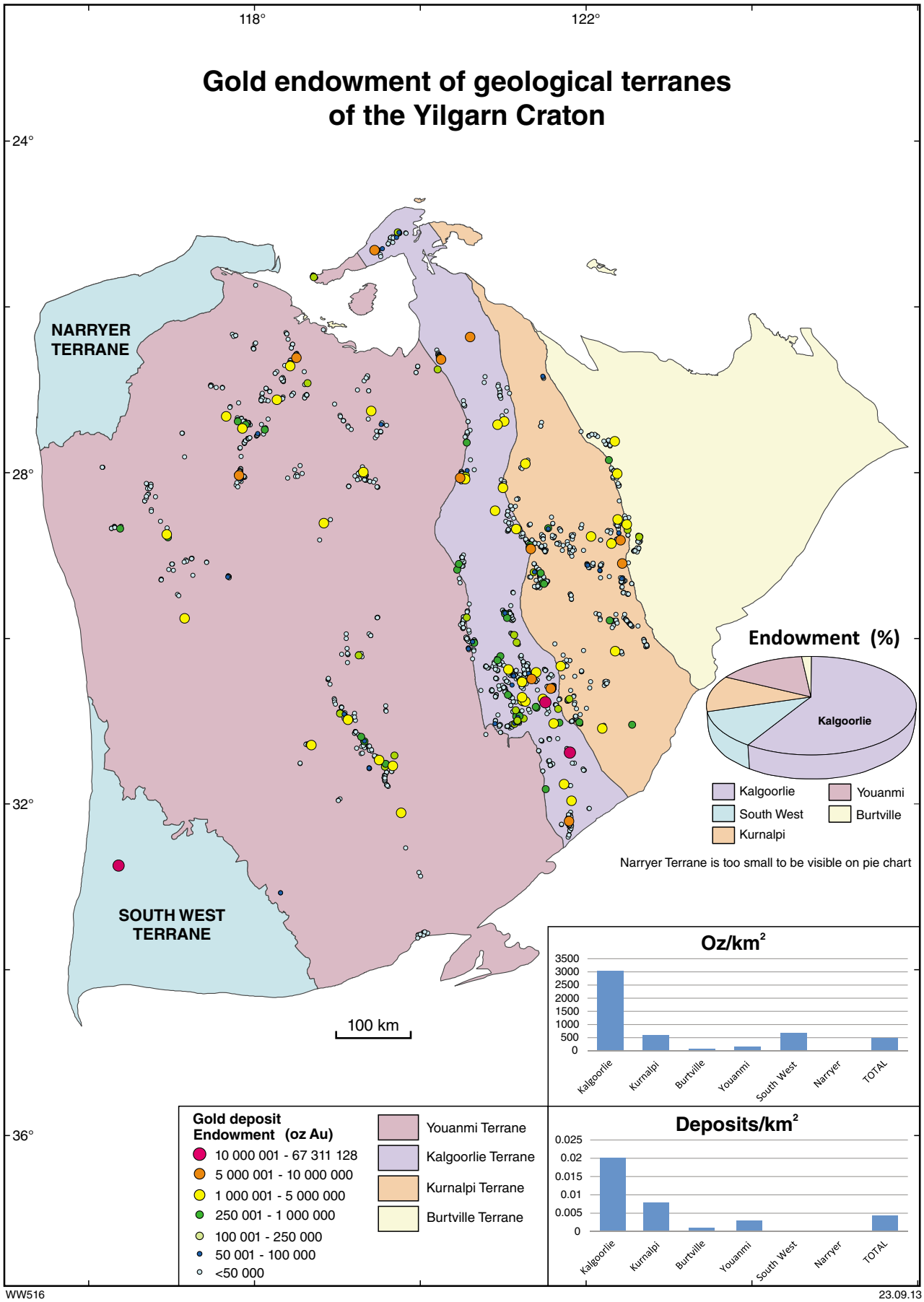

Figure 1.1. **Gold endowment of geological terranes of the Yilgarn Craton**

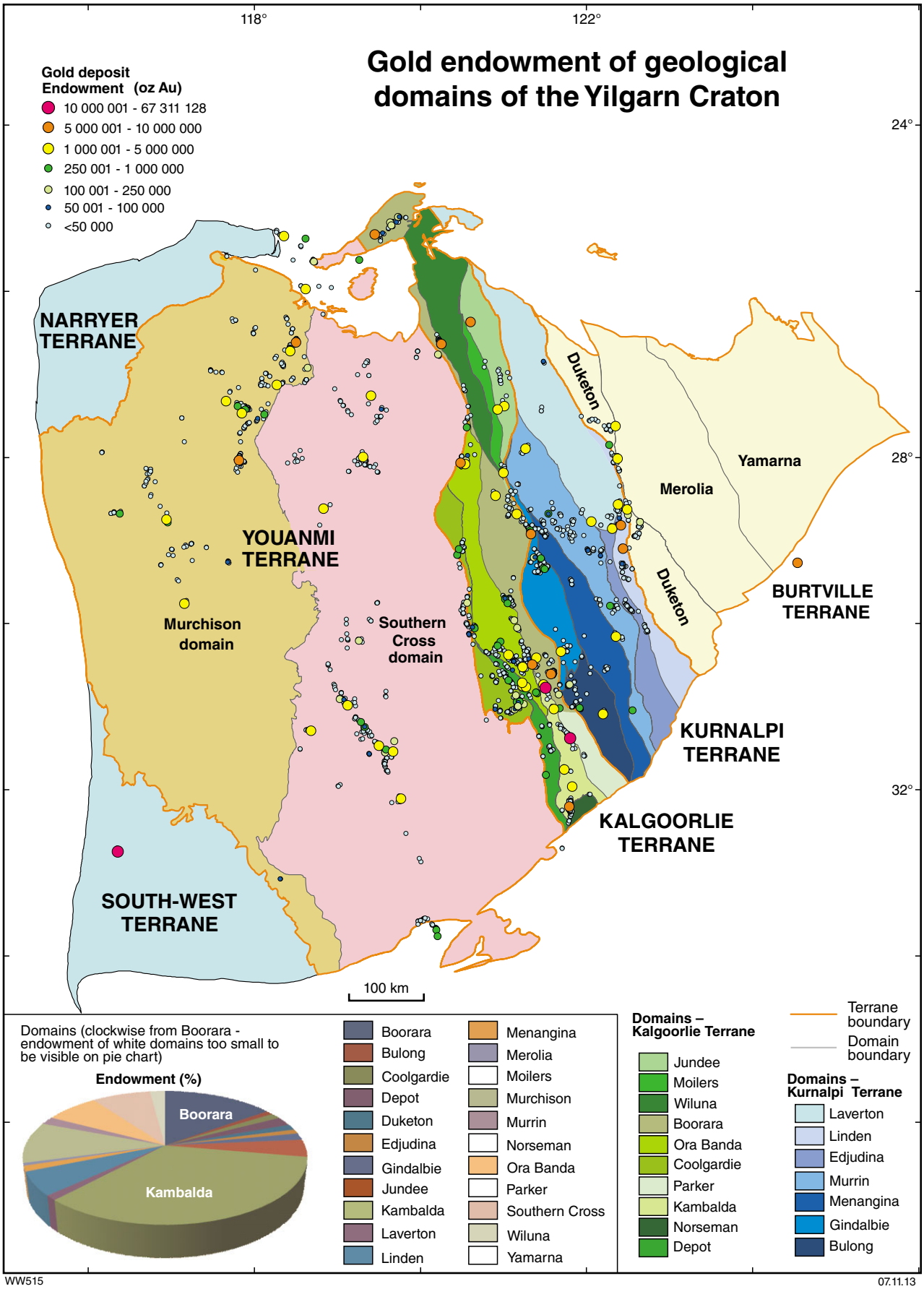

Figure 1.2. Gold endowment of geological domains of the Yilgarn Craton

Table 1.2. Comparison of gold endowment in the Yilgarn Craton, Western Australia (this study), with that of the Superior Province, Canada[a]

Craton	*Province/Superterrane*	*Terrane/domain*	*Endowment (oz/km^2)*
Superior	Entire craton		251
Yilgarn	Entire craton		476
Yilgarn	Eastern Goldfields Superterrane		1007
Yilgarn		Youanmi Terrane	144
Superior		Abitibi sub-province	1698
Superior		Uchi sub-province	1102
Superior		Wawa sub-province	428
Yilgarn		Murchison domain	168
Yilgarn		Southern Cross domain	121
Superior		Wabigoon districts	81
Superior		Sachigo districts	65

NOTE: (a) Endowments in Superior Craton from B Dubé and V Becu, 2011, Geological Survey of Canada, pers. comm., 11 February)

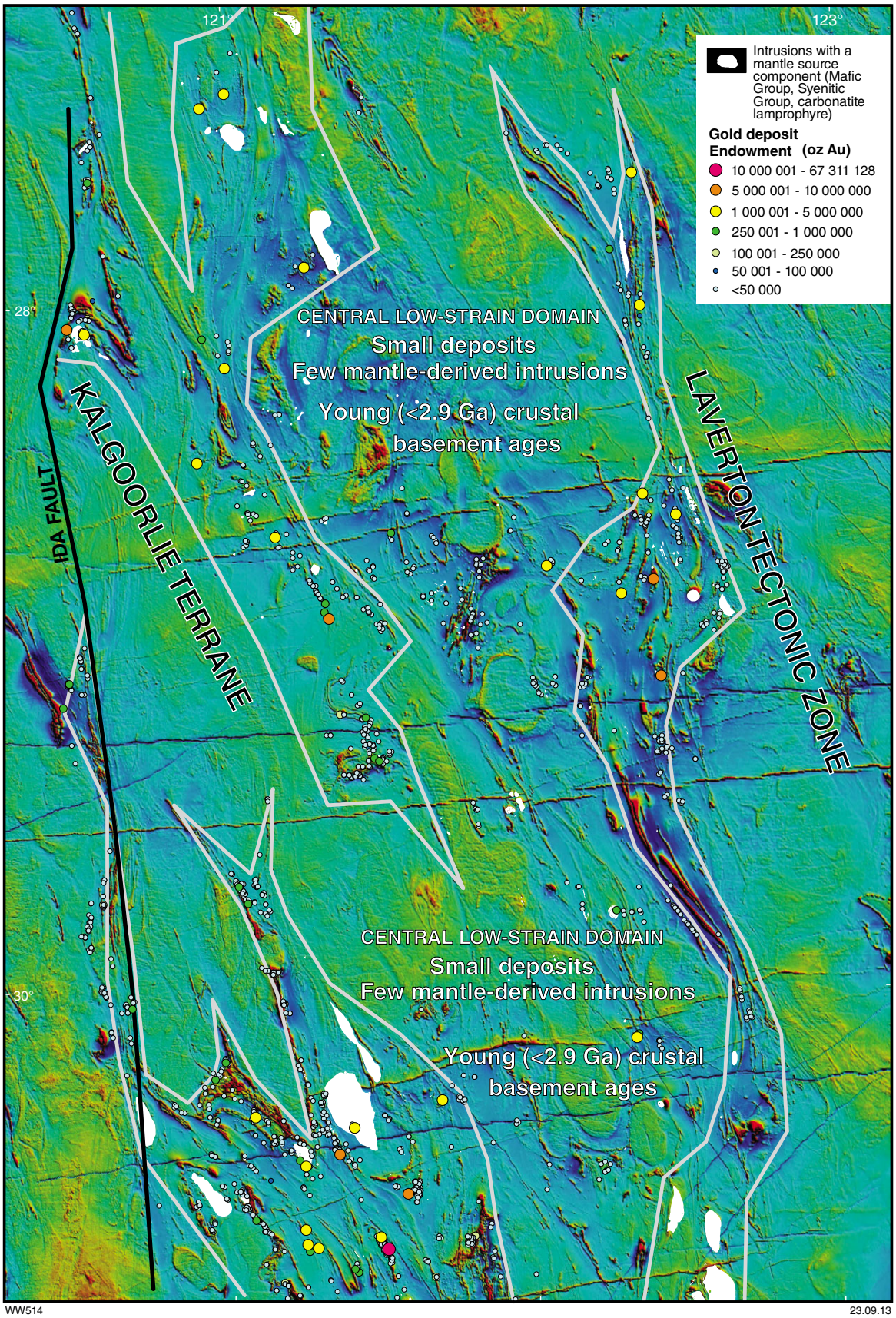

Figure 1.3. **Aeromagnetic image of a major portion of the Eastern Goldfields Superterrane showing distribution of gold deposits and intrusions with a mantle source component (white), both of which are concentrated in linear zones of deformation and high heat flow with connectivity to the mantle or lithospheric mantle (areas outlined in grey). These fertile zones (broadly equivalent to the Kalgoorlie Terrane and the Laverton Tectonic Zone) lie astride a central region of lower strain underlain by relatively young but competent crust.**

Targeting Criterion 1.1: Seismic tomography and tomographic edges

Seismic tomography uses energy received from near-surface disturbances (e.g. explosions, impacts) or deeper (e.g. earthquakes) sources to build a velocity image of the subsurface through which the seismic waves travelled (Goleby et al., 2006; Reading et al., 2003). Seismic data can be used to interpret the location of deeply penetrating structures that might have transported fluids and heat from the deep crust and/or mantle, potentially forming ore deposits. Seismic reflection profiling, derived from near-surface disturbances, has highlighted the presence of three east-dipping faults that penetrate the base of the greenstones and the base of the crust (Goleby et al., 2006). These structures correspond to the Mount George Shear Zone, near Leonora, the Laverton Shear Zone, near Laverton, and the Yamarna Shear Zone, near the remote eastern margin of the exposed Yilgarn Craton. Goleby et al. (2006) and Blewett et al. (2010b) proposed a spatial association between gold mineralization and the first two of these structures, and suggested there was exploration potential around the Yamarna Shear Zone. Subsequent exploration in the Yamarna greenstone belt by Gold Road Resources has identified combined Measured, Indicated, and Inferred resources of over 1 Moz gold on the Central Bore and Atilla Trends, including 101 738 oz of gold at 19.2 g/t in the high-grade Imperial Shoot (Gold Road Resources website, March, 2013; <www.goldroad.com.au/projects-central_bore.php>). The spatial association of gold mineralization with these deep, east-dipping structures has not been quantified, either in this Project, or in earlier publications. However, a more general association between gold and regional faults and fault vergence anomalies (west-dipping faults) is investigated in later sections of this Atlas.

In the Yilgarn Craton, seismic reflection data have generally been used to interpret the full crustal section (about 30 km) (Swager et al., 1997; Goleby et al., 2002, 2006). Velocity models of the upper mantle below the Yilgarn Craton have been derived from receiver function studies in which seismic data have been derived from earthquakes in areas surrounding the Australian continent (e.g. Reading et al., 2003; Fishwick and Rawlinson, 2012). These studies make use of surface wave and body wave datasets. Using absolute velocity variations determined by inversion of surface waves, Fishwick and Rawlinson (2012) showed that gold deposits in the Yilgarn and Pilbara Cratons display a spatial relationship with the margins of high-velocity mantle domains at depths of 100 km (Fig. 1.4).

Teleseismic S-wave velocities indicate the presence of a gently southeast-dipping, high-velocity (>4.8 km/s) lithospheric layer, 20–25 km thick at a depth of approximately 120 km beneath the Yilgarn Craton crust (Reading et al., 2003; Goleby et al., 2006). Blewett et al. (2008) reported a number of steps or tears in the high-velocity lithospheric layer, and these are portrayed in the *edges_s1_s9* shape file generated by pmd*CRC. They are shown as tomographic edges, projected from a depth of 120 km, in Figure 1.5. Blewett et al. (2010a) reported a spatial association between these tomographic edges and mantle-derived intrusions of Archean to Proterozoic age, including kimberlites, syenites, and carbonatites. Clustering of gold deposits, including those at Kalgoorlie and Laverton, are similarly close to these tomographic edges (Blewett et al., 2010a). Several models for Archean gold mineralization propose the mantle as a source of magmas that transfer heat and fluids to the middle to upper crust, or as a direct source for ore fluid (Rock et al., 1989; Walshe et al. 2008; Cassidy, 2010). Thus, tears in the lithospheric mantle provide potential pathways for magmas and fluids to access the upper crust where most Archean gold deposits are found. Czarnota et al. (2010a) assigned a 20 000 m buffer to these tomographic edges and used this feature as a factor in mapping the gold prospectivity of the eastern Yilgarn Craton (broadly equivalent to the Eastern Goldfields Superterrane).

A proximity analysis of the relationship between gold and tomographic edges results in a peak %Endowment/%Area ratio within the 30 000 m buffer (Table A1.5). This buffer captured 55.9% of the gold endowment (and 48.8% of deposits) within 27.2% of the analysis area (i.e. the Yilgarn Craton, excluding the Narryer and South West Terranes), equivalent to a %Endowment/%Area ratio of 2.06. This result seems to be heavily influenced by the inclusion of the giant Golden Mile deposit in the 30 000 m buffer. The peak number of deposits/square kilometre is captured by the 10 000 m buffer, where 18.9% of the deposits are within 9.55% of the analysis area. The size of the optimal buffers in this analysis is greater than for most of the other regional-scale spatial analyses described in this Atlas. However, given the scale of the target feature (the tomographic edges), buffers of 10 km and even 30 km do not seem unreasonable. Both the deposit density and ounces per square kilometre curves decrease consistently beyond the peak buffer (Table A1.5), supporting a meaningful geological relationship between gold and the tomographic edges. The average endowment of the 30 000 m buffer (998 oz/km^2) is roughly twice the average for the analysis area (485 oz/km^2 for the Yilgarn Craton, excluding the Narryer and South West Terranes), whereas the average deposit density for the 10 000 m buffer (0.01 deposits/km^2) is also approximately double the average for the analysis area (0.005 deposits/km^2). The analysis described here includes granite and greenstone areas of the Yilgarn Craton. The peak endowment figures for the tomographic edges analysis are actually much less than the Yilgarn average, if only greenstones are considered (2842 oz/km^2 and 0.025 deposits/km^2, Table A1.3). That is, the simple strategy of targeting greenstones as opposed to granites is 2.7 times more effective than targeting peak buffers around the tomographic edges. A combined strategy of targeting greenstones within the peak buffers around tomographic edges would be more effective than using either strategy alone.

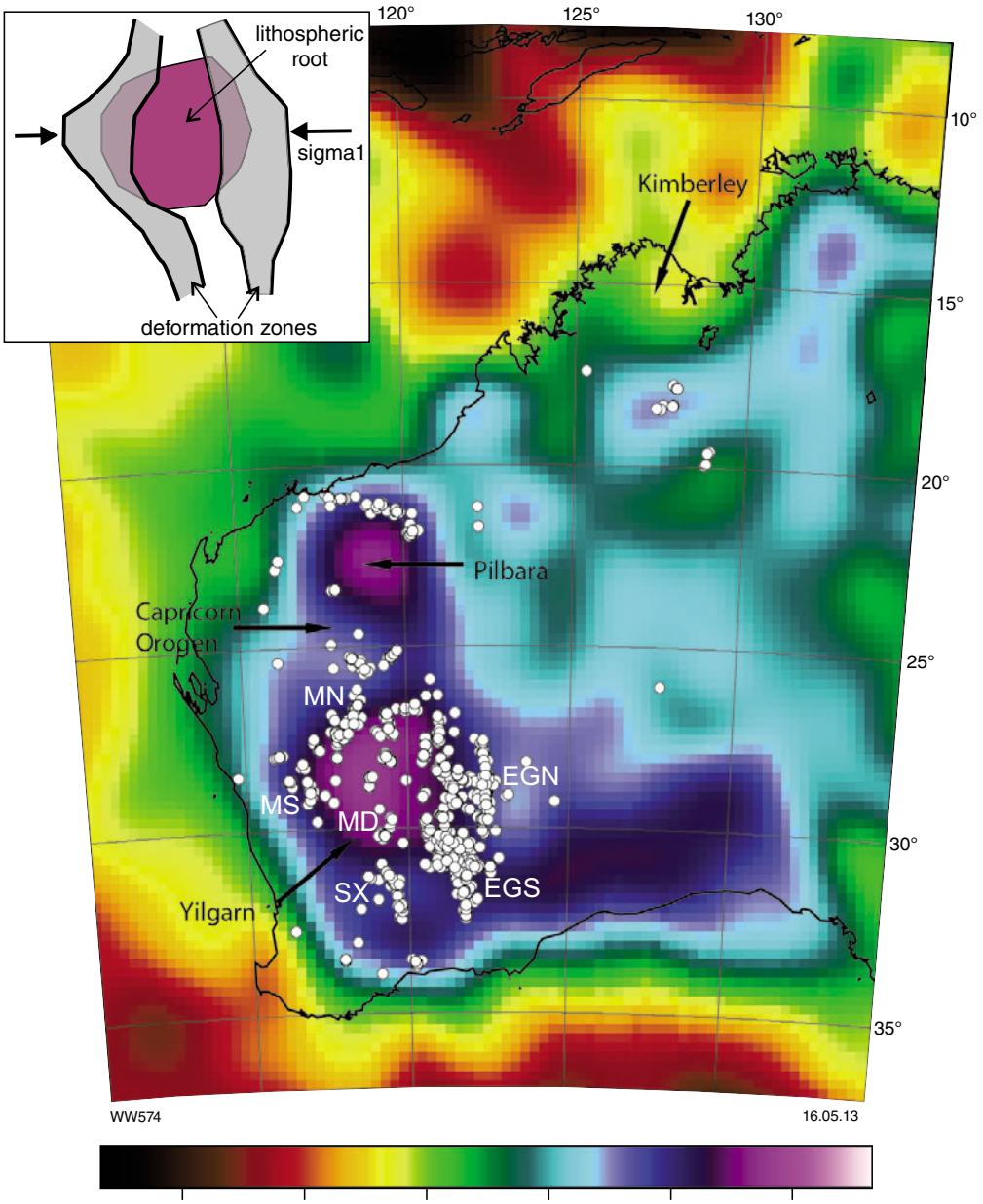

Figure 1.4. **Absolute surface wave velocities at 100 km depth below Western Australia, determined from surface wave inversion, and locations of major gold deposits (Geoscience Australia Australian Atlas of Mineral Resources, Mines and Processing Centres; <www.australianminesatlas.gov.au.>). Yilgarn Craton gold deposits are distributed around the margins of a high-velocity domain in the underlying lithospheric mantle (from Fishwick and Rawlinson, 2012). Abbreviations: EGN (Eastern Goldfields north), EGS (Eastern Goldfields south), MD (Marda-Diemals), MN (Murchison north), MS (Murchison south), SX (Southern Cross). Inset: schematic interpretation of the relationship between deformation zones and the thick lithospheric root beneath the Yilgarn Craton (cf. Oliver et al., 1990). The three subdivisions of the Eastern Goldfields Superterrane (described under the heading Terranes and domains: Gold endowment) are all within the eastern bounding deformation zone. The outer well-mineralized subdivisions shown in Figure 1.3, also within the eastern bounding deformation zone, correspond to the N-S clusters of high deposit density in the main part of this Figure.**

The spatial association of major gold deposits around the lithospheric root beneath the Yilgarn Craton is reminiscent of stress distribution models around rigid bodies undergoing regional deformation in the middle and upper crust (Oliver et al., 1990 and inset, Fig. 1.4). The distribution of major gold deposits in the Yilgarn Craton around the margins of the 100 km deep high-velocity domain (Fig. 1.4) suggests that these margins are zones of deformation in the lithospheric mantle, coincident with rheological gradients between rigid lithosphere and hotter, rheologically weaker lithosphere. Hronsky et al. (2012) drew attention to a similar relationship between gold mineralization and the margins of thick lithospheric roots at global scale. The Eastern Goldfields gold deposits formed along the eastern margin of the deep lithospheric root beneath the Yilgarn Craton, whereas the Murchison and Southern Cross deposits formed along its western margin. Deformation zones on the margins of the lithospheric root propagated to the north and south and were transferred into the overlying crust during one or more periods of regional deformation. These deformation zones provided access to heat, deeply sourced magmas, and the hydrothermal fluids that contributed, individually or in combination, to the formation of gold deposits. A small proportion of major gold deposits are central within the Yilgarn Craton, above the centre of the thick lithospheric root (Fig. 1.4). Some of these fall within the optimal 30 000 m buffer around the tomographic edge described above.

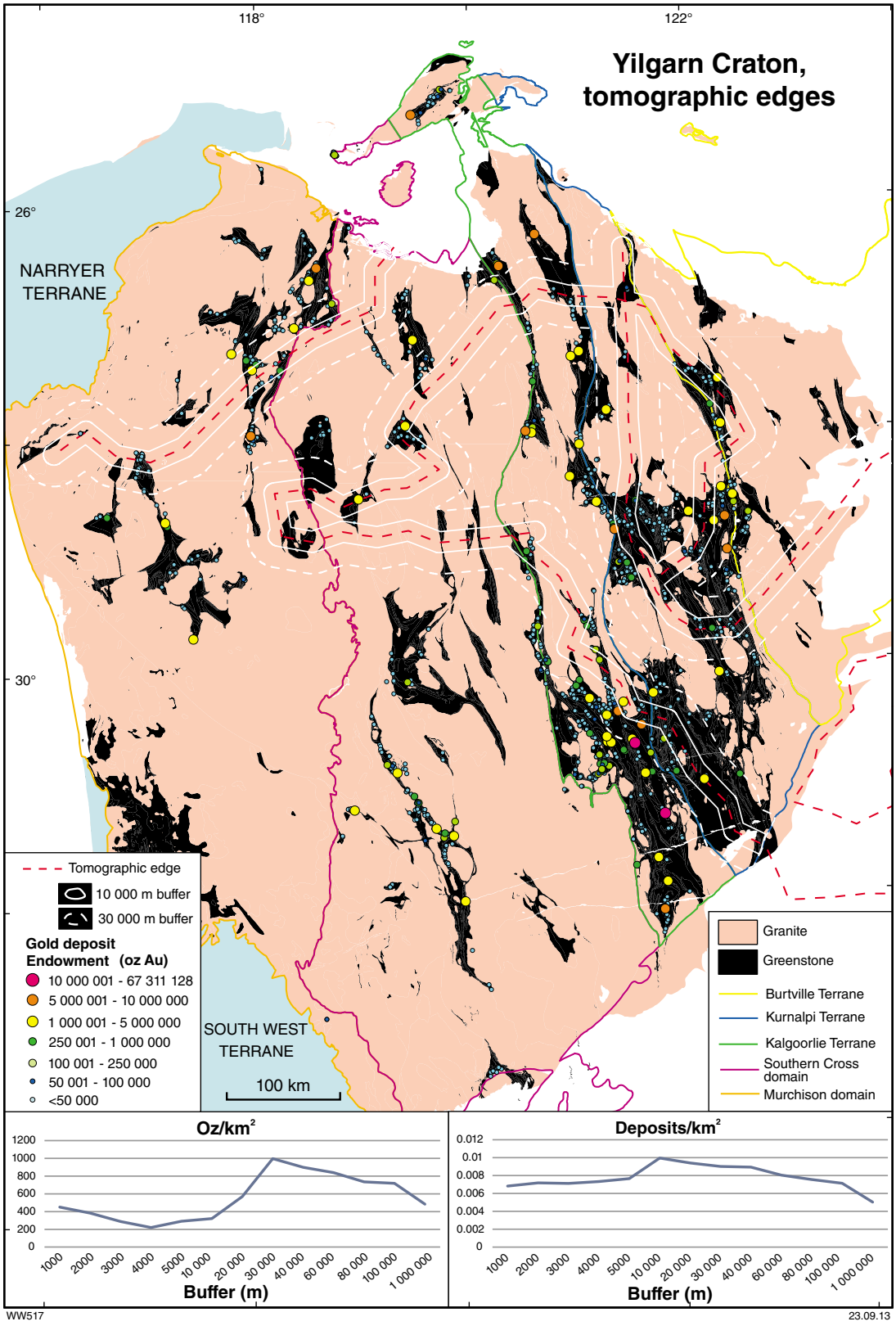

Figure 1.5. **Distribution of gold deposits in the Yilgarn Craton relative to deep tomographic edges based on teleseismic S-wave velocities at a depth of 120 km (Czarnota et al., 2010a)**

Targeting Criterion 1.2: Sm-Nd isotope basement domains and gradients

Champion and Cassidy (2007) published the first Nd isotope map of the Yilgarn Craton, based on Sm-Nd isotope ages of granites. This map effectively delineated the age at which the basement source rocks beneath the craton were extracted from the mantle. In effect, the Nd isotope map is a map of the age of the sub-Yilgarn greenstone basement. The map has undergone several revisions as more Sm-Nd isotope data have become available, and this study uses the most recent (unpublished) compilation available at the time of the study. This GSWA compilation incorporates the data of Champion and Cassidy (2007) as well as new data acquired by Geoscience Australia and GSWA (Fig. 1.6).

The Nd isotope map indicates relatively young basement (<2.85 Ga) beneath the Kurnalpi Terrane, and older basement to the east and especially to the west. The pattern defined by the Sm-Nd data has been interpreted by Blewett and Hitchman (2006) and Czarnota et al. (2010b) to indicate a relatively young basement rift on the eastern margin of the Youanmi Terrane (in effect the proto-Yilgarn Craton) and centred on the Kurnalpi Terrane. Slightly older basement to the east, beneath the Burtville Terrane, could be either a rifted fragment of the proto-Yilgarn Craton (Czarnota et al., 2010b) or an exotic terrane that was accreted to the Eastern Goldfields Superterrane. Similarly, the relatively young age of basement underlying the Murchison domain may represent a rifted basement province (Fig. 1.6).

Spatial analysis of the two-stage Nd isotopic domain map shows that areas underlain by intermediate aged basement (3.0 – 2.85 Ga) are the best endowed with respect to gold (Table A1.6). These areas, which dominate the Kalgoorlie Terrane and the relatively unexplored Burtville Terrane, also underlie the mineralized greenstone belts of the Murchison domain. They contain 66.9% of the gold endowment and 54.6% of deposits within 32.6% of the study area (Fig. 1.6), representing a %Endowment/%Area ratio of 2.05. Of the remaining Yilgarn Craton, the %Endowment/%Area ratio is much less than one, except in areas of very young basement (<2.85 Ga), which have a %Endowment/%Area ratio of a little less than one. However, the endowment of the <2.85 Ga areas is only 2.2% of the total. Deposit density also shows a substantial positive bias towards areas underlain by basement of 3.0 – 2.85 Ga age (0.008 deposits/km^2 relative to an average of 0.005 deposits/km^2 for the total analysis area). Greenstones above the youngest basement (<2.85 Ga), broadly centred on the Kurnalpi Terrane, contain a little less than the average deposit density for the analysis area.

For proximity analysis relating gold endowment to Sm-Nd gradients, steep Sm-Nd gradients were identified by two methods that gave similar but slightly different results (Fig. 1.6). Edge detection software (Intrepid Geophysics Ltd) was used to generate a series of lines, described as 'worms'[1], with various upward continued projection heights; the CET Grid Analysis Plug-in for ArcGIS (Geosoft Inc.) was used to generate curvilinear series of points. Although these curvilinear series are similar in distribution to the worms generated by the Intrepid software, they are generally shorter. The two sets of data were rationalized into a single shape file by duplicating the shapes of the curves generated by Intrepid, but restricting their extent to the shorter lengths of the point arrays generated by CET Grid Analysis (Fig. 1.6). Results of the proximity analysis relating gold endowment to steep gradients in Sm-Nd basement ages are presented in Table A1.7. The spatial relationships of proximity to steep Sm-Nd gradients for both gold endowment and number of deposits are extremely weak to non-existent. This poor association between mineralization and steep basement Sm-Nd age gradients is illustrated by the increase of endowment between the 10 000 and 50 000 m buffers, for both endowment and number of deposits.

The concentration of gold in areas underlain by basement of intermediate age (3.0 – 2.85 Ga) probably reflects rifting of older Archean crust and formation of younger, thinner crust onto which the 2.72 – 2.67 Ga greenstones that host gold mineralization were deposited (cf. Czarnota et al., 2010b). Rifts, and particularly rift margins, are potential zones of crustal weakness during subsequent orogenic events. High heat flow and igneous activity during rifting modifies the deep crust, possibly increasing its fertility when subsequent tectonothermal events are superimposed.

A more recent compilation of granite Sm-Nd isotopic data (Fig. 1.7; not available at the time of the spatial analysis presented here) provides additional perspective on this model. It is apparent (as in earlier compilations) that the superior endowment of the Kalgoorlie Terrane coincides with proximity to a steep Sm-Nd age gradient in the two stage Nd basement age model (Fig. 1.7). This gradient is broadly coincident with the Ida Fault and could be interpreted as marking the eastern margin of the stable proto-Yilgarn Craton. In younger geological environments, similar cratonic or continental margins are fertile economic zones (Hildenbrand et al., 2000; Grausch et al., 2003). If the rift scenario described above (Terranes and domains) is accepted, the steep gradient in basement age at the eastern edge of the Youanmi Terrane may represent a zone of relatively high heat flow at the western margin of the rift. Similarly, the eastern margin of the rift, represented by young (<2.9 Ga) basement crust, is broadly coincident with the well-mineralized Laverton Tectonic Zone, which is in turn broadly coincident with the Linden domain.

Craton-scale strain partitioning during the c. 2.64 Ga deformation of 2.71 – 2.67 Ga greenstones that resulted in accretion or re-accretion of crustal elements onto the eastern margin of the proto-Yilgarn Craton may have been an important factor in the localization of gold mineralization.

1 'Worms' are upward continued discontinuities or gradients, commonly used in analysis of potential field data (e.g. Hornby et al., 1999; Bierlein et al., 2006). See also Targeting Criteria 1.4 and 1.5.

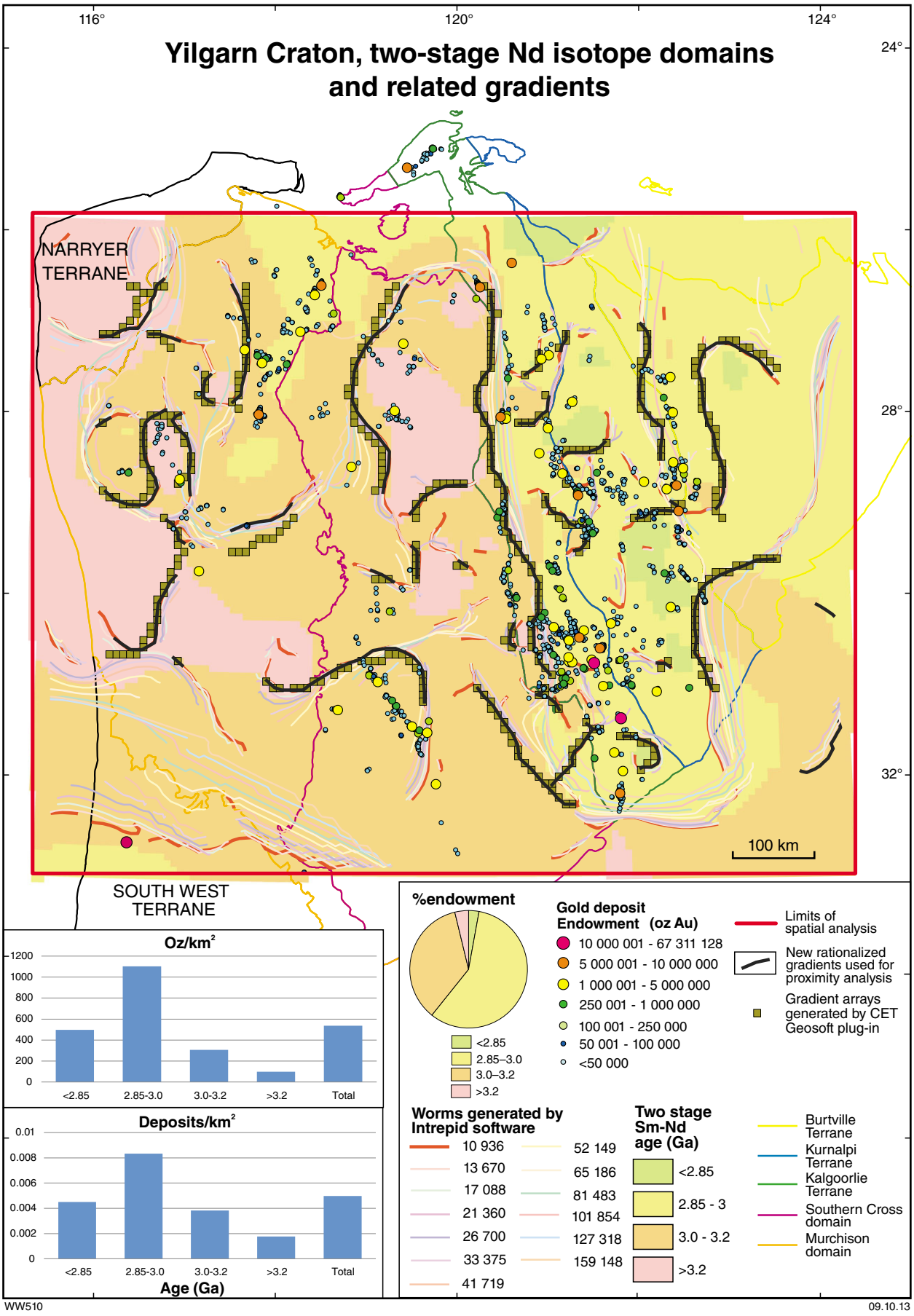

Figure 1.6. **Relationship of Sm-Nd basement domains and steep gradients in Sm-Nd data to gold endowment in part of the Yilgarn Craton**

The highly mineralized zones represented by the Kalgoorlie Terrane and Laverton Tectonic Zone were probably zones of crustal weakness with high heat flow and high fluid flux during the c. 2.64 Ga accretionary event with which gold mineralization was associated (see also Fig. 1.3). The results of our craton-wide proximity analysis relating gold endowment to other steep Sm-Nd basement gradients indicate that these smaller scale features are not effective targeting criteria in the Yilgarn Craton.

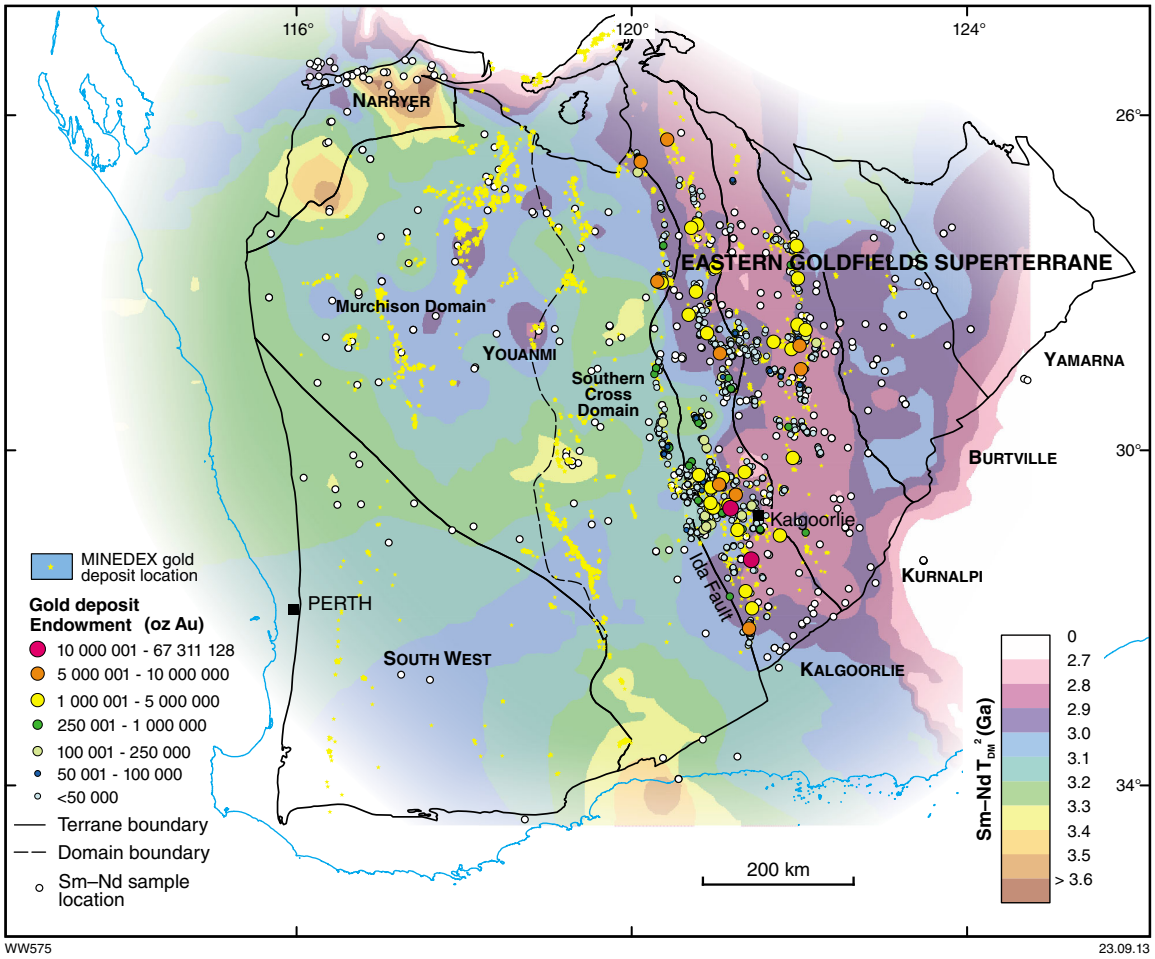

Figure 1.7. **Sm-Nd basement map, based on ages of granites, for the Yilgarn Craton (Wyche et al., 2012). Also shown are gold deposit data from the Barrick Gold Corporation and MINEDEX databases.**

Targeting Criterion 1.3: Granite groups

The genetic relationship between gold mineralization and various types of granites in Archean greenstone belts has long been keenly debated. Opinions range between those who advocate granites as a source for the ore fluid (Cameron and Hattori, 1987; Spooner, 1993; Penczak and Mason, 1997) and those who view intrusions as passive participants in deposit formation (Witt, 1992; Cassidy et al., 1998; Groves et al., 2000). In the latter case, the common association of gold deposits with felsic to intermediate intrusions is explained as the result of magmatic melts and ore fluids exploiting the same deeply penetrating structures, and perhaps even produced by the same deep-crustal or mantle-generated thermal event (Goldfarb et al., 2005). In this view, intrusions are relatively competent bodies and therefore contribute to rheological gradients and consequent stress heterogeneity during externally imposed deformation. Quantitative GIS spatial analysis of the relationship between gold mineralization and various granitic suites in the Yilgarn Craton has not previously been published. In this study, we used shape files developed by pmd*CRC and acquired from David Champion (Geoscience Australia, pers. comm., May 2010), which show the location and extent of granitic intrusions in the Yilgarn Craton, grouped by 'granite group' or supersuite. There are five main granite groups, described originally by Champion and Sheraton (1997) based on petrographic and geochemical criteria, and subsequently adopted by Blewett et al. (2010a) and Czarnota et al. (2010b). The most voluminous granites in the Yilgarn Craton belong to the High-Ca and Low-Ca Groups, whereas the High Field Strength Element Enriched (HFSE), Mafic, and Syenitic Groups[2] are generally relatively small and less widely distributed. For the GIS spatial analyses, buffers were created at 1000 m spacing to 10 000 m for suites in which individual intrusions are large (High-Ca and Low-Ca granites), and at 500 m spacing to 5000 m for the remaining groups, in which most individual intrusions are relatively small.

HFSE granites represent the earliest pulse of intrusive activity in the Eastern Goldfields Superterrane (Fig. 1.8). These granites were intruded before 2675 Ma and are broadly contemporaneous with the eruption between 2720 and 2675 Ma of chemically similar felsic volcanic rocks in the Kurnalpi Terrane (Cassidy et al., 2002). They have not been documented outside the Kalgoorlie and Kurnalpi Terranes, although some intrusions of the Eelya Suite in the Murchison domain reportedly have high-HFSE geochemical characteristics (Van Kranendonk and Ivanic, 2009). Spatial analyses of gold endowment in successively increasing buffers from 500 to 5000 m show a peak endowment at 1500 m, beyond which endowment remains approximately constant for successively larger buffers (Table A1.8). The 1500 m buffer contains only 4.1% of the endowment in 3.7% of the analysis area, equivalent to a %Endowment/%Area ratio of 1.11. The number of deposits peaks in the most proximal (500 m) buffer and slowly declines in successively larger buffers (Table A1.8). The average deposit size increases steeply, reaching a plateau at 1500 m, but increases again in the most distal (>5000 m) buffer (Table A1.8). These relationships suggest that if there is a meaningful spatial relationship between gold and HFSE granites, this relationship concerns only a small (<5%) proportion of relatively small deposits (Fig. 1.8).

The next pulse of granite intrusions is included in the widespread High-Ca granites (Fig. 1.9), intruded mainly between 2685 and 2655 Ma (Cassidy et al., 2002). In the Eastern Goldfields Superterrane, emplacement of these granites overlapped deposition of the felsic to intermediate volcaniclastic Black Flag Group in the Kalgoorlie Terrane, formation of late-stage sedimentary basins, and most of the Wangkathaa Orogeny. The Wangkathaa Orogeny of Blewett et al. (2004) incorporates D_2 through D_4 of Czarnota et al. (2010b) and Blewett et al. (2010a). Spatial analysis of gold endowment in successively increasing buffers from 1000 to 10 000 m around High-Ca granite intrusions results in flattish curves that do not support a meaningful spatial relationship with gold deposits or gold endowment (Table A1.9). There is a peak of capture of gold within the 6000 m buffer (52.5% of the gold endowment in 44.7% of the area, equivalent to %Endowment/%Area of 1.18), but this does not represent an effective targeting tool for gold exploration and the shape of the curves does not support a meaningful geological relationship between High-Ca granites and gold mineralization.

Overlapping the latter part of the High-Ca granite 'bloom', the main pulse of intrusion of the Mafic and Syenitic granites was between 2675 and 2655 Ma (Czarnota et al., 2010b). The peak emplacement age of these intrusions was coincident with D_3 extension and formation of the late sedimentary basins, but emplacement overlapped D_2 and D_4 shortening events (Czarnota et al., 2010b; Blewett et al., 2010a). Lamprophyres, which are mostly small plugs and dykes, show a close spatial and temporal association with syenites and can probably be added to this group of broadly syn-D_3 intrusions. Although not well dated by geochronological techniques, the lamprophyres commonly display an intimate spatial association with Syenitic granites in the Kurnalpi Terrane. In the Archean Abitibi greenstone belt (Wyman and Kerrich, 1988) and in younger geological terranes (Sheppard and Taylor, 1992), lamprophyres and syenites are also spatially and temporally related.

A 1000 m buffer around Mafic granite intrusions (Fig. 1.10) captures 43.1% of the gold endowment in only 0.9% of the spatial analysis area (Table A1.10). This equates with a maximum %Endowment/%Area of 50.4. The steadily declining curves defined by buffers >1000 m suggests there is a real and significant geological relationship between gold endowment and proximity to Mafic granites. The number of deposits defines a similar relationship, with deposit density declining from a peak of 0.146 deposits/km^2 in the most proximal (500 m) buffer (Table A1.10).

2 For simplicity, 'Group' is omitted hereafter and these five groups are referred to in the form High-Ca granites, Low-Ca granites, HFSE granites, Mafic granites, and Syenitic granites.

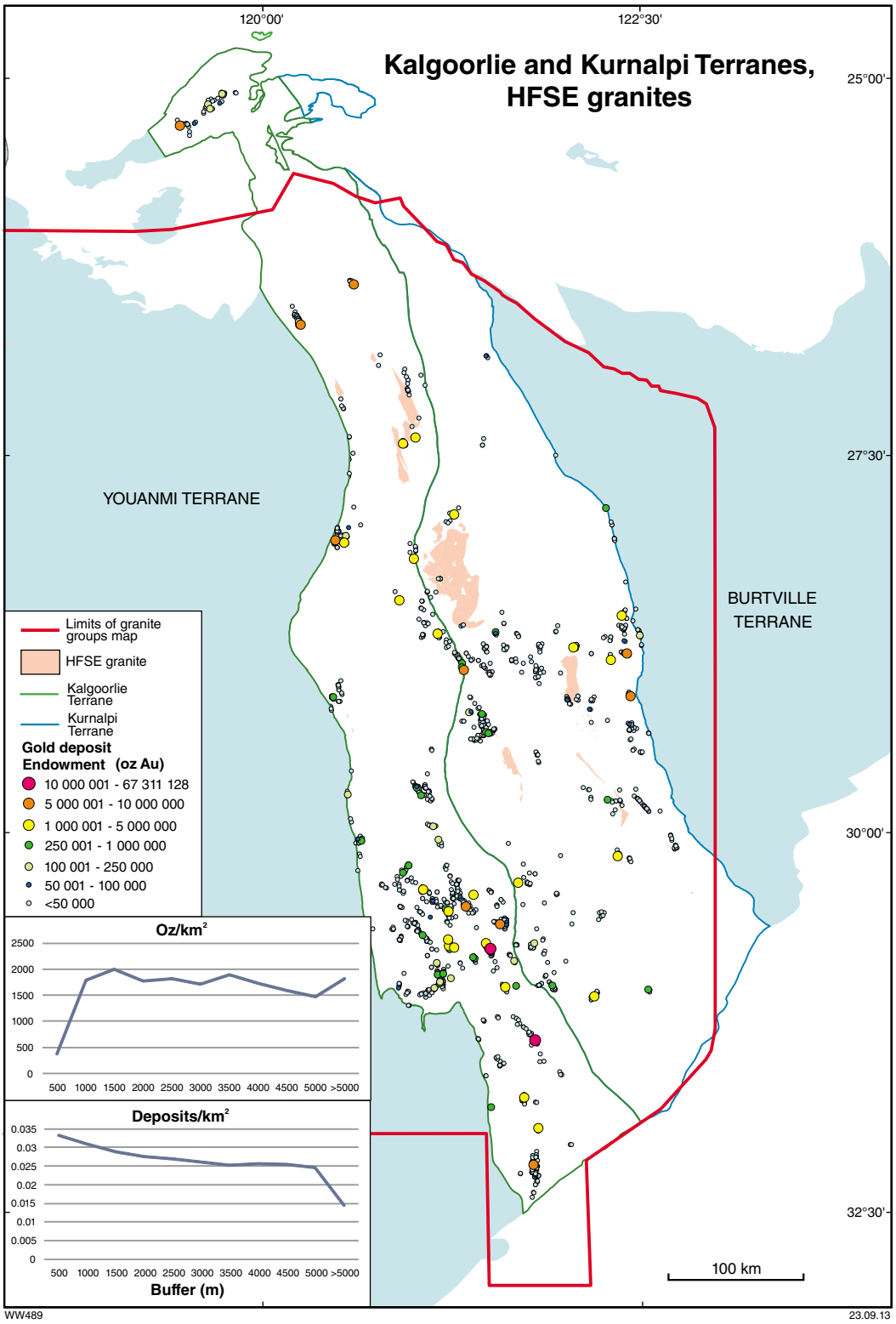

Figure 1.8. **Distribution of gold deposits in the Kalgoorlie and Kurnalpi Terranes relative to HFSE-enriched granite intrusions**

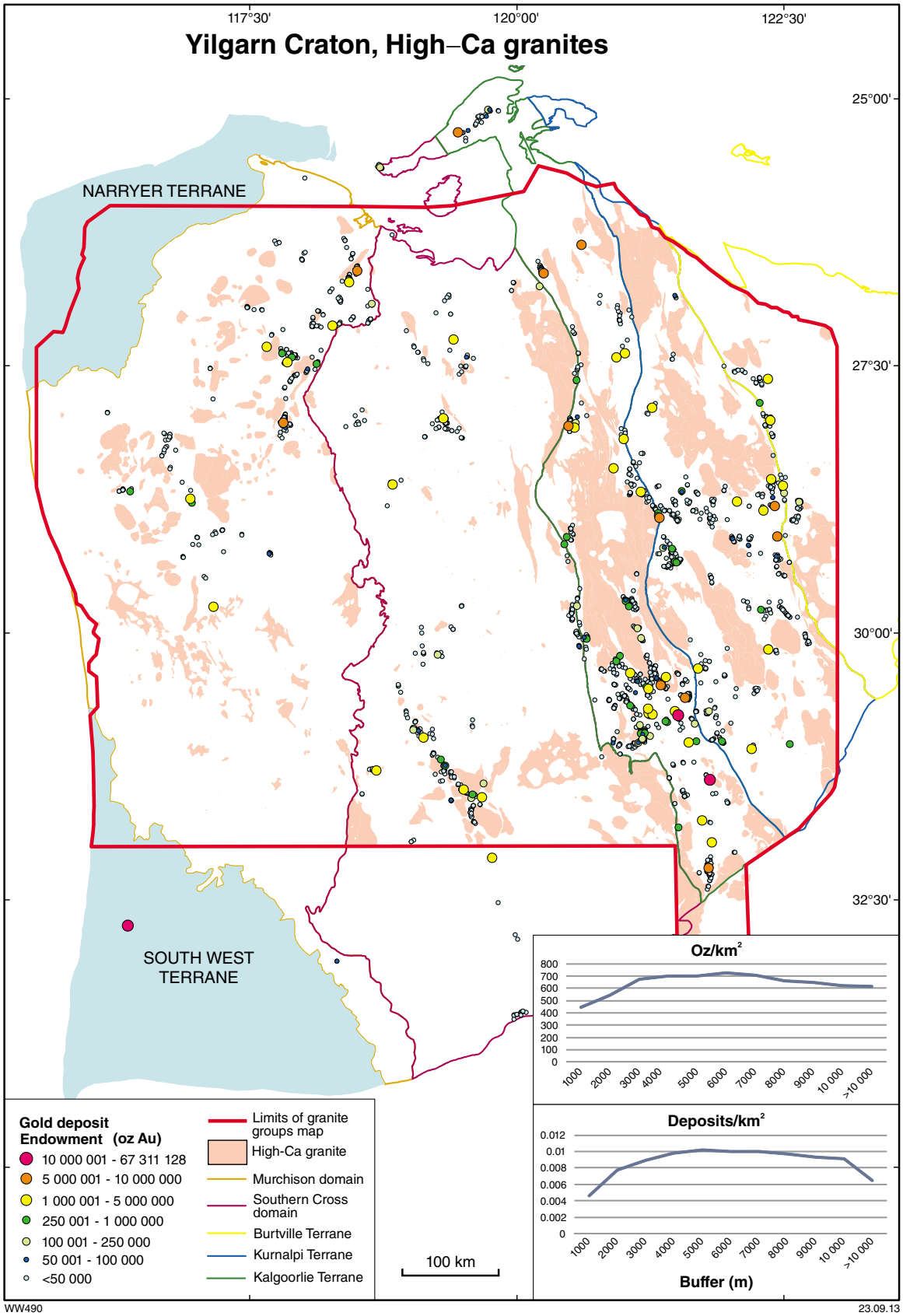

Figure 1.9. Distribution of gold deposits in the Yilgarn Craton relative to High-Ca granite intrusions

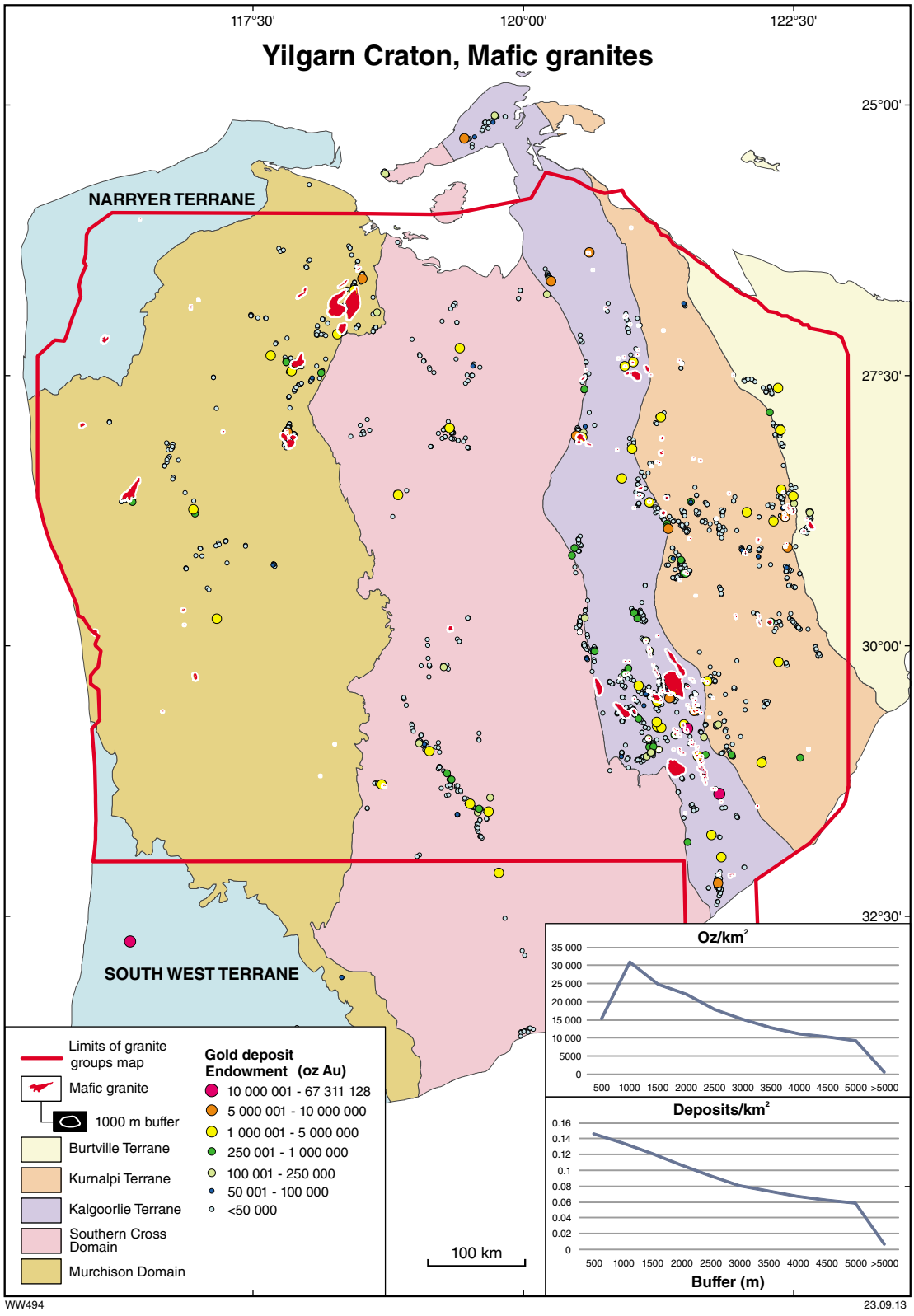

Figure 1.10. Distribution of gold deposits in the Yilgarn Craton relative to Mafic granite intrusions

This figure can be compared with an average deposit density over the analysis area of 0.006 deposits/km^2. If the spatial analysis is confined to the Kalgoorlie and Kurnalpi Terranes (Fig. 1.11), a peak %Endowment/%Area ratio of 28.4 is achieved within the 1000 m buffer (Table A1.11). The average deposit size (361 927 oz Au) is also greatest within the 1000 m buffer. The number of deposits decreases steadily with increasing distance from the most proximal buffer (500 m) where the deposit density is >10 times the average for the analysis area. Within the Murchison domain (Fig. 1.12), the optimum buffer distance for Mafic granites is 1500 m, where 36.3% of the gold endowment is captured within 1.1% of the area, equivalent to a %Endowment/%Area ratio of 32.8 (Table A1.12). As for the combined Kalgoorlie and Kurnalpi Terranes, average deposit size is coincident with peak %Endowment/%Area, in the 1500 m buffer, whereas the number of deposits declines from a peak of 0.116 deposits/km^2 in the most proximal (500 m) buffer (Table A1.12). The deposit density within the 500 m buffer is >30 times the average deposit density for the Murchison analysis area (0.003 deposits/km^2).

Syenitic granite intrusions are found mainly in the Kurnalpi Terrane of the Eastern Goldfields Superterrane (Fig. 1.13). Despite a well-known association of some gold deposits with syenitic intrusions in the Kurnalpi Terrane (e.g. Duuring et al., 2000; Salier et al., 2005; Witt et al., 2009), spatial analysis at the scale of the Eastern Goldfields Superterrane shows that the proportion of gold proximal to Syenite granites is very limited (e.g. 1.2% of the total endowment within the 500 m buffer; Table A1.13). Beyond the 500 m buffer, endowment decreases steadily to about 3500 m, after which the endowment consistently increases. There is an inverse relationship between the number of deposits and proximity (Table A1.13). A notable feature of the analysis is the overall decrease in average deposit size with distance from Syenitic granite intrusions, which suggests that the relatively few deposits in the most proximal buffers are larger than average for the Eastern Goldfields Superterrane. This result is influenced by the location of the Wallaby deposit (2.8 Moz Au) in and around Syenitic granite intrusions of the Kurnalpi Terrane.

When the spatial analysis of gold and Syenitic granite intrusions is confined to the Kurnalpi Terrane (Fig. 1.14), the relationships described above are maintained but the proportion of the gold endowment captured in proximal buffers is higher. The most proximal buffer (500 m), representing 3.4% of the analytical area, captures 7.1% of the gold endowment (Table A1.14). This equates to a maximum ratio of %Endowment/%Area of 2.08. Average deposit size declines progressively with increasing buffer distance. The number of gold deposits increases with distance from Syenitic granite intrusions, again suggesting relatively few but relatively large deposits in the most proximal buffers. Observations derived from spatial analyses in the Eastern Goldfields Superterrane and Kurnalpi Terrane suggest there may be a relationship between a small proportion of gold deposits and proximity to Syenitic granite intrusions. This relationship is stronger in the Kurnalpi Terrane than in the Kalgoorlie Terrane. The deposits that are proximal to Syenitic granite intrusions tend to be larger than average. However, at best, a very small proportion of the gold in the Eastern Goldfields Superterrane may be targeted on the basis of proximity to Syenitic granite intrusions. The large resources inferred to be proximal to Syenitic granite intrusions are strongly influenced by the Wallaby deposit. Wallaby includes a dominant component of mineralization that is associated with a late-stage hydrothermal event (Salier et al., 2004), which is not recorded or is not well developed in most deposits associated with Syenitic granite intrusions.

Lamprophyres are known in the Murchison and Southern Cross domains but have only been mapped systematically in the Eastern Goldfields Superterrane. Consequently, the following spatial analysis is limited to the Eastern Goldfields Superterrane (Fig. 1.15, Table A1.15). Even in the Eastern Goldfields Superterrane, the documentation of lamprophyres should be regarded as incomplete, as these intrusions are mostly very small and poorly exposed; consequently, they are preferentially recognized where exposed in active mining areas. Because of their size, they are partly obscured by gold deposit symbols and difficult to see in Figure 1.15. They are found in four main swarms (Leonora, Murrin, Laverton, and Boulder–Lefroy), which are highlighted in Figure 1.15. A %Endowment/%Area ratio of 26.6 is achieved using a 1000 m buffer, which captures about 4% of the gold endowment in only 0.15% of the area (Fig. 1.15). The number of deposits peaks in the most proximal (500 m) buffer and declines steadily in larger buffers (Table A1.15). The peak deposit density in the 500 m buffer is 0.523 deposits/km^2, compared to an average of 0.013 deposits/km^2 for the analysis area. Both in terms of gold endowment and number of gold deposits, there is a fairly steady decrease with distance from the peak buffer. The endowment trend is interrupted by a sharp peak at 5000 m, which reflects capture of the Golden Mile. When the analysis is restricted to the better exposed and better documented Kalgoorlie and Kurnalpi Terranes (Fig. 1.16), a similar relationship is established (Table A1.16). The 1000 m buffer around lamprophyric intrusions captures 4.1% of the gold endowment within 0.18% of the area, equivalent to a %Endowment/%Area ratio of 22.9 (Table A1.16). Deposit numbers decline steadily from the most proximal (500 m) buffer, which contains 0.523 deposits/km^2, compared to an average of 0.015 deposits/km^2 for the analysis area. The 5000 m buffer contains only 10.2% of all deposits, illustrating that like Syenitic granite intrusions, lamprophyres show a spatial relationship with a relatively small proportion of Yilgarn gold deposits. Unlike the Syenitic granite intrusions, there is no indication that these lamprophyre-associated deposits are larger than average.

The Mafic and Syenitic granite intrusions and lamprophyre intrusions have been combined in a spatial analysis in the Kalgoorlie and Kurnalpi Terranes (Fig. 1.17), the results of which are summarised in Table A1.17. A 1000 m buffer around all of these intrusions is a very effective targeting tool, capturing 54.1% of the gold endowment and 19.4% of deposits in only 4.8% of the area (Table A1.17). This represents a %Endowment/%Area ratio of 11.35. Deposit density is highest in the most proximal (500 m) buffer and declines steadily in progressively larger buffers. The peak deposit density of 0.061 deposits/km^2 captures 14.7% of deposits at four times the average for the analysis area. Average deposit size peaks in the 1000 m buffer (345 213 oz) and declines progressively in larger buffers (Table A1.17).

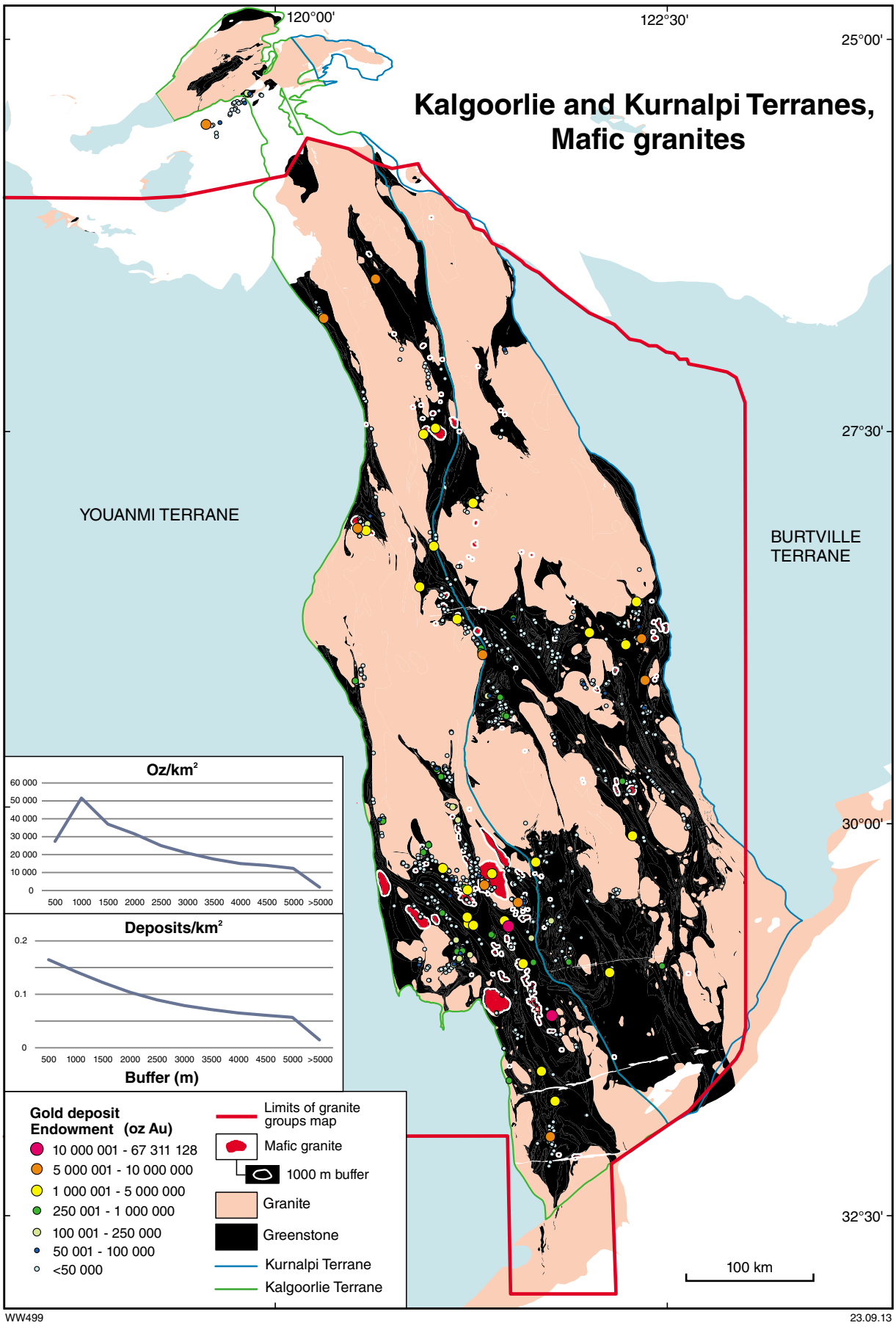

Figure 1.11. Distribution of gold deposits in the Kalgoorlie and Kurnalpi Terranes relative to Mafic granite intrusions

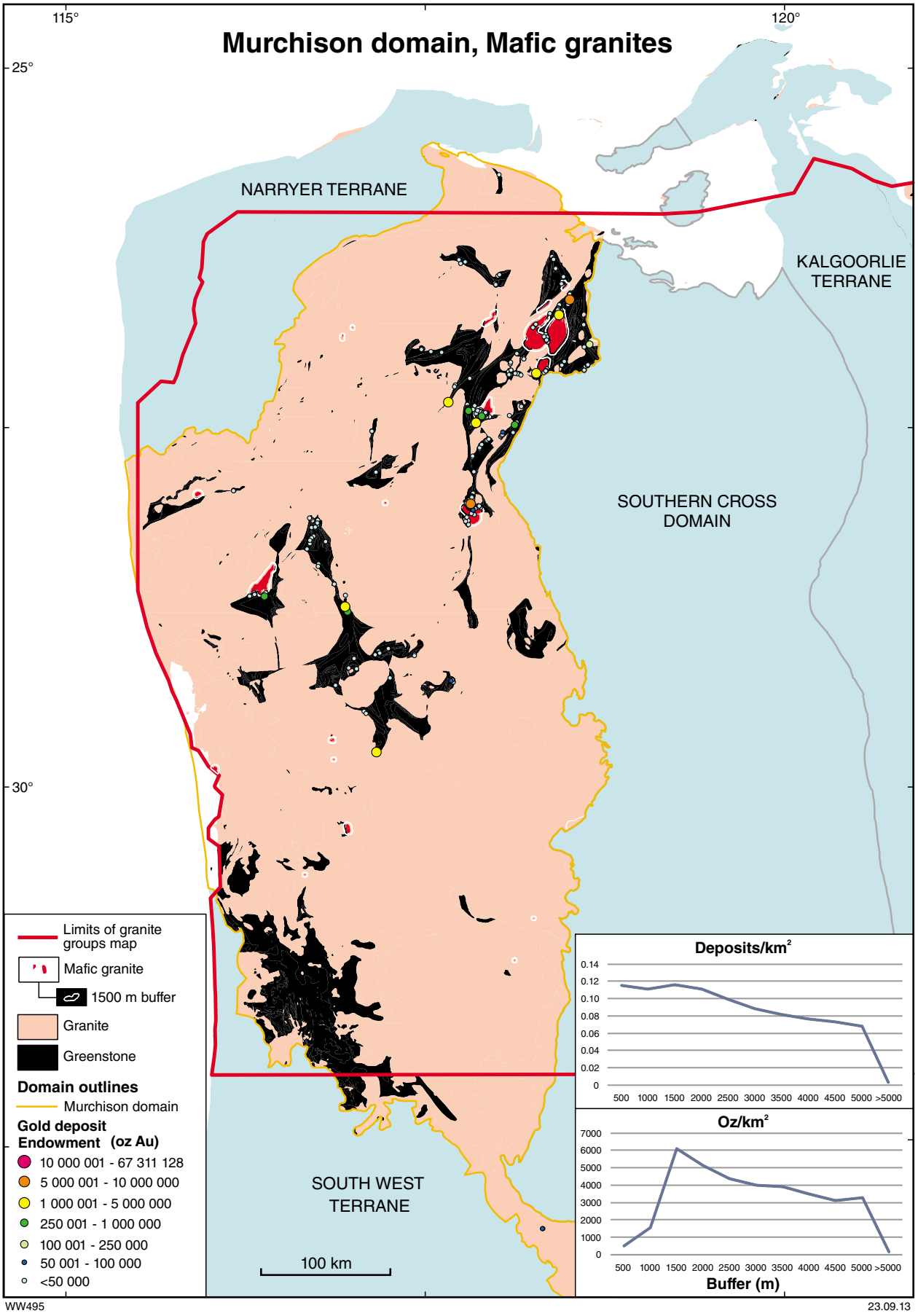

Figure 1.12. Distribution of gold deposits in the Murchison domain relative to Mafic granite intrusions

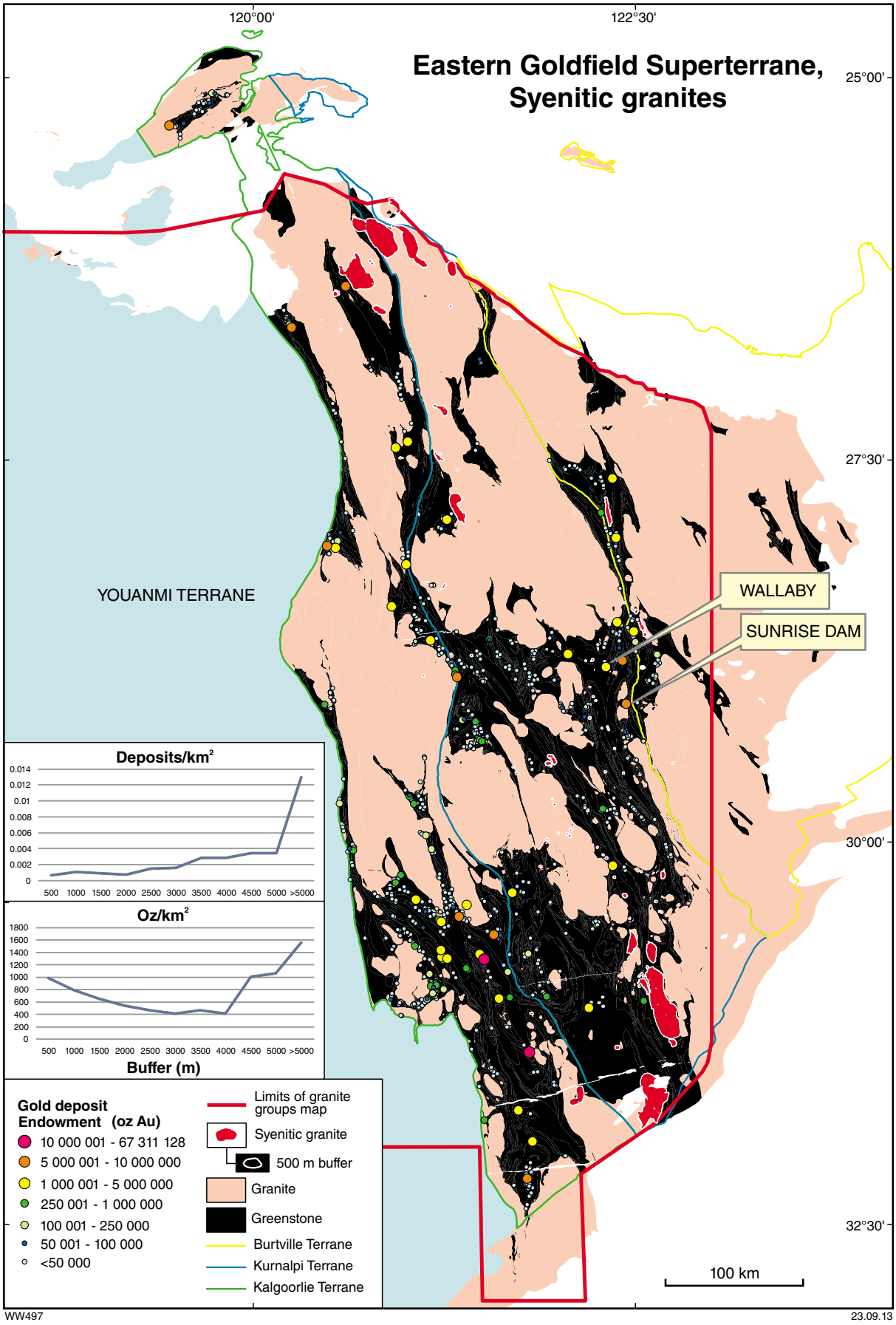

Figure 1.13. Distribution of gold deposits in the Eastern Goldfields Superterrane relative to Syenitic granite intrusions

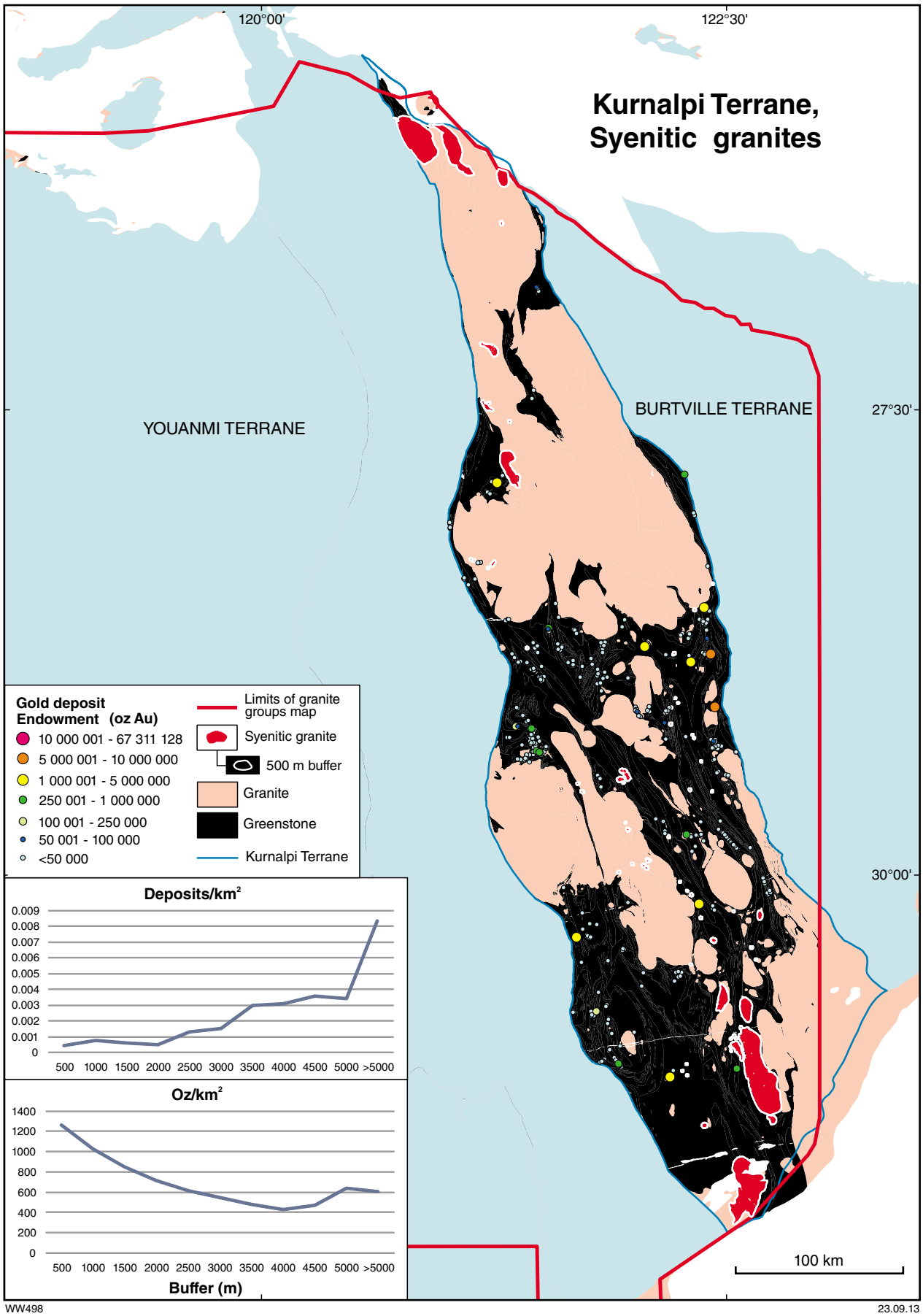

Figure 1.14. Distribution of gold deposits in the Kurnalpi Terrane relative to Syenitic granite intrusions

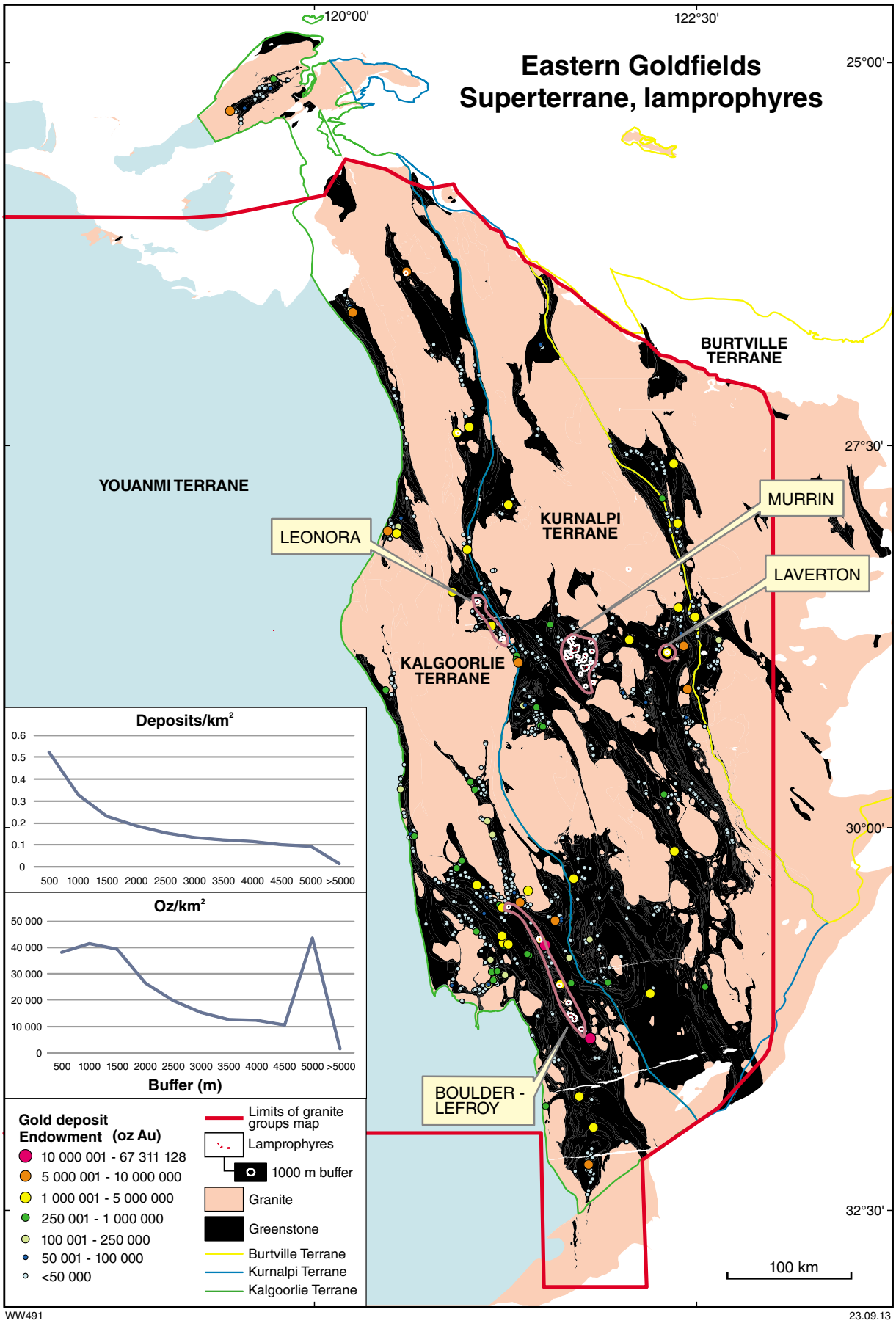

Figure 1.15 **Distribution of gold deposits in the Eastern Goldfields Superterrane relative to lamprophyre intrusions**

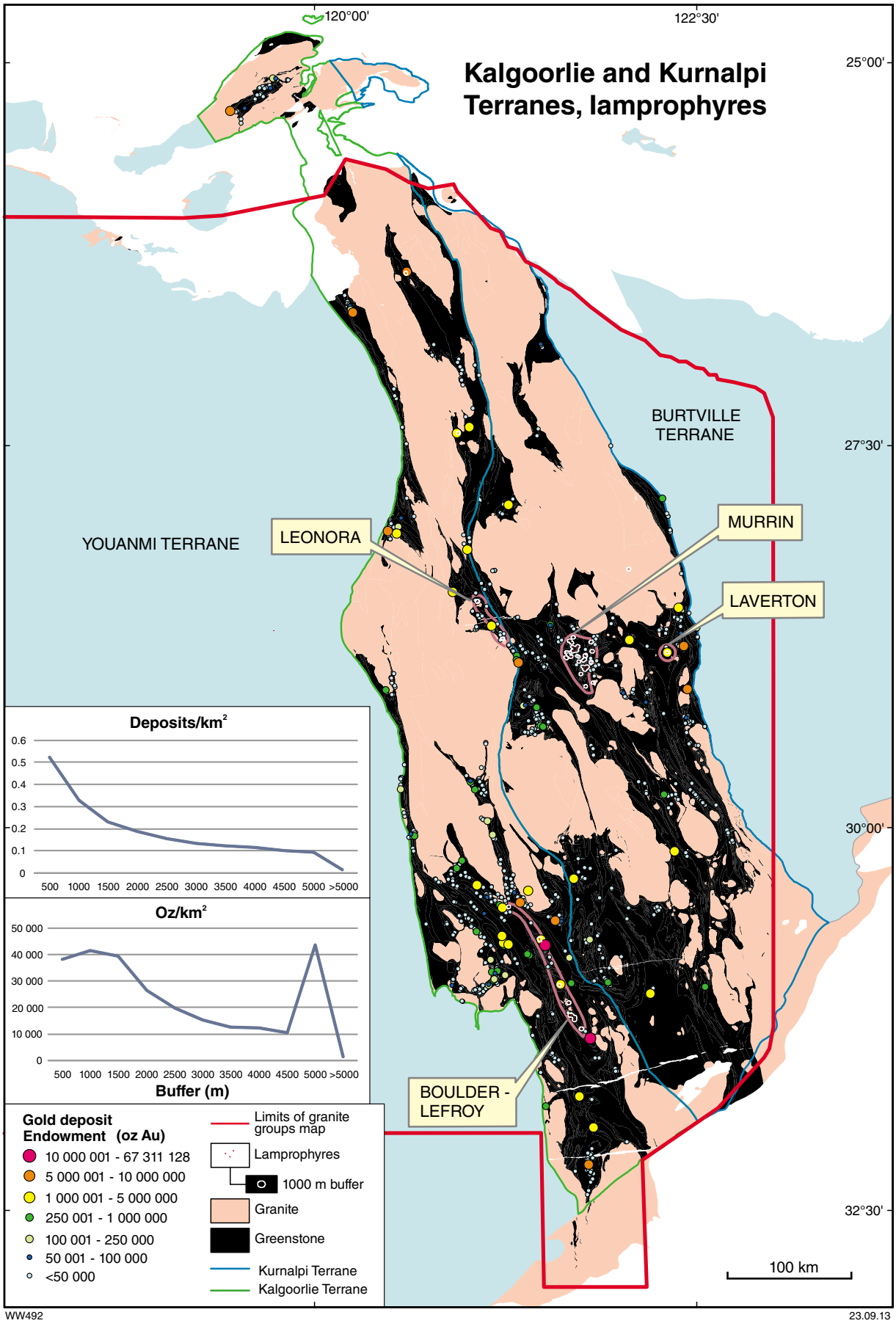

Figure 1.16. Distribution of gold deposits in the Kalgoorlie and Kurnalpi Terranes relative to lamprophyre intrusions

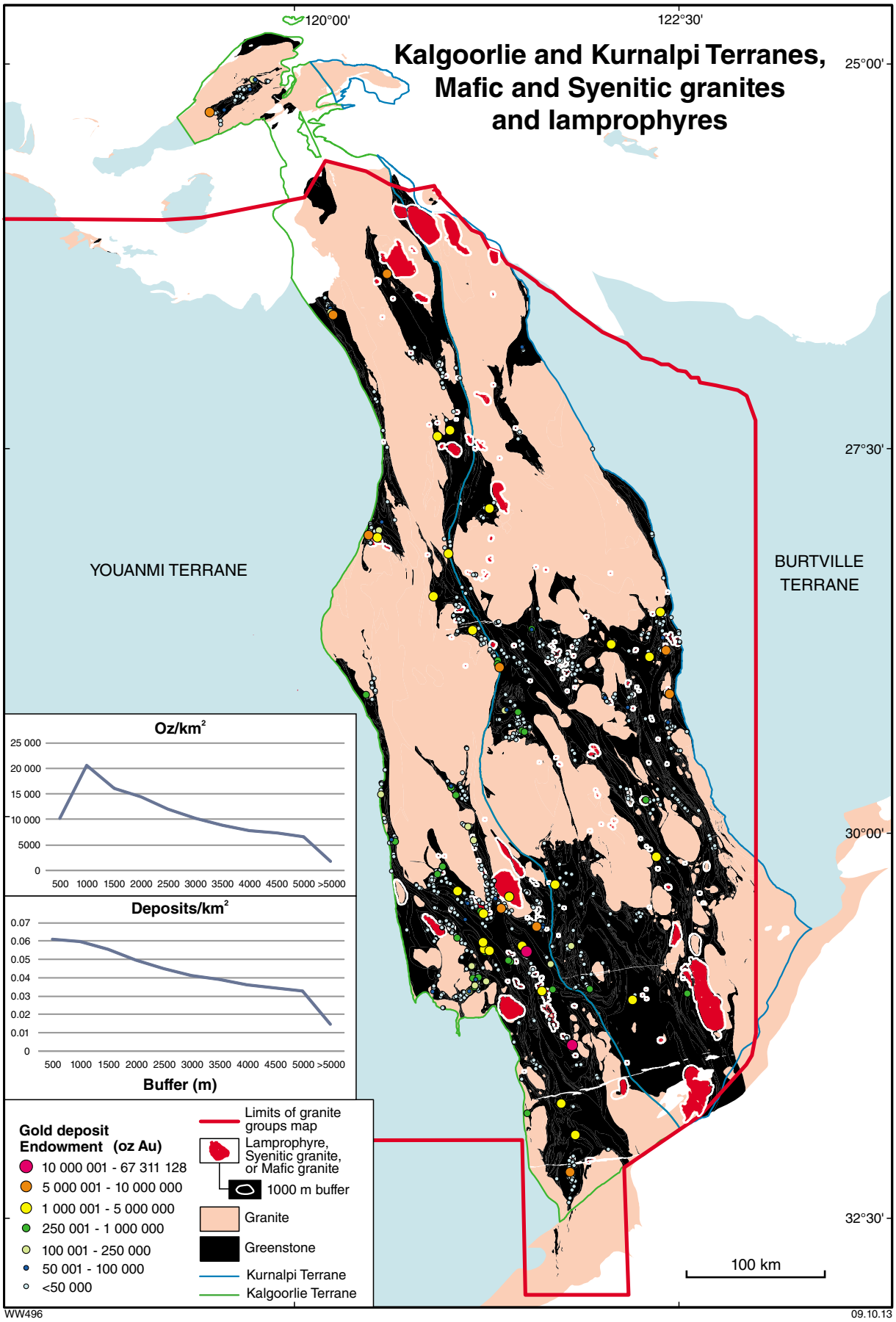

Figure 1.17. **Distribution of gold deposits in the Kalgoorlie and Kurnalpi Terranes relative to Mafic granite, Syenitic granite, and lamprophyre intrusions**

The final major episode of granite magmatism in the Yilgarn Craton produced widespread intrusions of Low-Ca granites (Fig. 1.18). Low-Ca magmatism took place mainly after 2650 Ma and postdates D_4 of Czarnota et al. (2010b). It is broadly coincident with the final stages of the Wangkathaa Orogeny (Blewett et al., 2004). The spatial analysis of the relationship of gold endowment to Low-Ca granite intrusions is most effective using a 3000 m buffer (7.5% of the gold endowment in 21.9% of the area) but a negative (O-E)/E value for all buffers indicates that the relationship is not useful for gold exploration (Table A1.18).

This series of spatial analyses indicates that proximity to Mafic granites and lamprophyric intrusions, and to a lesser degree Syenitic granite intrusions, are very useful exploration targeting criteria for gold, at least in the Kalgoorlie and Kurnalpi Terranes. In the Eastern Goldfields Superterrane, these intrusions are broadly contemporaneous with D_3 of Czarnota et al. (2010b), but emplacement ages range from late greenstone deposition (equivalent to Black Flag Group ages) to at least D_4 times (Czarnota et al., 2010b). Genetic models for Mafic granites and lamprophyres include a significant mantle or metasomatized mantle source component (Rock and Groves, 1988; Champion and Sheraton, 1997; Cassidy et al., 2002). Smithies and Champion (1999) interpreted an anhydrous crustal source for Syenitic granites in the Eastern Goldfields Superterrane, but even this model requires a thermal input from the mantle. However, the source region for Syenitic granites in the Eastern Goldfields Superterrane is uncertain; a metasomatized mantle source has been suggested by Witt and Davy (1997) and Czarnota et al. (2010b).

The above results are certainly influenced by the giant endowment of the Golden Mile, which appears within the 1000 m buffer around Mafic granites, but the relationship of gold to intrusions with a metasomatized mantle-source component is supported by analyses that exclude the endowment of the Golden Mile. These include relations between mantle-sourced intrusions and the number of deposits (endowment ignored) in the combined Kalgoorlie and Kurnalpi Terranes, and the number of deposits and gold endowment in the Murchison domain. In fact, taken alone, the association of gold with Mafic granites in the Murchison Terrane (peak %Endowment/%Area of 32.8) is stronger than that in the combined Kalgoorlie and Kurnalpi Terranes (peak %Endowment/%Area of 28.4). Only the latter analysis is influenced by the Golden Mile. One of the strongest associations with gold was achieved by combining all intrusions with a metasomatized mantle-source component (Mafic and Syenitic granites, and lamprophyres) in the combined Kalgoorlie and Kurnalpi Terranes, which resulted in capture of 54.1% of the gold endowment and 19.4% of deposits in the 1000 m buffer: a %Endowment/%Area ratio of 11.35.

Previously, Halley (2007) hinted at a genetic association between gold and enriched mantle-derived intrusions and suggested that mixing of mantle-derived magmas and felsic magmas was an effective means of generating a gold ore fluid. The close association of at least some gold with enriched mantle-derived intrusions, particularly Mafic granites, is striking and consistent with the model of Halley (2007). However, other explanations also need to be considered. It is commonly suggested (e.g. Goldfarb et al., 2005) that the association between gold and mantle-derived intrusions reflects a common structural control that permits independent access from mantle or deep crustal source regions to gold depositional sites in the upper crust. Given the large scale of the zones of structural weakness under discussion (see Terranes and domains: Gold endowment, and Targeting Criterion 1.2), this model does not appear to explain the very close association of gold endowment with mantle-derived intrusions (peak results in 500 to 1000 m buffers). Furthermore, the timing of peak mantle-derived magma emplacement during D_3 extension is not compatible with the evidence for emplacement of most gold deposits during the compressive D_4b and D_5 events of Czarnota et al. (2010b) or, more generally, their emplacement in Precambrian granite–greenstone terranes during regional shortening and under high fluid pressures (Groves et al., 2000; Robert et al., 2005).

Most Syenitic granite intrusions and some Mafic granite intrusions are associated with halos of hydrothermal alteration that contain biotite or amphibole, typically with metasomatic magnetite (e.g. Wallaby, Salier et al., 2004; McAuliffe Well, Roberts et al., 2004; Mount Shea, Mueller, 2007; Karari, Witt et al., 2009; Witt and Hagemann, 2013). Iron-rich rocks can provide an effective chemical trap for gold carried in solution by ore fluids in which gold is transported as some form of sulfide complex (Phillips and Groves, 1983); this depositional model might contribute to the close association between gold and mantle-derived intrusions indicated by the spatial analyses described above.

In the light of the data presented above, the association of gold with Mafic granite intrusions, and to a lesser extent Syenitic granite and lamprophyric intrusions, can be interpreted in terms of crustal structure and access to heat and fluids from the mantle. The mantle-derived intrusions delineate deeply penetrating structures or zones of crustal weakness with access to the mantle (e.g. Fig. 1.3). Although the main episode of magmatism and intrusion was during D_3 extension, ongoing heat and fluid flow in these zones of weakness provided further access to deeply sourced ore fluids during subsequent regional shortening (D_{4b} and D_5), which were the main periods of gold mineralization (Czarnota et al., 2010b). Intrusions emplaced during D_3 provided rheological contrasts that were important for the formation of fractures, ore fluid focusing, and gold deposition. Gold deposition was promoted by reaction of the ore fluid with pre-existing Fe-rich alteration assemblages in and around the margins of the intrusions. Additionally, some gold and copper may have been deposited from hydrothermal fluids derived from the Mafic and Syenitic granite intrusions (e.g. Wallaby, Miller et al., 2007; Karari, Witt et al., 2009; Mount Shea, Mueller, 2007; Admiral Hill, Majestic, Witt and Hagemann, 2013), but the overall proportion of Yilgarn Craton gold derived from these sources is probably quite low.

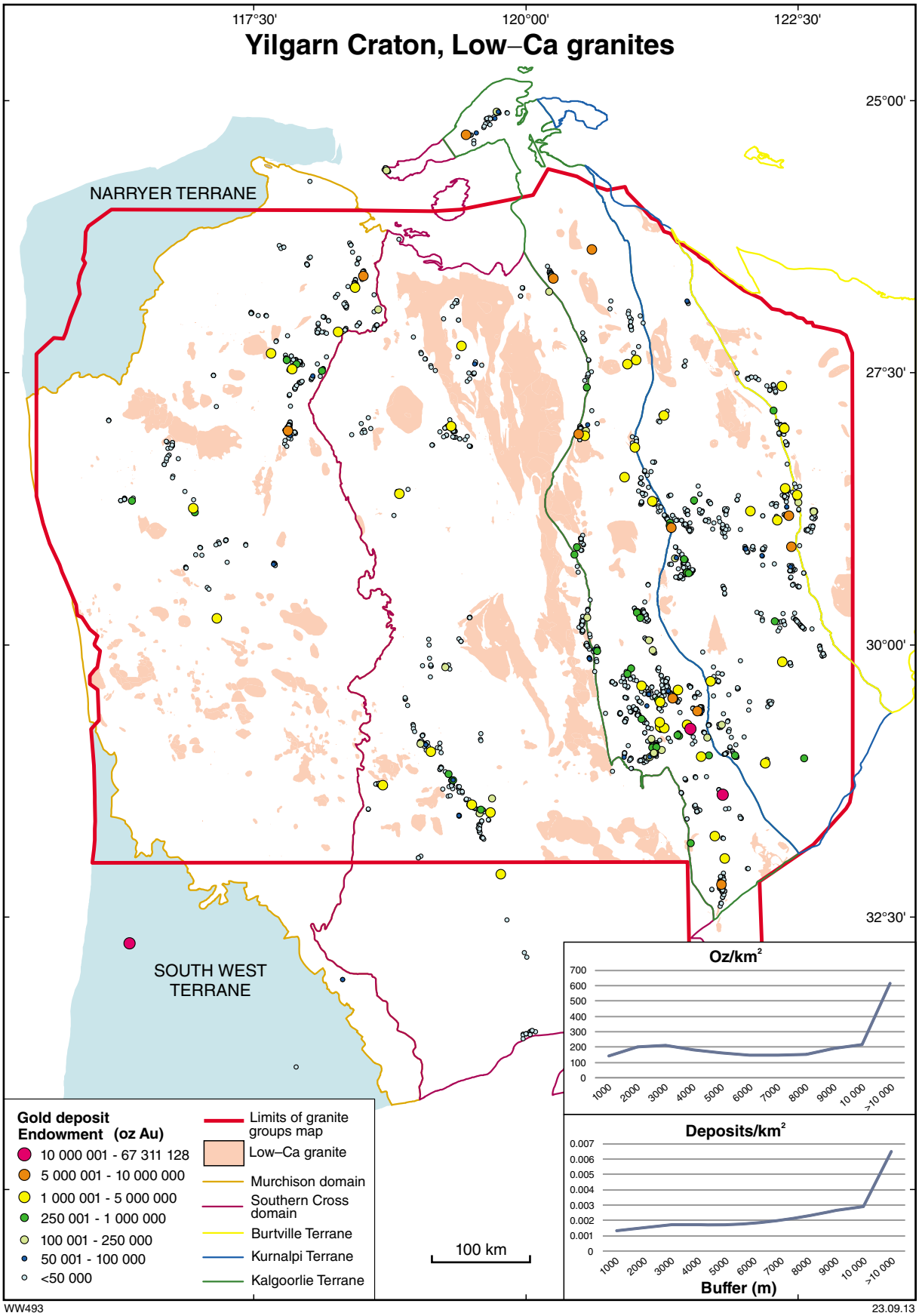

Figure 1.18. Distribution of gold deposits in the Yilgarn Craton relative to Low-Ca granite intrusions

Targeting Criterion 1.4: Regional gravity lineaments

A spatial relationship between deep gravity lineaments and a range of metal deposits, including gold, was proposed for western North America by Hildenbrand et al. (2000) and Grauch et al. (2003). A similar relationship between gold mineralization and proximity to regional gravity lineaments in the Eastern Goldfields Superterrane was proposed by Archibald et al. (2001) and Czarnota et al. (2010a). The relationship was investigated quantitatively by Bierlein et al. (2006), using data from Geoscience Australia's MINLOC and OZMIN databases for gold deposit location and endowment, respectively (Ewers et al., 2002a,b), and a regional gravity survey from Geoscience Australia <www.ga.gov.au/minerals/index.html>. Bierlein et al. (2006) used height- and length-weighted buffers around the near-surface expression of gravity lineaments (concatenated gravity 'worms') from the Eastern Goldfields Superterrane and found a gradual increase in gold endowment with proximity for both sets of buffers, although there was a decrease for the most proximal buffer. Bierlein et al. (2006) interpreted these spatial relationships to indicate that the distribution of gold in the Eastern Goldfields Superterrane is strongly correlated with long and deep gravity gradients (worms upward continued for distances of up to 60 km).

All gravity datasets used in this study are from a compilation of diverse ground surveys integrated into a single dataset referred to as the Australian National Gravity Database, available at the Geoscience Australia website <www.ga.gov.au/minerals/projects/current-projects/continental-geophysics/gravity.html>. Digitally generated worms (Archibald et al., 2001) were derived from grids of these data by using edge detection software (Intrepid Geophysics Ltd). Worms portray steep gradients in the gravity data projected upwards to various heights above the land surface. Greater heights of projection above the land surface represent deeper penetrating structures. For convenience, we categorize sets of worms by their upward continued height (e.g. 2500 m worms). We used a set of gravity worms developed by pmd*CRC (Y4 Project Team, 2008) for the Eastern Goldfields Superterrane (eastern Yilgarn Craton of pmd*CRC). Equivalent datasets are not available for the Southern Cross or Murchison domains; for these domains, worms were generated by GSWA from the Geoscience Australia regional gravity data described above. The shallowest gravity worm developed by pmd*CRC in the Eastern Goldfields Superterrane was at 960 m. Because spatial analysis of the relationship of shallow worms to gold endowment provided the best results in the Southern Cross domain, additional shallow worms were generated by GSWA using the same regional gravity dataset that formed the basis of the Southern Cross and Murchison worms. The 500 m and 2500 m worms from this dataset were used in the Eastern Goldfields Superterrane analysis.

The approach of Bierlein et al. (2006) involves a degree of subjective interpretation; firstly, in deciding which set of upwardly projected worms should be correlated to a particular structure and, secondly, how to interpret the shallow expression of deep structures where worms at shallow levels are relatively short and discontinuous or otherwise displaced from the upward projection of equivalent, longer and more continuous, deeper worms. An alternative and more objective approach adopted for this Atlas has been to quantify the spatial association of gold with individual sets of gravity worms representing a particular level of upward continuation. Additionally, a more subjective analysis of the association of gravity worms with gold endowment in the Eastern Goldfields Superterrane was carried out using the shallow expression of selected deeply penetrating structures based on gravity data.

For the Eastern Goldfields Superterrane, worms derived from the gravity data were generated for 500, 2500, 5264, 9864, 21 626, 47 415, 64 907, 75 941, and 88 851 m levels of upward continuation. Using successively wider buffers around worms at each of these levels, the best results are for the two shallowest (500 and 2500 m) worm sets (Tables A1.19 and A1.20). Peak endowments occur within the 1500 m buffer around the 500 m worms and within the 500 m buffer around the 2500 m worms (Figs 1.19 and 1.20). The highest %Endowment/%Area ratio of 1.70, for the 500 m buffer around the 2500 m worm, captures 13.4% of the gold endowment and 11.7% of deposits in 7.9% of the analysis area (Table A1.20). The 1500 m buffer around the 500 m worms captures 69.7% of the gold endowment and 59.2% of deposits in 43.4% of the analysis area, equivalent to a %Endowment/%Area ratio of 1.61 (Table A1.19). The results for the 500 m worms (but not the 2500 m worms) are strongly influenced by inclusion of the giant endowment of the Golden Mile. In each case, average deposit size peaks with the %Endowment/%Area ratio, and deposit density decreases (albeit very slowly) outward from the most proximal buffer (Tables A1.19 and A1.20). The proximal (500 m) buffers around the 500 and 2500 m worms both contain 0.015 deposits/km^2, compared to an average of 0.010 deposits/km^2 for the analysis area.

Analyses for most deeper worms (5264, 21 626, 47 415, 64 907, and 88 851 m) from the Eastern Goldfields Superterrane generate erratic or flat curves that cannot be confidently interpreted to indicate a meaningful relationship between gold endowment and individual gravity worm sets (Tables A1.21 to A1.25). Steadily decreasing numbers of deposits in progressively larger buffers around the 47 415 m worms suggests a valid spatial relationship, but the peak %Endowment/%Area ratio (1.25) is relatively modest. These results for the 47 415 m worms are not biased by inclusion of the Golden Mile in the more proximal buffers. The results are at variance with the assumptions used by Czarnota et al. (2010a) to map prospectivity in the Eastern Goldfields Superterrane (i.e. that the deep, 45 km worms should show the closest spatial correlation with gold).

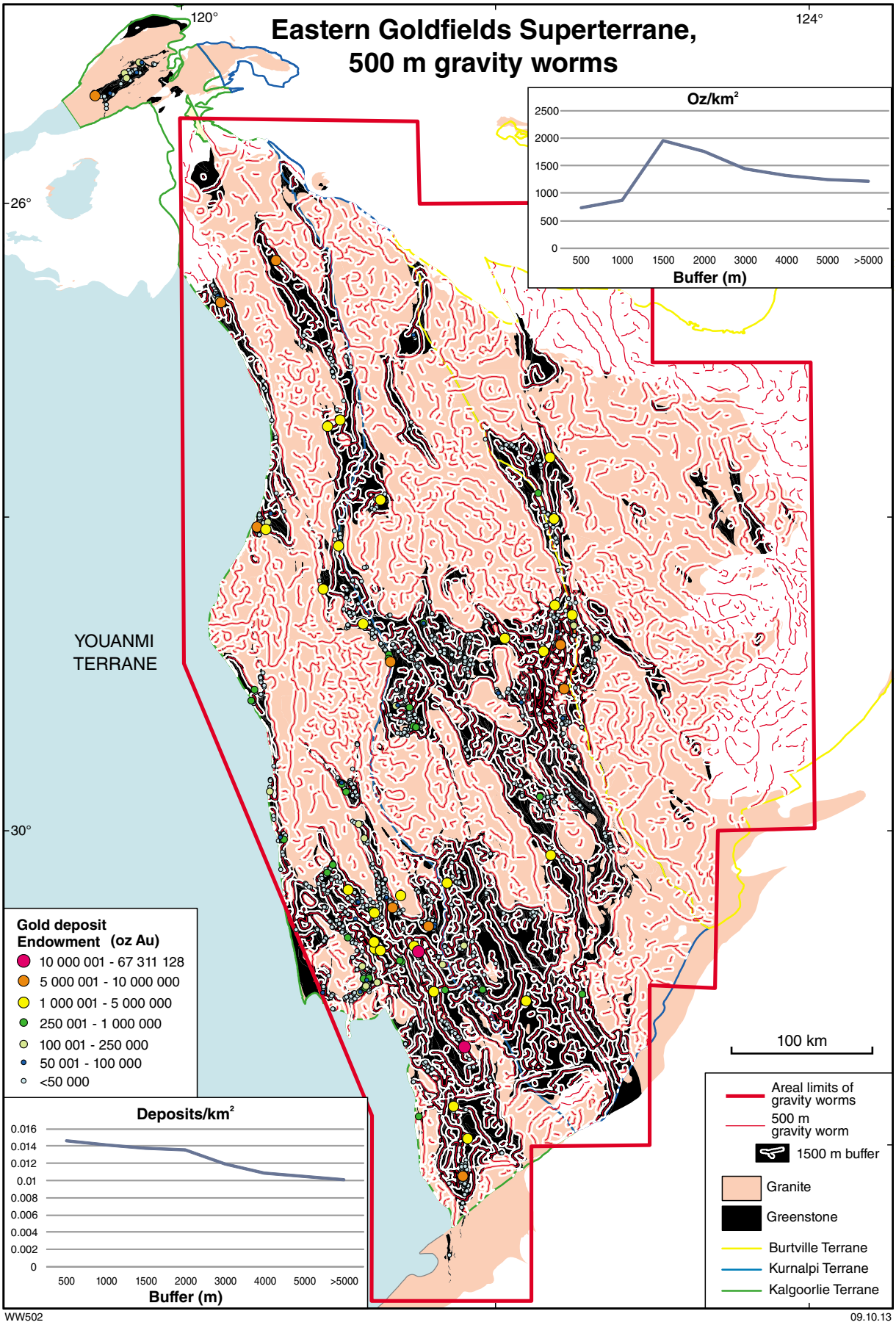

Figure 1.19. **Distribution of gold deposits in the Eastern Goldfields Superterrane relative to 500 m gravity worm sets**

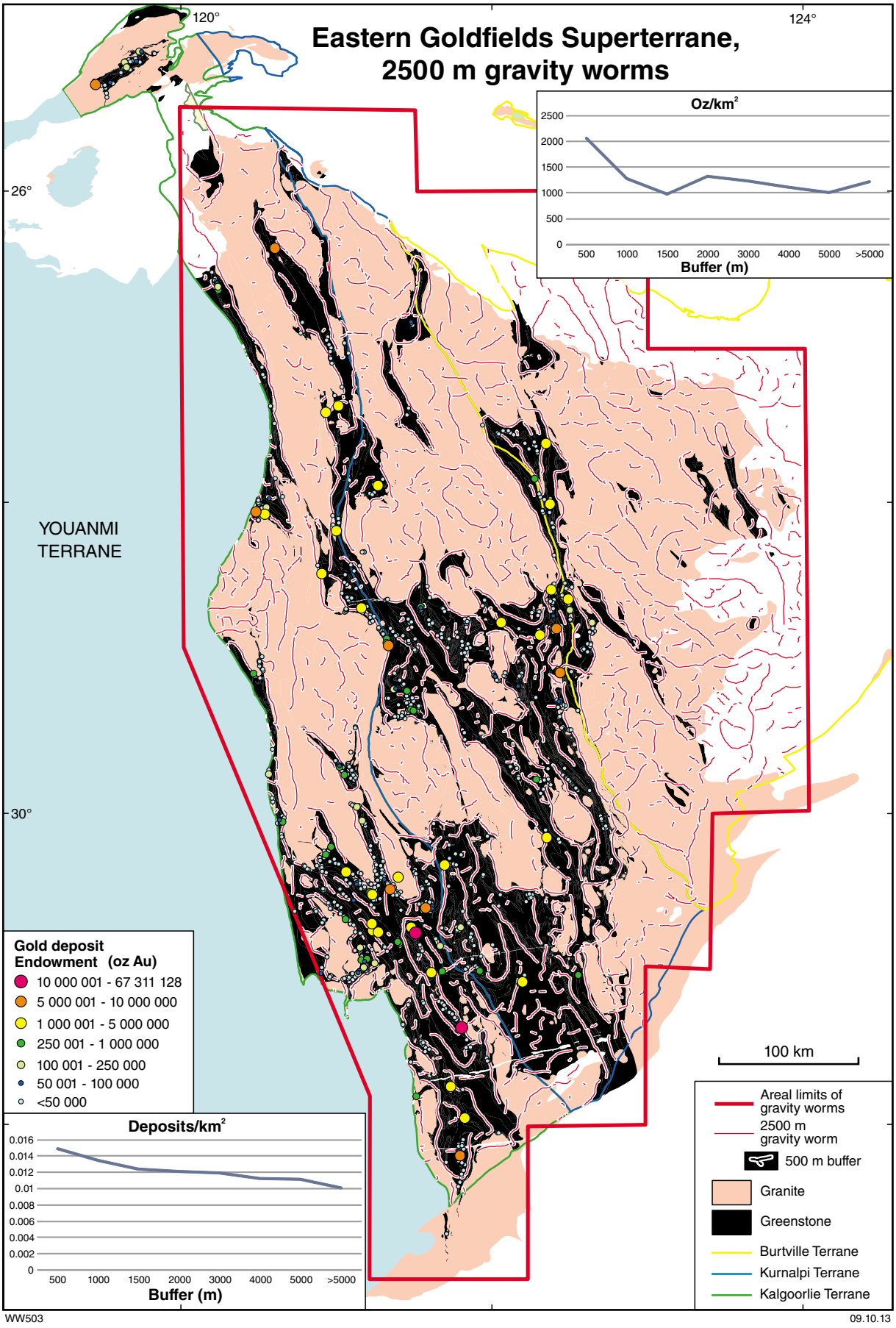

Figure 1.20. Distribution of gold deposits in the Eastern Goldfields Superterrane relative to 2500 m gravity worm sets

For the Southern Cross domain, shallower gravity worms (140, 255, 464, and 2807 m) also gave the best results (Tables A1.26 to A1.31). Curves for the deeper worms are either erratic (e.g. 41 803 m worms) or show a positive correlation between endowment and buffer distance (e.g. 16 990 m worms). A preliminary analysis of the 6905 m worms (not presented) also produced erratic curves. The 140, 255, 464, and 2807 m worms each produced steadily decreasing endowments in successively larger buffers, from a maximum in or near the most proximal buffer. The best results were achieved for the 2807 m worms, for which a 1000 m buffer captured 43.8% of the total gold endowment and 16.6% of deposits in 11.8% of the analysis area, representing a %Endowment/%Area ratio of 3.7 (Fig. 1.21). The average size of deposits generates a similar curve, whereas deposit density falls only slightly beyond the 2000 m buffer (Table A1.29). This suggests these data may be influenced by the inclusion of a small number of large deposits within the 1000 m buffer. Inspection of buffer contents indicates that the Marvel Loch deposit is most likely to account for the observed patterns. At 4.3 Moz Au, Marvel Loch is considerably larger than the next largest deposit (Westonia, 2.7 Moz Au) in the Southern Cross domain. Similar results were obtained from the 255 m worms, except that peak %Endowment/%Area (2.36) was achieved with the 1500 m buffer (Fig. 1.22). This buffer captures 68.4% of the gold endowment and 33.7% of deposits in 29.0% of the analysis area (Table A1.27).

In contrast to the Eastern Goldfields Superterrane and the Southern Cross domain, gravity worms in the Murchison domain show few positive spatial relationships with gold endowment (Tables A1.32 to A1.36), although increasing distance from the shallower worms (308 and 3244 m) are negatively correlated with numbers of deposits (Tables A1.32 and A1.33). For example, a 1000 m buffer around the 3244 m worms (Fig. 1.23) captures 19.1% of the gold endowment and 12.1% of deposits in 12.9% of the analysis area (equivalent to %Endowment/%Area of 1.47). Deposit density peaks within the 3000 m buffer, which contains 0.009 deposits/km^2, compared to an average of 0.006 deposits/km^2 for the total analysis area. The 7500 m buffer around the 6359 m worms captures 97.7% of the gold endowment and 96.7% of deposits in 76.4% of the analysis area (Fig. 1.24). However, the %Endowment/%Area ratio is modest (1.28) and the significance of the results achieved with such a large buffer is doubtful. Curves for deeper worm sets tend towards negative correlations between gold and proximity to the target features.

The above results of spatial analysis relating gold endowment to gravity worms indicate a modest increase in gold endowment with proximity to shallow worms in the Eastern Goldfields Superterrane, and a more pronounced increase with proximity to shallow worms in the Southern Cross domain. Although some of the endowment results for the Eastern Goldfields Superterrane are influenced by inclusion of the Golden Mile, deposit density also decreases consistently with distance from the 500 and 2500 m worms. Endowment results in the Southern Cross domain are also supported by similar results in terms of number of deposits. For the Murchison domain, curves for all worms are erratic in terms of endowment, or otherwise fail to support a meaningful relationship of endowment to proximity to gravity worms. The better results for shallower worms in the proximity analyses for the Eastern Goldfields Superterrane and Southern Cross domain is perhaps unsurprising because the shallow worms represent an approximation of the intersection of the concatenated gravity lineaments with the present erosion surface, which is where the known gold deposits are located. Deeper worms representing the same gravity gradients (or structures) are displaced from the surface expression of the structures they represent, unless the structures are vertical. The results of the analyses described above were achieved without filtering out those shallow worms that are not related to deeper structures. The results presented here contrast with those from spatial analyses relating gold endowment to aeromagnetic worms (see Targeting Criteria 1.5), where relatively deep worms show the closest spatial association with gold. The latter results were interpreted to relate gold to deeply penetrating structures represented by the deepest aeromagnetic worms. In contrast, the relatively shallow gravity worms with which gold is associated represent features in the upper crust. Because the main density variance in the Yilgarn Craton is between granite (low density) and greenstones (high density), these relatively shallow-seated features probably represent variations in thickness of the greenstone sequence overlying a middle and lower crust of granitic composition. In effect, the gravity data is dominated by variations in the depth to the base of the greenstones. Over large parts of the Eastern Goldfields Superterrane, seismic data and combined seismic and gravity modelling have shown that this depth ranges between 3 and 12 km (Swager, 1997; Goleby et al., 2004; Blewett et al., 2010a). We conclude that the shallow gravity data are dominated by density contrasts between greenstones and the underlying granitic rocks and continental (felsic) crust, and that many of the shallow gravity lineaments represent faults that displace the base of the greenstones. Our spatial analytical results from the Eastern Goldfields Superterrane and the Southern Cross domain suggest that these faults are prospective for gold.

The results presented above contrast with those of Bierlein (2005) and Bierlein et al. (2006), who found a stronger correlation of gold with shallow gravity worms that represent deeply penetrating structures in the eastern Yilgarn Craton (Eastern Goldfields Superterrane). This contrast probably reflects a different approach by Bierlein et al. (2006), who concatenated worms from different depths into near-surface lineaments, and applied weighting to buffers depending on the strike length and depth penetration of the lineaments. Their results emphasized an association of gold with the near-surface expression of deeply penetrating structures; in contrast, our results show a weak to modest association with undivided relatively shallow and unweighted worms.

Intuitively and anecdotally, a relationship between gold and deeply penetrating structures is predicted by models in which the ore fluid is derived, directly or indirectly, from deep crustal or mantle sources (e.g. Czarnota et al., 2010a). Deep-seated gravity lineaments reflect deep

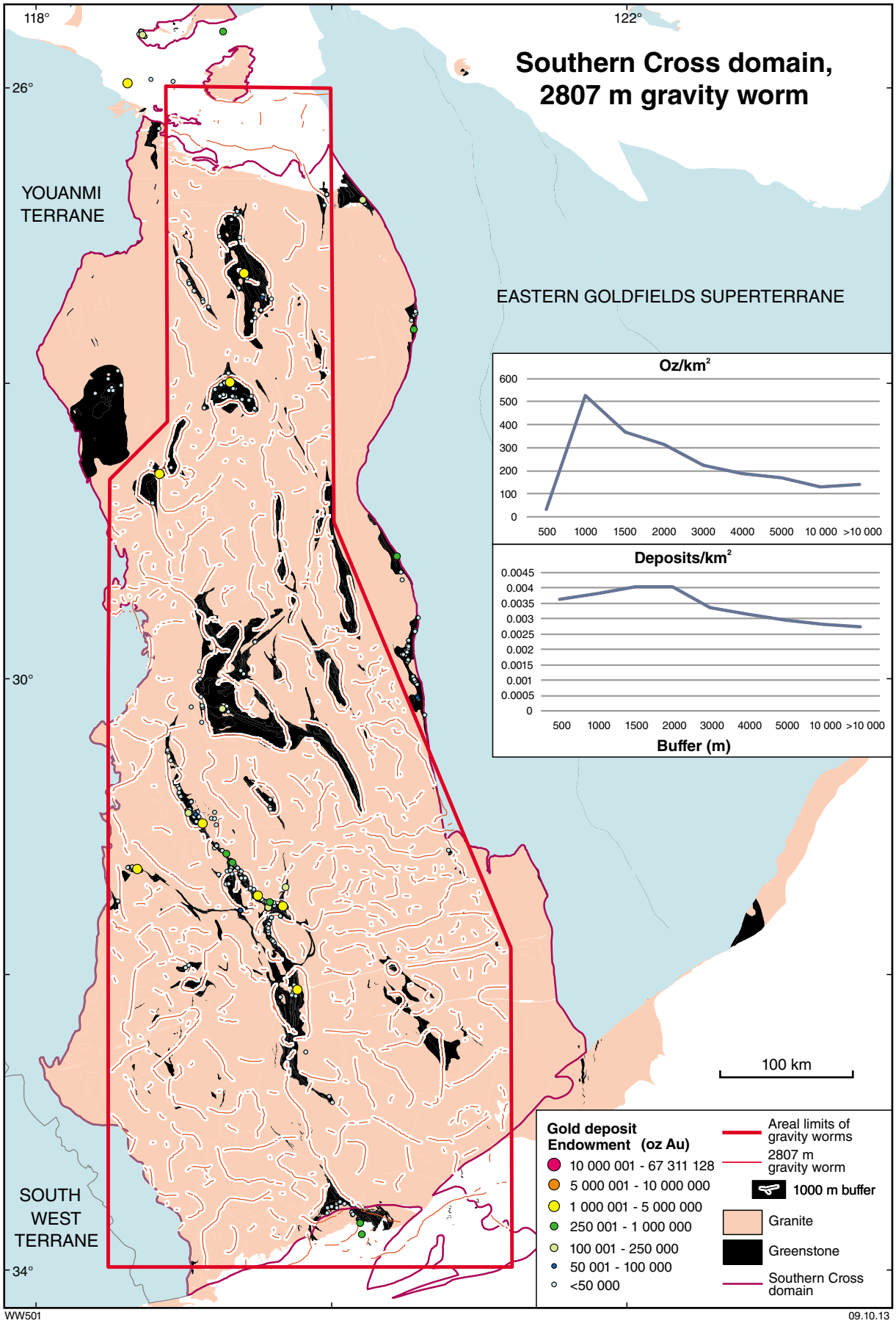

Figure 1.21. Distribution of gold deposits in the Southern Cross domain relative to 2807 m gravity worm sets

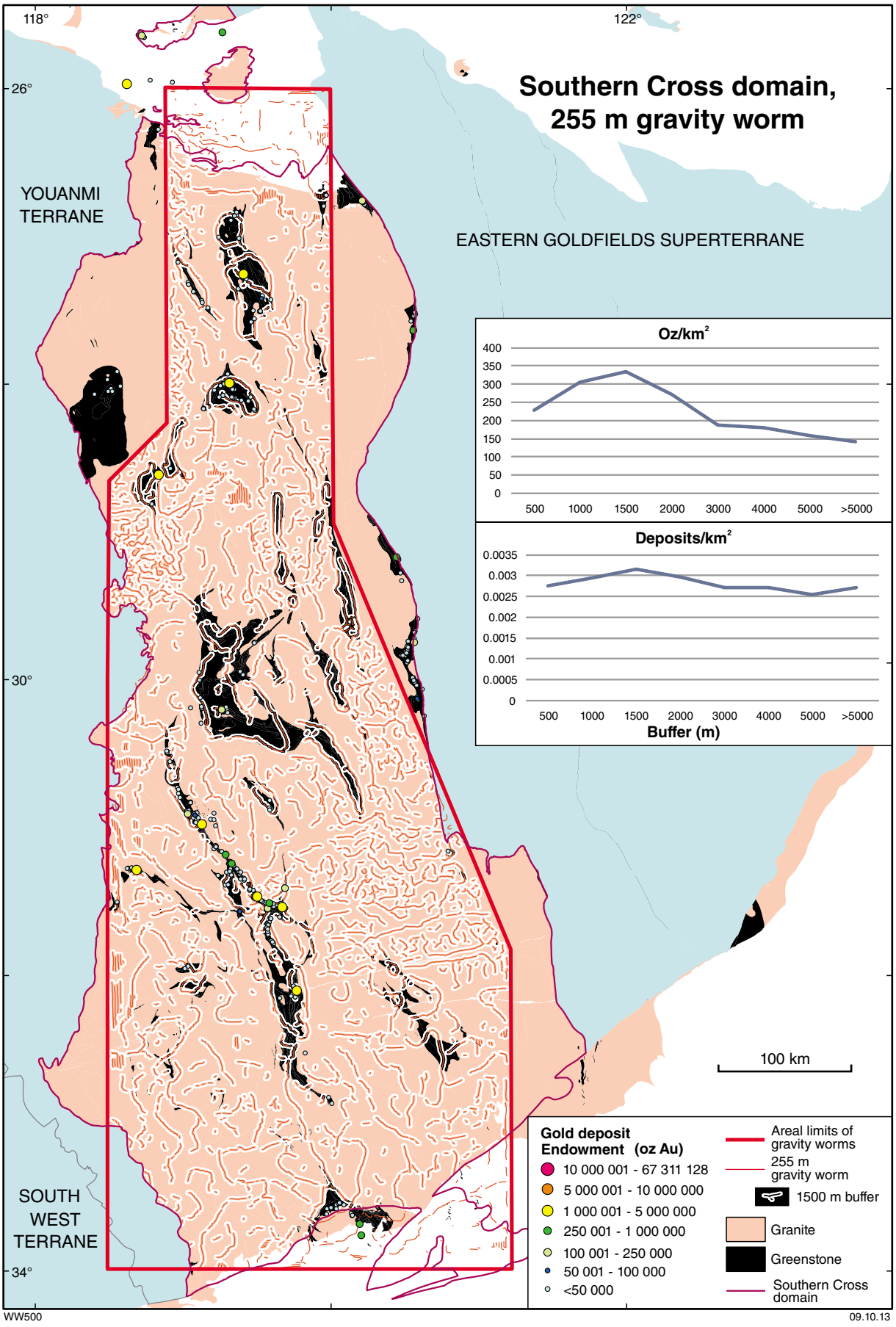

Figure 1.22. Distribution of gold deposits in the Southern Cross domain relative to 255 m gravity worm sets

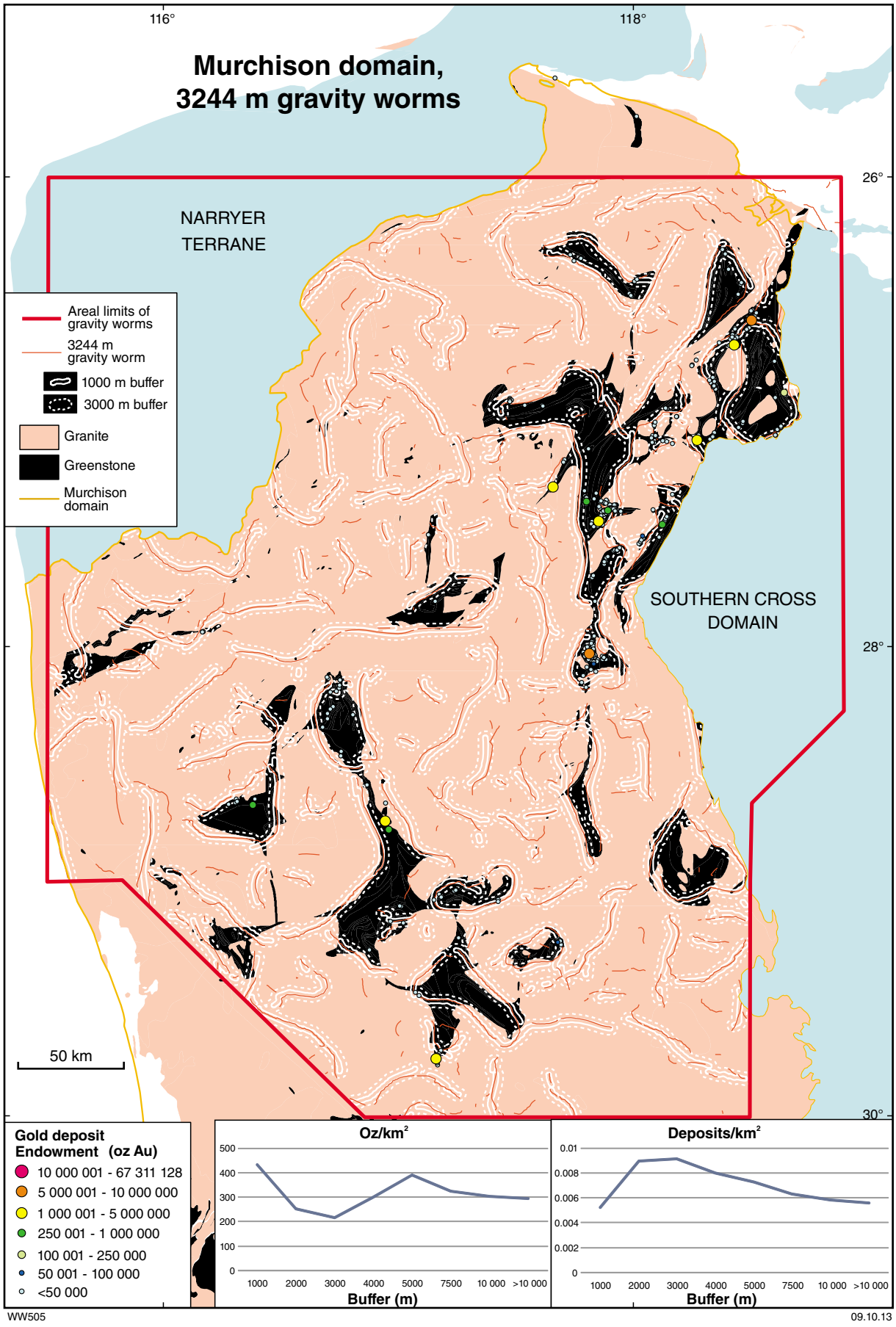

Figure 1.23. Distribution of gold deposits in the Murchison domain relative to 3244 m gravity worm sets

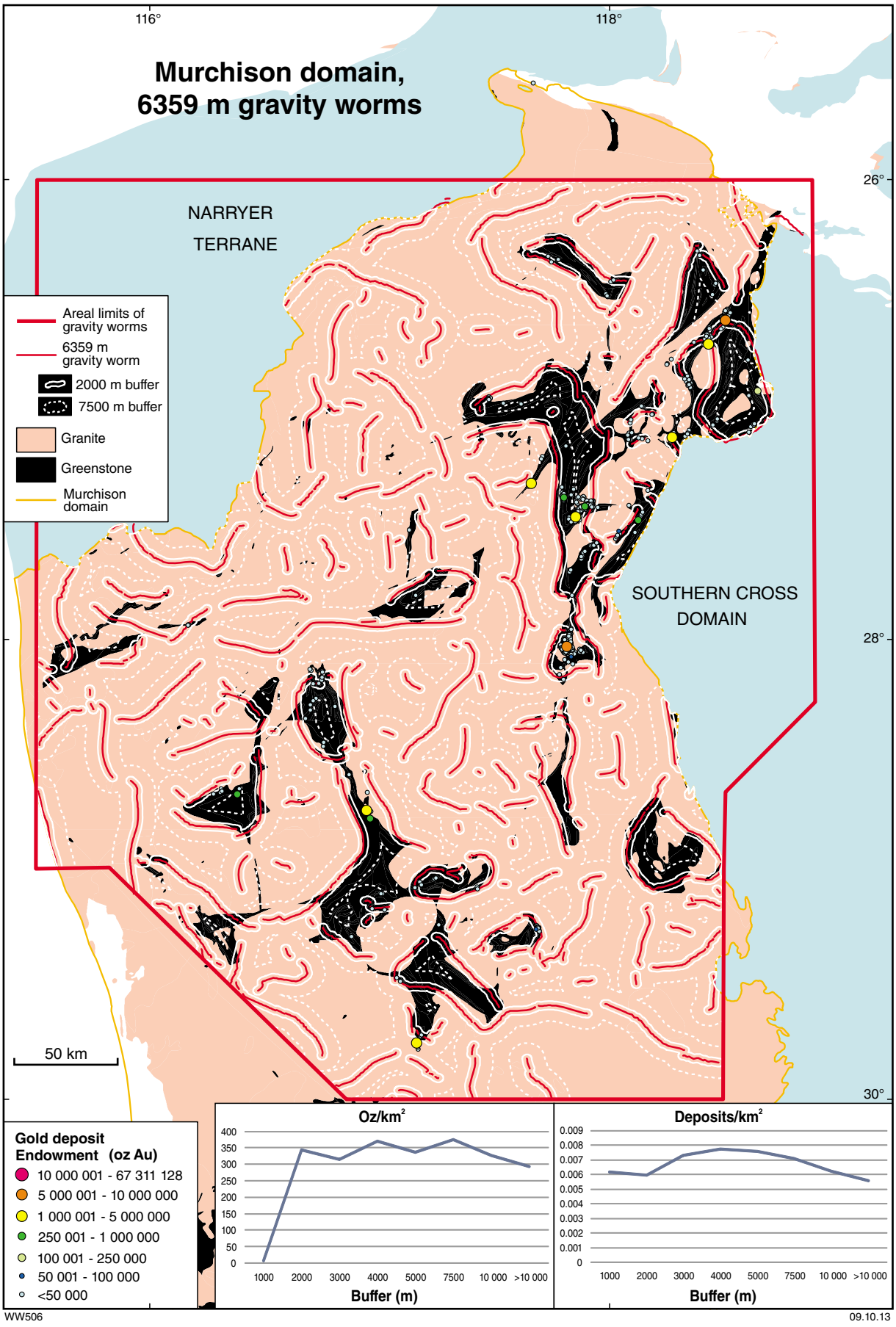

Figure 1.24. Distribution of gold deposits in the Murchison domain relative to 6359 m gravity worm sets

crustal structures extending into the basement below the greenstones and possibly into the base of the crust (Bierlein et al. (2006). For genetic models that relate gold to deeply sourced ore fluids (from below the base of the greenstones), such profound gravity lineaments represent potential conduits through which gold may have been transported into the middle to upper crust. However, not all deeply penetrating gravity lineaments were necessarily connected to an ore fluid source region, so some deeply penetrating gravity lineaments may be better targeting criteria than others.

To further investigate the potential of gravity worms as a targeting tool for gold in the Eastern Goldfields Superterrane, selected deeply penetrating gravity lineaments were assessed in a separate spatial analysis. These lineaments were defined as those extending to a depth of at least 32.5 km, equivalent to the 64 907 m worms. From a depth of approximately 32.5 km, deeper and shallower worms judged equivalent to the same gravity lineament were selected. The resulting gravity lineaments (Fig. 1.25), defined by multiple worm depths, include a large component that is oriented at a high angle to the dominant north-northwesterly striking structural trends in the upper crust (granite–greenstone terranes), at least in their deeper expressions. These oblique trends are not apparent in aeromagnetic images. To be selected for analysis, worms had to at least partly define the overall gravity lineament, although in some cases, shallow and deep worms that define the same lineament diverge. For example, the western end of the southern, approximately east–west gravity lineament is defined by deep worms that rotate into a north-northwest orientation and shallow worms that rotate to the south (Fig. 1.25). Shallower worms without deep equivalents have been eliminated from the dataset. A prominent northeast-striking gravity lineament at the southeastern margin of the Yilgarn Craton has also been eliminated because it is believed to be related to the post-Archean Albany–Fraser Orogeny (Clark et al., 2000; Spaggiari et al., 2012). The set of gravity lineaments so selected approximately delineate large areas of granite and granite gneiss that were interpreted by Williams and Whitaker (1993) and Blewett et al. (2010a) as regional-scale extensional domes. One of the prominent deeply penetrating gravity worms is broadly coincident with the Keith–Kilkenny fault, a major northwest-striking structure separating the southwest and northeast Eastern Goldfields Superterrane (Fig. 1.25).

The spatial analysis relating gold endowment to the selected gravity lineaments shown in Figure 1.25 is confined to the combined Kalgoorlie and Kurnalpi Terranes and the 9864 m (~10 000 m), 21 626 m (~20 000 m) and 75 941 m (~75 000 m) worms (representing crustal penetration depths of approximately 5, 11, and 38 km, respectively; Tables A1.37 to A1.39). As for previous proximity analyses, the best result on the selected gravity lineaments were derived from the relatively shallow 9864 m worms (Table A1.37). A 2500 m buffer around the 9864 m worm captures 14.7% of the gold endowment and 14.3% of deposits in 6.0% of the analytical area, equivalent to a %Endowment/%Area ratio of 2.43 (Fig. 1.26). Deposit density in the most proximal buffer (0.033 deposits/km^2) is more than twice the average density for the analysis area (0.014 deposits/km^2). Steadily declining endowment and number of deposits in progressively larger buffers (Table A1.37) supports a meaningful relationship between gold and proximity to the relatively shallow expression of these selected gravity lineaments. This result is not influenced by inclusion of the Golden Mile deposit.

To summarize, the results of spatial analysis described above indicate a modest correlation of gold endowment and number of deposits with proximity to unprocessed shallow gravity worms (<3000 m upward continued height or 1.5 km depth penetration) in the Eastern Goldfields Superterrane and Southern Cross domain. Results in the Murchison domain are less clear, but do suggest an increase in the number of gold deposits with proximity to shallow worms. The work of Bierlein et al. (2006) indicates that improved results can be achieved by concatenating the worms for individual lineaments and weighting buffers according to the length and vector height (upward continued height) of the worms. Gravity worms can be generated by a range of structures, including faults, granite–greenstone contacts, and contacts between greenstones of contrasting density, and the basic analyses described here do not attempt to distinguish between these various sources. The exercise using selected worms in the Eastern Goldfields Superterrane indicates that judicious classification and quarantining of gravity lineaments can lead to improved proximity analysis results. In particular, the example shown here suggests that gravity lineaments that outline areas of uplifted granite and granite gneiss may provide a useful targeting criterion for regional gold exploration in the Yilgarn Craton.

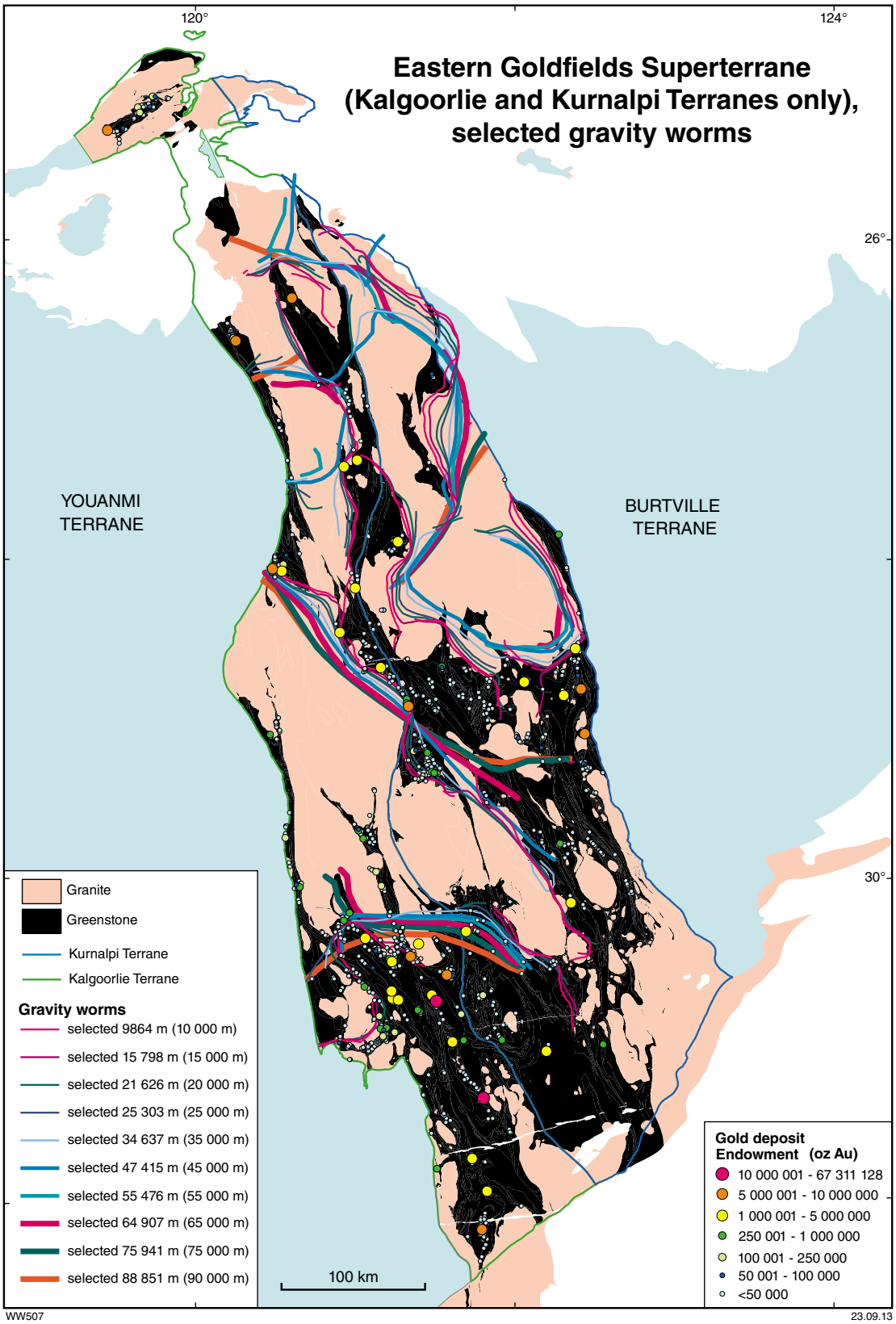

Figure 1.25. **Distribution of gold deposits in the Eastern Goldfields Superterrane (Kalgoorlie and Kurnalpi Terranes only) relative to selected deeply penetrating structures interpreted from gravity worm sets**

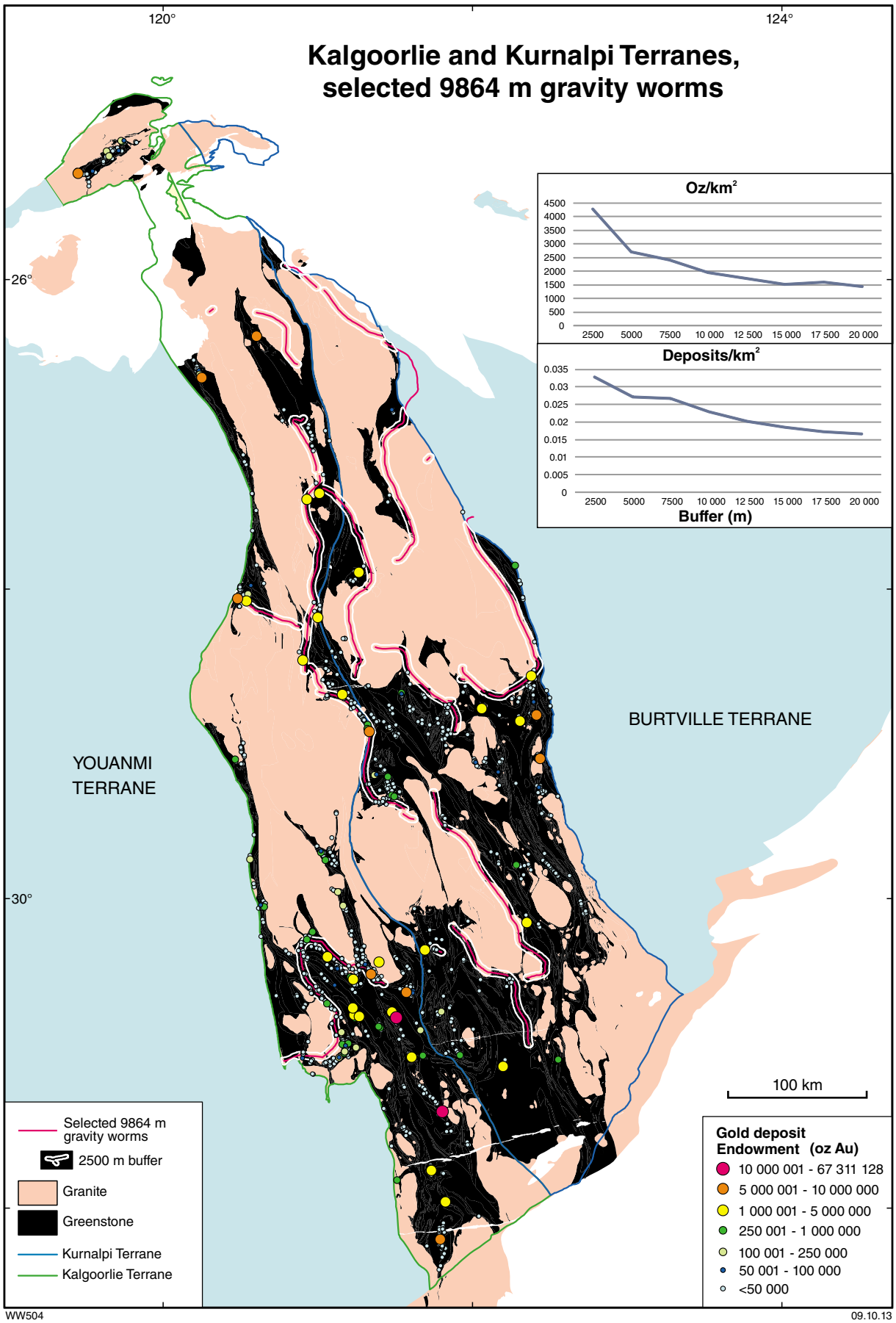

Figure 1.26. Distribution of gold deposits in the Kalgoorlie and Kurnalpi Terranes relative to selected 9864 m gravity worm sets

Targeting Criterion 1.5: Aeromagnetic discontinuities

As was the case for Targeting Criteria 1.2 and 1.4, worms have been used in our analysis of discontinuities in aeromagnetic data (Hornby et al., 1999; Bierlein et al., 2006). Spatial relationships between aeromagnetic worms and gold mineralization were assessed using a combination of new data and data derived from the pmd*CRC A1 Project (Bierlein (2005). For the Eastern Goldfields Superterrane, worms prepared by the pmd*CRC Project, and derived from an undocumented data source, were used without modification. For the Southern Cross and Murchison domains, aeromagnetic worms were generated using Intrepid Geophysics Ltd software to process an aeromagnetic mosaic generated in house by GSWA from diverse sources and covering the entire Yilgarn Craton. The worms represent discontinuities between magnetic trends in the potential field dataset, which might be caused by faults or the contacts of intrusions. Higher magnitudes of upward continuation reflect more deeply penetrating discontinuities.

In the Eastern Goldfields Superterrane, a preliminary analyses of the spatial relationships of gold with magnetic worms upward continued to heights of 1011, 1769, 3558, 6223, 8230, and 16 553 indicated that the deepest worm set (16 533 m) showed the closest association with gold; the results for shallow and intermediate depth worms were less satisfactory. A subsequent re-investigation of the relationships between gold and only the 1011, 6233, 12 516, and 16 553 m worms, broadly reflects the results of the preliminary investigation (Tables A1.40 to A1.43, Figs 1.27 and 1.28). The best results were achieved for the 12 516 m worm set, representing the second most deeply penetrating magnetic discontinuities investigated (Table A1.42). A 1000 m buffer around this set of worms captures 28.7% of the gold endowment within 1.7% of the analysis area, equivalent to a %Endowment/%Area ratio of 17.1 (Fig. 1.27). Extending the buffer distance to 2500 m captures 32.7% of the gold endowment in 5.2% of the analysis area (%Endowment/%Area ratio of 6.3). Both results are influenced by capture of the Golden Mile deposit in the most proximal buffer. Although the curves for both ounces per square kilometre and deposit density show strongly asymptotic curves that support a meaningful relationship between gold and the 12 516 m worm set, the proportion of gold deposits captured by these proximal buffers is small (4.4% for the 1000 m buffer and 8.7% for the 2500 m buffer; Table A1.42). Peak endowment associated with the 16 533 m worms is within the 2500 m buffer, which captures 47.6% of gold endowment and 33.5% of deposits in 20.2% of the analysis area (Fig. 1.28). These figures equate with a %Endowment%Area ratio of 2.4 (Table A1.43). Although the 2500 m buffer also captures the Golden Mile, thus biasing endowment relationships, the steadily decreasing deposit density supports the relationship between endowment and proximity to the 16533 m worms. Shallow and intermediate height worms produce irregular curves (Tables A1.40 and A1.41), suggesting these are less useful as exploration targeting tools for gold.

In the Southern Cross and Murchison domains, analyses were based on worms derived from a different potential field dataset to that used for the Eastern Goldfields Superterrane (as discussed above). In a preliminary investigation, the spatial relationships of gold with magnetic worms upward continued to heights of 255, 464, 1141, 2079, 5115, 9322, 16 990, and 30 965 m were investigated in the Southern Cross domain, and with worms upward continued to heights of 112, 431, 1182, 2317, 4542, 8903, 17 450, 34 202, and 67 036 m in the Murchison domain. Final spatial analyses were completed for only the 1141, 5115, 9322, 16 990, and 30 965 m worms in the Southern Cross domain and only the 1182, 4542, 8903, 17 450, and 34 202 m worms in the Murchison domain. Although some shallow worms in these analyses produced curves that suggest a meaningful geological relationship with gold endowment (Tables A1.44 to A1.53), the extensive distribution of shallower magnetic worms produces proximal buffers that encompass a high proportion of the total area and therefore yield modest peak %Endowment/% area ratios (e.g. 1.7 for the 500 m buffer around 1141 worms in the Southern Cross domain, and 1.8 for the 500 m buffer around the 1182 worms in the Murchison domain (Tables A1.44 and A1.49).

Stronger relationships were achieved using deeper worms, especially in the Southern Cross domain where the 9322 and 30965 m worms are particularly effective (Tables A1.46 and A1.48). A peak %Endowment/%Area ratio of 2.5 is achieved with a 2500 m buffer around the 9322 m worm (Fig. 1.29). This buffer captures 69.1% of the gold endowment and 43.9% of deposits within 27.9% of the analysis area. For the 30965 m worm, a 1000 m buffer captures 18.6% of the gold endowment and 12.7% of deposits within 3.1% of the analysis area, representing a %Endowment/%Area ratio of 6.1 (Fig. 1.30). It should be noted, however, that the peak buffers around both sets of worms are achieved by the inclusion of Marvel Loch (4.3 Moz Au), the largest deposit in the Southern Cross domain. The endowment curves for the 16 990 m worms (Table A1.47) are complicated by the location of Marvel Loch, between 7.5 and 10 km from the nearest worm. Nevertheless, deposit density decreases steadily from the most proximal buffer (1000 m) around each of the three deepest worms (9322, 16990, and 30 965 m), suggesting that these worms provide useful targeting criteria (Tables A1.46 to A1.48). The 1000 m buffer around the 9322 m worms contains 0.004 deposits/km^2, approximately 1.6 times the average for the analysis area. The 1000 m buffer around the 30 965 m worms contains 0.011 deposits/km^2, approximately 3.7 times the average for the analysis area (Figs 1.29 and 1.30).

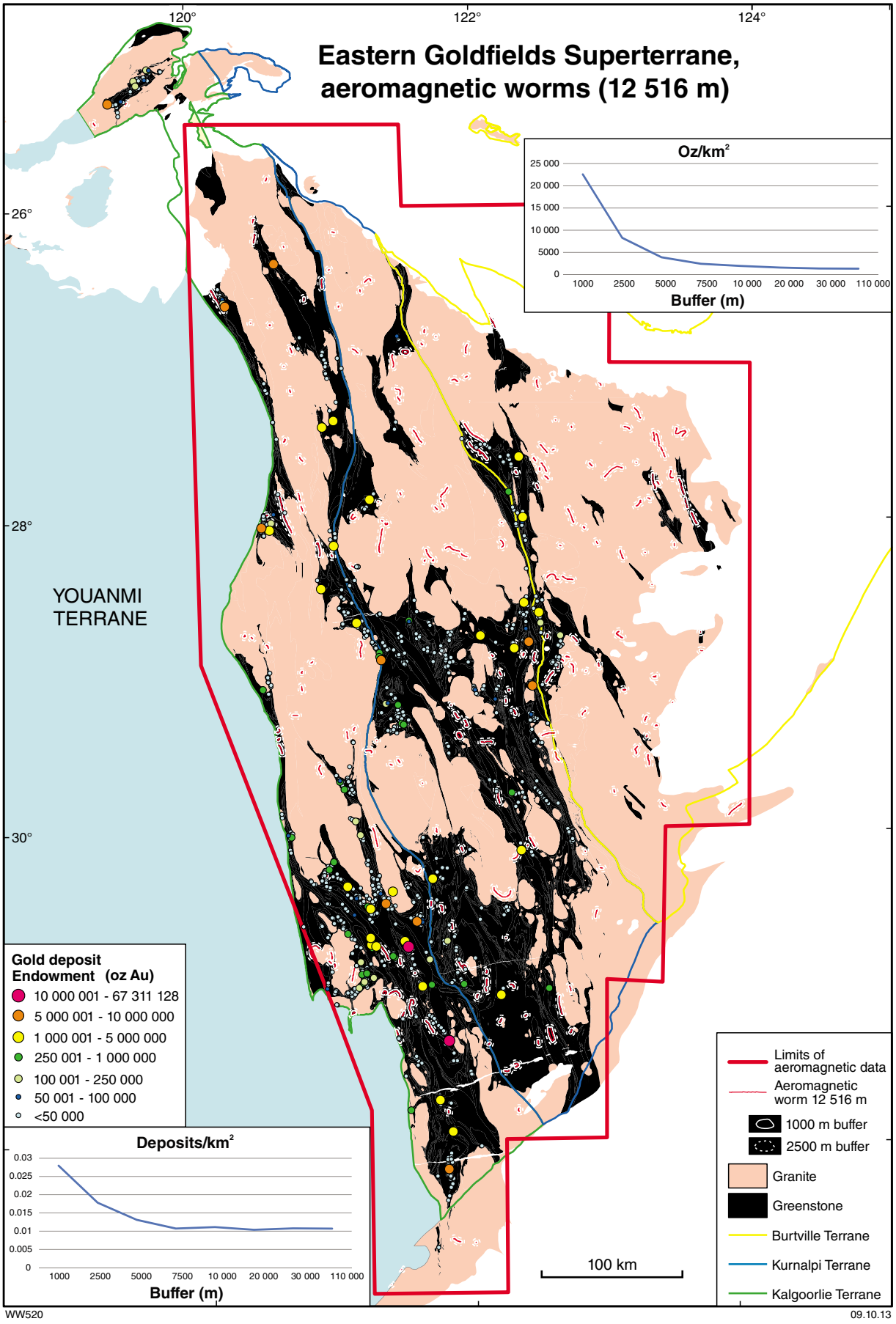

Figure 1.27. **Distribution of gold deposits in the Eastern Goldfields Superterrane relative to selected 12 516 m aeromagnetic worm sets**

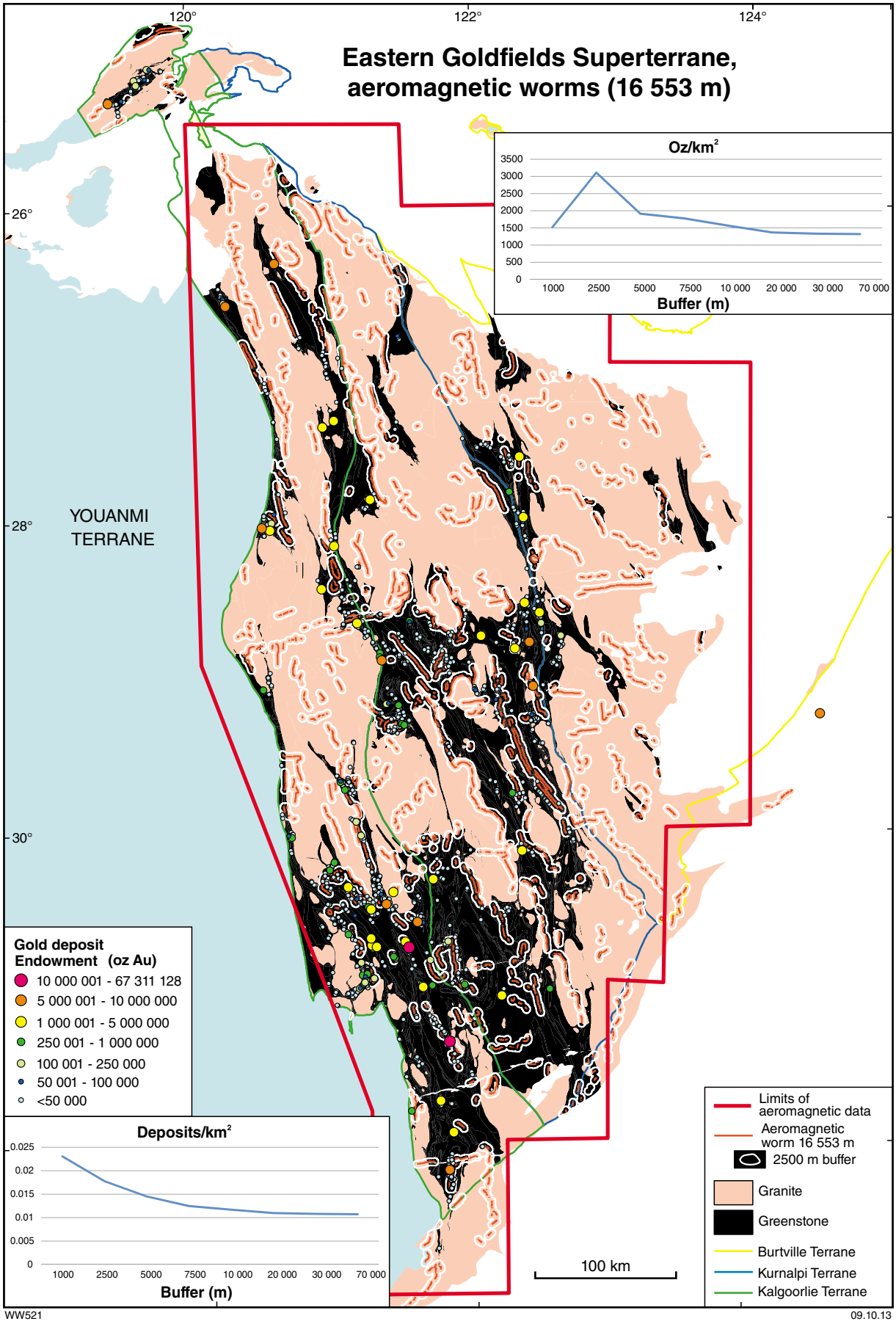

Figure 1.28. **Distribution of gold deposits in the Eastern Goldfields Superterrane relative to 16553 m aeromagnetic worm sets**

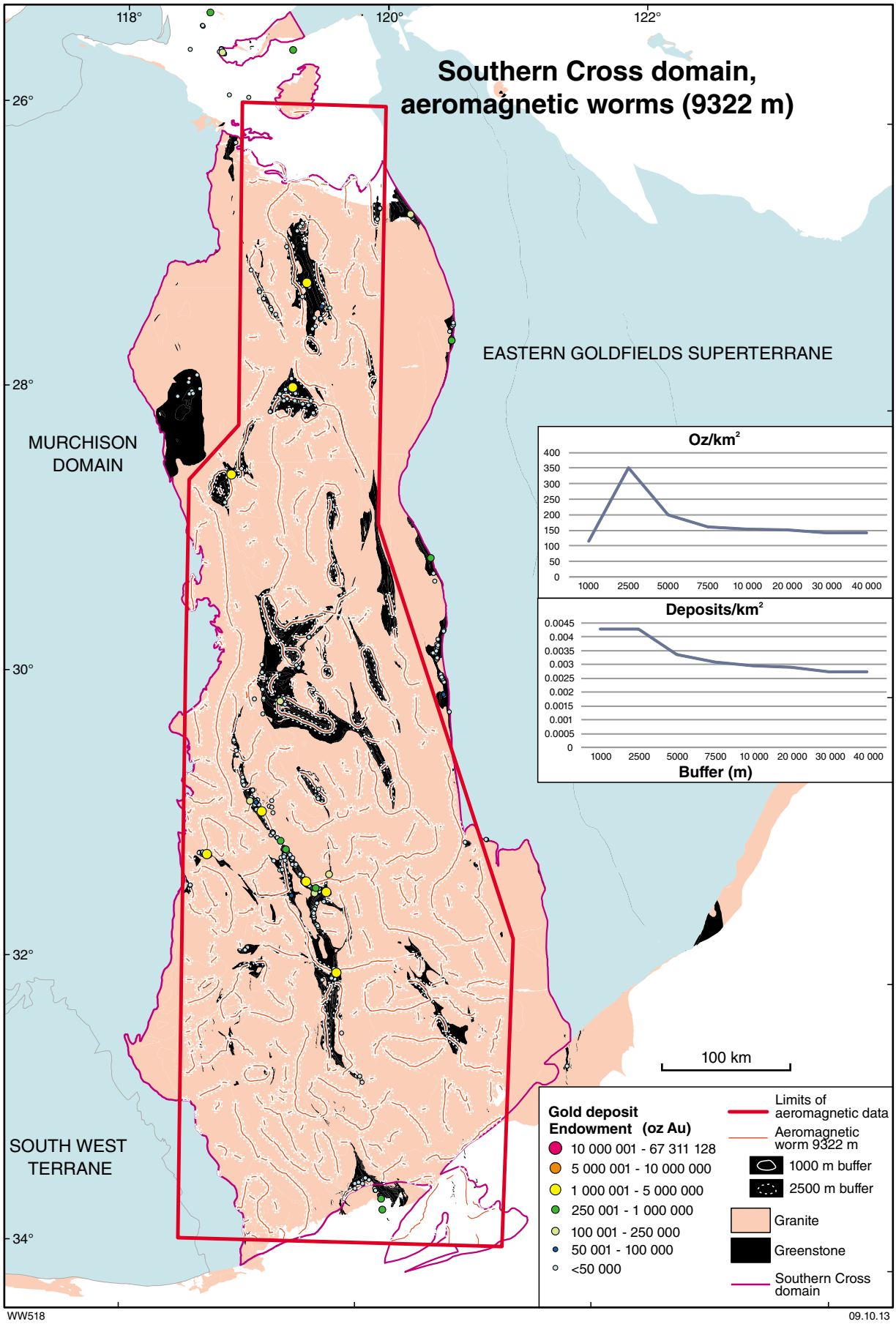

Figure 1.29. Distribution of gold deposits in the Southern Cross domain relative to 9322 m aeromagnetic worm sets

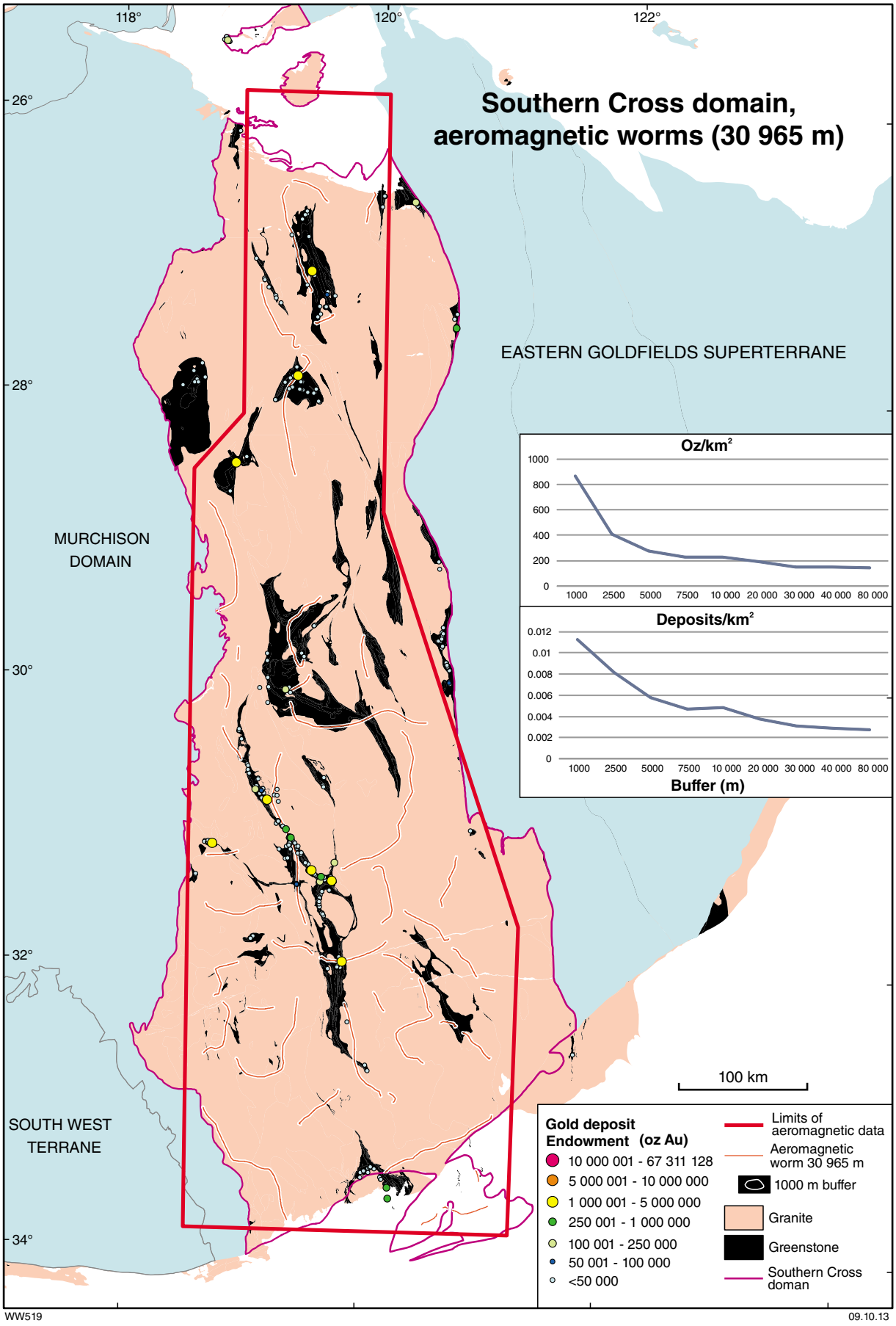

Figure 1.30. Distribution of gold deposits in the Southern Cross domain relative to 30 965 m aeromagnetic worm sets

In the Murchison domain, the deepest worm (34 202 m) did not produce a curve that suggests utility as an exploration targeting tool. However, intermediate depth worms (4542, 8903, and 17 450 m) produced curves that suggest a role in exploration targeting (Tables A1.49 to A1.53). For example, the 500 m buffer around the 4542 m worms captures 25.0% of the gold endowment in 9.3% of the area (Fig. 1.31), a %Endowment/%Area ratio of 2.7. A 2500 m buffer around the 17 450 m worms captures 39.1% of the gold endowment in 15.6% of the area (Fig. 1.32), a %Endowment/%Area ratio of 2.51. Spatial analyses for all three sets of worms (4542, 8903, and 17 450 m) produce curves that define an overall declining deposit density in progressively larger buffers (Tables A1.50 to A1.52). Minor peaks at 2500 m (4542 m worms) and 5000 m (8903 m worms) relate to capture of the Mount Magnet group of deposits (8.1 Moz Au). The best result is for the 1000 m buffer around 17 450 m worms, which captures 11.0% of deposits at a density of 0.010 deposits/km^2, 1.9 times the average deposit density for the analysis area (Table A1.52, Fig. 1.32).

In summary, proximity analyses relating gold endowment to shallow aeromagnetic worms (upward continued heights of 3000 m or less) in the Eastern Goldfields Superterrane, Southern Cross domain, and Murchison domain indicate that proximal (500 m) buffers capture a high percentage of the gold endowment, but the gold is contained within a large proportion of the analysis area because the shallow worms are extensively distributed. Spatial analyses of the deepest worms (>30 000 m) in the Eastern Goldfields Superterrane and the Murchison domain did not produce meaningful curves, probably reflecting lateral displacement of the worms from the intersection of the structural surface they represent with the present day erosion surface. Intermediate depth worms provide the best compromise between problems associated with shallow and deep worms. The best results in all three areas are provided by analyses of worms representing upward continued heights of between 3000 and 30 000 m (equivalent to projected depths of 1.5 and 15 km below the surface). The most effective buffers for intermediate height worms range from 500 to 5000 m with a peak %Endowment/% area ratio of 17.0 achieved with a 1000 m buffer around the 12 516 m worms in the Eastern Goldfields Superterrane. For the Southern Cross and Murchison domains, the best %Endowment/% area ratio was 6.1, achieved using a 1000 m buffer around the 30 965 m worms in the Southern Cross domain analysis area. Both these peak results are influenced by incorporation of the largest deposit in the respective analysis areas; however, these and most other analyses of the relationship between gold and aeromagnetic worms of intermediate depth produced curves for deposit density that support a meaningful proximity relationship.

Aeromagnetic worms are commonly interpreted to represent faults or lithological contacts between units of contrasting magnetite content. The relationships between aeromagnetic worms and gold described here suggest that the intermediate depth worms most closely approximate the near-surface location of relatively deep faults that penetrate the base of the greenstones, and perhaps the entire crust, and that these faults acted as conduits for gold ore fluids. Some of the proposed target worms, particularly in the Southern Cross domain, appear to reflect fractures subsequently intruded by east–west Proterozoic dolerite dykes of the Widgiemooltha Dyke Suite (Sofoulis, 1966). The size of the buffers required to effectively capture a high proportion of gold (up to 5000 m) is consistent with the common observation that gold-bearing lodes are in second- and third-order structures related to major faults and, less commonly, in the faults themselves (Groves et al., 1995, 1998; Eisenlohr et al., 1989).

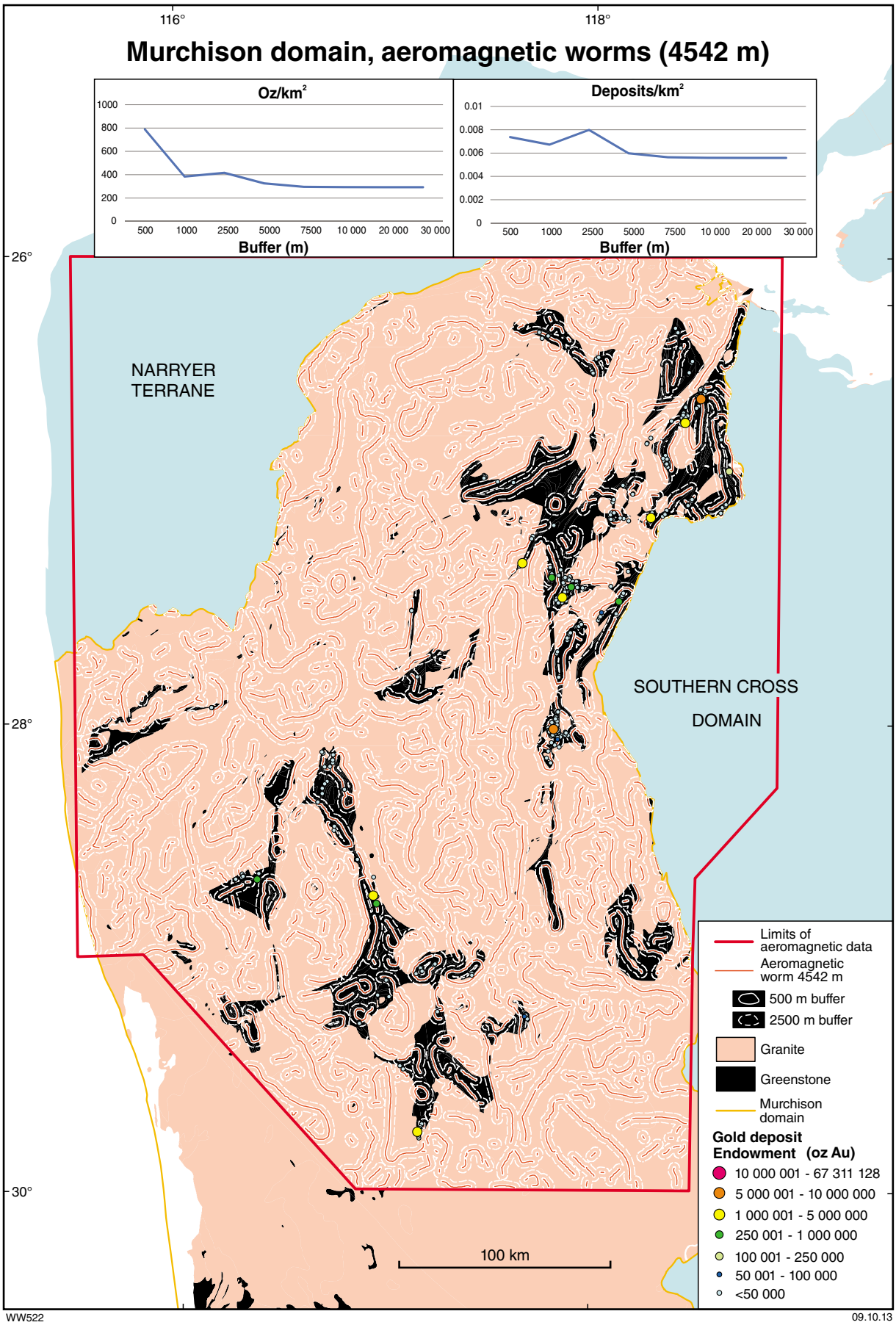

Figure 1.31. Distribution of gold deposits in the Murchison domain relative to 4542 m aeromagnetic worm sets

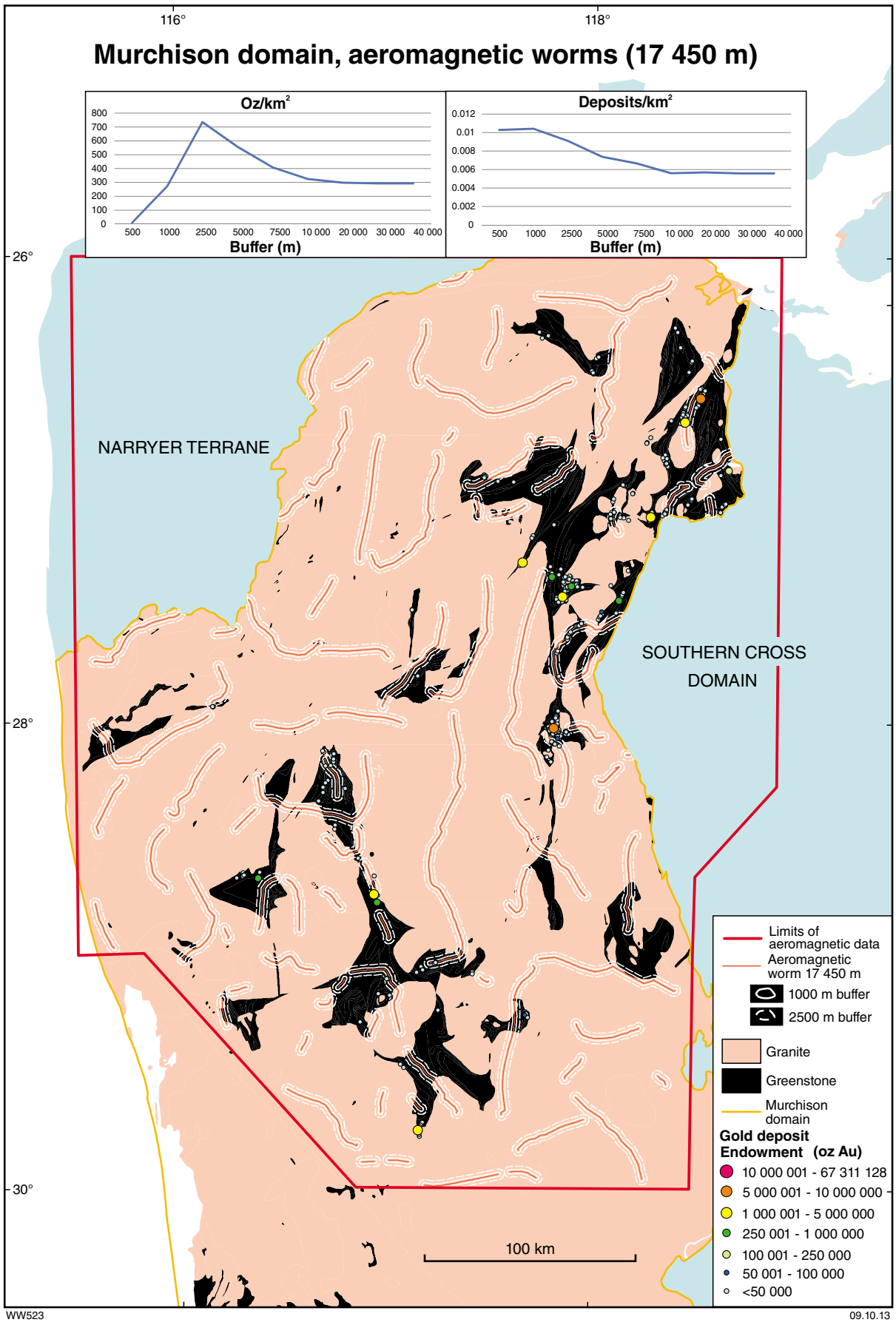

Figure 1.32. Distribution of gold deposits in the Murchison domain relative to 17 450 m aeromagnetic worm sets

Targeting Criterion 1.6: Greenstone thickness

The thickness of the greenstones in the Eastern Goldfields Superterrane varies to a maximum of around 9 km, based on the results of seismic reflection surveys along two major east–west profiles (Goleby et al., 2004). The greenstone thickness has been extrapolated north and south of the seismic sections, by the pmd*CRC Y4 Project Team (2008), using regional gravity data. The results were presented as a set of contours representing the elevation at the interpreted base of the greenstone sequence. Polygons representing five classes of greenstone thickness (less than 1000, 1000 to 3000, 3000 to 5000, 5000 to 7000, and more than 7000 m) have been digitized from those contours (Fig. 1.33).

A containment analysis relating gold endowment to estimated greenstone thickness (Table A1.54) shows a strong association of gold endowment with greenstones of intermediate thicknesses (3000 to 5000 m). This association is influenced by the location of the giant Golden Mile deposit within the 3000 to 5000 m interval. Although the areas of 3000 to 5000 m greenstone thickness provide 36.6% of the endowment of the total area of greenstones, and a %Endowment/%Area ratio of 2.96, these results are strongly dependent on the giant Golden Mile deposit. Exclusion of the Golden Mile from the results produces an endowment of approximately 13 Moz, considerably lower than those of both of the thinner greenstone intervals (Table A1.54).

Given the bias introduced into the endowment by the Golden Mile deposit, the results in terms of number of deposits are particularly important. These results show that there is a steady increase in deposit density with increasing greenstone thickness up to the 3000 to 5000 m class, beyond which thicker greenstones contain fewer deposits (Table A1.54). The peak deposit density, in the 3000 to 5000 m thickness range, is 0.052 deposits/km^2, 1.7 times the average of 0.031 deposits/km^2 for greenstones in the Eastern Goldfields Superterrane.

Although the areas of shallow greenstones (<1000 m thickness) represent 42.5% of the total area, they contain only 23.8% of the endowment and 28.6% of the deposits, suggesting that shallow greenstones are not particularly favourable for gold mineralization (Table A1.54). Nevertheless, some significant gold-producing centres (e.g. St Ives) are in greenstone sequences that are less than 1000 m thick (Fig. 1.33). The areas of deepest greenstones (>7000 m thickness) also have a poor gold endowment, but these account for only 0.6% of the total analysis area (Fig. 1.33). The maximum endowment is in greenstones of thickness from 3000 to 5000 m, where an endowment of 11 724 oz/km^2 compares with an average of 3736 oz/km^2 for greenstones (only) in the entire Eastern Goldfields Superterrane. All other greenstone thickness domains have an endowment that is less than or only marginally in excess of the average of 3956 oz/km^2 for the total (granites and greenstones) analysis area (Table A1.54).

The average size of gold deposits increases with increasing greenstone thickness to peak in the 5000 to 7000 m thickness range at 347 280 oz (Table A1.54). Although this thickness range contains only 22 deposits, this is an interesting result considering that the Golden Mile deposit is not included. The largest deposits in the 5000 to 7000 m class are Bronzewing, Darlot, and Day Dawn (north of Norseman, Fig. 1.33).

Intuitively, an association between gold and steep gradients at the base of the greenstones seems likely, particularly as most of these steep gradients are oriented roughly normal to the direction of regional shortening at the time of gold mineralization (proposed variously as northeast–southwest to east-southeast–west-northwest by a range of authors; e.g. Witt and Vanderhor, 1998; Groves et al., 2000; pmd*CRC Y4 Project Team, 2008; Blewett et al., 2010a). In such circumstances, the steep gradient in the surface separating greenstones from underlying granitic rocks potentially represents a regional-scale rheological gradient capable of partitioning strain and focusing fluid flow (cf. Ridley, 1993; Oliver et al., 2001). The results of proximity analyses relating gold to shallow gravity lineaments were interpreted in the same way (section 1.4). To investigate this potential relationship, a triangular irregular network (TIN) was built by interpolating the elevation points on the greenstone depth contours into a contiguous triangular surface. The TIN was used to generate a digital elevation model (DEM) representing the base of the greenstone sequence. Next, a slope map that represents the maximum rate of change in elevation between each cell and its neighbours was generated from the DEM. Values representing greenstone contours with a gradient greater than 30° were isolated and converted into vector format, which provided the basis for the proximity analysis.

The results of a proximity analysis (Table A1.55) show that the peak gold endowment is achieved by the 1000 m buffer, which captures 25.2% of the gold in 14.0% of the area of the Eastern Goldfields Superterrane (Fig. 1.34), equivalent to a %Endowment/%Area ratio of 1.79 (Table A1.55). The 1000 m buffer includes the area within the outlines of the >30º domain and extends to 1 km beyond. The endowment falls away fairly slowly with increasing distance from the >30º domains, supporting a weak relationship between gold endowment and proximity to the steeper sections of the basal greenstone contact. The giant Golden Mile deposit is captured only by the 20 000 m buffer. The 0 m buffer, equivalent to a containment analysis relating gold endowment to greenstones overlying a basal contact with a gradient of >30°, contains the greatest deposit density and that parameter decreases steadily with distance from the steep gradient domains (Table A1.55). Although the deposit density in greenstones overlying steep basal gradients (0.043 deposits/km^2) is 1.4 times the average for greenstone areas in the Eastern Goldfields Superterrane (0.031 deposits/km^2), it is 3.4 times the average for greenstones in the analysis area (0.013 deposits/km^2). The endowment captured by the steep basal gradient domains is only 9.7% of the total endowment, and the %Endowment/%Area ratio is a modest 1.21. The 1000 m buffer (which includes the area within the >30º domain) captures 42.6% of deposits at a deposit density of 0.038 deposits/km^2, which is three times the average for greenstones in the analysis area (Table A1.55).

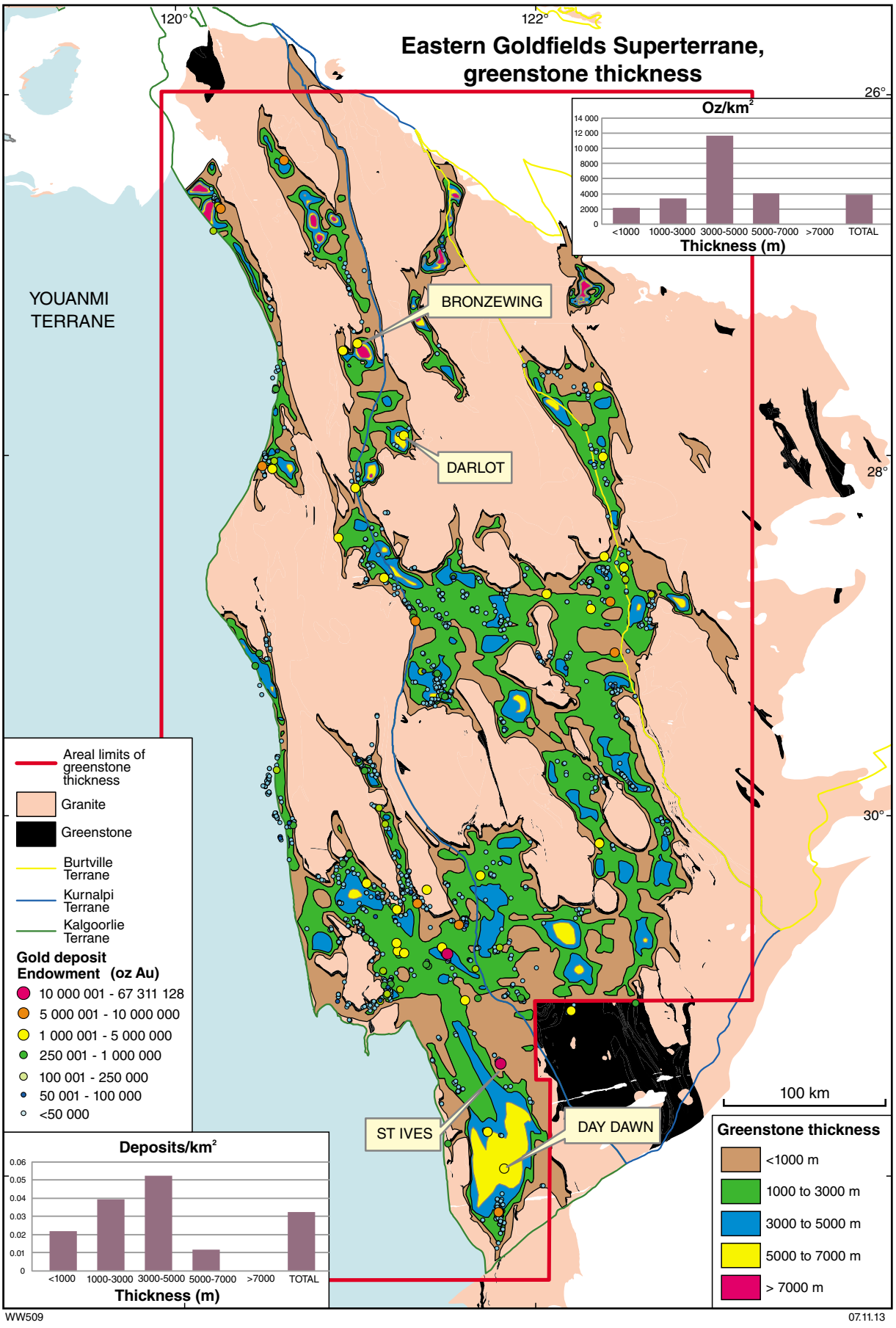

Figure 1.33. Distribution of gold deposits in the Eastern Goldfields Superterrane relative to interpreted greenstone thickness

In summary, currently available data from the Eastern Goldfields Superterrane suggest that gold endowment is not influenced greatly by greenstone thickness, if the skewing effect of the Golden Mile is discounted. However, there is an apparent tendency for deposit density to increase with greenstone thickness, to a maximum of 5000 m, after which it decreases in the regions of thickest greenstones (<5000 m). The average size of deposits (excluding the Golden Mile) also increases in greenstones sequences that are thicker than 3000 m (Table A1.54). There is a statistical advantage to exploring within 1000 m of steep (>30°) gradients in the basal contact of the greenstones, if discovery rather than tonnage is the main incentive. However, this approach provides only a weak advantage in terms of endowment and would miss some of the larger gold deposits (e.g. Golden Mile, St Ives, Wallaby, Granny Smith, and Sunrise Dam). There is, in fact, an inverse relationship between deposit size and distance from the steep (>30°) gradients in the Eastern Goldfields Superterrane (Table A1.55).

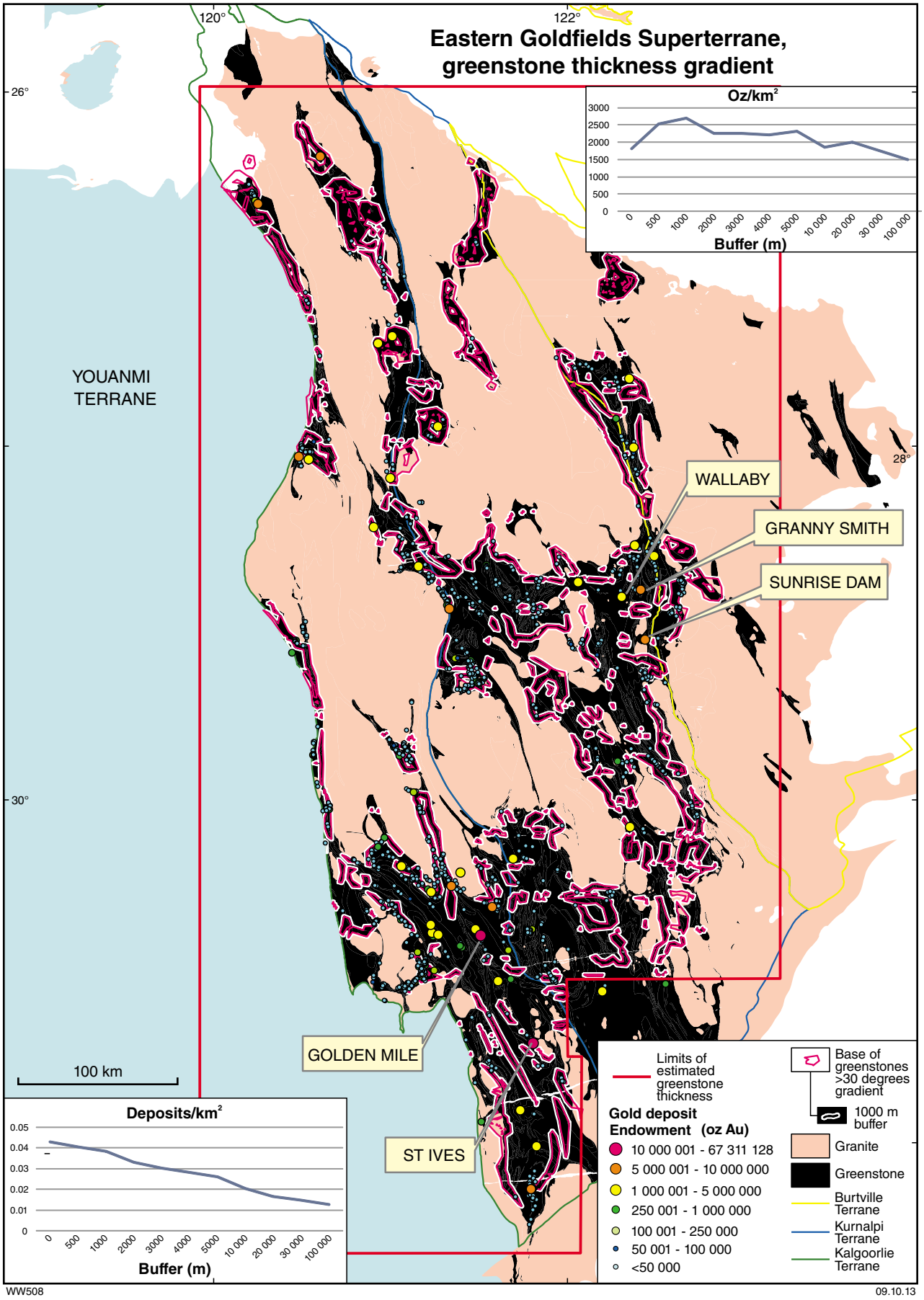

Figure 1.34. Distribution of gold deposits in the Eastern Goldfields Superterrane relative to steep gradient segments in interpreted greenstone thickness

Targeting Criterion 1.7: Regional faults

A close spatial relationship between gold mineralization and proximity to regional faults, in the Yilgarn Craton and elsewhere, has long been posited (Groves and Phillips, 1987; Groves et al., 1989, 2000; Goldfarb et al., 2005; Robert et al., 2005; Sheldon and Micklethwaite, 2007). The relationship was previously investigated for the Eastern Goldfields Superterrane by Bierlein et al. (2006), using Geoscience Australia's MINLOC and OZMIN databases for gold deposit location and endowment (Ewers et al., 2002a,b), and fault trends derived from GSWA's digital map coverage.

Bierlein et al. (2006) did not specify which GSWA regional fault set they used but, using fixed width buffers (1, 2, 3, 4, and 5 km), they found that gold endowment increased steadily in successively more proximal buffers. They also noted a decrease in the endowment of 2 km buffers around long strike-length faults compared with a maximum endowment in short strike-length faults (<20 km). In a separate analysis, Bierlein et al. (2006) created buffers with widths that were weighted according to the strike length of the fault. Using these length-weighted buffers, they showed that gold endowment was substantially greater for small faults within 4 km of >100-km-long faults than in small faults from more distal locations. They interpreted their results to reflect the common observation that gold is concentrated in second- and third-order structures adjacent to major faults (see references in first paragraph of this section). The ratio of gold endowment to the area of the fault buffers (%Endowment/%Area) was improved by the use of buffers that were weighted to reflect fault length.

In this study, we specifically addressed longer strike-length faults, commonly referred to as regional faults. All faults were similarly buffered; they were not weighted according to strike length. For the Eastern Goldfields Superterrane, these faults were represented by the *projected fault system* shape file interpreted from geological outcrop and aeromagnetic imagery, and reported by pmd*CRC (Y4 Project Team, 2008). Equivalent files are not available for the Southern Cross or Murchison Domains; for these domains the *geolin01* shape file, a 1:2 500 000 state-wide cache of faults developed by GSWA was used.

In the Eastern Goldfields Superterrane, spatial analysis of gold endowment in successively increasing buffers from 500 to 110 000 m results in a peak %Endowment/%Area ratio of 5.90 within the 1000 m buffer and decreasing returns in progressively larger buffers (Table A1.56). The 1000 m buffer captures 44.8% of the gold endowment in 7.6% of the analysis area (Fig. 1.35). The most proximal buffer (500 m) is less well-endowed than the 1000 m buffer. These data essentially repeat the results of the Bierlein et al. (2006) study, though more quantitatively. The average deposit size (ounces) also peaks in the 1000 m buffer, beyond which it decreases slowly with increasing buffer distance. These results are influenced by incorporation of the giant Golden Mile deposit within the 1000 m buffer. In terms of deposit density, there is a steady decline from the most proximal (500 m) buffer (Table A1.56). The 500 m buffer captures 13.9% of deposits at 0.038 deposits/km^2 (almost four times the average for the analysis area, 0.011 deposits/km^2). Even the 4000 m buffer, which captures more than 50% of deposits, contains approximately twice the average deposit density of the analysis area (the Eastern Goldfields Superterrane). The shapes of the curves for ounces per square kilometre and deposit density support a meaningful spatial relationship between gold mineralization and the regional faults identified by the pmd*CRC Y4 Project in the eastern Yilgarn Craton.

Similar results were generated in the Southern Cross domain, where a maximum %Endowment/%Area ratio of 5.36 was achieved using a 1000 m buffer around the GSWA regional fault set (*geolin01* shape file) (Fig. 1.36). The 1000 m buffer captures 37.4% of the endowment in 7.0% of the analysis area (Table A1.57). It also holds the maximum average deposit size (75 265 oz) of all the buffers. Deposit density is also greatest within the 1000 m buffer, beyond which there is a steady decrease. The 1000 m buffer captures 21.9% of deposits at 0.009 deposits/km^2, compared to an average of 0.003 deposits/km^2 for the Southern Cross domain. The 3000 m buffer captures 53.3% of deposits at more than twice the average deposit density for the analysis area (Fig. 1.36). The shapes of the curves for ounces per square kilometre and deposit density support a meaningful spatial relationship between gold and regional faults identified by the GSWA in the Southern Cross domain.

In the Murchison domain, relatively high %Endowment/%Area ratios (between 3.1 and 4.9) are found for buffers extending 1000 to 5000 m around regional faults (Table A1.58). The analysis produced irregular curves that do not support a close geological relationship between gold and regional faults. The irregularity of the endowment curves are influenced by the capture of Meekatharra (5 Moz Au), Mount Magnet (8.1 Moz Au), and Great Fingall (2 Moz Au) in the 1500, 4000, and 5000 m buffers, respectively. Nevertheless, the 1500 m buffer captures 32.8% of the gold endowment in 6.7% of the analysis area, equivalent to a %Endowment/%Area ratio of 4.92 (Fig. 1.37). The 5000 m buffer captures 85.9% of the gold endowment and 49.4% of deposits in 21.0% of the analysis area (the Murchison domain). The deposit density within the 5000 m buffer (0.008 deposits/km^2) is 2.4 times the average for the Murchison domain.

Results of proximity analyses relating gold endowment to regional faults in the Eastern Goldfields Superterrane and the Southern Cross domain produce smooth curves that suggest a meaningful association between the two.

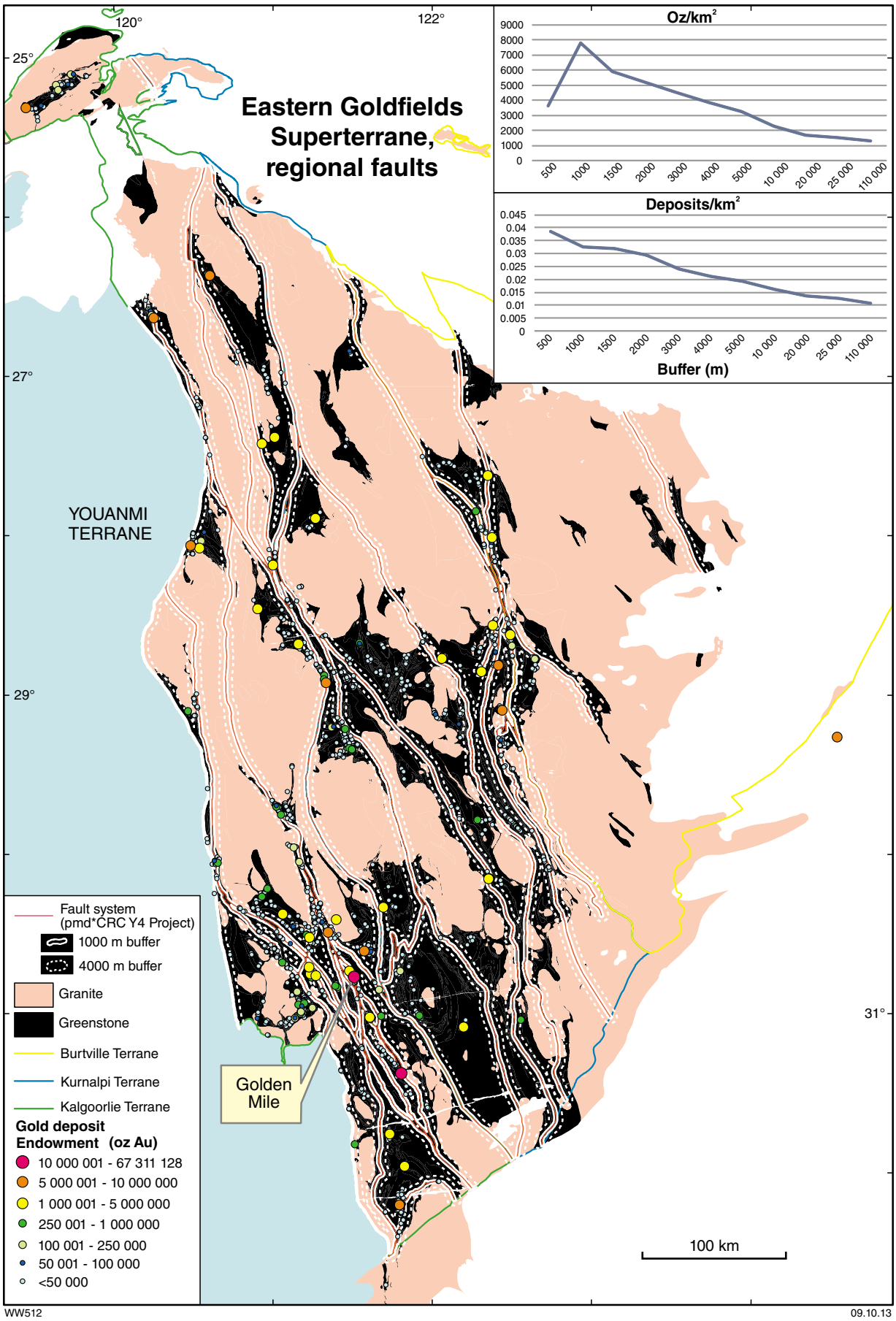

Figure 1.35. Distribution of gold deposits in the Eastern Goldfields Superterrane relative to regional faults

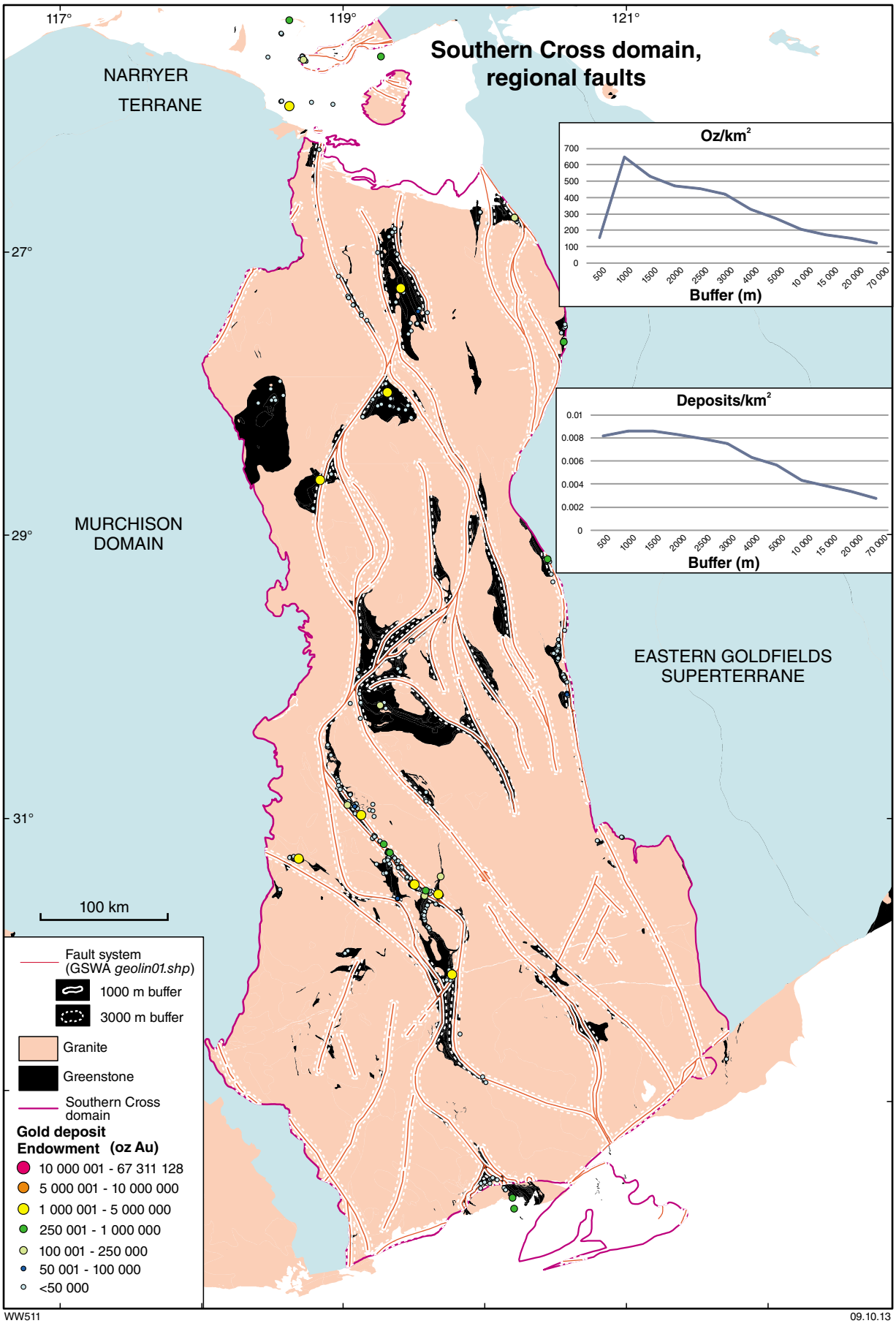

Figure 1.36. Distribution of gold deposits in the Southern Cross domain relative to regional faults

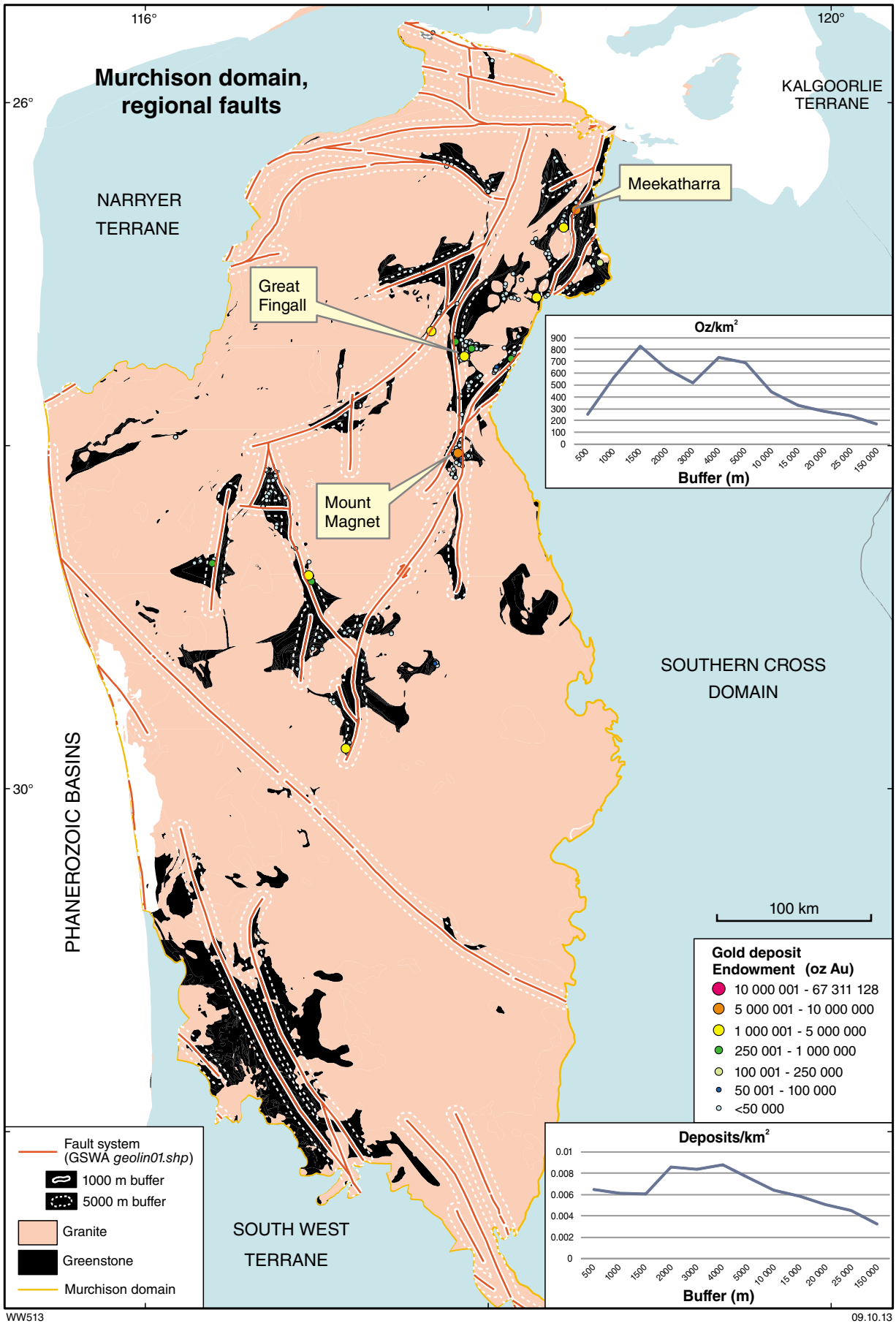

Figure 1.37. Distribution of gold deposits in the Murchison domain relative to regional faults

Maximum gold endowment (ounces) is within the 1000 m buffer in both regions and, as for the number of deposits, decreases steadily from the most proximal buffers. Despite the influence of the Golden Mile on the endowments in the Eastern Goldfields Superterrane, the supportive results for endowment in the Southern Cross domain, and the deposit density in both areas, strengthen the argument for a significant spatial association between gold and regional faults. The maximum %Endowment/%Area ratio in the second-closest (1000 m) buffer is consistent with the common observation that gold is concentrated in second- and third-order structures adjacent to major faults (e.g. Groves and Phillips, 1987; Groves et al., 1989, 2000; Goldfarb et al., 2005; Robert et al., 2005; Sheldon and Micklethwaite, 2007), and is consistent with the results of Bierlein et al. (2006). In the Southern Cross domain, there appears to be a strong spatial association between gold deposits and relatively few of the regional faults and their intersections with greenstone belts (Fig. 1.36). The situation in the Eastern Goldfields Superterrane is more complex, though the association of gold with the Boulder–Lefroy Fault is well documented (Groves and Phillips, 1987; Witt and Vanderhor, 1998; Robert et al., 2005).

The less satisfactory outcomes for proximity analysis in the Murchison domain may reflect the less detailed mapping available for that area at the time of the analyses presented here. Nevertheless, the relatively high %Endowment/%Area ratios for buffers between 1000 and 5000 m may still be useful for exploration targeting in the Murchison domain.

Targeting Criterion 1.8: Regional fault density

Fault density was calculated using the ArcGIS Density Tool in Spatial Analyst to analyse the *regional fault system* shape file of the pmd*CRC (Y4 Project Team, 2008) for the Eastern Goldfields Superterrane, and the GSWA 1:2500000 *geolin01* shape file for the Southern Cross and Murchison domains. Fault density is expressed as kilometres of fault length per square kilometre, based on an analytical cell size of 100 m and a search radius of 10 km. The Eastern Goldfields Superterrane and the Southern Cross and Murchison domains have been divided into polygons according to the calculated fault density (Figs 1.38 to 1.40). Containment analyses were carried out relating gold endowment to fault density for each of these areas (Tables A1.59 to A1.61).

For the Eastern Goldfields Superterrane, the containment analysis shows a fairly even spread of endowment through each of the fault density ranges. When normalized by area, however, a distinct enrichment of gold is evident in areas with maximum fault density (>0.25 km/km^2), which have a %Endowment/%Area ratio of 108.9. The huge Golden Mile deposit accounts for more than 90% of the gold endowment for this category of fault density. If the endowment of the Golden Mile is discounted, the areas of >0.25 km/km^2 fault density are still the most prospective, but less markedly so, possessing a %Endowment/%Area ratio of 7.95, compared to 4.46 for the next most highly endowed fault density (0.15 to 0.2 km/km^2). Areas with fault densities of 0.15 to 0.20 km/km^2 in the Eastern Goldfields Superterrane (Table A1.59, Fig. 1.38), which account for 2.8% of the analysis area, contain 12.6% of the total gold endowment. Discounting the bias caused by inclusion of the Golden Mile in the highest fault density category, there is a trend towards greater gold endowment (%Endowment/%Area) in areas of relatively high fault density in the Eastern Goldfields Superterrane, with polygons containing <0.15 km/km^2 distinctly less well-endowed (Fig. 1.38).

In terms of deposit density, the maximum fault density range again stands out, capturing 7.1% of deposits at 0.244 deposits/km^2, compared to an average of 0.010 deposits/km^2 for the entire analysis area. Average deposit size decreases fairly steadily with decreasing fault density, from a maximum in the highest fault density range (Table A1.59).

Gold endowments in the Southern Cross and Murchison domains peak within the fault density range 0.1 – 0.15 km/km^2 (Tables A1.60 and A1.61). In the Southern Cross domain, areas with fault densities of 0.1 to 0.15 km/km^2 occupy 6.4% of the total analysis area and contain 53.6% of the gold endowment (Fig. 1.39). Deposit density peaks in the highest fault density range, although this represents only a little over 1% of all deposits. The 0.1 to 0.15 km/km^2 range captures 31.3% of deposits at 0.013 deposits/km^2, or 4.8 times the average for the Southern Cross domain. The average deposit size is also highest (75 146 oz) for this range. In the Murchison domain, areas with fault densities of 0.1 to 0.12 km/km^2 occupy 2.3% of the total analysis area and contain 48.5% of the gold endowment (Fig. 1.40). Deposit density peaks in the areas of 0.14 – 0.16 km/km^2 fault density, although this range captures only 4% of all deposits (Table A1.61). The fault density range of 0.10 to 0.12 km/km^2 captures 18.6% of deposits at 0.025 deposits/km^2, almost eight times the average for the Murchison domain.

In summary, only the Eastern Goldfields Superterrane shows maximum endowment in the highest fault density range. In terms of deposit density, the highest fault density range is optimal in the Eastern Goldfields Superterrane and Southern Cross domain. However, by combining all fault density ranges above 0.10 km/km^2, better results are achieved. In the Eastern Goldfields Superterrane, this captures 54.7% of the endowment and 30.8% of deposits in 11.1% of the total area. This is equivalent to a %Endowment/%Area ratio of 4.93 and a deposit density (0.027 deposits/km^2) that is 2.7 times the average for the Eastern Goldfields Superterrane. In the Southern Cross domain, the same combination of fault density ranges provides 53.6% of the total endowment and 33.7% of all deposits in 7.7% of the total analysis area. These figures equate to a %Endowment/%Area ratio of 6.96 and a deposit density (0.012 deposits/km^2) that is 4 times the average for the Southern Cross domain. In the Murchison domain, equivalent figures are 49.1% of total endowment at a %Endowment/%Area ratio of 14.8, and 37.8% of deposits captured at a density of 0.027 deposits/km^2 or 8.9 times the average for the Murchison domain.

Considering that most models for lode gold mineralization in the Yilgarn Craton involve focusing of hydrothermal fluids via fracture-controlled permeability (Hagemann and Cassidy, 2000; Cox et al., 2001; Goldfarb et al., 2005), the above relationships between gold and moderate to high fault densities are to be expected. However, it is only in the Eastern Goldfields Superterrane that peak %Endowment/%Area and peak deposit density are within the maximum fault density range; the former is attributed in part to the influence of the Golden Mile deposit. The absence of a direct correlation between gold mineralization and fault density may in part be a reflection of the closely spaced major fault systems (at least in the Eastern Goldfields Superterrane), which allow partial accommodation of regional stresses by fracturing of the intervening low-strain domains in which regional fault densities are low (e.g. the Ora Banda domain; Witt, 1993).

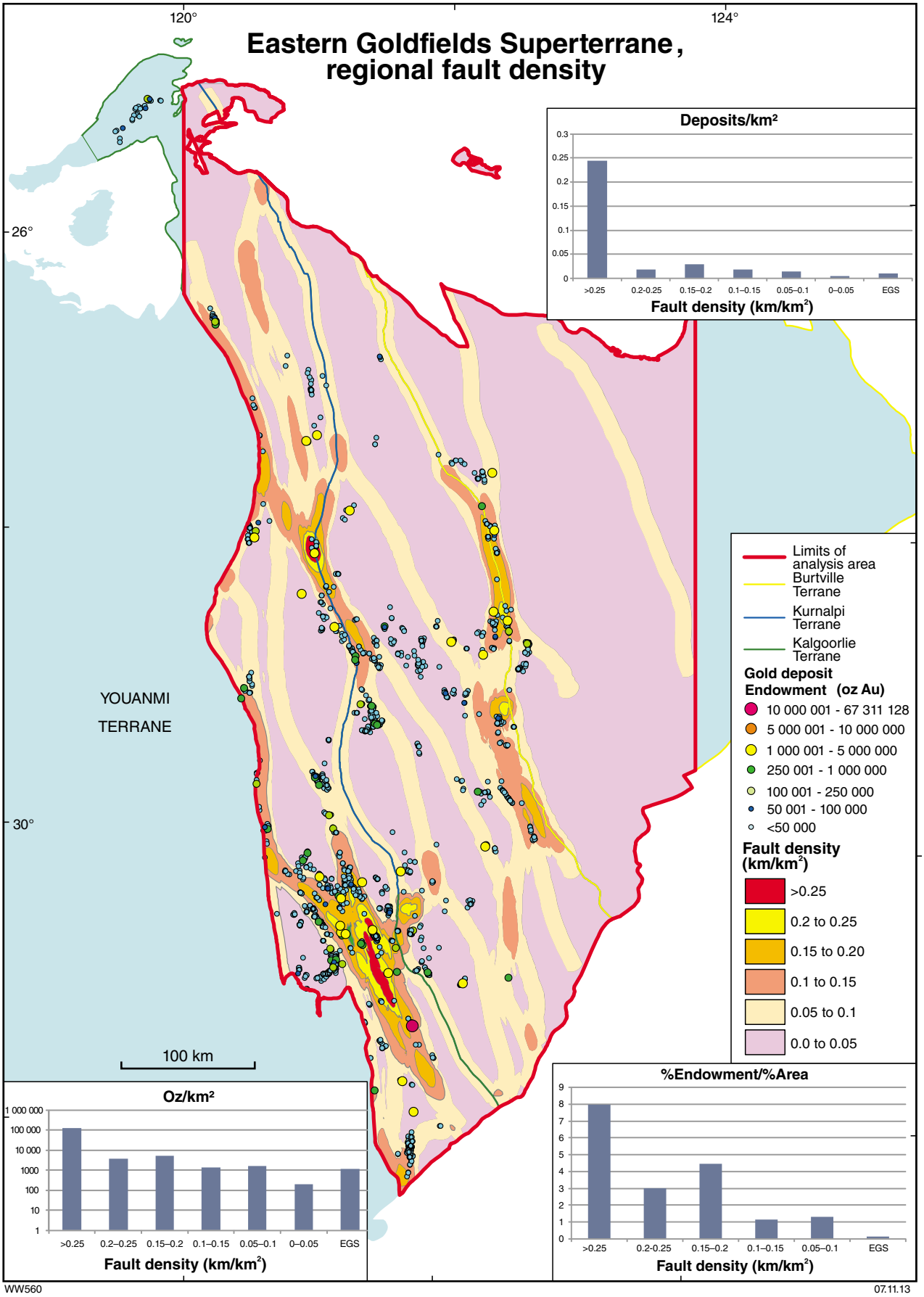

Figure 1.38. Distribution of gold deposits in the Eastern Goldfields Superterrane relative to regional fault density

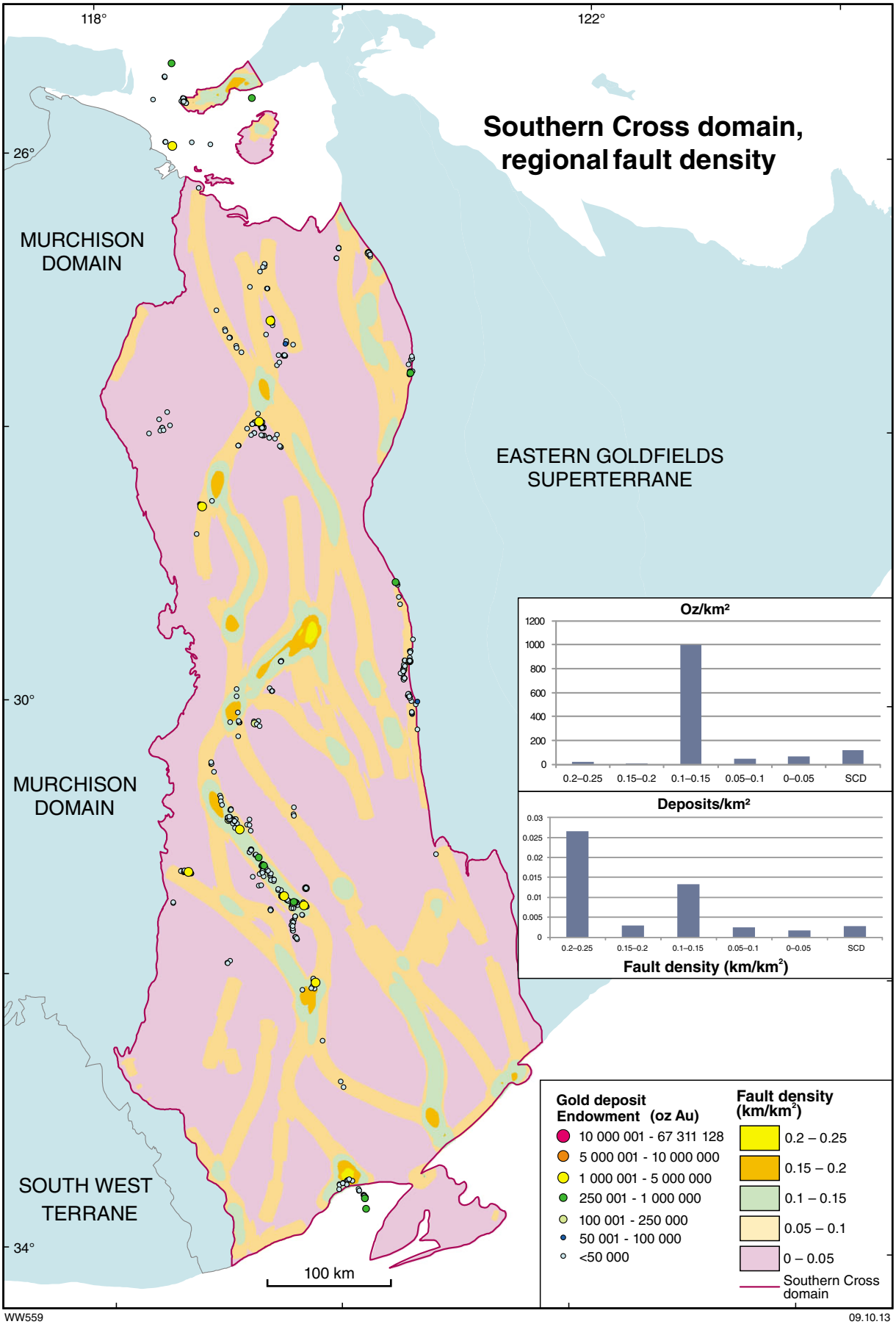

Figure 1.39. Distribution of gold deposits in the Southern Cross domain relative to regional fault density

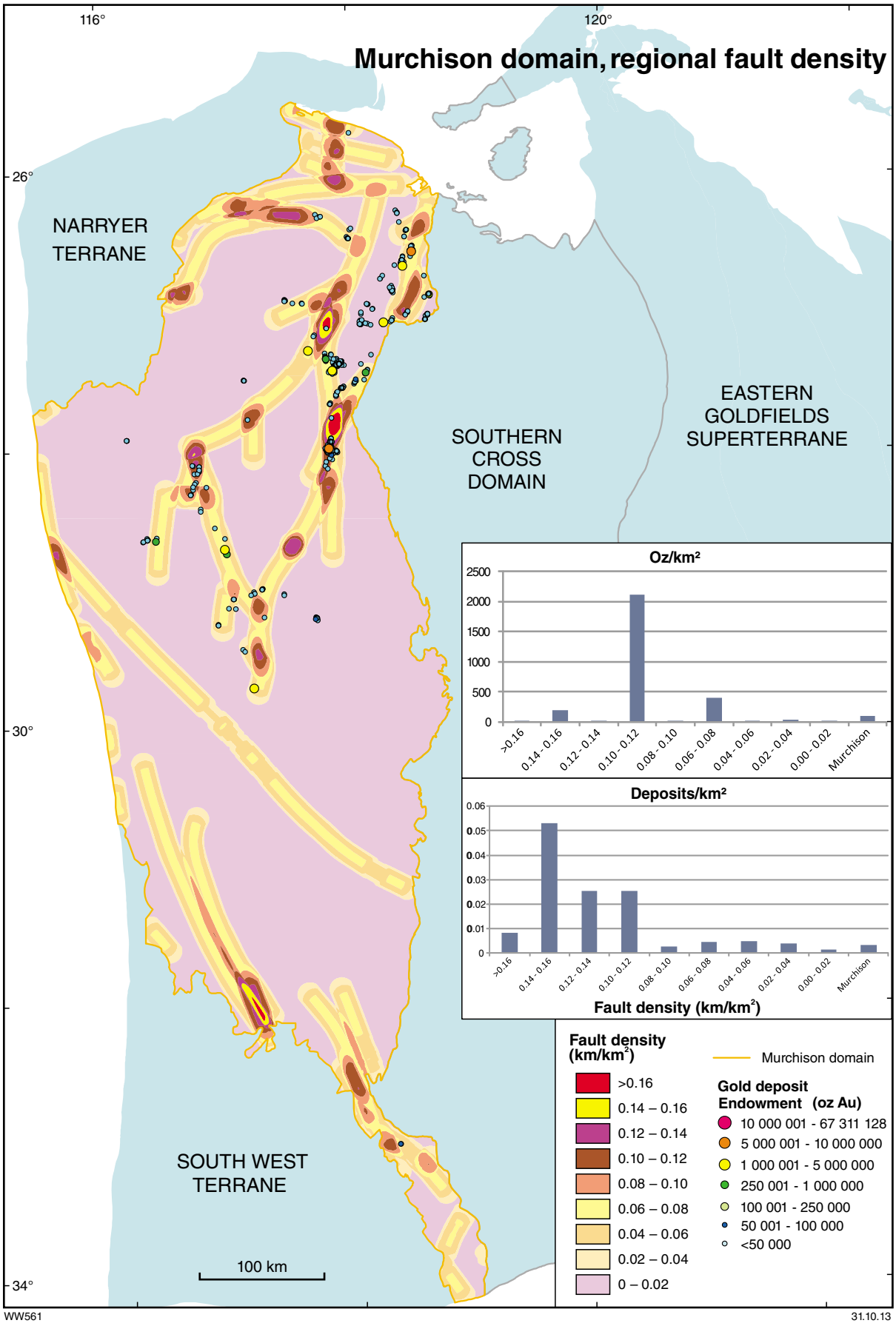

Figure 1.40. Distribution of gold deposits in the Murchison domain relative to regional fault density

Targeting Criterion 1.9: Regional fault intersections

Intersecting structures, particularly the intersection of two or more faults, have long been recognized as significant controls on gold mineralization, and on high-grade shoots within gold deposits (O'Driscoll, 1968, 1990; Woodall, 1994; Walshe et al., 2006). To investigate this relationship quantitatively at regional scale, spatial analyses were directed at intersections between regional faults and high-angle oblique faults in the Eastern Goldfields Superterrane, the Southern Cross domain, and the Murchison domain (Figs 1.41 to 1.43). The intersections were digitized manually using ArcGIS software. Oblique faults intersect regional structures at angles of 40° to 90°. Intersections include some relatively low-angle splays within the regional fault sets. However, low-angle (<40º) intersections between faults defined in different datasets were excluded to avoid the risk of including false intersections created by different interpretations of the same structure.

The *projected fault system* shape file developed by pmd*CRC (Y4 Project Team, 2008) was used to represent regional faults in the Eastern Goldfields Superterrane. High-angle intersections were created where this fault set was cut or joined by oblique faults from the GSWA Eastern Yilgarn GIS dataset (*2_5m_geology98_EYC* shape file). In this file, lines classified as faults largely duplicate the north-northwesterly striking regional fault system and were therefore not used. Intersecting oblique faults and fractures in the *2_5m_geology98_EYC* shape file are classified as dykes. It is inferred that these dykes (mainly belonging to the Widgiemooltha Dyke Suite) intruded long-lived fractures that were possibly active during the formation of gold deposits in the late Archean (cf. Isles et al., 1989). The oblique faults were extended for distances of up to 5 km to generate intersections with regional faults.

For the Southern Cross and Murchison domains, regional faults were taken from the GSWA *geolin01* shape file (see also Targeting Criterion 1.7: Regional faults). Intersecting oblique faults in the Southern Cross domain were generated from the GSWA *500K_interpstrucl* shape file (available from the GSWA Central Yilgarn GIS dataset). Only aeromagnetic lineaments were selected from this file because the faults and shears largely duplicate the faults in the *geolin01* shape file. The extent of the *500K_interpstrucl* file is limited to the northern part of the Southern Cross domain, so the 1141 aeromagnetic worm set was used as a substitute for oblique faults and high-angle intersections of these worms with the *geolin01* shape file were recorded throughout the analysis area. Intersecting oblique faults in the northern Murchison domain were generated from the *interpstrucl* shape file (available from the 2006 GSWA Murchison Geological Exploration Package). The analysis was confined to the northern Murchison domain because detailed structural files were not available for the southern Murchison.

For the Eastern Goldfields Superterrane, the spatial analysis relating gold endowment to regional fault intersections yields a maximum %Endowment/%Area ratio of 1.45 within the 5000 m buffer (Table A1.62). Within this buffer, 17.2% of the gold endowment is captured within 11.8% of the area of the Eastern Goldfields Superterrane. Within the 3000 m buffer, 6.4% of the gold endowment is captured within 5.0% of the area, representing a %Endowment/%Area ratio of 1.28. These low %Endowment/%Area ratios suggest that fault intersections are not particularly useful targeting criteria for gold exploration at regional scale, at least using the digital datasets employed in this study. The results may be critically influenced by a lack of fault intersections between about 30.5°S and 31°S (reflecting the absence of dykes in the *2_5m_geology98_EYC* shape file between these latitudes; Fig. 1.41), which means that the giant Golden Mile deposit is not captured until the 37 000 m buffer is considered.

When viewed in terms of the number of deposits rather than endowment, the results are slightly more encouraging. For example, the 3000 m buffer captures 9.1% of the deposits in 5.0% of the total analytical area (Table A1.62). This buffer contains 0.020 deposits/km^2, or 1.8 times the average deposit density of the Eastern Goldfields Superterrane. The 1500 m buffer captures 3.2% of the deposits in 1.4% of the total analytical area. Although, the overall negative relationship between buffer distance and %Endowment*(%Endowment/%Area) does not support a meaningful relationship between gold mineralization and fault intersections (as defined in this analysis) in the Eastern Goldfields Superterrane (Table A1.62), support for such a relationship is provided by the steady decline in deposit density with increasing distance from a peak density within the 1500 m buffer.

Regional fault intersections in the central Southern Cross domain produce an overall negative relationship between buffer distance and %Endowment*(%Endowment/%Area), and the irregular curves for deposit density (Table A1.63) do not support a meaningful relationship between gold mineralization and fault intersections (as defined in this analysis) in the Southern Cross domain. A peak %Endowment/%Area ratio of 5.4 is associated with the 1000 m buffer. However, the 1000 m buffer accounts for only 3.3% of the gold endowment of the Southern Cross domain. Larger buffers at 4000 and 15 000 m capture more significant proportions of the gold endowment, but with lower %Endowment/%Area ratios. For example, the 4000 m buffer captures 19.3% of the gold endowment in 6.5% of the area, equivalent to a %Endowment/%Area ratio of 2.98 (Table A1.63). The 4000 m buffer captures 6.2% of deposits, but in 6.5% of the analysis area. Deposit density peaks at 15 000 m with 59.3% of deposits captured within 40.3% of the area, which is 1.5 times the average for the central Sothern Cross domain (Table A1.63).

Spatial analyses relating gold endowment to regional fault intersections in the northern Murchison domain provide similar results. Note that the analysis area nominally denoted as the Murchison domain actually includes parts of the Southern Cross domain to the east (Fig. 1.43). The Murchison domain analyses yielded a maximum %Endowment/%Area ratio of 6.7 for the 2000 m buffer (Table A1.64). This buffer captures 19.6% of the endowment within 2.9% of the analytical area.

Apart from an anomalous dip at buffer distance 3000 m (Fig. 1.43), the endowment curves decrease slowly beyond the 2000 m buffer. The peak deposit density is within the 5000 m buffer, where 40.0% of the deposits are captured within 13.5% of the analysis area (Table A1.64). This buffer also captures 75.0% of gold endowment at a %Endowment/%Area ratio of 5.6.

Given the regional scale of the analyses, a five kilometre buffer around fault intersections does not seem to represent an unreasonably large area within which to target exploration in the Murchison domain. The buffer distances are geologically reasonable if the nature and extent of structural damage around fault intersections can be viewed as similar to those around fault bends or jogs (Cox and Ruming, 2004; Micklethwaite and Cox, 2004). In fact, detailed investigations at fault intersection sites may show that many of them are coincident with fault jogs caused by interference or refraction as one fault intersects another (Miller et al., 2010; Alibone et al., 2002). However, the statistics generated by these analyses, particularly in the Eastern Goldfields Superterrane and Southern Cross domain, suggest that caution is required if applying the results to regional gold exploration. The questionable results provide little support for the notion that intersections of Proterozoic dykes with regional shear zones (e.g. Isles et al., 1989) can be used to target gold mineralization.

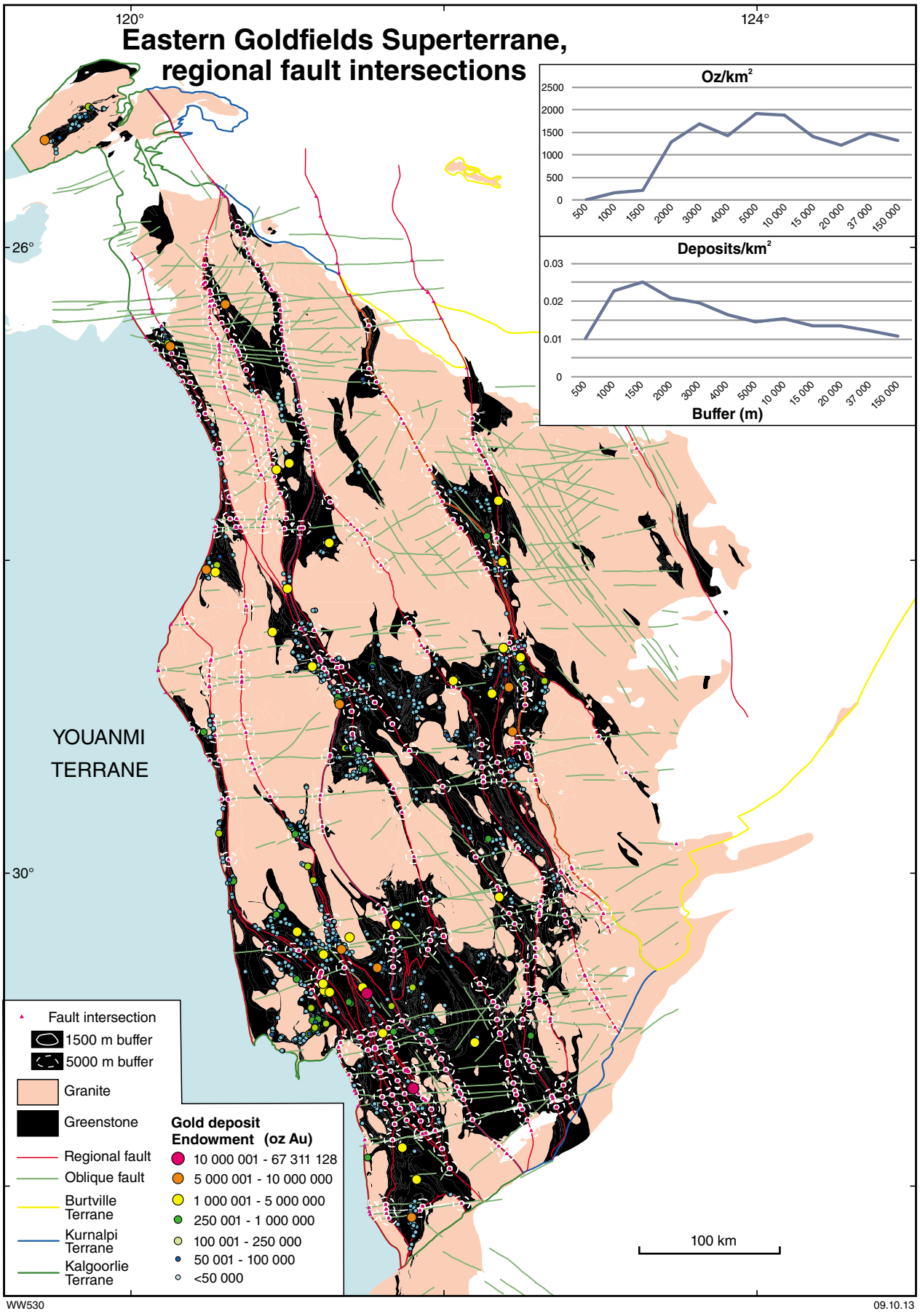

Figure 1.41. Distribution of gold deposits in the Eastern Goldfields Superterrane relative to regional fault intersections

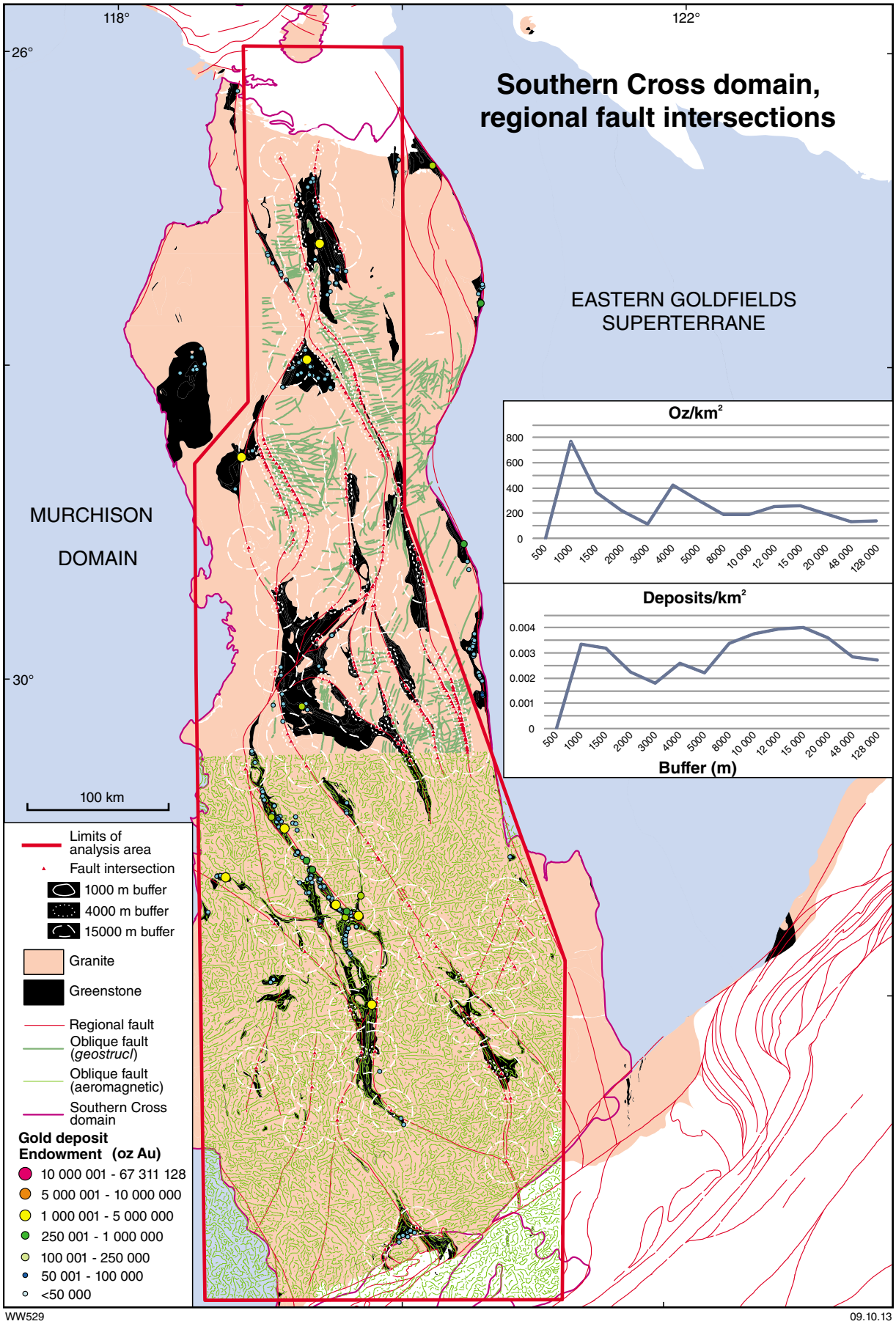

Figure 1.42. Distribution of gold deposits in the Southern Cross domain relative to regional fault intersections

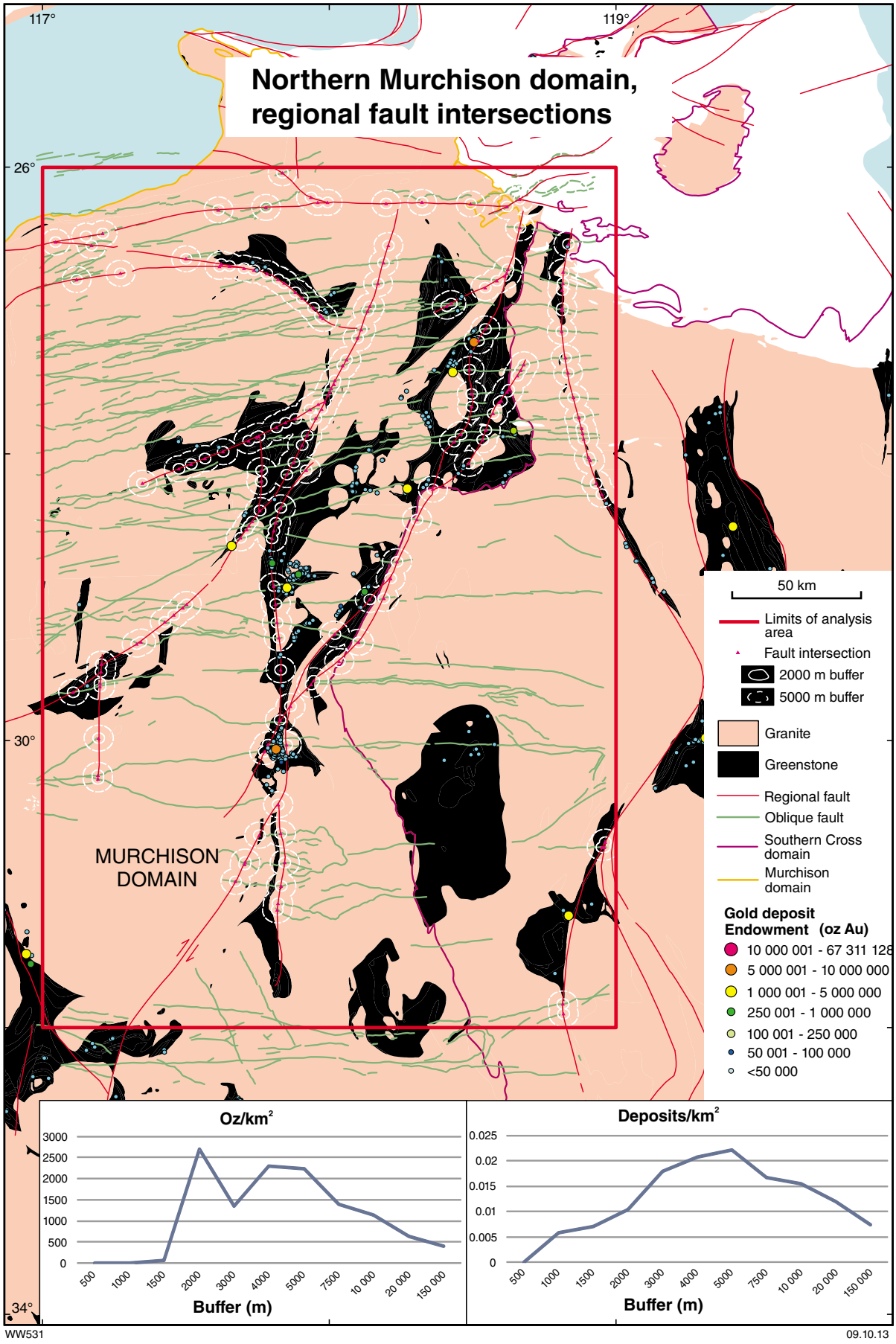

Figure 1.43. Distribution of gold deposits in the northern Murchison domain relative to regional fault intersections

Targeting Criterion 1.10: Regional fault bends

Fault bends and jogs have long been recognized as significant controls for both gold mineralization in general and high-grade shoots within gold deposits (Colvine et al., 1984; Nguyen et al., 1998; Goldfarb et al., 2005; Micklethwaite and Cox, 2004; Weinberg et al., 2004). Changes in the strike and dip of faults produce damage zones comprising a network or array of faults and fractures that can focus and sustain regional and local fluid flow, a prerequisite for significant gold accumulation (Sheldon and Micklethwaite, 2007). The origin of fault bends is not always clear, but potential mechanisms include intersections with fold axes, other faults, or lithological contacts (particularly those involving significant rheological contrasts), and deviations around rigid bodies (e.g. granite intrusions). The various origins of fault bends are not distinguished in this study. Bierlein (2005) reported a 'clear relationship' of fault bends and jogs to gold mineralization in the Eastern Goldfields Superterrane, but did not provide details of how the analysis was designed or detailed results. Bierlein (2005) also found a relationship between fault-hosted base metal mineralization and 'fault roughness' in the Mount Isa Inlier, Queensland. The analyses described here do not specifically address 'fault roughness', but it is noted that 'rough' faults will contain more fault bends than 'smooth' faults. Therefore, any positive relationship between gold and fault jogs and bends will be at least equally applicable to faults that incorporate numerous irregularities such as fault jogs and bends.

For this study, fault bends have not been distinguished from fault jogs because it is considered likely that both would be portrayed as fault bends on regional-scale maps. They are therefore referred to collectively as fault bends in the remainder of this section. Fault bends were generated from the same regional fault files used for regional fault proximity (*projected fault_system* shape file for the Eastern Goldfields Superterrane; *geolin01* shape file for other areas) by using the Fault Bend Analysis tool of MapInfo Spatial Data Modeller. Fault bends were defined as those exhibiting bend angles between 5 and 15°, and bend lengths between 200 and 5000 m. For the Eastern Goldfields Superterrane, fault bends were classified as either clockwise or anticlockwise bends, according to the direction of strike variation. This classification is more objective than trying to classify fault bends as dilational or contractional: firstly, because the kinematic movement sense of the faults is not always known and, secondly, because many regional faults have been reactivated under variable stress orientations (e.g. Davis et al., 2010; Henson, et al., 2010; Miller et al., 2010) so that clockwise bends may reflect either dilational or contractional stresses at different stages of their movement history. Fault bends in the Southern Cross and Murchison domains were not classified as clockwise or anticlockwise.

For the Eastern Goldfields Superterrane, the spatial analysis relating gold endowment to regional fault bends yields a maximum %Endowment/%Area ratio of 11.9 within the 1000 m buffer (Table A1.65). Within this buffer, 35.9% of the gold endowment is captured within 3.0% of the area of the Eastern Goldfields Superterrane (Fig. 1.44). Successively larger buffers result in consistently decreasing endowments and %Endowment/%Area ratios. This result compares with a maximum %Endowment/%Area ratio of 5.90 (also for the 1000 m buffer) generated by the proximity analyses for regional faults (see Targeting Criterion 1.7), thus illustrating that fault bends are approximately twice as prospective for gold compared to the undivided regional faults that host the bends. A separate analysis of clockwise and anticlockwise fault bends (Tables A1.66 and A1.67) shows that anticlockwise bends are slightly more prospective than clockwise bends and that selective targeting of either is almost three times more efficient than targeting undivided faults. For example, the %Endowment/%Area ratio is 18.4 for a 1000 m buffer around anticlockwise bends (Table A1.67), compared with a maximum %Endowment/%Area ratio of 5.90 for a 1000 m buffer around regional faults (Table A1.56). The foregoing results are influenced by capture of the giant Golden Mile deposit within the 1000 m buffer. However, deposit density also decreases consistently in successive buffers around fault bends, in this case from the most proximal buffer at 500 m. This is true for undivided, clockwise, and anticlockwise fault bends (Table A1.65 to A67). The 500 m buffer around anticlockwise fault bends captures 4.9% of deposits in 0.6% of the analysis area, equivalent to 0.093 deposits/km^2, which is 8.4 times the average for the Eastern Goldfields Superterrane.

Regional fault bends (undivided) in the Southern Cross domain also produce a peak %Endowment/%Area ratio (49.0) associated with the 1000 m buffer (Table A1.68). This buffer accounts for 21.0% of the gold endowment of the Southern Cross domain within only 0.4% of the total area of the analysis (Fig. 1.45). Progressively larger buffers are associated with sharply declining %Endowment/%Area ratios. As was the case for the Eastern Goldfields Superterrane, the peak deposit density is achieved by the most proximal (500 m) buffer, but this captures only 0.4% of the deposits in 0.1% of the analysis area. A more practical interpretation of the results suggests that 11.2% of deposits is captured in 5.7% of the analysis area using a 4000 m buffer. The deposit density in this buffer (0.005 deposits/km^2) is approximately twice the average for the Southern Cross domain (Table A1.68).

Spatial analysis relating gold endowment to regional fault bends in the Murchison domain yields results that imply a much broader spatial association with gold mineralization. The maximum %Endowment/%Area ratios of 12.4 is achieved within the 5000 m buffer, although the ratio for the 3000 m buffer (11.7) is only a little lower (Table A1.69). The 5000 m buffer captures 60.4% of the gold endowment in only 4.9% of the analysis area (Fig. 1.46). The highest deposit density is similarly generated by a relatively wide buffer (4000 m), which captures 32.5% of the deposits in 3.3% of the analysis area (Table A1.69). The 4000 m buffer contains 0.032 deposits/km^2, almost ten times the average for the analysis area. The reason for the much broader association of gold with fault bends compared to the Eastern Goldfields Superterrane and Southern Cross domain is not known, but may reflect

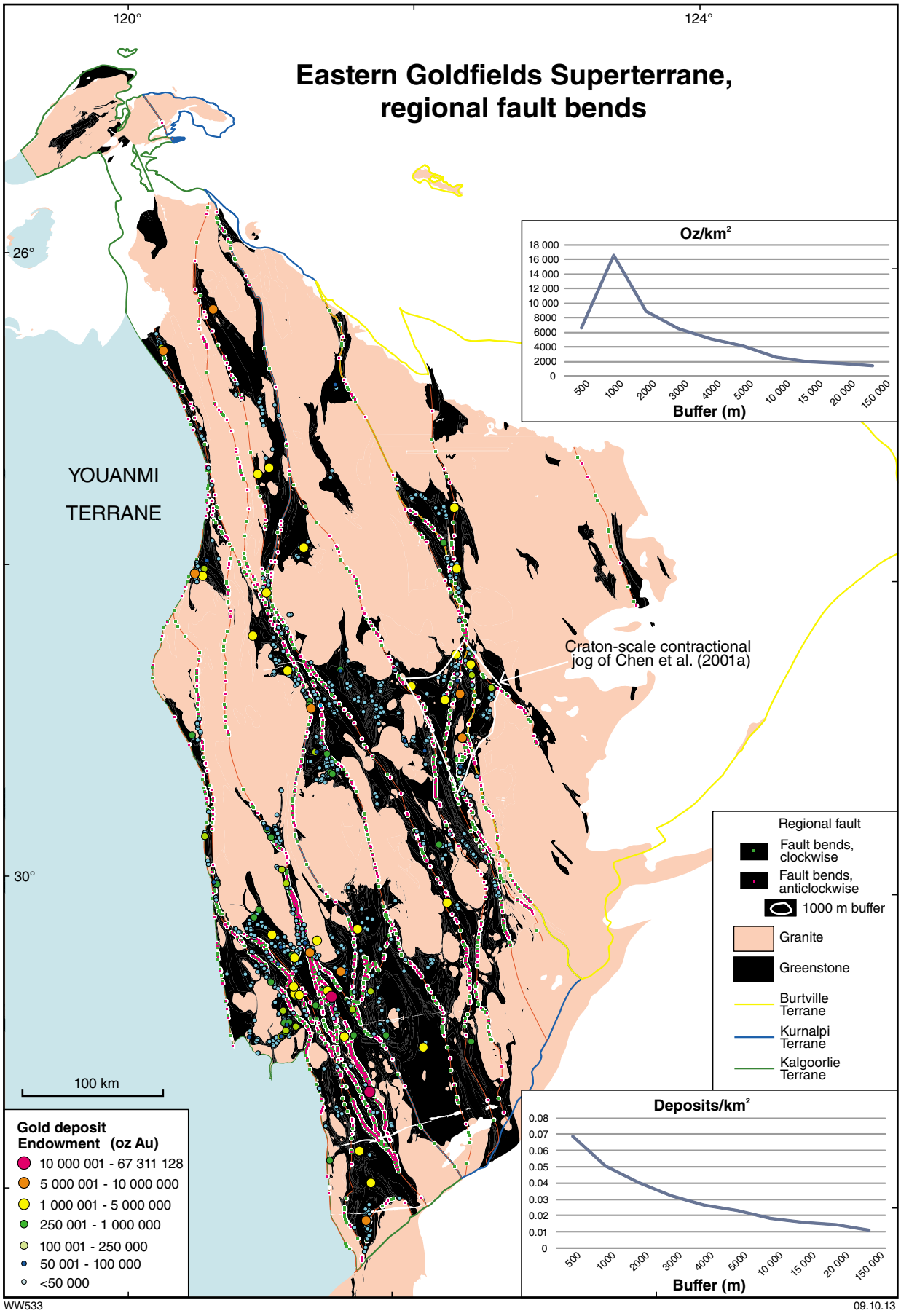

Figure 1.44. Distribution of gold deposits in the Eastern Goldfields Superterrane relative to regional fault bends

poorer definition of regional faults in the shape file used for the Murchison domain. The inconclusive trends of the curves for endowment and deposit density versus buffer distance (Table A1.69) may reflect inaccuracy in the underlying regional fault files. Fault bends nevertheless appear to represent a reasonably effective broad-scale targeting tool in the Murchison domain.

The results presented above demonstrate a strong association between gold mineralization and fault bends at regional scale, with evidence from the Eastern Goldfields Superterrane indicating little difference in the prospectivity of clockwise versus anticlockwise fault bends. The clockwise and anticlockwise fault bends cannot be translated into dilational and anti-dilational categories, unless the sense of strike-slip movement on the faults is known. As a generalization, the strikes of most regional faults in the Eastern Goldfields Superterrane range from approximately northwest to north and the regional stress vector during the major gold mineralization event is generally agreed to be approximately east–west (e.g. Groves et al., 2000). Under these circumstances, the strike-slip component of movement on regional faults is likely to be sinistral and, therefore, the anticlockwise jogs are likely to be dilational. Recent studies both at the scale of the Eastern Goldfields Superterrane and of individual gold camps (e.g. Czarnota et al., 2010a; Davis et al., 2010; Henson et al., 2010, Miller et al., 2010) concluded that a major gold depositional event took place during northeasterly to east-northeasterly shortening. In this case, the anticlockwise fault bends would have been contractional. However, significant gold camps are found in both contractional (St Ives; Nguyen et al., 1998) and dilational (Mount Pleasant; Micklethwaite and Cox, 2004) settings.

It is worth noting, in conclusion, that some large-scale fault bends or jogs are not captured by the automated technique used in this analysis. For example, the strongly mineralized Laverton Tectonic Zone has been interpreted as a craton-scale contractional jog (Chen et al., 2001a; Henson et al., 2010), but this structure was not recognized as a change of strike of a single fault by the Fault Bend Analysis function of MapInfo. At a more detailed scale, the regional approach trialled here did not recognize the known jog or overstep in the Western – Far East Fault of the Laverton Tectonic Zone, which contains the Sunrise Dam deposit (Part 2 of this Atlas). Consequently, Sunrise Dam is not captured until the 4000 m buffer is considered in this regional analysis, whereas the manual analysis presented in Part 2 (Targeting criterion 2.6) of the Atlas indicates that this world-class deposit is within a dilational fault jog. From these observations, it can be surmised that the association between gold and fault bends or jogs has probably been underestimated by the spatial analysis reported here.

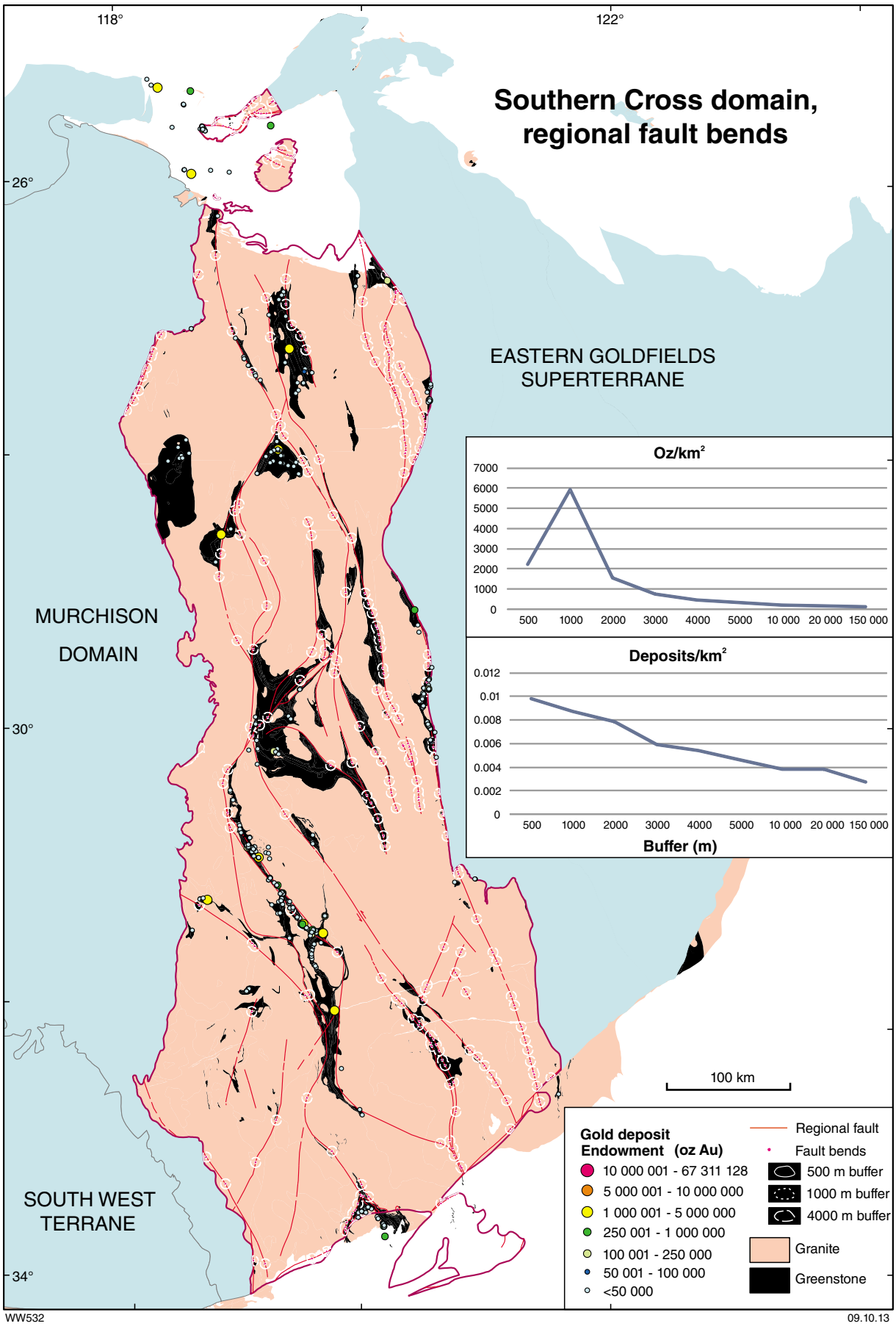

Figure 1.45. Distribution of gold deposits in the Southern Cross domain relative to regional fault bends

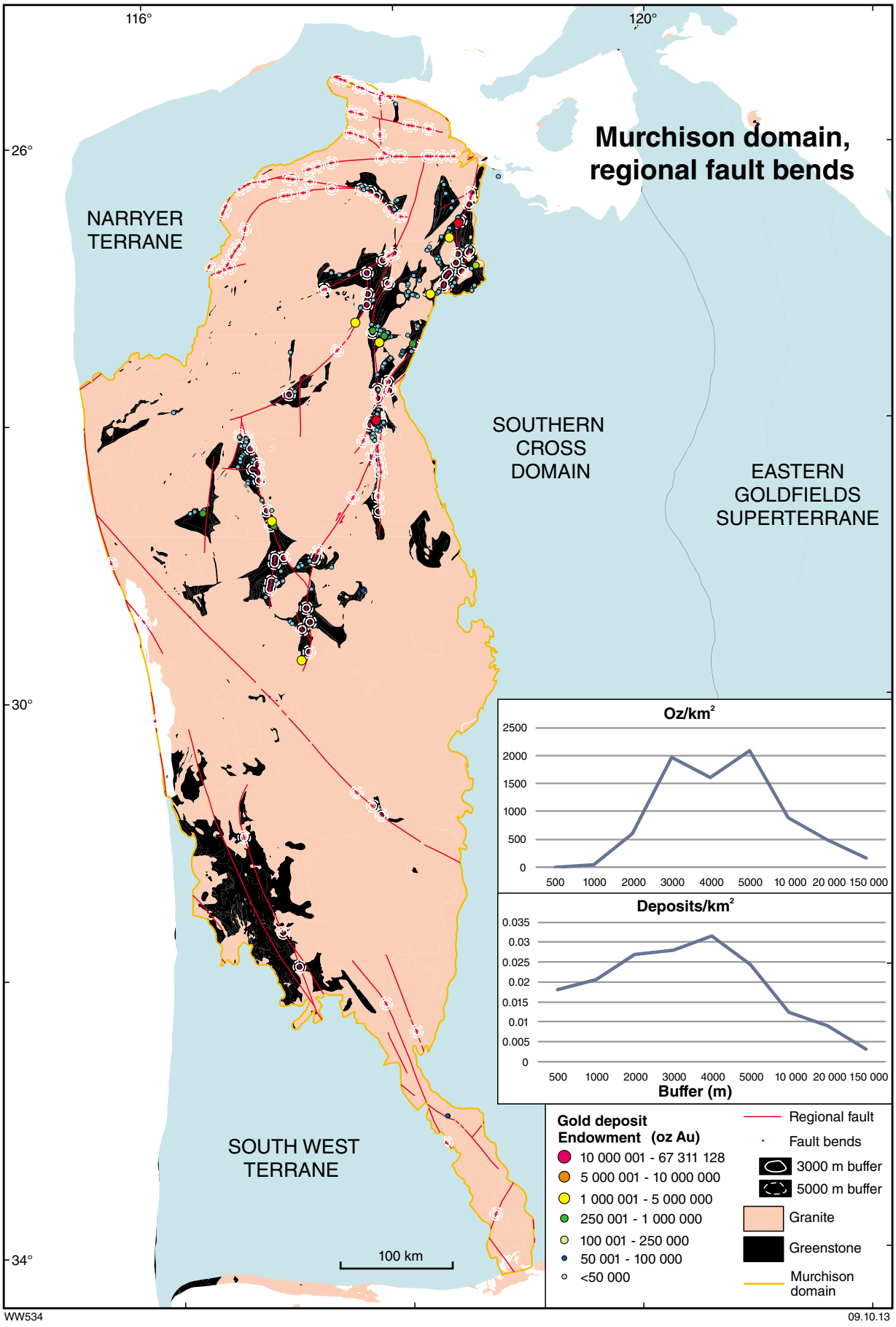

Figure 1.46. Distribution of gold deposits in the Murchison domain relative to regional fault bends

Targeting Criterion 1.11: Fault vergence anomalies

Seismic traverses across the Eastern Goldfields Superterrane show that most of the regional faults dip at moderate angles to the east, suggesting a westerly vergence (Swager et al., 1997; Goleby et al., 2004). On seismic sections, a few of these major faults display evidence for a westerly dip and therefore represent vergence anomalies. The possible significance of west-dipping structures for gold exploration was first identified by Hall (1998) using the Bardoc Tectonic Zone as an example. Hall (1998) postulated that anomalous west-dipping faults might focus fluid flow into the upper crust from deeper sources. Other prominent individual west-dipping faults include the Zuleika Shear Zone and the Emu Fault (Figure 1.47). Areas in which several closely spaced faults show evidence of anomalous westerly dips are shown as west-dipping fault domains in Figure 1.47. Anomalous west-dipping fault domains (which include two or more west-dipping faults) include those bounded by the east and west Zuleika Faults, a domain west of the Speedway Fault, another east of the Boorara Shear Zone, and, further east, the Laverton Tectonic Zone. West-dipping structures have been identified from seismic data, but major seismic transects were not available at the time of the analyses presented here for the Southern Cross and Murchison domains. Therefore, the spatial analyses are limited to the Kalgoorlie and Kurnalpi Terranes (Fig. 1.47). Even in the Eastern Goldfields Superterrane, regional seismic traverses have been recorded only in the south (around 30.5°S) and central (around 29°S) areas. West-dipping faults have been extrapolated into the northern part of the Eastern Goldfields Superterrane but further seismic surveys are required to confirm the dips of the faults in the north.

The spatial analysis of west-dipping fault domains shows that they contain 3.2% of deposits and 9.1% of the endowment in greenstones of the combined Kalgoorlie and Kurnalpi Terranes (Table A1.70). However, the endowment of individual domains is quite variable, from no endowment in the Speedway anomalous domain to 2.7% of deposits and 8.4% of endowment in the Laverton Tectonic Zone. In comparison with the combined Kalgoorlie and Kurnalpi Terranes, west-dipping fault domains contain 9049 oz/km^2 and 0.025 deposits/km^2, representing respectively 2.2 times and 0.8 times the averages for the entire analysis area. Only the Laverton Tectonic Zone shows a greater than average deposit density (0.037 deposits/km^2). Because the endowment is greater than the average and the deposit density less than the average, it can be concluded that deposits hosted by domains of anomalous fault vergence contain deposits of larger average size than the combined Kalgoorlie and Kurnalpi Terranes (Table A1.70). This result is particularly significant in that the Golden Mile deposit lies outside the anomalous vergence domains. It is noteworthy that there is a strong spatial association between domains of anomalous vergence and late-stage sedimentary basins (cf. Figs 1.47 and 1.59), such that significant portions of the former are probably obscured by the latter. In this respect, the greenstones beneath the unconformity at the base of the late-stage basins might be similarly endowed with larger than average gold deposits.

The spatial analysis of gold endowment in successively larger buffers around west-dipping faults (Table A1.71) shows a peak %Endowment/%Area ratio of 7.7 for a buffer of 2000 m. The 2000 m buffer captures 48.2% of the gold endowment within 6.3% of the area of the combined Kalgoorlie and Kurnalpi Terranes. The same analysis shows that the 20 000 m buffer captures 86.8% of the total gold endowment in less than 50% of the total area of the two terranes (Table A1.71, Fig. 1.47). Only four >1 Moz camps (Darlot, Mount Morgans, Carosue Dam, and Lindsays Find) are excluded by this constraint. The 2000 m buffer captures just over 20% of all gold deposits in the analysis area, including the Golden Mile. However, the maximum deposit density is achieved with the 1500 m buffer, which contains 17.5% of the deposits in 4.8% of the entire analysis area (Table A1.71). The deposit density of 0.050 deposits/km^2 is 1.5 times the deposit density for greenstones in the combined Kalgoorlie and Kurnalpi Terranes (Table A1.70). Although not directly comparable, the peak buffer around faults with anomalous vergence contains 13 451 oz/km^2 compared with 7798 oz/km^2 for the peak buffer around undivided regional faults in the Eastern Goldfields Superterrane. Similarly, the peak buffer around faults with anomalous vergence (1500 m) in the combined Kalgoorlie and Kurnalpi Terranes contains 0.050 deposits/km^2 compared with 0.038 deposits/km^2 in the peak buffer (500 m) around undivided faults in the Eastern Goldfields Superterrane (see Targeting Criterion 1.7). These comparisons between the combined Kalgoorlie and Kurnalpi Terranes and the Eastern Goldfields Superterrane are probably reasonable, given the few regional faults within the Burtville Terrane and the absence of any deposits within associated proximal buffers (Fig. 1.35).

The apparent success of proximity to west-dipping faults as a targeting criterion for gold exploration in the Eastern Goldfields Superterrane can probably be explained by the effect that anomalous vergence has on regional stress patterns. West-dipping faults and fault domains represent structural anomalies that, in turn, create stress anomalies in response to regional shortening, with the potential to generate fractures and dilation in competent rock units or at the boundaries between rock units of contrasting rheological properties (Groves et al., 1989, 2000). The generation of fractures in these domains leads to focusing of regional fluid flow with the potential to concentrate gold in the resulting fracture arrays (Ridley, 1993; Oliver et al., 1990).

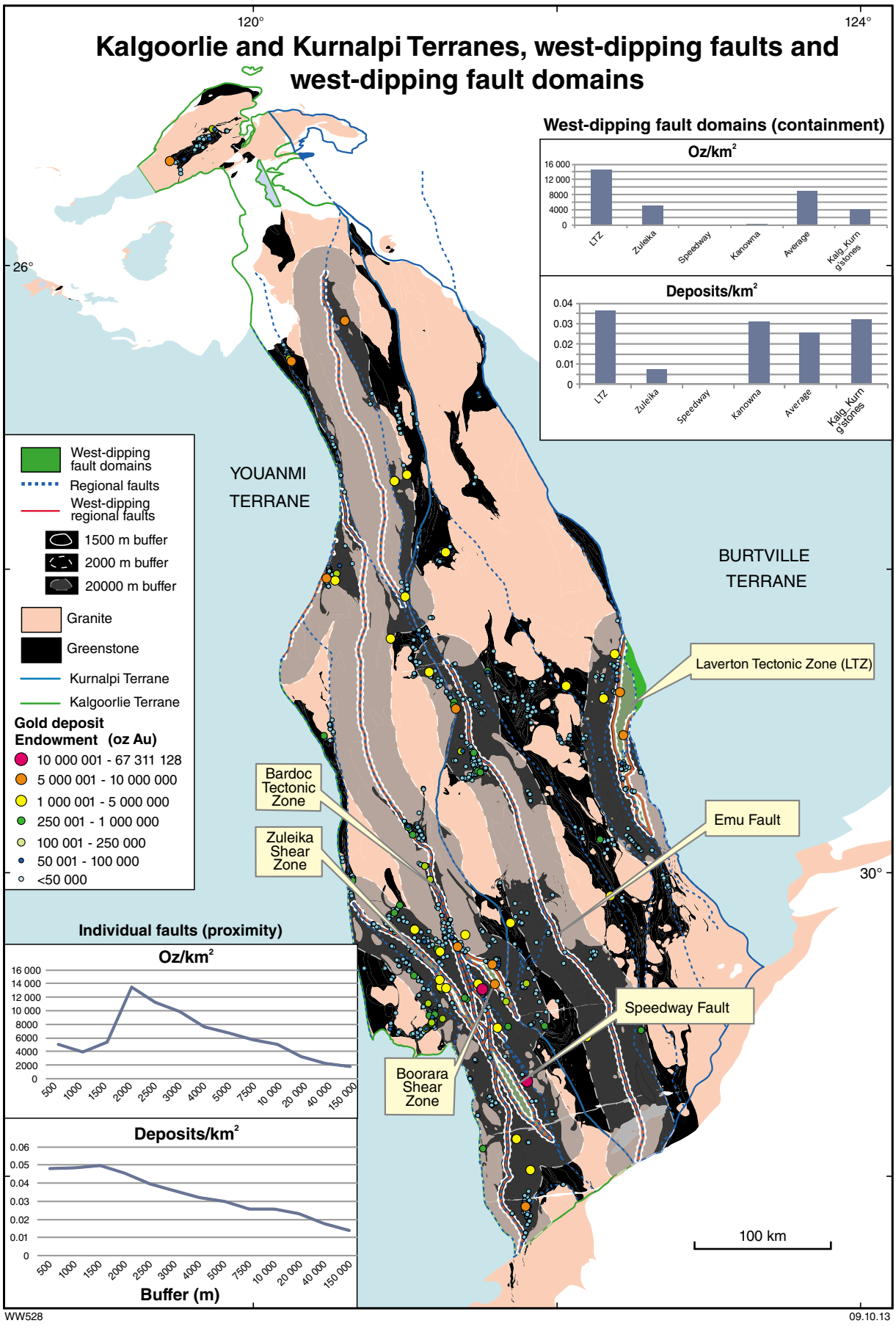

Figure 1.47. **Distribution of gold deposits in the Kalgoorlie and Kurnalpi Terranes relative to regional faults with anomalous vergence (west-dipping)**

Targeting Criterion 1.12: Constriction zones

Constriction zones (also known as bottlenecks), largely interpreted from aeromagnetic data, are areas where faults or shear zones converge. These are areas where greenstone volumes are structurally attenuated, probably through vertical movement of greenstones in response to strike-slip faulting (e.g. positive flower structures; Harding et al., 1983). The high density of faults and other structural elements in these areas creates favourable conditions for the generation of fracture and dilation as relatively thick greenstone packages are dismembered and displaced relative to one another within the limited volume of the constriction zones. Accordingly, it can be anticipated that constriction zones will be relatively favourable environments for gold mineralization, and this seems to be borne out by casual observation of some constriction zones in the Yilgarn Craton (e.g. Paddington, Fig. 1.48; Meekatharra, Fig. 1.49). For the following spatial analysis, several of the more significant constriction zones in the Yilgarn Craton have been digitized, based on aeromagnetic data and GSWA 1:500 000-scale geology maps.

A containment analysis of gold endowment in constriction zones of the combined Kalgoorlie and Kurnalpi Terranes of the Eastern Goldfields Superterrane (Table A1.72) indicates that, overall, they are better endowed (6321 oz/km^2) than the average for the combined Kalgoorlie and Kurnalpi greenstone areas (4064 oz/km^2). Similarly, gold deposits (0.057 deposits/km^2) are more abundant than the average (0.032 deposits/km^2) for greenstone areas. Relative to the greenstone areas of the Kalgoorlie and Kurnalpi Terranes, the %Endowment/%Area ratio of the undivided constriction zones (Fig. 1.48) is 1.55. However, closer inspection of the same data (Table A1.73) reveals that any prospectivity advantage (as measured by %Endowment/%Area) can be attributed almost entirely to the Paddington constriction zone, which is almost six times more prospective than the constriction zones as a whole. The Paddington constriction zone contains 37 818 oz/km^2 and 0.293 deposits/km^2. The Thunderbox and Laverton constriction zones also contain greater endowments than the average for the combined areas of greenstones within the Kalgoorlie and Kurnalpi Terranes, but the endowments of the Kathleen, Pinjin, and Davyhurst constriction zones are poor (Table A1.73). On average, the size of deposit in the constriction zones is somewhat smaller than those in undivided greenstones of the combined Kalgoorlie and Kurnalpi Terranes.

The analysis of the Murchison domain was confined to areas north of 30°S because the distribution of constriction zones in the southern Murchison is not well understood. Constriction zones in the northern Murchison domain (Table A1.74) are far better endowed (10 014 oz/km^2 and 0.113 deposits/km^2) than average greenstones of the Murchison domain (1178 oz/km^2 and 0.020 deposits/km^2), and also better endowed than the relatively fertile northern Murchison domain greenstones (1869 oz/km^2 and 0.032 deposits/km^2), where all of the known constriction zones are located (Fig. 1.49). The average size of deposits in the constriction zones (88 249 oz) is also greater than the average for the north Murchison greenstones (57 425 oz), though this comparison relies heavily on the Big Bell constriction zone (Table A1.74). However, the absolute endowment of constriction zones (~5.6 Moz Au) in the northern Murchison is relatively low (22.25% of the northern Murchison greenstone total). Individually, the Meekatharra, Tuckabianna, and Big Bell constriction zones are better endowed (in oz/km^2) than the average northern Murchison greenstones, but all have greater than average deposit densities (Table A1.74). The prominent endowment of the Big Bell constriction is of uncertain significance because it is almost entirely attributed to the Big Bell deposit. Big Bell has been interpreted by some (e.g. Phillips and De Nooy, 1988) as a pre-metamorphic deposit, so the geological rationale behind the putative prospectivity of the constriction zones may not apply to the Big Bell constriction. However, the timing of gold mineralization at Big Bell, with respect to metamorphism, is contentious (e.g. Mueller et al., 2008; Wilkins, 1993).

The results of the above spatial analyses suggest that constriction zones contain more gold ounces and gold deposits per square kilometre than the average for greenstones in the same geological terrane. However, the endowment captured by constriction zones is small compared to the total gold endowment of the host terrane, and the endowment of individual constriction zones is very variable. Constriction zones have rarely been emphasized in analyses of gold mineralization in other Archean terranes, so there are few examples that can be used for comparative purposes. In one example, Bateman et al. (2008) identified a constriction domain in a contractional jog on the Porcupine–Destor Fault, Abitibi greenstone belt, Canada, with which gold mineralization at the Dome and Buffalo–Ankerite mines is spatially associated. However, mineralization at these deposits largely pre-dates constriction and only the late-stage ladder veins at Buffalo–Ankerite may be genetically related to the constriction event.

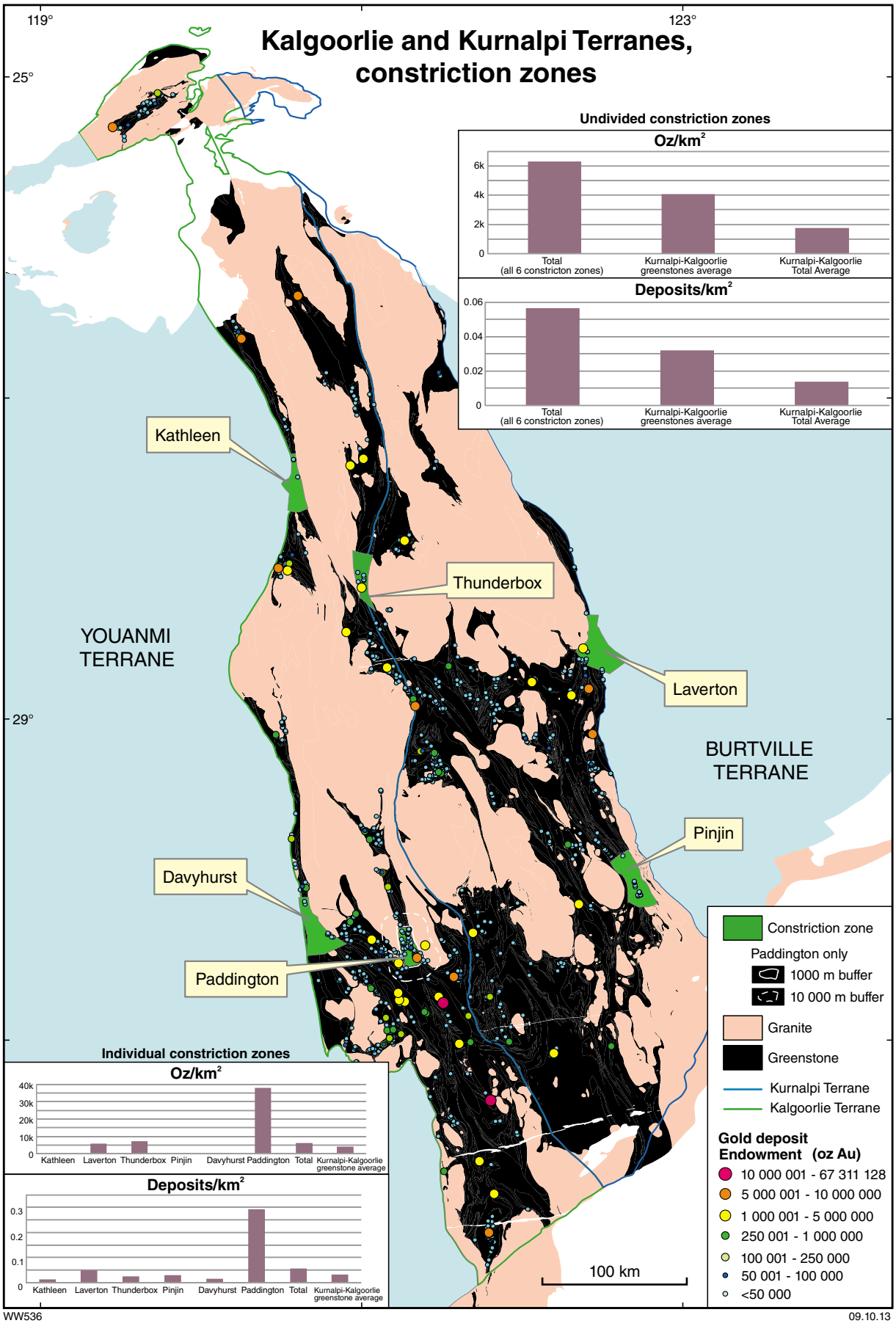

Figure 1.48. **Distribution of gold deposits in the Kalgoorlie and Kurnalpi Terranes relative to constriction zones**

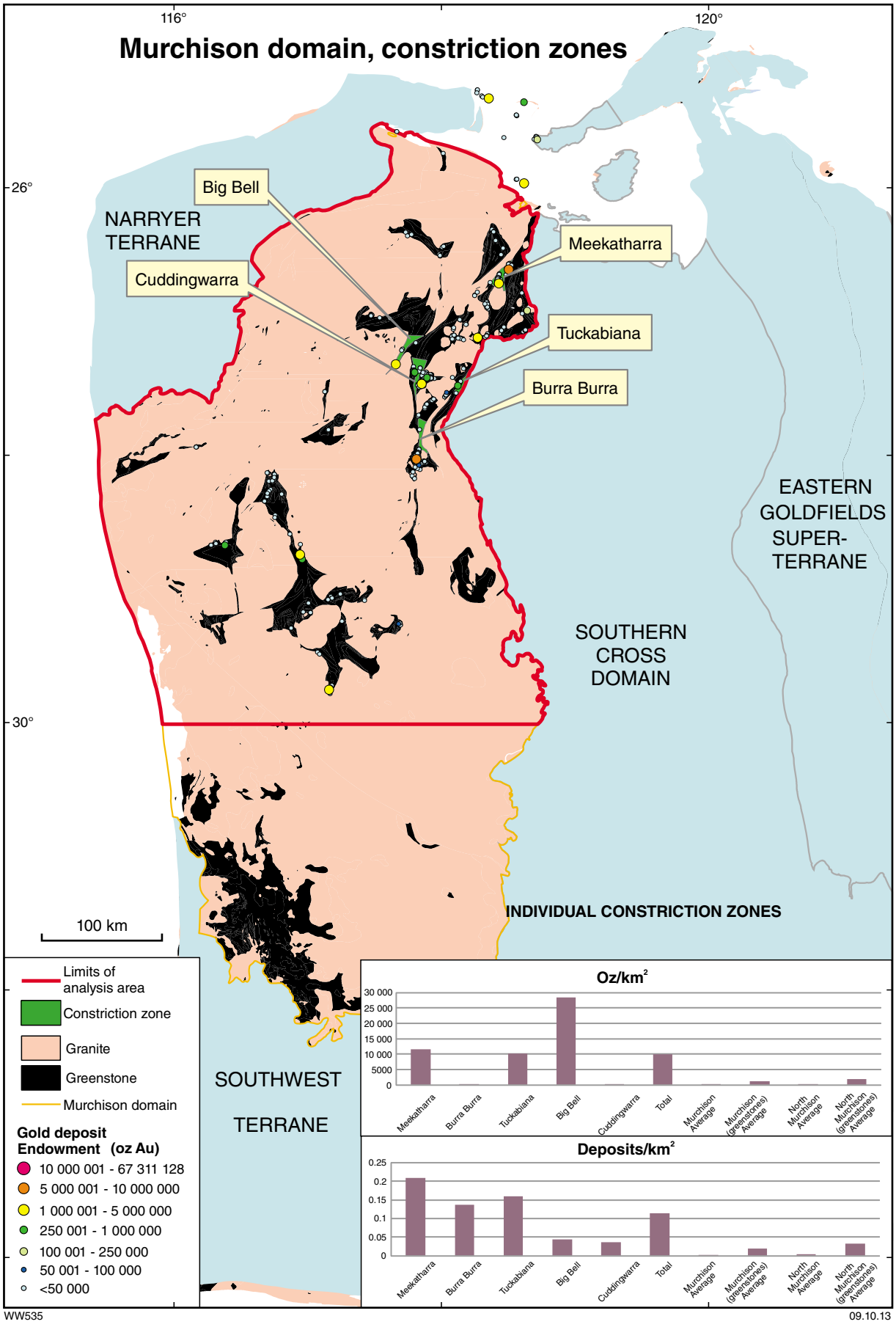

Figure 1.49. Distribution of gold deposits in the Murchison domain relative to constriction zones

Targeting Criterion 1.13: Domes

Blewett et al. (2010b), Davis et al. (2010), and Henson et al. (2010) emphasized the role of granite-cored domes and antiforms within greenstones, and domal structures in gneissic basement below the greenstones, as providing a favourable architecture for focusing fluids sourced at depth into a more confined volume of greenstones in the upper crust. These authors further proposed that strain was focused around the flanks of domes in the Eastern Goldfields Superterrane and, as a result, upward fluid flow was focused along the dome flanks and into the apical regions above the domes. In some cases, as at St Ives, it is argued that a domal shape at the base of the greenstones reflects a granitic intrusive complex (Walshe et al., 2006). This latter view emphasizes the dome as a source of oxidized hydrothermal fluids, rather than a structural pathway. In some ways, this aspect of gold targeting mirrors the advice of Groves and Phillips (1987) that gold is concentrated in uplifted portions of greenstone belts, including anticlines. The problem with this approach to gold targeting is to define just what are the limits of domes or otherwise uplifted regions. The pmd*CRC Y4 Project Team (2008) used gravity data to define the elevation of the base of the greenstones and defined domes as those greenstone regions projected along strike from granite domes and defined by the apex and inflection points in the depth to base of greenstones contours (Y4 Project Team, 2008, p. 65). The granite domes themselves, which are not well mineralized, are not included in the *domes_clip* shape file used for this analysis. Although an imperfect representation of areas of uplifted greenstones, the shape file resulting from the pmd*CRC Y4 Project Team (2008) investigation has been used here as the best available basis for a spatial analysis relating domes to gold mineralization. Availability of data restricts the spatial analysis to part of the Eastern Goldfields Superterrane (Fig. 1.50). Note that the extent of the *domes_clip* shape file does not fully cover either the Eastern Goldfields Superterrane or the combined area of the Kalgoorlie and Kurnalpi Terranes. However, the shape file covers roughly 90% of the latter, and the remaining 10% is relatively poorly mineralized. None of the deposits recorded in the Barrick gold database lie in the 10% of the Eastern Goldfields Superterrane that is not covered by the analysis area.

As defined here, domes occupy an area of 24 631 km^2 or 13.8% of the analysis area (including granites) and 42.3% of the greenstone areas of the Eastern Goldfields Superterrane (Table A1.75). The endowment of the domes is 7 781 987 oz, or 3162 oz/km^2, equivalent to a %Endowment/%Area ratio of 2.39. These figures can be compared with an endowment of 157 907 114 oz at 1027 oz/km^2 (equivalent to %Endowment/%Area of 0.78) outside the domes, figures that include the Golden Mile deposit at Kalgoorlie. Domes contain 768 deposits, equivalent to 0.031 deposits/km^2, compared with 1144 deposits at 0.007 deposits/km^2 outside the domes. The results of this analysis suggest that exploration within domes (as defined by the *domes_clip* shape file) is warranted. For example, in endowment terms, exploration within domes is approximately three times more likely to lead to discovery of a gold deposit, and 2.4 times more likely to result in discovery of gold ounces than random exploration within the analysis area. These comparisons do not provide a true reflection of the relative prospectivity of the domes because the domes are limited to greenstone areas, whereas the area outside the domes includes a large component of granite (Fig. 1.50). A better test is to compare the endowment of the domes with the average for greenstones in the combined Kalgoorlie and Kurnalpi Terranes and the larger Eastern Goldfields Superterrane. In fact, the endowment of the domes as defined in this analysis (3162 oz/km^2) is less than the average for greenstone areas in either the combined Kalgoorlie and Kurnalpi Terranes (4064 oz/km^2) or the total Eastern Goldfields Superterrane (3736 oz/km^2). In terms of deposit density, the endowment of the domes is similar to the average for greenstones in both the combined Kalgoorlie and Kurnalpi Terranes and the Eastern Goldfields Superterrane (Table A1.75). The average size of gold deposits in domal areas is less than that outside those areas, no doubt strongly influenced by the giant Golden Mile deposit being excluded from the domes (Fig. 1.50).

Proximity to domes was defined by buffers around dome boundaries, excluding the areas within the domes but extending outwards into both greenstone and granite areas (Fig. 1.50). The spatial analysis relating gold endowment to proximity to domes shows a nearly consistent decrease in the number of deposits in successively larger buffers, from a maximum 0.032 deposits/km^2 in the 500 m buffer (Table A1.76). The 500 m buffer contains 47.1% of the deposits in 15.9% of the analysis area. The gold endowment also declines from a maximum 3180 oz/km^2 in the 500 m buffer (%Endowment/%Area of 2.41), but peaks again at the 7500 m buffer, strongly influenced by the inclusion of the Golden Mile deposit. The 500 m buffer contains 38.4% of the gold endowment within 15.9% of the analysis area (Table A1.76). The 7500 m buffer contains 90.5% of the endowment in 37.9% of the analysis area, equivalent to a %Endowment/%Area ratio of 2.4. Interestingly, the Golden Mile deposit is in a nadir almost equidistant from four nearby domes (Fig. 1.50).

The relationships described above suggest that, contrary to the recent suggestions of Blewett et al. (2010b), Davis et al. (2010), and Henson et al. (2010), domal areas are not preferentially mineralized in comparison to the average for greenstones in the same region. The apparent advantage of targeting domes provided by the results of the containment analysis described here is almost entirely due to restriction of the *domes_clip* shape file to areas of greenstone dominance. Some very large deposits, including the Golden Mile, Sunrise Dam, Granny Smith, and, more controversially, Kanowna Belle (cf. Davis et al., 2010), lie outside interpreted dome regions (Fig. 1.50). More interestingly, a 500 m buffer around domal areas captures 38.4% of the gold endowment and 47.1% of the gold deposits in 15.9% of the analysis area. This result suggests that it is not so much the uplifted areas that are favourable for gold mineralization, but the margins of the domes, where deformation and fluid flow may have become focused as a result of strain partitioning (Davis et al., 2010).

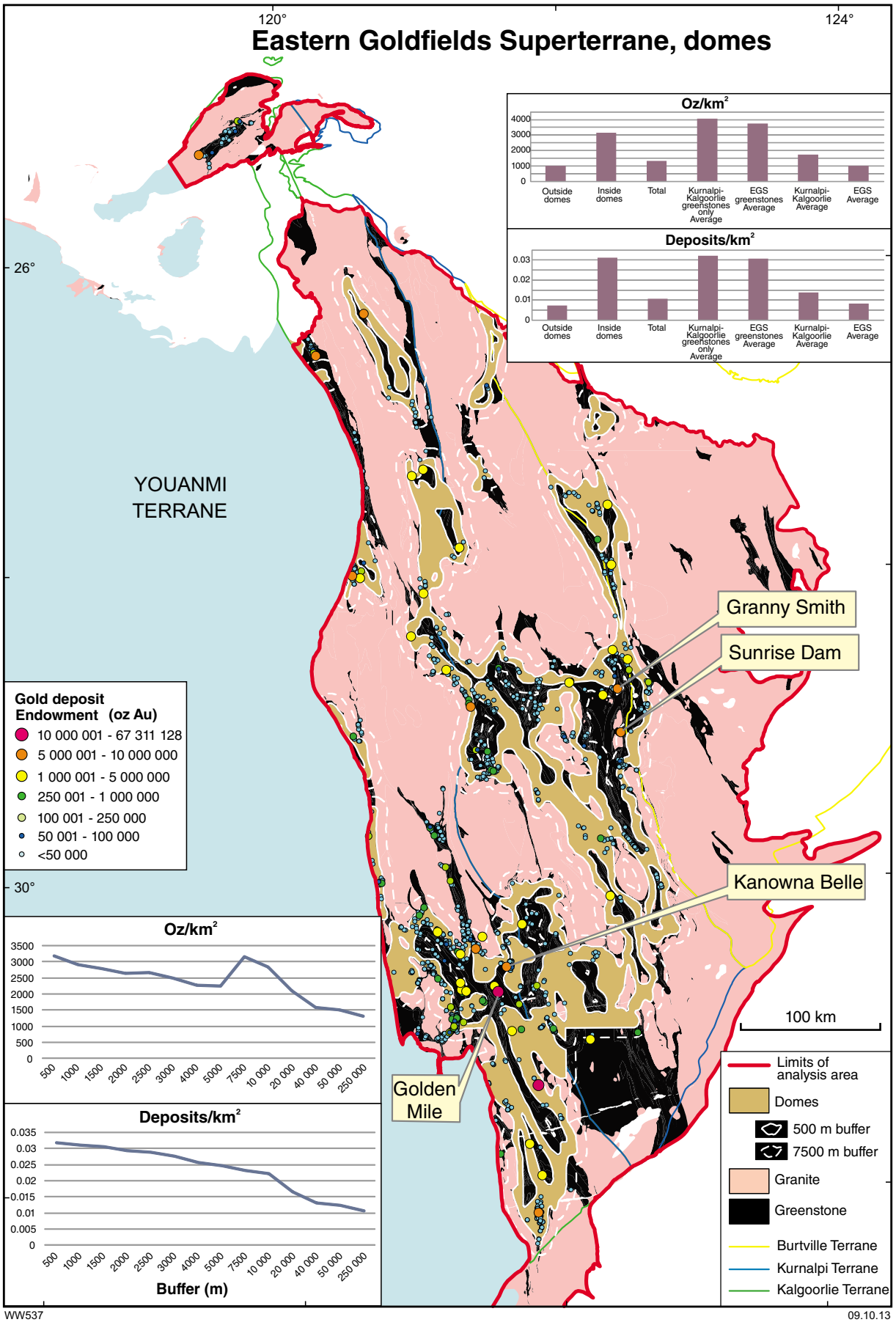

Figure 1.50. Distribution of gold deposits in the Eastern Goldfields Superterrane relative to domes

Targeting Criterion 1.14: Granite–greenstone contacts

Contacts between granite and greenstone represent sites of juxtaposition of rocks with contrasting rheological properties. In theory, the resultant competency contrasts favour failure by fracture under regional stress (Oliver et al., 1990; Ridley, 1993); many significant gold deposits in the Eastern Goldfields Superterrane (e.g. Tarmoola, Granny Smith, Wallaby, Tower Hill, Harbour Lights, and Sons of Gwalia) are in fractures at or close to contacts between granite and greenstones (Fig. 1.51). In most cases, these are the contacts of greenstones with internal granites (i.e. granite intrusions within greenstone belts; Sofoulis, 1963). In contrast, many deposits in the Southern Cross domain are close to contacts between greenstones and external granites (i.e. large areas of granite that surround greenstone belts; Sofoulis, 1963). Some granite bodies are not readily classified as internal or external (e.g. the Raeside batholith, on the margin of which lies the Sons of Gwalia deposit; the Mulliberry and Birthday complexes; the Goongarrie – Mount Pleasant and Scotia–Kanowna domes; Witt and Davy, 1993; Fig. 1.51). This ambiguity has prevented the distinction of internal and external granite contacts, so the following spatial analysis is limited to the relationship between gold endowment and undivided granite–greenstone contacts. For this Atlas, separate spatial analyses have been carried out for the Eastern Goldfields Superterrane, Southern Cross domain, and Murchison domain. Each analysis uses granite–greenstone contacts derived from the GSWA's *500k_geologyp08* shape file. The analysis area is limited to the extents of this shape file within each region. Buffers extend in both directions from the contacts, thus incorporating areas of both granite and greenstone.

For the Eastern Goldfields Superterrane, the spatial analysis relating gold endowment to granite–greenstone contacts shows gold endowment (and number of deposits) decreasing erratically in successively larger buffers, from a maximum %Endowment/%Area ratio of only 1.43 within the 500 m buffer (Table A1.77). This most proximal buffer contains 9.6% of the known gold endowment of the Eastern Goldfields Superterrane within 6.7% of the analysis area. The buffer contains 0.018 deposits/km^2 compared to an average of 0.008 deposits/km^2 for granite–greenstone areas of the Eastern Goldfields Superterrane, indicating that it is more than twice as prospective in terms of number of deposits compared to the undivided Eastern Goldfields Superterrane. The average size of deposits within the 500 m buffer is 106 141 oz of gold, a little less than the average for the Eastern Goldfields Superterrane (123 315 oz). However, because this analysis does not distinguish between internal and external granite contacts, the results might mask a more positive relationship between gold endowment and the contacts of small granite intrusions within the greenstone belts, and overestimate that relationship with external granite contacts. It is worth noting that the giant Golden Mile deposit is far from any exposed granite–greenstone contact and is captured only by the 150 000 m buffer.

Better results are produced by the spatial analysis relating gold endowment to granite–greenstone contacts in the Southern Cross domain (Table A1.78). Gold endowment decreases more or less steadily from a peak %Endowment/%Area ratio of 8.52 within the 1000 m buffer. Within this buffer, 57.4% of the gold endowment is within 6.7% of the total area of the Southern Cross domain. The maximum deposit density (0.015 deposits/km^2) is also within the 1000 m buffer and is substantially greater than the average deposit densities for both the Youanmi Terrane and the Southern Cross domain (both 0.003 deposits/km^2). The average size of deposits within the 1000 m buffer (72 181 oz) is also greater than the average deposit size for greenstones in the Southern Cross domain (47 406 oz). Granite–greenstone contacts in the Southern Cross domain are dominated by external granite contacts. Although greenstone belts in the Southern Cross domain are narrower than those in both the Eastern Goldfields Superterrane and the Murchison domain, the 1000 m buffer represents an area significantly smaller than the total area of greenstones in the Southern Cross domain (Fig. 1.52).

For the Murchison domain, the spatial analysis was restricted to the area north of 30°S because this area captures all of the gold deposits recorded in the Barrick gold deposits database for this domain (Fig. 1.53). The resultant curves are somewhat erratic, showing a maximum %Endowment/%Area ratio of 3.59 within the 4000 m buffer (Table A1.79). The 4000 m buffer also captures the maximum average deposit size (54 823 oz), slightly lower than the average (57 425 oz) for deposits in greenstones in the entire Murchison domain (the latter figure includes the largely unmineralized southern Murchison domain, Fig. 1.53). The 4000 m buffer captures virtually the entire gold endowment within the northern Murchison domain within 27.8% of the analysis area. Similarly, the 3000 m buffer captures 78.6% of the gold endowment within 22.3% of the total area. The peak deposit density (0.023 deposits/km^2) is captured by the 2000 m buffer, which contains 72.6% of the deposits in 16.0% of the analysis area. The average deposit density for the Murchison domain is 0.020 deposits/km^2, although this includes the largely unmineralized southern Murchison domain.

The results of spatial analyses relating gold endowment to granite–greenstone contacts shows that there is an advantage in directing exploration towards these contacts. Buffer distances of 500 to 1000 m are most effective in the Eastern Goldfields Superterrane and Southern Cross domain, but the advantage in the Eastern Goldfields Superterrane, particularly in terms of ounces per square kilometre, is limited. The substantially greater prospectivity advantage gained by targeting granite–greenstone contacts in the Southern Cross domain is probably influenced markedly by the concentration of deposits in the Corinthia – Hopes Hill and Frasers–Lenneberg shear zones, both of which are close to greenstone belt margins (Bloem et al., 1994; see also Targeting criterion 2.13, Atlas Part 2). The reason for the much broader peak prospectivity buffers for the Murchison domain analyses compared to those of both the Southern Cross domain and the Eastern Goldfields Superterrane is unclear, but is in accord with less satisfactory results for several other criteria for the Murchison domain (e.g. proximity to regional faults). For the Yilgarn Craton as a whole, it is concluded that greenstones within a few kilometres of granite–greenstone contacts are relatively well-endowed in terms of numbers of deposits but, within that distance there is only a modest advantage in terms of expected ounces per square kilometre or average size of deposit.

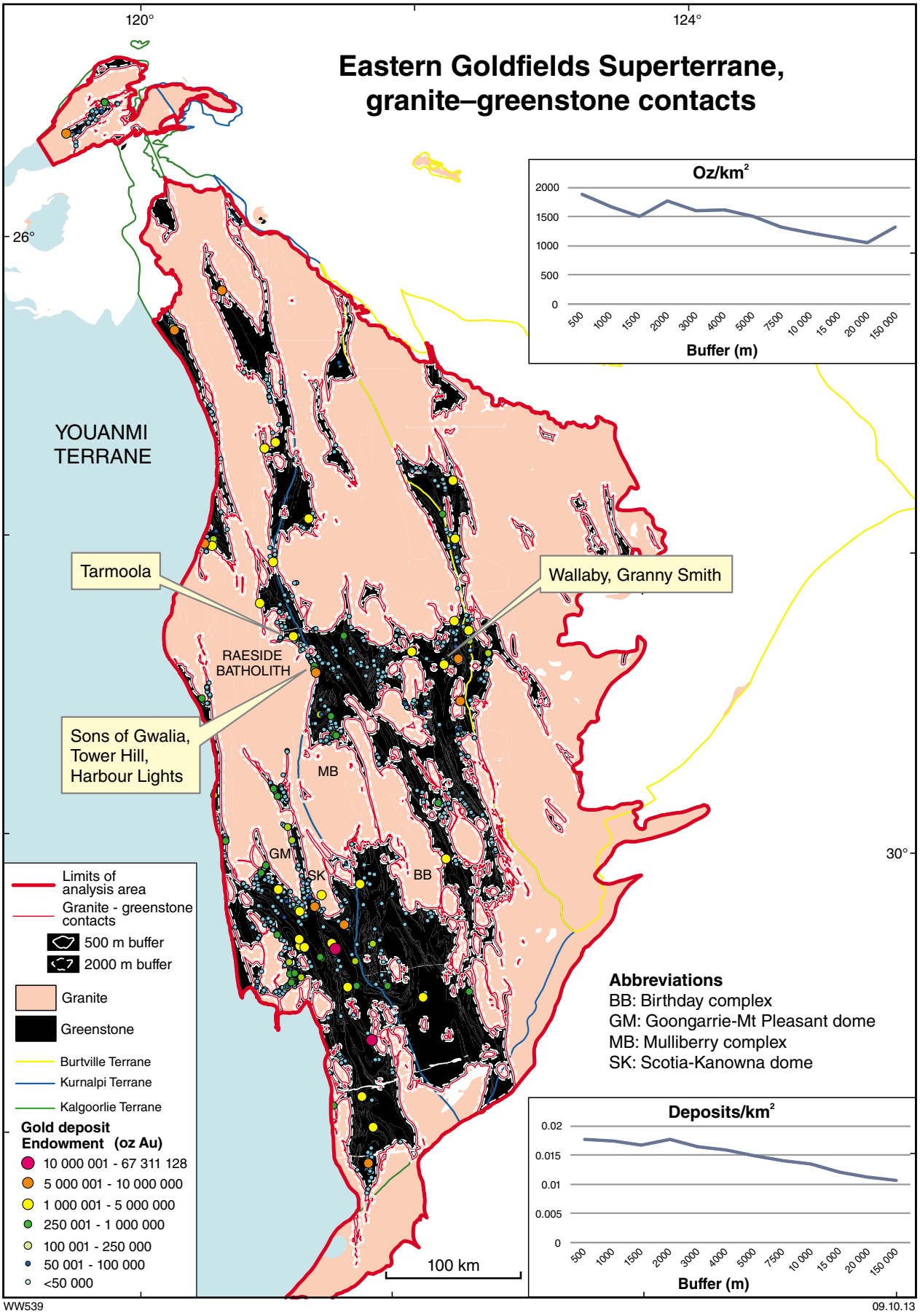

Figure 1.51. Distribution of gold deposits in the Eastern Goldfields Superterrane relative to granite–greenstone contacts

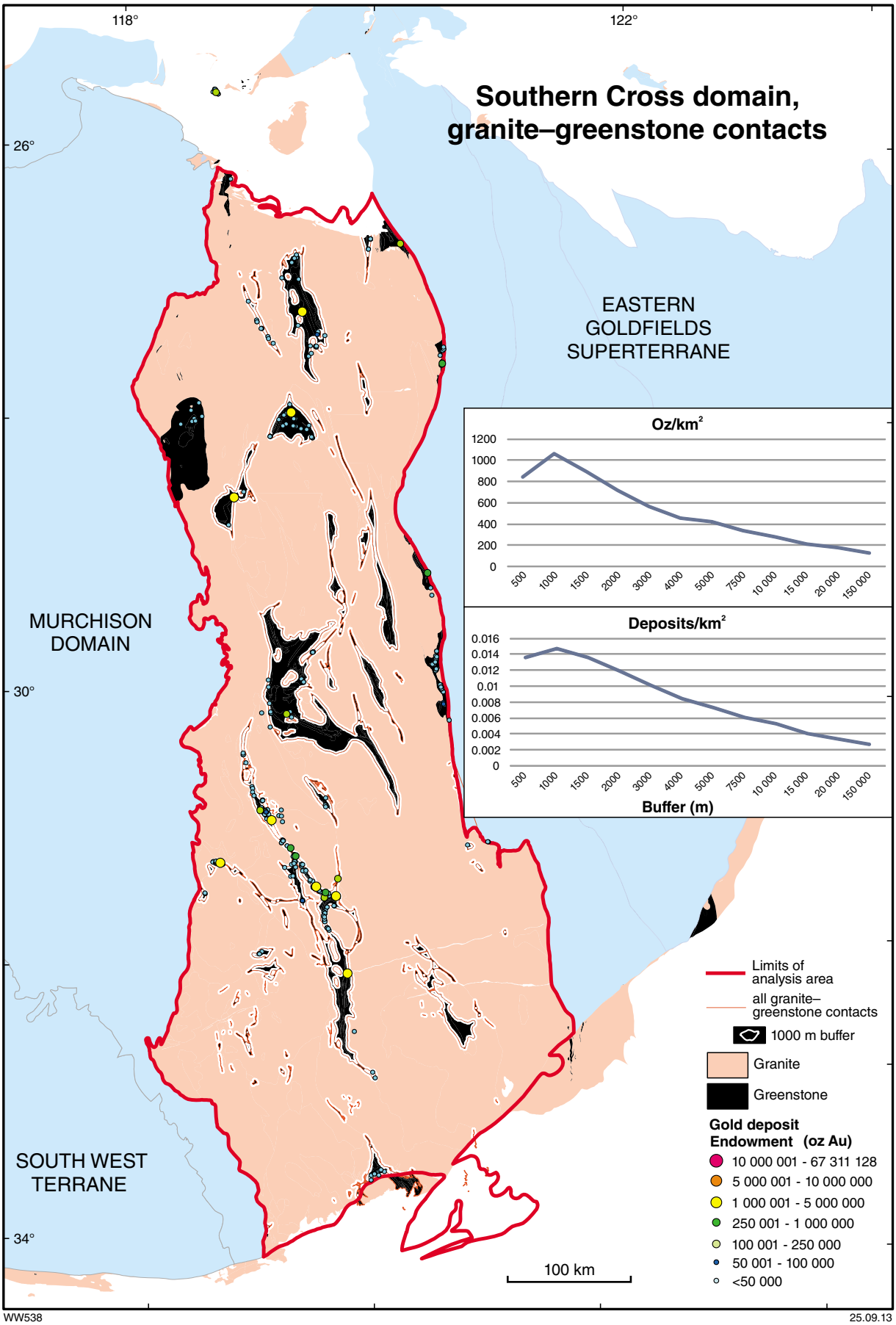

Figure 1.52. **Distribution of gold deposits in the Southern Cross domain relative to granite–greenstone contacts**

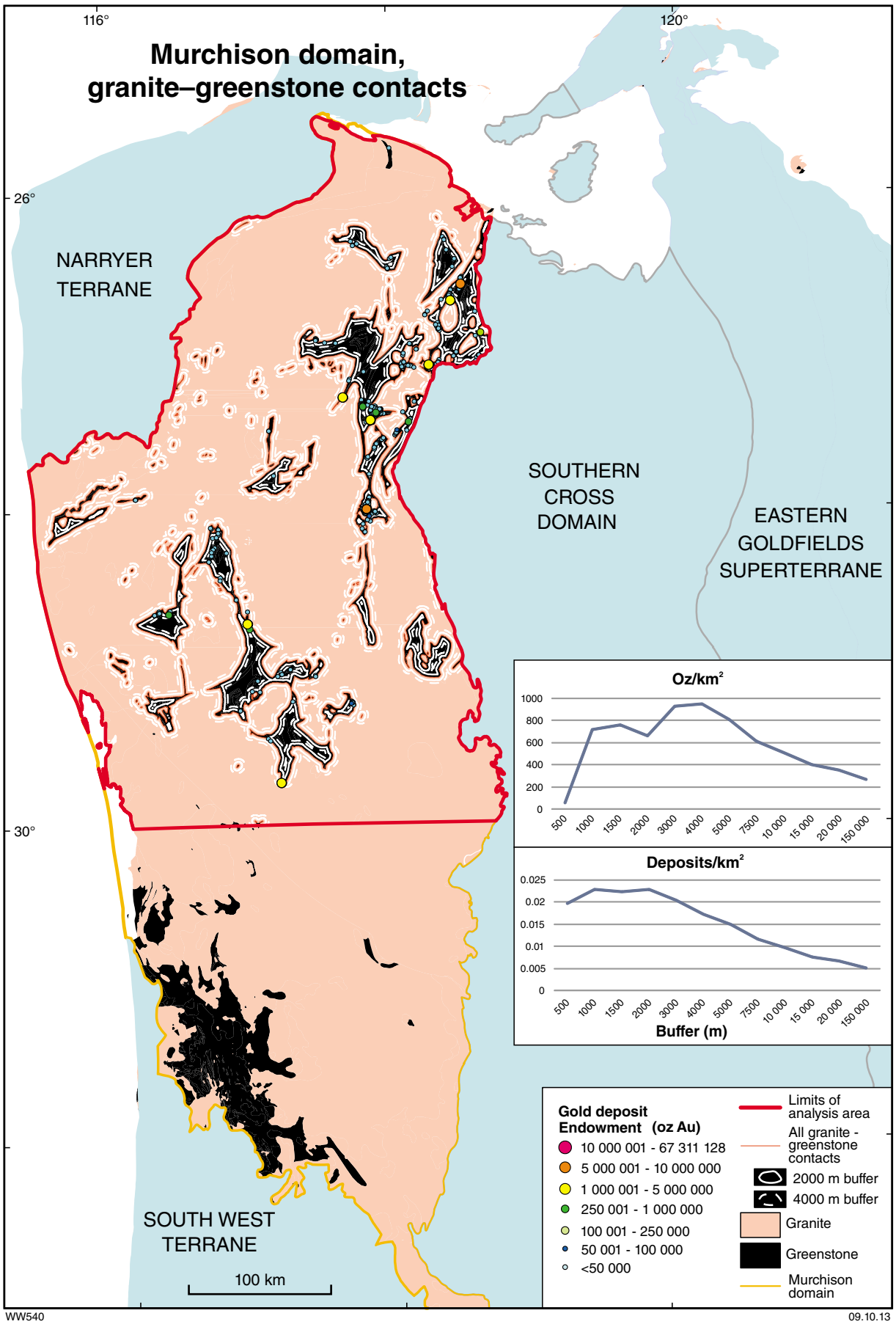

Figure 1.53. Distribution of gold deposits in the northern Murchison domain relative to granite–greenstone contacts

Targeting Criterion 1.15: Regional metamorphic domains and regional strain

In a detailed metamorphic study of a major part of the Eastern Goldfields Superterrane, Goscombe et al. (2009) recognized four significant metamorphic episodes (M_a, M_1, M_2, and M_3). The areal extents of the assemblages representing M_a and M_1, which formed during greenstone deposition, are quite restricted and are not included in the spatial analyses described here. The M_2 event was broadly contemporaneous with the earliest shortening deformation and emplacement of early High-Ca granites (Y4 Project Team, 2008). M_2 assemblages are dominant in the Eastern Goldfields Superterrane. M_3 was a long-lived event extending from c. 2665 to 2620 Ma. Early M_{3a} was contemporaneous with regional extension and emplacement of mantle-derived intrusions (Mafic granites and Syenitic granites). M_{3a} assemblages are closely related to the formation of late-stage sedimentary basins and are found mainly in spaced zones of D_3 extension and in the overlying upper-plate greenstones. Metamorphism during M_{3a} lagged D_3 by 5 to 10 m.y. (Y4 Project Team, 2008). Later M3b metamorphism was dominated by hydrothermal alteration at gold depositional sites and shear zones and M3b assemblages have a widespread but patchy distribution (Goscombe et al., 2009). Spatial analyses presented here were confined to the intersection of the dataset of Goscombe et al. (2009) with the limits of the exposed Eastern Goldfields Superterrane (i.e. within the area of the combined Kalgoorlie, Kurnalpi, and Burtville Terranes).

Some models for gold mineralization in the Yilgarn Craton appeal to metamorphic fluids generated at the amphibolite–greenschist transition as a source of ore fluids (Powell et al., 1991; Phillips and Powell, 2010). Given that M_2 and M_{3a} are inferred to be the volumetrically dominant metamorphic events and are most closely related in time to the gold depositional event, these were the metamorphic events chosen for investigation in this study. Goscombe et al. (2009) produced maps showing the locus of D_3 deformation and the upper plate during D_3 extension, and a total accumulated strain map. The relationships of gold endowment to these features have also been investigated here. The relationship between gold endowment and M_{3b} metamorphism could not be quantitatively investigated because no maps showing the distribution of M_{3b} assemblages are available. However, a close relationship can be anticipated because M_{3b} metamorphism is defined by gold-related hydrothermal alteration (Goscombe et al., 2009). Witt (1991) and Witt et al. (1997) demonstrated a spatial correlation between the metamorphic field gradient and the thermal stability of the alteration assemblages in gold deposits (M_{3b} of Goscombe et al., 2009) in the southern Kalgoorlie Terrane. However, the metamorphic field gradient in those studies is the end product of several temporally distinct but spatially overlapping metamorphic events.

The spatial analysis of the relationship between gold endowment and M_2 metamorphic facies domains (Fig. 1.54) indicates that gold is concentrated in low-pressure lower greenschist facies domains and in medium-pressure lower amphibolite facies domains (Table A1.80). This relationship is remarkable, considering that both of these facies domains contain more than three times the average gold endowment of the Eastern Goldfields Superterrane greenstones (3736 oz/km^2). All other metamorphic domains contain less gold than the average endowment of the Eastern Goldfields Superterrane greenstones. It should be noted that, in absolute terms, the medium-pressure lower amphibolite domains have a restricted distribution (1.0% of the total area) and contain a relatively small amount (5.4%) of the total endowment. On the other hand, the low-pressure lower greenschist facies domains contain 45.8% of the gold endowment in 9.2% of the total area, albeit biased by inclusion of the Golden Mile (>67 Moz Au). Ignoring the endowment of the Golden Mile in the low-pressure lower greenschist total brings the endowment of this metamorphic domain into line with the other metamorphic domains, and the revised endowment (~33 Moz Au) is approximately half of that contained in the low-pressure upper greenschist facies domains. An alternative view that avoids the bias imparted by the very large endowment of the Golden Mile is to examine the deposit density (Table A1.80). This approach shows a more even distribution of gold through the various metamorphic domains. Of the seven low-pressure facies domains that comprise >95% of the study area, the deposit density decreases fairly regularly from sub-greenschist facies domains to upper amphibolite facies domains. Only the sub-greenschist and lower greenschist facies domains contain deposit densities greater than the average for Eastern Goldfields Superterrane greenstones.

Areas of preserved M_{3a} metamorphic assemblages are within late-stage sedimentary basins and extend as thermal anomalies into adjacent greenstone areas where they overprint M_2 assemblages. These areas amount to about 25% of greenstones in the spatial analysis area (Fig. 1.55). In combination, these areas are almost three times better endowed with gold (10 424 oz/km^2, Table A1.81) compared to the average endowment for all greenstones in the Eastern Goldfields Superterrane (3736 oz/km^2). Expressed as %Endowment/%Area, the combined areas of M_{3a} metamorphism are 2.79 times more prospective than the total area of all greenstones in the Eastern Goldfields Superterrane. Again, these results are biased by the inclusion of the Golden Mile. In terms of deposit density, M3a domains (0.036 deposits/km^2) are only slightly better endowed than the average for greenstones in the Eastern Goldfields Superterrane (0.031 deposits/km^2). Amongst the subdivisions of the M_{3a} metamorphic areas, the highest %Endowment/%Area ratio (8.0) is in the small areas of contact metamorphism around some syn-M_{3a} intrusions (Fig. 1.55). This ratio is not biased by inclusion of the Golden Mile deposit, but does include Wallaby – Granny Smith and Nimary–Jundee, and represents a relatively small proportion of the total Eastern Goldfields Superterrane gold endowment (9.1%, Table A1.81).

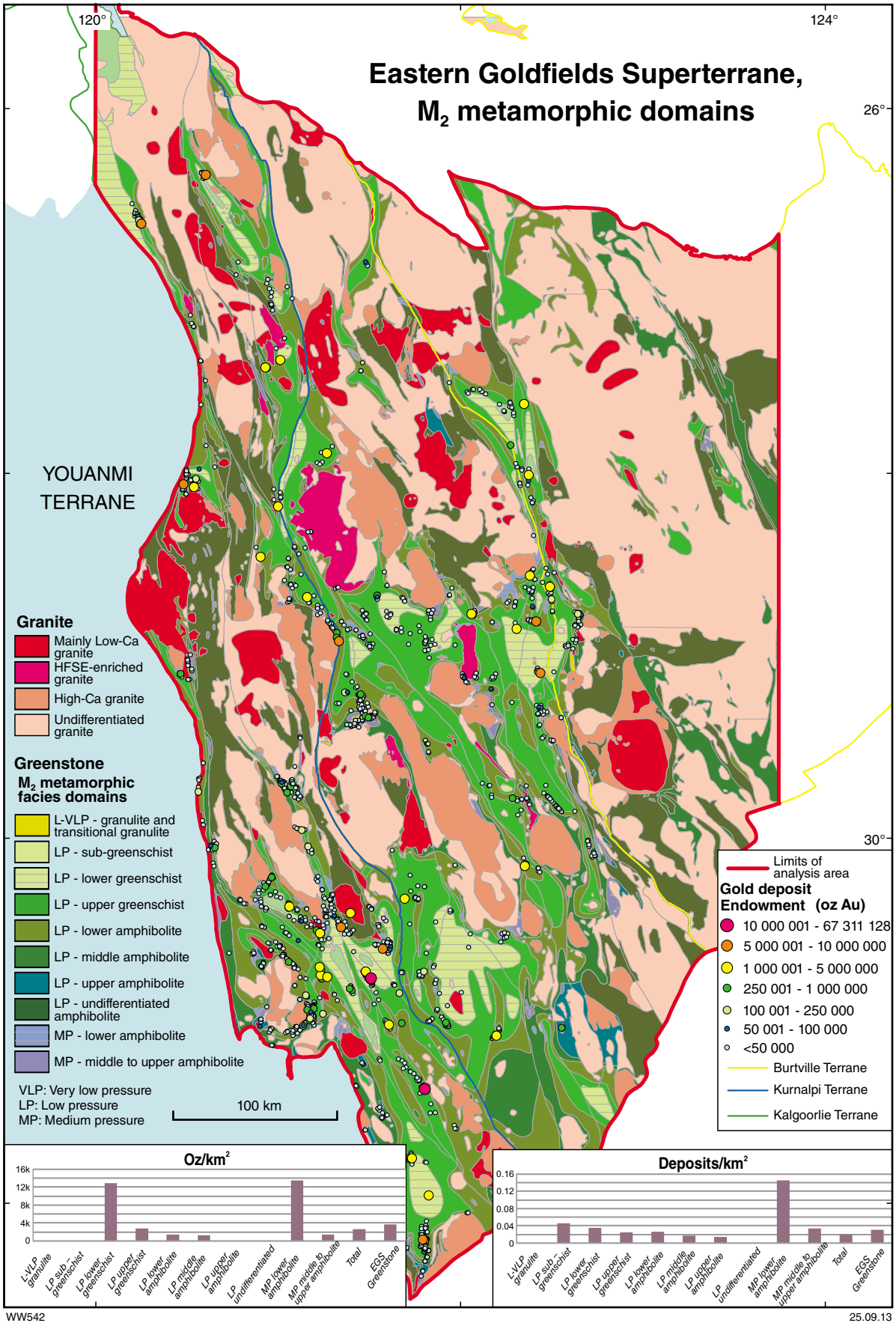

Figure 1.54. **Distribution of gold deposits in the Eastern Goldfields Superterrane relative to M_2 metamorphic domains. Best-endowed domains marked with horizontal lines.**

Areas of contact metamorphism around syn-M_{3a} intrusions have an average endowment of 83 533 oz/km^2, more than 22 times that for the Eastern Goldfields Superterrane greenstones. This association seems to reflect the proximal location of some gold deposits with respect to intrusions with a mantle source component (previously noted in Targeting Criterion 1.3). The interpreted extent of the M_{3a} thermal anomaly (Fig. 1.55) is represented by annular domains extending beyond areas of late-stage sedimentary basins where M_{3a} metamorphism has overprinted M_2 in the underlying greenstones; they represent a little over half of the total area of M_{3a} domains, but contain 85.4% of the 515 deposits within areas of M_{3a} metamorphism (Table A1.81). These annular domains represent 14.6% of the area of the Eastern Goldfields Superterrane greenstones but contain 3.9 times the endowment (57.0% of total endowment at 14 628 oz/km^2) and 1.7 times the deposit density (24.7% of all deposits at 0.052 deposits/km^2).

D_3 extensional deformation zones (i.e. the locus of the D_3 metamorphic event; Fig. 1.56) are well-endowed compared with areas (including granite) outside D_3 deformation zones (Table A1.82). However, an endowment of 2914 oz/km^2 is less than the average for all greenstone areas of the Eastern Goldfields Superterrane (3736 oz/km^2). The D_3 deformation zones have a %Endowment/%Area ratio of 2.35, representing 16.7% of the gold endowment captured within 7.1% of the spatial analysis area (Table A1.82). The giant Golden Mile deposit is not contained within the locus of D_3 metamorphism. The locus of D_3 metamorphism domains has a higher deposit density than areas (including granite) outside these domains (Table A1.82), but it is still lower than the average for the Eastern Goldfields Superterrane greenstones (0.031 deposits/km^2).

A proximity analysis relating gold endowment to D_3 deformation zones demonstrates that both endowment and deposit density decrease consistently with increasing buffer distance (Table A1.83). Buffers include and extend beyond the zones of D_3 deformation into the upper and lower plates. The curves relating these parameters to buffer distance suggest a meaningful geological relationship between the two, but the %Endowment/%Area ratios are modest, with a maximum of 1.5 in the most proximal (1000 m) buffer, within which 43.5% of the gold endowment is captured in 28.6% of the spatial analysis area (Fig. 1.56). This endowment (2325 oz/km^2) is significantly greater than the average for granite–greenstone areas of the combined Kalgoorlie and Kurnalpi Terranes (1750 oz/km^2). Deposit density in the most proximal (1000 m) buffer (0.024 deposits/km^2) is also almost twice the average for granite–greenstone areas of the combined Kalgoorlie and Kurnalpi Terranes (0.013 deposits/km^2).

The upper plate during M_3 lies above the D_3 deformation zones and is better endowed (1495 oz/km^2) than the lower plate (Table A1.84). The upper plate, which includes granite areas, has a %Endowment/%Area ratio of 1.20, representing 25.2% of the gold endowment captured within 20.9% of the spatial analysis area (Fig. 1.56). This endowment is less than that of the D_3 deformation zones, but is greater than those for both the analysis area (1241 oz/km^2) and the Eastern Goldfields Superterrane (1007 oz/km^2). The upper plate contains the giant Golden Mile deposit, thus biasing these results. The deposit density for the upper plate (0.025 deposits/km^2) is four times that of areas outside the upper plate (0.006 deposits/km^2) and three times the average deposit density (0.008 deposits/km^2) for the Eastern Goldfields Superterrane (Table A1.84). The lower plate includes higher proportions of granite (Fig. 1.56), which are less well-endowed than the greenstones. Endowment for the lower plate can be calculated as the difference between those shown as 'Outside D_3 Upper Plate' in Table A1.84 and 'Inside D_3 Locus of Meta Event' in Table A1.82. So calculated (Table A1.84), the endowment for the lower plate is relatively poor (1001.7 oz/km^2 and 0.004 deposits/km^2). However, the 592 deposits in the lower plate have a higher average size than those in the upper plate or within the locus of the D_3 metamorphic event (Table A1.84).

Goscombe et al. (2009) estimated the total accumulated strain resulting from the extended deformation history of the Eastern Goldfields Superterrane (Fig. 1.57, major faults are shown for reference). A containment analysis of the relationship between gold endowment and strain (Table A1.85) shows that only the moderate-, high-, and very high-strain domains are significantly better endowed than the average for granite–greenstone areas of the Eastern Goldfields Superterrane (1007 oz/km^2). Peak results (%Endowment/%Area of 2.12) are in domains of high strain, in which 11.9% of the endowment is contained within 5.6% of the analysis area. More usefully perhaps, 47.8% of the endowment and 32.0% of deposits are contained within domains of moderate strain, representing 27.8% of the analysis area (Table A1.85). The results for gold deposit density contrast markedly with those for endowment, as they show an almost asymptotic increase in deposit/density as strain increases (Table A1.85). This somewhat surprising result conforms with the observations that moderate-strain domains contain relatively large deposits (average 179 428 oz), and high strain domains contain more but smaller deposits (average 58 908 oz). As shown in Table A1.85, the largest deposits are preferentially located in adjacent domains of weak to moderate strain (Fig. 1.57). The larger deposit size in moderate strain domains is influenced by inclusion of the giant Golden Mile deposit, but it should be noted that weak-strain domains also have a similar average deposit size (173 155 oz). In summary, deposit density increases with increasing strain, but the larger deposits are found in weak- to moderate-strain domains that comprise about 46% of the analysis area.

In conclusion, although the M_2 metamorphism of Goscombe et al. (2009) pre-dates the main periods of gold deposition, the lower greenschist facies domains of low-pressure M_2 metamorphism are clearly the best endowed in terms of ounces per square kilometre, average deposit size, and %Endowment/%Area. These domains capture 45.8% of the total endowment and 15.7% of all gold deposits in the Eastern Goldfields Superterrane. Lower amphibolite facies domains of medium-pressure metamorphism also have a high %Endowment/%Area ratio, but are restricted in area and capture only 5.4% of

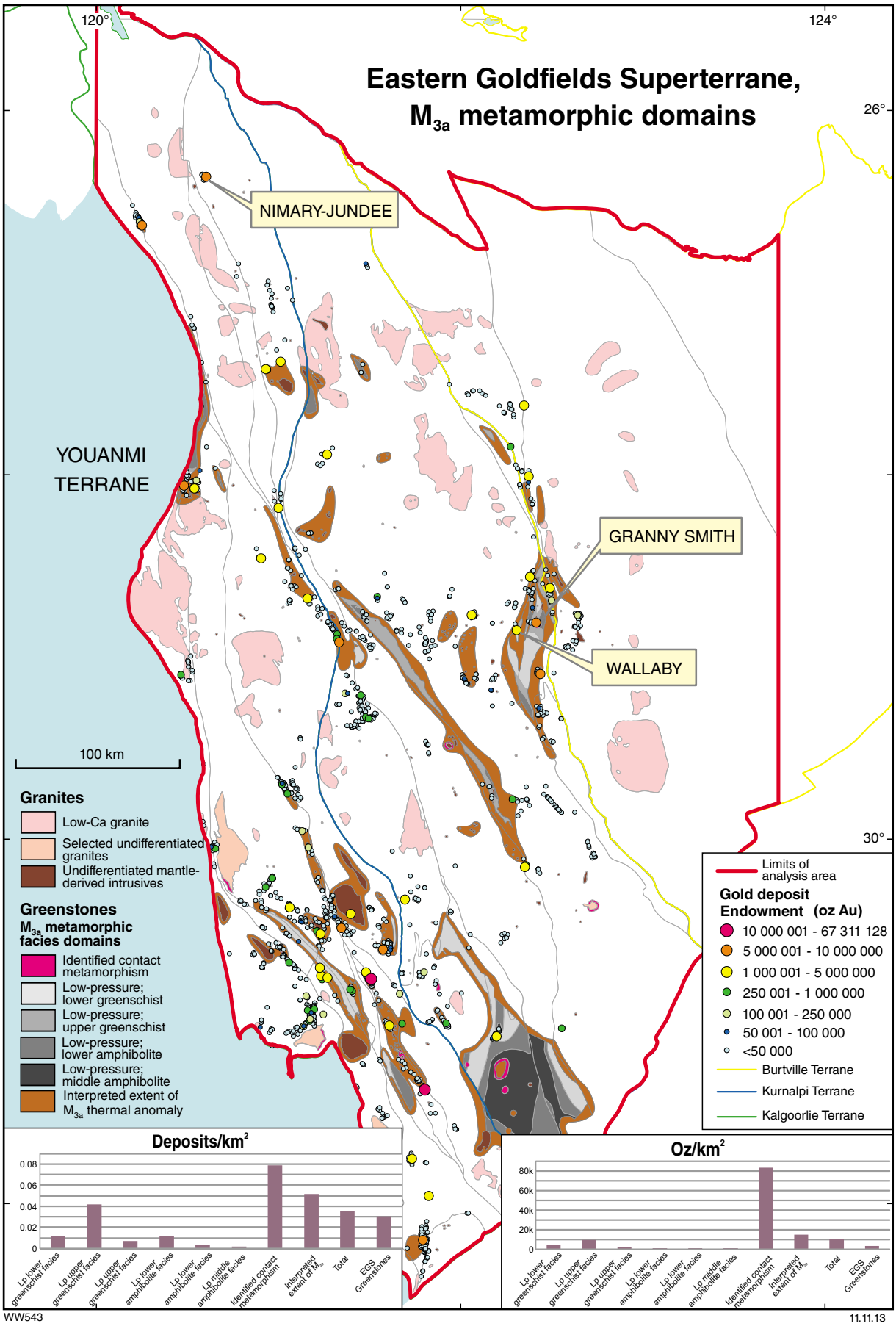

Figure 1.55. Distribution of gold deposits in the Eastern Goldfields Superterrane relative to M_{3a} metamorphic domains

the endowment and 7.3% of deposits. Areas of syn-M_3 contact metamorphism are the best endowed of the M_{3a} facies domains, but contain relatively small proportions of both total gold endowment (9.1%) and number of gold deposits (2.5%). This association is interpreted to reflect the association of some gold deposits with intrusions with a mantle-source component (mainly of the Mafic and Syenitic Groups of Cassidy et al., 2002). The loci of D_3 deformation (D_3 deformation zones) are roughly twice as prospective as undivided granite–greenstone areas of the combined Kalgoorlie and Kurnalpi Terranes. Both gold endowment and deposit density increase slightly with proximity to D_3 deformation zones, and the most proximal buffer contains a greater endowment and deposit density than undivided granite–greenstone areas of the combined Kalgoorlie and Kurnalpi Terranes. The D_3 upper plate is preferentially mineralized relative to the lower plate, but neither contain as large an endowment as the undivided greenstones in the combined Kalgoorlie and Kurnalpi Terranes. The upper plate shows almost twice the deposit density of that of undivided granite–greenstone areas of the combined Kalgoorlie and Kurnalpi Terranes, and only slightly less than that within D_3 deformation zones. Exploration for gold in the Eastern Goldfields Superterrane should target domains of moderate to high strain, which have the highest endowments and amongst the larger average deposit sizes.

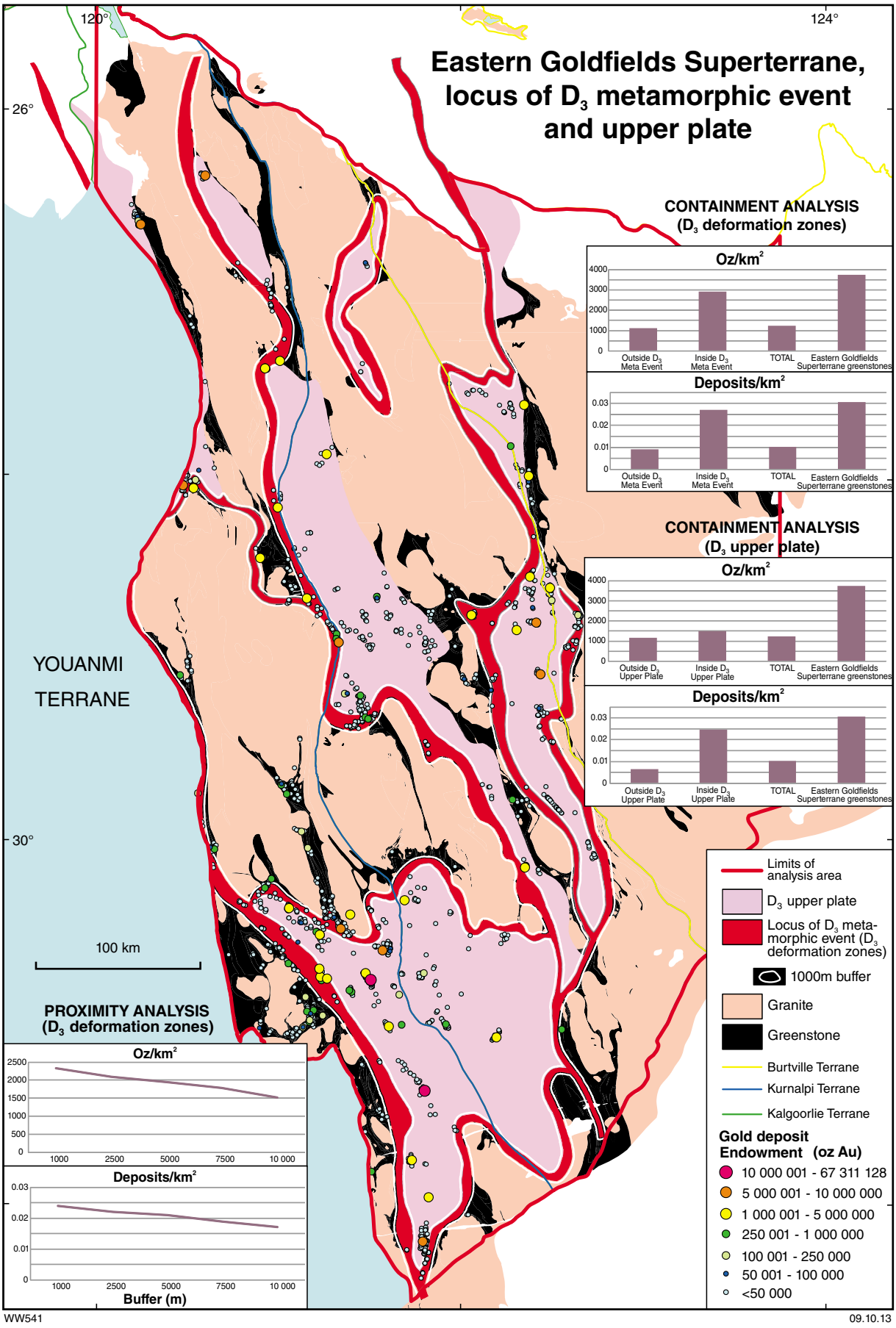

Figure 1.56. **Distribution of gold deposits in the Eastern Goldfields Superterrane relative to D_3 deformation zones and the D_3 upper plate**

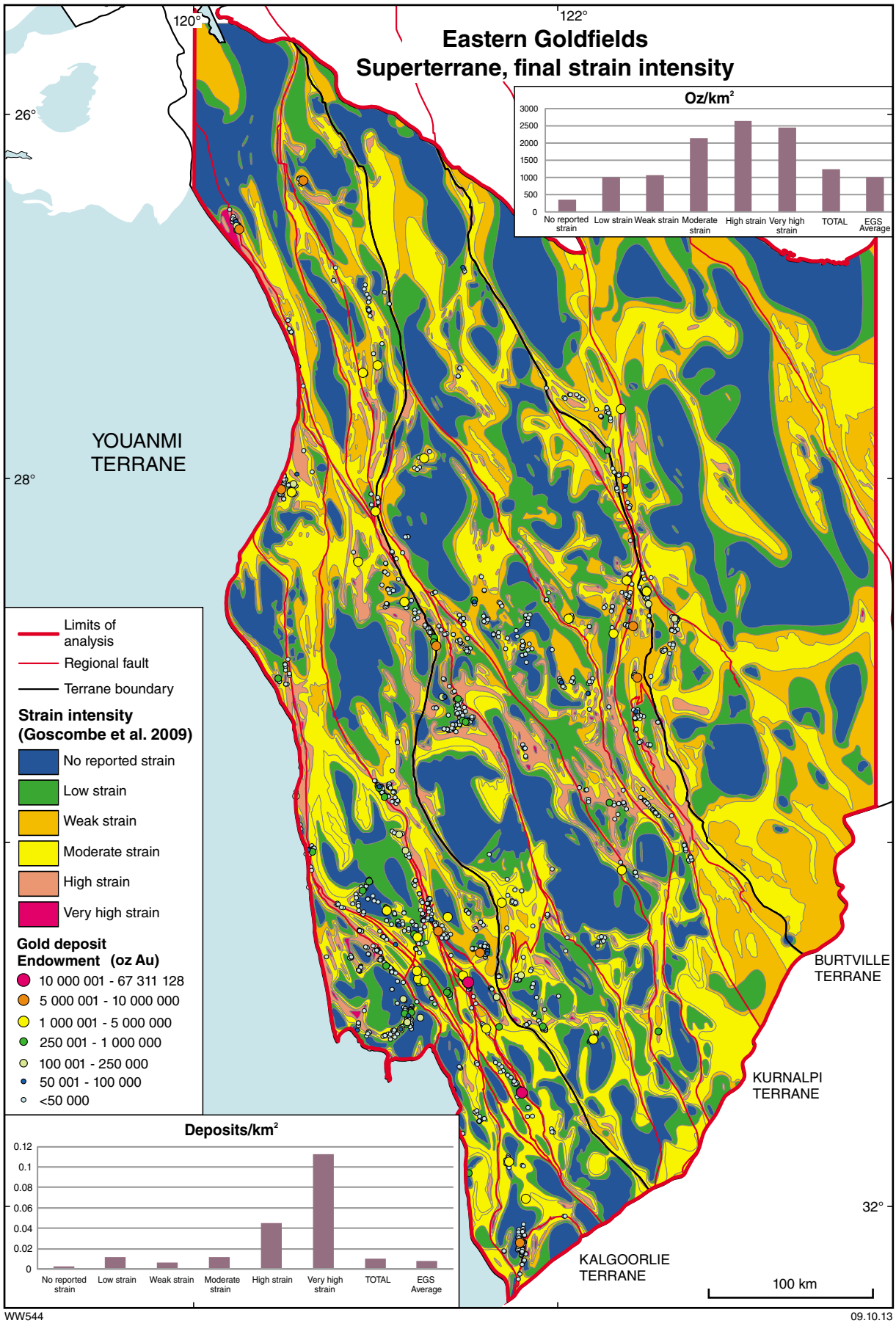

Figure 1.57. Distribution of gold deposits in the Eastern Goldfields Superterrane relative to final strain intensity

Targeting Criterion 1.16: Regional strain partitioning

A superficial examination of geological maps of the Yilgarn Craton reveals the heterogeneous nature of strain, comprising anastomosing shear zones that enclose domains of relatively low strain. Well-preserved stratigraphic sequences can be recognized in large low-strain domains such as the Margaret–Murrin sector and the Ora Banda low-strain domain, whereas the bounding high-strain zones are geologically more complex (Hallberg, 1985; Witt, 1990). Four such regions of strain partitioning have been singled out to investigate the distribution of gold endowment between high- and low-strain environments (Fig. 1.58). These regions of strain partitioning are of larger scale than the strain subdivisions of Goscombe et al. (2009) that were analysed in relation to gold endowment under Targeting Criterion 1.15.

There are no formal definitions of the low- and high-strain domains investigated here. In particular, the Laverton Tectonic Zone, although widely recognized, is portrayed inconsistently in a range of publications (e.g. Hallberg, 1985; Ojala et al., 1993; Salier et al., 2004; Henson et al., 2010). For this study, shape files outlining the zones of high and low strain were generated using aeromagnetic data and GSWA 1:500 000-scale geological mapping (*500k_geologyp08* shape file). High-strain zones are characterized by thin, elongate, commonly discontinuous geological or magnetic units of strong preferred orientation, typically in the regional north-northwest to north–south orientation, but including north-northeast to northeast orientations (e.g. Youanmi Terrane). The geological map was used as a guide to the boundaries of the domains, but the boundaries were modified locally to follow magnetic trends and contacts more closely. For example, thin greenstone units (magnetic) that overlie granite (weakly magnetic) were excluded where the magnetic contact is sharp and displaced from the geological contact determined from surface outcrops. The high- and low-strain domains are independent of geological terranes and domains (see Terranes and domains: Gold endowment). All regions examined here exclude the Golden Mile deposit, so there is no bias derived from inclusion of this giant deposit.

The Leonora–Laverton region includes a large area of low strain coincident with a belt of granitic intrusions and anomalous northeast to east–west greenstone orientations. This low-strain region includes the Mount Kilkenny area in the north and the Galvalley Monzogranite in the south (Fig. 1.58) and is broadly equivalent to the Murrin–Margaret sector of Hallberg (1985). Primary igneous and sedimentary textures are widely preserved in this domain, which is bounded to the east by the Laverton Tectonic Zone and to the west by the Keith–Kilkenny fault zone. A spatial (containment) analysis shows that the high-strain Laverton Tectonic Zone is far better endowed with gold than either the Murrin–Margaret low-strain zone or the Keith–Kilkenny high-strain zone (Table A1.86). The endowment of the Murrin–Margaret low-strain domain is much greater than that of the Keith–Kilkenny high-strain domain. The Laverton Tectonic Zone contains 69.3% of the total gold endowment of the three zones, even though it represents only 26.8% of their combined area. It contains 45.5% of the gold endowment in 5.1% of the area of the Kurnalpi Terrane. The Laverton Tectonic Zone also contains the greatest deposit density (0.025 deposits/km^2) of the three zones but contains a lower absolute number of deposits than the Murrin–Margaret low-strain domain (Table A1.86). The endowment of the Laverton Tectonic Zone (5087 oz/km^2) is much greater than the average for the Kurnalpi Terrane (576.4 oz/km^2, or 944.5 oz/km^2 for greenstone areas only), as is the deposit density (0.008 deposits/km^2, or 0.017 deposits/km^2 in greenstone areas only). The deposit density of the Murrin–Margaret domain is comparable with the average for the Kurnalpi Terrane (greenstones only), whereas that of the Keith–Kilkenny zone is somewhat lower (Table A1.86).

The Ora Banda region includes a large domain in which igneous textures are widely preserved and a coherent stratigraphy can be mapped over a strike length of several hundred kilometres (the Ora Banda domain; Witt, 1990). This low-strain domain is bounded to the east by the Bardoc Tectonic Zone and to the west by the Zuleika Shear Zone (Fig. 1.58). The spatial analysis of the Ora Banda region shows that the high-strain Bardoc Tectonic Zone has the best endowment of the three domains (%Endowment/%Area of 3.5 and 0.250 deposits/km^2). The Bardoc Tectonic Zone captures 44.6% of the endowment and 33.3% of deposits in 12.8% of the total area (Table A1.87). It contains 5.4% of the gold endowment in 1.7% of the area of the Kalgoorlie Terrane greenstones and contains ten times the deposit density of the Laverton Tectonic Zone, but with just over half the total endowment (10 Moz compared with 18 Moz Au). Unlike the Leonora–Laverton example, the low-strain domain of the Ora Banda region is the least endowed (3761 oz/km^2), although in terms of deposit density the Ora Banda low-strain domain and the Zuleika Shear Zone are comparable (Table A1.87). It should be cautioned that the results for the Ora Banda region are somewhat distorted by the gold deposit database, which attributes a significant amount of production from low-strain domains in the Mount Pleasant and Kanowna areas to Paddington in the Bardoc Tectonic Zone, where there is a treatment plant. However, this disparity is not considered serious enough to change the relative magnitudes of the endowments in the three domains examined.

In the Youanmi Terrane, the bounding high-strain domains of the Windimurra region are better endowed than the Youanmi Terrane average (Table A1.88). In this case, the western bounding high-strain zone is the better endowed (4001 oz/km^2), in contrast to the Laverton and Ora Banda regions where the eastern high-strain zone is superior. The Windimurra low-strain domain is also less well-endowed than the Youanmi Terrane average (143.6 oz/km^2). The relative endowment of the three domains is not changed by considering deposit density. In the Sandstone region, the low-strain domain is better endowed than the bounding high-strain zones but all three zones are less well-endowed than the Youanmi Terrane average. All three domains in the Sandstone area exceed the average deposit density for granite–greenstone areas in the Youanmi Terrane (0.003 deposits/km^2). The prominent endowment of

the low-strain domain within the Sandstone analysis is unexpected because it is dominated by granite, whereas the high-strain zones are focused on narrow greenstone belts (Fig. 1.58). However, the gold deposits in the Sandstone low-strain domain are in greenstones at the northern and southern ends of a large body of granite that could be viewed as the necks of a large-scale boudin (cf. the Southern Cross mega-boudin, see Part 2.13 of this Atlas).

In summary, the results of this spatial analysis on four examples of regional strain partitioning show that most high-strain zones are better endowed with gold than the average of the terranes within which they occur (the Sandstone area is an exception). Within these regions of strain partitioning, the central low-strain domain is dominated by smaller deposits, whereas the premium gold endowment is in one or other of the bounding high-strain domains. In the Eastern Goldfields Superterrane, the eastern high-strain domain is favoured, whereas the western high-strain zone is superior in the Windimurra region. It is interesting to note from seismic data that the eastern high-strain zones in the Laverton and Ora Banda regions are both zones of anomalous vergence (i.e. dominated by west-dipping faults within a larger terrane dominated by east-dipping faults; see Targeting criterion 1.11). Interpretation of a recently released seismic profile across the Youanmi Terrane (line 10GA-YU1) suggests that the relatively well-endowed western high-strain zone of the Windimurra region is a similarly anomalous east-dipping structure within a province dominated by west-dipping regional faults (Zibra et al., 2013). Though the number of spatial analyses presented here is limited, the results suggest that regional strain partitioning creates a favourable structural setting for gold mineralization and that one or other of the bounding high-strain zones will contain the highest endowment. This result can be compared with those derived from spatial analysis of the various strain domains of Goscombe et al. (2009) in the Eastern Goldfields Superterrane, where relatively low-strain domains are also poorly endowed in terms of both ounces of gold and numbers of deposits (see Targeting Criterion 1.15). The results are also of interest as they support the favourable prospectivity of regional faults characterized by anomalous vergence (Targeting criterion 1.11).

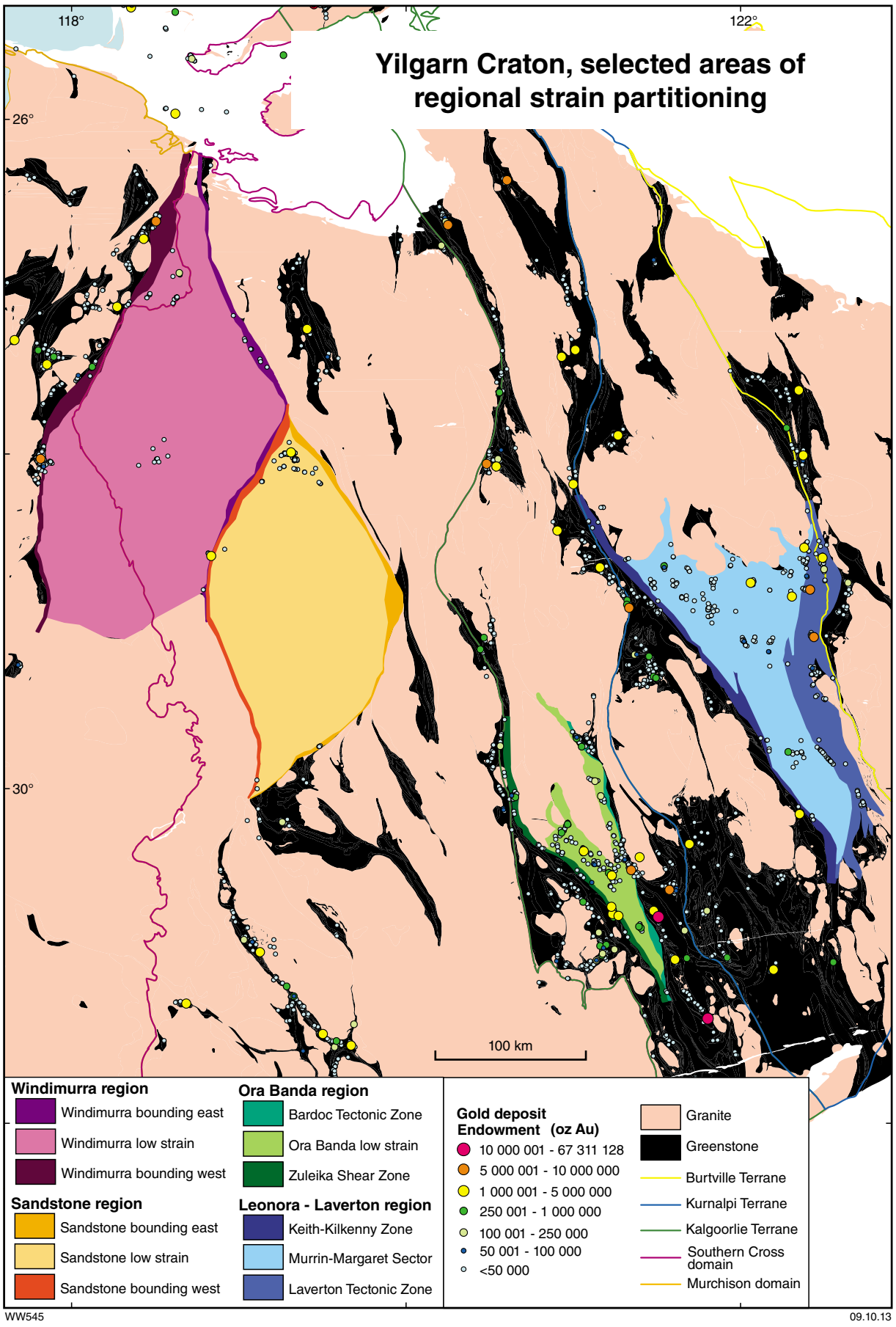

Figure 1.58. Distribution of gold deposits relative to selected low-strain domains and adjacent bounding high-strain zones in part of the Yilgarn Craton

Targeting Criterion 1.17: Late-stage basins

Krapez et al. (2000, 2008), Kositcin et al. (2008), and Krapez and Pickard (2010) identified several late-stage basins that unconformably overlie an older folded volcano-sedimentary greenstone sequence in the Eastern Goldfields Superterrane (see also Blewett et al., 2004). Krapez et al. (2000) subdivided these late-stage basins into alluvial sequences dominated by braided stream deposits (e.g. Merougil basin) and turbidite sequences dominated by deep marine deposits (e.g. Kurrawang basin). Krapez et al. (2000) also suggested that these depositional basins were originally more continuous over the Eastern Goldfields Superterrane. Most of the late-stage basins are modestly endowed with gold (the Wallaby and Agnew deposits are major exceptions), but the unconformity at the base of the late-stage basin(s) represents a potential barrier to upward flow of hydrothermal fluids. Walshe et al. (2006) and Hall (2007) noted that many gold deposits are within 1 km of the unconformity. High fluid pressure immediately below the unconformity would have promoted rock failure and exposed large volumes of rock to any ore fluid sourced from below the late-stage sedimentary deposits. Thus, Hall (2007) advocated exploration for gold in footwall sequences near the remnants of late-stage basin(s) presently exposed at the surface in the Eastern Goldfields Superterrane. In addition to acting as a regional seal, the basal unconformity of the late-stage basins was potentially a site of fluid mixing (Sheldon and Ord, 2004). If the seal was breached by fault or fracture, numerical modelling suggests that basinal fluids from the overlying sedimentary sequence would have been drawn down through the breaching structure to mix with ambient fluids in the underlying greenstone sequence. Robert et al. (2005) and Dubé and Gosselin (2007) have noted an association between unconformities at the base of late-stage basins and large gold-producing camps in the Superior Province of Canada.

The location and extent of late-stage basins used in this spatial analysis are based on data encapsulated by the GSWA 1:500 000-scale shape file (*500k_geologyp*, Fig. 1.59). It is similar to the late-stage basin file generated by pmd*CRC (Y4 Project team, 2008), but has been modified to include recently recognized late-stage basins in the Kanowna area (Tripp et al., 2007; Tripp, 2013), and the Lake Carey basin, in accordance with Standing (2008) and Krapez and Pickard (2010). The data are limited to the Kalgoorlie and Kurnalpi Terranes, which are therefore used as the areal extent of the spatial analysis. The resulting distribution of late-stage basins is similar to, but different in detail from, maps of late-stage basins published by Krapez and Pickard (2010). In particular, the late-stage Penny Dam sedimentary basin extends well to the south on the Krapez and Pickard (2010) map to include the Mount Belches Formation. However, Hall (2006) found two deformation fabrics in the Mount Belches Formation and concluded they should not be included with other late-stage basins. Therefore, they have been excluded from the data used in this analysis.

A containment analysis shows that the late-stage basins contain 16.4 Moz of gold, equivalent to about 7.8% of the total for greenstones in the combined Kalgoorlie and Kurnalpi Terranes (Table A1.89). Almost all of this endowment is contained within the Lake Carey and Jones Creek/Scotty Creek basins; the remaining basins contain little or no known gold. Similarly, 34 of the 49 known gold deposits hosted by late-stage basins are in the Lake Carey and Jones Creek/Scotty Creek basins. The most productive deposits in the Lake Carey basin are Granny Smith (8.0 Moz Au) and Lancefield (1.8 Moz Au); those in the Jones Creek/Scotty Creek basin are the deposits of the Agnew camp (approximately 6.2 Moz Au). Note that because of limitations in the accuracy of either or both of the deposit database and the *500k_geologyp* shape file, the Wallaby deposit (2.8 Moz) is incorrectly excluded from the Lake Carey basin (Fig. 1.59). Inclusion of Wallaby, which is hosted by hydrothermally altered conglomerate of the Lake Carey late-stage basin (Salier et al., 2004), would further enhance the endowment of the late-stage basins. Even excluding Wallaby, the average endowment of the late-stage basins (6020 oz/km^2) is still substantially larger than the average endowment of greenstones in the combined Kalgoorlie and Kurnalpi Terranes (4064 oz/km^2). In terms deposit density, the late-stage basins (0.018 deposits/km^2) are less prospective than greenstones of the combined Kalgoorlie and Kurnalpi Terranes (0.032 deposits/km^2). These observations suggest that compared to the combined Kalgoorlie and Kurnalpi Terranes greenstones, the late-stage basins contain fewer gold deposits, but those that are present are larger than average. Late-stage basins have traditionally been viewed as poor host rocks for gold mineralization. The large endowment of two of the eleven late-stage basins recognized here, and the small quantities of known gold in the other nine, suggests that some late-stage basins may be under-explored.

The spatial analysis relating gold endowment to proximity to late-stage basins shows both the peak %Endowment/%Area ratio of 5.98 and the maximum deposit density at a buffer distance of 7500 m (Table A1.90). Although a rather large buffer, it does not necessarily relate directly to distance below the unconformity, which may have been a relatively short distance above the gold deposit at the time of mineralization and before subsequent erosion. The 7500 m buffer captures 64.9% of the gold endowment and 27.4% of deposits in 10.9% of the combined area of the Kalgoorlie and Kurnalpi Terranes. These results are not strongly influenced by the giant Golden Mile deposit, which is captured by the 5000 m buffer. For comparison, the 1000 m buffer captures 7.4% of the gold endowment and 4.1% of the deposits in 3.4% of the area (%Endowment/%Area of 2.19).

Lack of detailed information prevents extending the analysis of late-stage basins into the Southern Cross and Murchison domains. However, recent regional mapping suggests there are possible remnants of late-stage depositional sequences in the Marda Dam greenstone belt (the Diemals Formation; Chen et al., 2001b). The nearest gold deposit is more than 10 km from the Diemals Formation. Other possible late-stage basins have been noted in the Sandstone area and the Gum Creek greenstone belt (S. Wyche, GSWA, pers. comm., Oct 2010). Both of these areas contain deposits (Sandstone and Gidgee, respectively) with >1 Moz of gold within 3000 m of the sedimentary rock units. However, exposure in both areas is poor and the stratigraphic significance of these basins remains to be established.

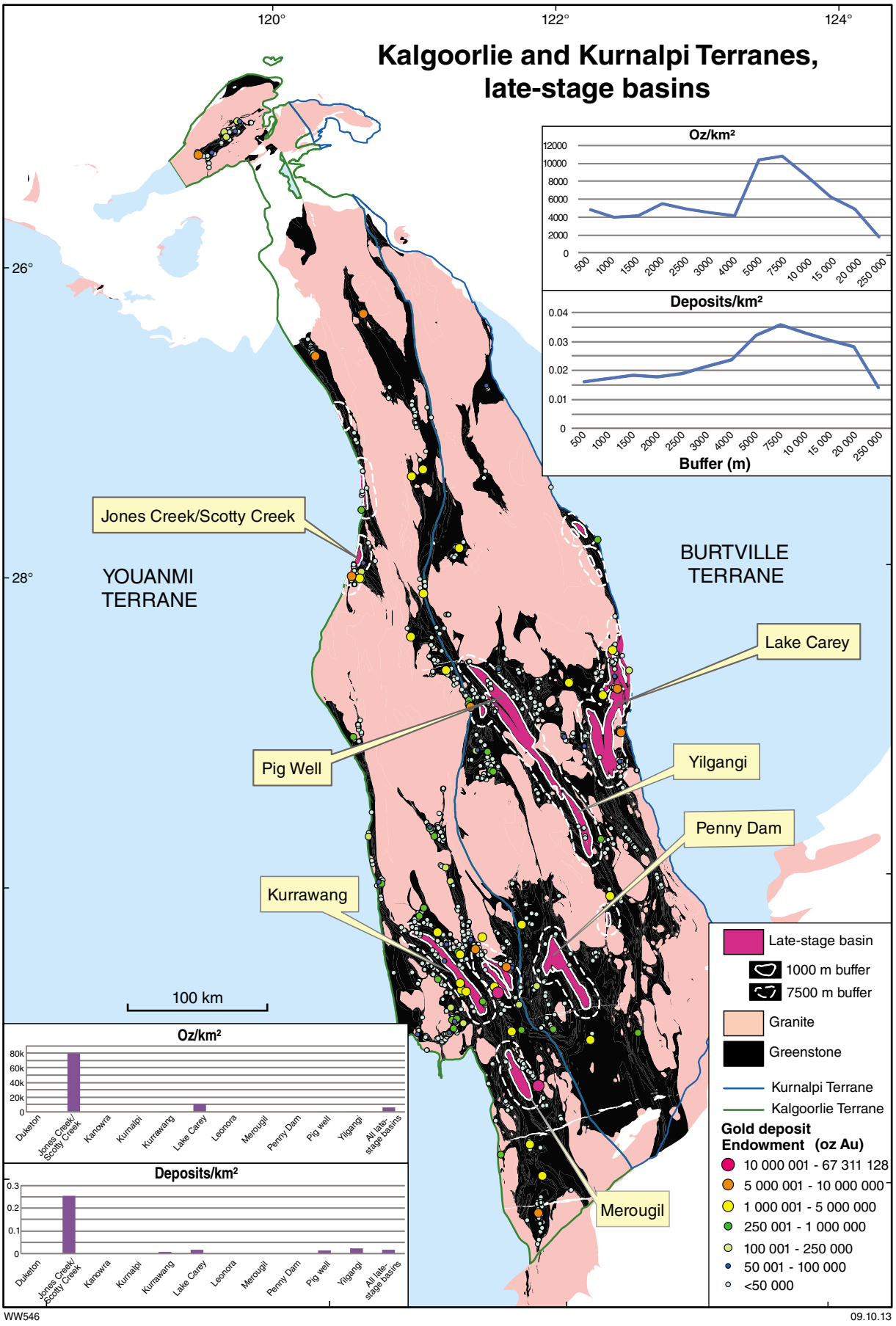

Figure 1.59. Distribution of gold deposits in the Kalgoorlie and Kurnalpi Terranes relative to late-stage basins

Targeting Criterion 1.18: Regional geological complexity

Geological complexity was measured as a fractal dimension, calculated using a box-counting method similar to that of Hodkiewicz et al. (2005). The method involves placing a grid of squares with side dimension *d* over a geological map and counting those squares that contain one or more lines (e.g. geological contacts and structures). The side dimension of the boxes is then halved and the number of squares that contain lines counted again. The process is repeated by halving the side dimension of the squares several times. In the study of the Yilgarn Craton by Hodkiewicz et al. (2005), four sets of boxes (with side dimensions of 10, 5, 2.5, and 1.25 km) were counted. The fractal dimension (*D*) is calculated as the slope of the line of best fit on a plot of log *Nd* versus log *d* (where *Nd* is the number of boxes containing one or more lines, and d is the side dimension of the boxes). *D*, which is a measure of geological complexity, typically ranges between one and two, but can be less than one in those parts of maps where no lines are present. The analyses presented here made use of gold deposit data from the MINEDEX database as well as the Barrick gold deposit database. The MINEDEX database lacks endowment figures but contains more deposits, with good locational accuracy.

The script used by Hodkiewicz et al. (2005) to calculate fractal dimension was written for Avenue, the programming language available to users of Arc 3.2 software at the time, but is no longer compatible with current versions of ArcGIS. New scripts that are compatible with ArcGIS versions 9.3.1 and 10, and carry out the same function, have been developed by GSWA. The new script for ArcGIS v.9.3.1 was used here to investigate geological complexity at regional scale in the Yilgarn Craton. Although Hodkiewicz et al. (2005) mapped the geological complexity of the whole craton, the updated script has been used here for separate analyses of the Eastern Goldfields Superterrane and the Southern Cross and Murchison domains (Fig. 1.60). In a further departure from the Hodkiewicz et al. (2005) study, five rather than four iterations of box side dimension were used.

The efficiency of using geological complexity as a targeting tool for gold was assessed by plotting gold endowment and number of gold deposits against fractal dimension for each of the first (largest) set of boxes in the study area. The degree of correlation between these two parameters is viewed as an indication of the strength of the relationship between gold mineralization and geological complexity. The results of the analyses are summarized in Table 1.3. In a separate test, logistic regression was used to determine the likelihood that boxes containing gold had a different fractal dimension to boxes without gold mineralization (Fig. 1.61).

The analytical area used to assess geological complexity in the Eastern Goldfields Superterrane covers most of the Kalgoorlie and Kurnalpi Terranes and the better-exposed western part of the Burtville Terrane, thus encompassing most of the larger gold mining districts (Fig. 1.60). For the Eastern Goldfields Superterrane, digital data from the GSWA Eastern Yilgarn GIS dataset (2009 update) was used. The solid geology polygon file *500k_geologyp08* was first converted to a polyline shape file and then merged with the *500k_geolstrucl08* and *geostrucl* shape files to create a single polyline shape file for complexity analysis. An initial box dimension of 20 000 m was chosen and subsequent iterations used box dimensions of 10 000, 5000, 2500, and 1250 m. The results of the analysis using a maximum *d* of 20 000 m are shown in Figure 1.62. Most boxes over greenstone belts gave fractal dimensions between 1.8 and 2.0. Plots comparing *D* and gold endowment from the Barrick gold deposit database show that the two quantities are poorly correlated (Table A1.91a; Fig. 1.63). Similarly, correlations between geological complexity and the number of deposits (from the Barrick and MINEDEX databases) are poor (Tables A1.91a and A1.91b). Although a few gold deposits are within tiles defined by $D < 1.5$, significant gold endowment is confined to tiles with $D > 1.5$. Selection of only tiles with $D > 1.5$ improves the correlation between gold endowment and fractal dimension in some cases, but the best coefficient of correlation is only about 0.25, using the number of deposits from the MINEDEX database (Table A1.91b; Fig. 1.63). A box plot summarizing the results of a logistic regression test indicates that mineralized boxes have marginally higher fractal dimension than unmineralized boxes (Fig. 1.61).

The area selected for analysis of geological complexity in the Southern Cross domain is the northern part of the domain where greenstones and gold deposits are moderately common (Fig. 1.60). Equivalent GIS data for the better-endowed gold districts in the southern part of the domain were not available at the time of this study. The analysis of geological complexity made use of a polyline shape file of merged digital data from the GSWA Central Yilgarn GIS (2008 update). The geology polygon shape file (*500K_interpgeop*) was first converted to a polyline shape file and then merged with linear geology (*500K_interpgeol*) and linear structure (*500K_interpstrucl*) shape files. The resulting merged dataset represents a network of geological contacts, faults, lineaments, and (relatively few) fold axes across part of the northern Southern Cross domain (Fig. 1.64). The initial box dimension chosen was 20 000 m and subsequent iterations used box dimensions of 10 000, 5000, 2500, and 1250 m. As was the case for the Eastern Goldfields Superterrane, tiles that contain mainly greenstone areas have *D* between 1.8 and 2.0 (Fig. 1.64). Also in common with the Eastern Goldfields Superterrane data, significant gold endowment is restricted to tiles with $D > 1.5$. The correlations between *D* and both gold endowment and number of gold deposits are similarly poor (Table A1.92, Fig. 1.65). The best correlation coefficient (0.2371) was found for the number of deposits derived from the MINEDEX database restricting the analysis to those tiles with $D > 1.5$. As for the Eastern Goldfields Superterrane analysis, a logistic regression test indicated that mineralized boxes have marginally higher fractal dimension than unmineralized boxes (Fig. 1.61).

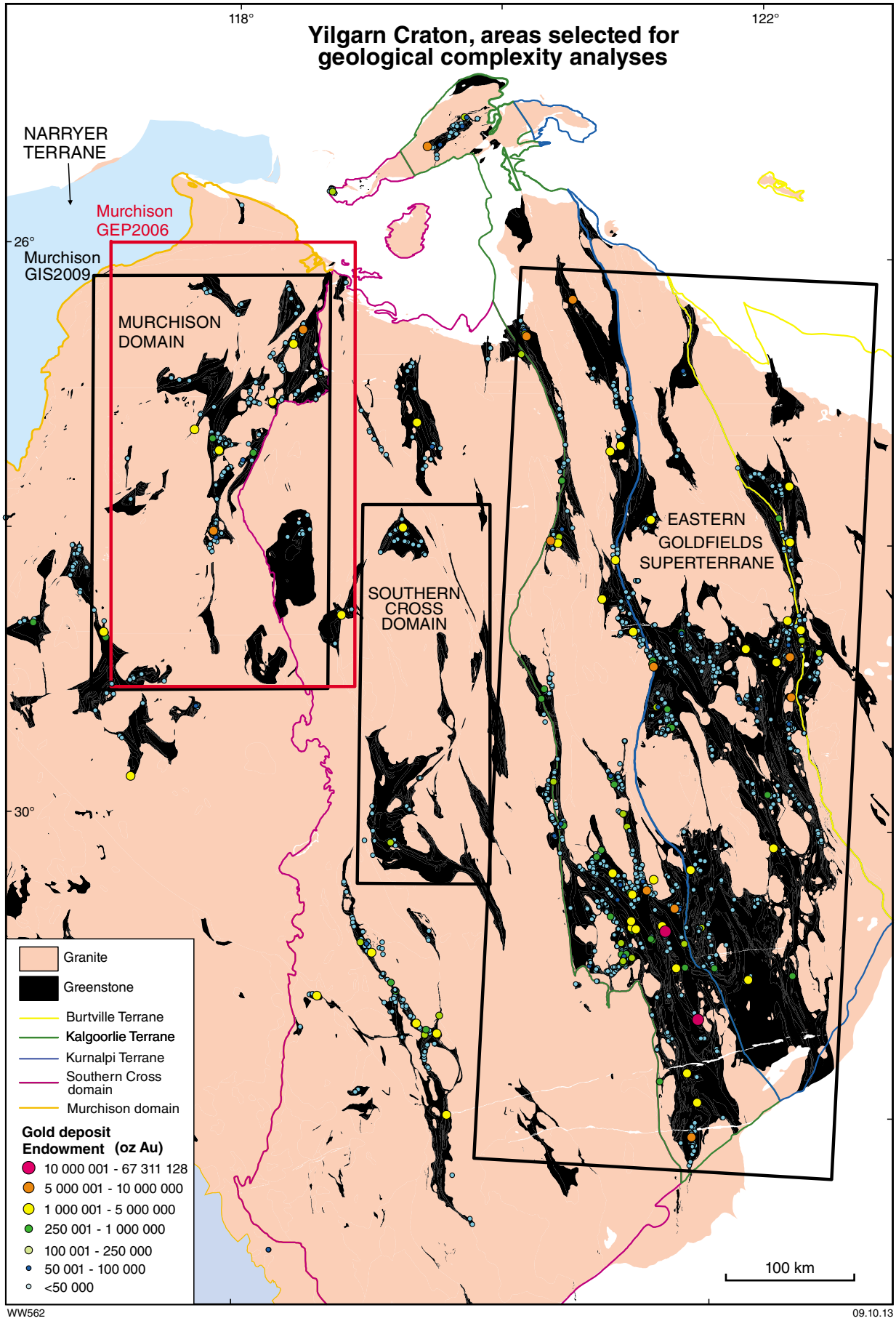

Figure 1.60. Areas of the Yilgarn Craton selected for investigation of geological complexity

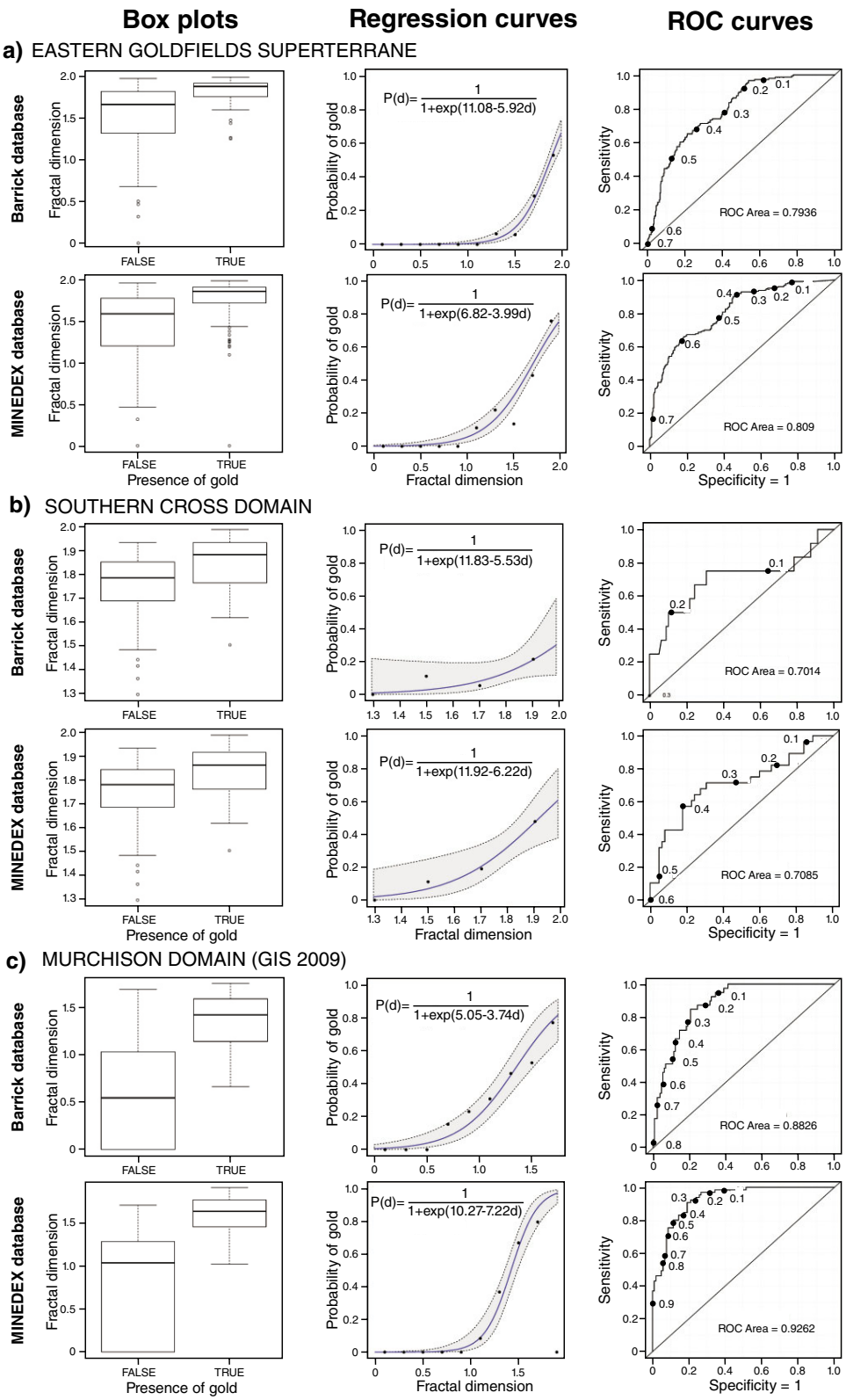

The box plots show the median value (thick line) and the first and third quartiles as the lower and upper boundaries of the box respectively; the mean minus (and plus) ¾ of the data range define the lower (and upper) ends of the whiskers; small circles are outliers. The regression curves show the predicted values and the enveloping broken line curves represent 95% confidence intervals on predictions. The ROC curves represent the accuracy of the test, which is proportional to the area under the curve.

WW573 02.10.13

Figure 1.61. Results of logistic regression analysis relating gold deposits to fractal dimension (*D*) for analyses of geological complexity

The analysis of geological complexity in the Murchison domain involved the use of two datasets for comparison. Both datasets extend into the Southern Cross domain of the Youanmi Terrane (Fig. 1.60). The more recent data is from the GSWA Murchison GIS (2009 update). After converting the *500K_interpgeologyp08* polygon shape file to a polyline file, the polyline file was merged with the *500K_geostrucl08* polyline shape file, and the resulting file used for the analysis. The second dataset was from the GSWA Murchison Geological Exploration Package (2006), which contains an older but more extensive and uniform dataset that covers almost the same area of the Murchison domain. The areas selected for analysis represent a major part of the northern Murchison domain, incorporating greenstone belts between Golden Grove in the southwest and Meekatharra in the northeast, and the main gold-producing areas of the domain. Although more detailed (1:100 000 scale) data are available for the area between Cue and Weld Range, this area was considered too small for an assessment of geological complexity as a regional targeting tool. For comparative purposes, two analyses were completed for each dataset; the first used box-side dimensions of 20 000, 10 000, 5000, 2500, and 1250 m and the second used box-side dimensions of 10 000, 5000, 2500, 1250, and 625 m.

The distributions of calculated geological complexity for the Murchison domain using these various parameters are shown in Figures 1.66 to 1.69. Compared to analyses of the Southern Cross domain and Eastern Goldfields Superterrane, complexity analyses of the Murchison domain using the 2009 dataset result in lower overall fractal dimensions, and significant gold endowments are found in tiles with D as low as 1.09 (Table 1.3; Figs 1.68 and 1.69). This is not the case for analyses using the more detailed data derived from the 2006 dataset, where fractal dimensions of tiles over greenstones are commonly in the range 1.8 to 2.0 (Figs 1.66 and 1.67), in common with the results from the Eastern Goldfields Superterrane and Southern Cross domain. The analysis using the 2006 dataset and starting with d of 10 000 m generates greater variability of geological complexity in areas of greenstone than the analysis starting with d of 20 000 m. This is also true of the analyses using the 2009 dataset. Compared to the analysis for d of 20 000 m, the analysis of the 2006 dataset for d of 10 000 m produces fewer tiles with high values of D: 24 tiles with $D > 1.9$ for d = 20 000 m; 6 tiles with $D > 1.9$ for d = 10 000 m (Tables A1.93 and A1.94; Figs 1.66 and 1.67).

The correlations between fractal dimension and gold endowment and number of gold deposits are summarized in Figures 1.70 to 1.73 and Table 1.3. The best result from all of the Murchison analyses was achieved using the 2009 dataset and a maximum tile dimension of 20 000 m (Tables A1.95 and A1.96). The correlation coefficient of 0.3115, relating the number of deposits (from the MINEDEX database) to fractal dimension, still does not convincingly support a relationship between the two. For both datasets, all analyses using the 10 000 m starting dimension resulted in lower correlation coefficients than the equivalent analysis using the 20 000 m starting dimension (Table 1.3). Because more intensive interrogation of a dataset should provide a more accurate result, this observation appears to contradict any suggestion of a relationship between geological complexity and either gold endowment or deposit density in the Murchison domain. However, a box plot using the 2009 dataset (Fig. 1.61) shows that tiles containing mineralization have higher fractal dimensions than those without mineralization and that there is a greater separation between the two in comparison to results from corresponding tests in the Eastern Goldfields Superterrane and Southern Cross domain (Fig. 1.61).

The results of this study of the relationship between gold and geological complexity do not support the initially promising results reported by Hodkiewicz et al. (2005) and Ford and McCuaig (2010). Qualitatively at craton scale, the maps produced by Hodkiewicz et al. (2005) appear to show increased geological complexity in the main areas of gold endowment, although the authors did not quantify this relationship. That study emphasized an association between gold mineralization and steep gradients in the fractal dimension, illustrated by transects along the well-mineralized Boulder and Bardoc fault systems and the Laverton Tectonic Zone. At a more detailed scale (the Kurnalpi Terrane), Ford and McCuaig (2010) found low correlation coefficients (similar to those reported here) for the relationship between fractal dimension and gold endowment. These authors reported somewhat better correlation coefficients for fractal dimension versus number of deposits (up to 0.57). It should be noted that the maps used by Hodkiewicz et al. (2005) and some of those used by Ford and McCuaig (2010) were not the same as those used in this study. The 1:500 000-scale interpretive geology map used by Ford and McCuaig (2010) is the same as that used in this study, but they used only part of the coverage used here. The correlation coefficient of 0.450 between number of deposits (from the MINEDEX database) and fractal dimension reported by Ford and McCuaig (2010) is better than that determined here (0.250) for the larger areal extent of the Eastern Goldfields Superterrane using the same data sources. Ford and McCuaig (2010) reported better results when using larger scale (1:250 000 and 1:100 000) outcrop maps rather than interpreted structure maps, but the significance of these results is not clear. Ford and McCuaig (2010) were unable to repeat the relationship between gold and fractal dimension gradient reported by Hodkiewicz et al. (2005) and, in fact, established a negative relationship between the two for the Kurnalpi Terrane.

The results reported here indicate that geological complexity is not a useful targeting criterion at regional scale, at least using the datasets available at the present time. In all regions investigated, the fractal dimensions of granite-dominated areas are lower than those of areas of greenstone. This can be attributed partly to more intensive mapping and interpretation of aeromagnetic data in greenstone belts, which are lithologically more diverse than areas of granite, and of greater economic interest. However, qualitative observations of outcrops on the basis of regional geological mapping of the Yilgarn Craton suggest that there is less geological heterogeneity in areas

underlain by granite, and that the lower *D* values for these areas are probably genuine. Furthermore, the range of *D* values in greenstone areas is relatively restricted (mostly 1.8 to 2.0) in the Eastern Goldfields Superterrane and Southern Cross domain, thus limiting the effectiveness of this approach. The small but positive correlation coefficients for the relationship between gold endowment and fractal dimension may simply be a reflection of the well-known tendency for gold mineralization to be in greenstone belts rather than in the surrounding areas of granite. The positive results of logistic regression tests may reflect the same tendency. The strategy used here to assess the relationship between gold endowment and geological complexity may be improved by investigating smaller areas in which greenstone areas are dominant, and by using datasets based on the interpretation of aeromagnetic data. The latter approach may provide more objective results than geological field mapping, which can be subject to human bias (e.g. closer attention to accessible areas of good outcrop). The results of application of these alternative approaches are described in Part 2 of this Atlas.

Table 1.3. Summary statistics for geological complexity analyses, Yilgarn Craton

Region	*Max. d*	*Max. D*	*R [B(oz)]*	*R [B(N)]*	*R [M(N)]*
Eastern Goldfields Superterrane	20	1.9826	0.1002	0.2119	0.2496
Southern Cross domain	20	1.9861	0.1655	0.1858	0.2106
Murchison domain[(a)]	20	1.7501	0.1857	0.2135	0.3115
Murchison domain[(a)]	10	1.9062	0.1250	0.1542	0.2152
Murchison domain[(b)]	20	1.9827	0.1450	0.1833	0.2403
Murchison domain[(b)]	10	1.9456	0.1084	0.1690	0.2203

NOTES: (a) GSWA 2009 GIS dataset

(b) GSWA 2006 GEP dataset

d = side dimension of box; *D* = fractal dimension; *R* = correlation coefficient; *B* (Barrick gold deposit database); *M* (MINEDEX database); (oz) (gold endowment in ounces); (*N*) (gold endowment as number of deposits).

Correlations are for full dataset (*D*>0) whereas those shown in map Figures are confined to tiles with *D* between 1.5 and 2.0, or between 1 and 2 for Murchison domain analyses.

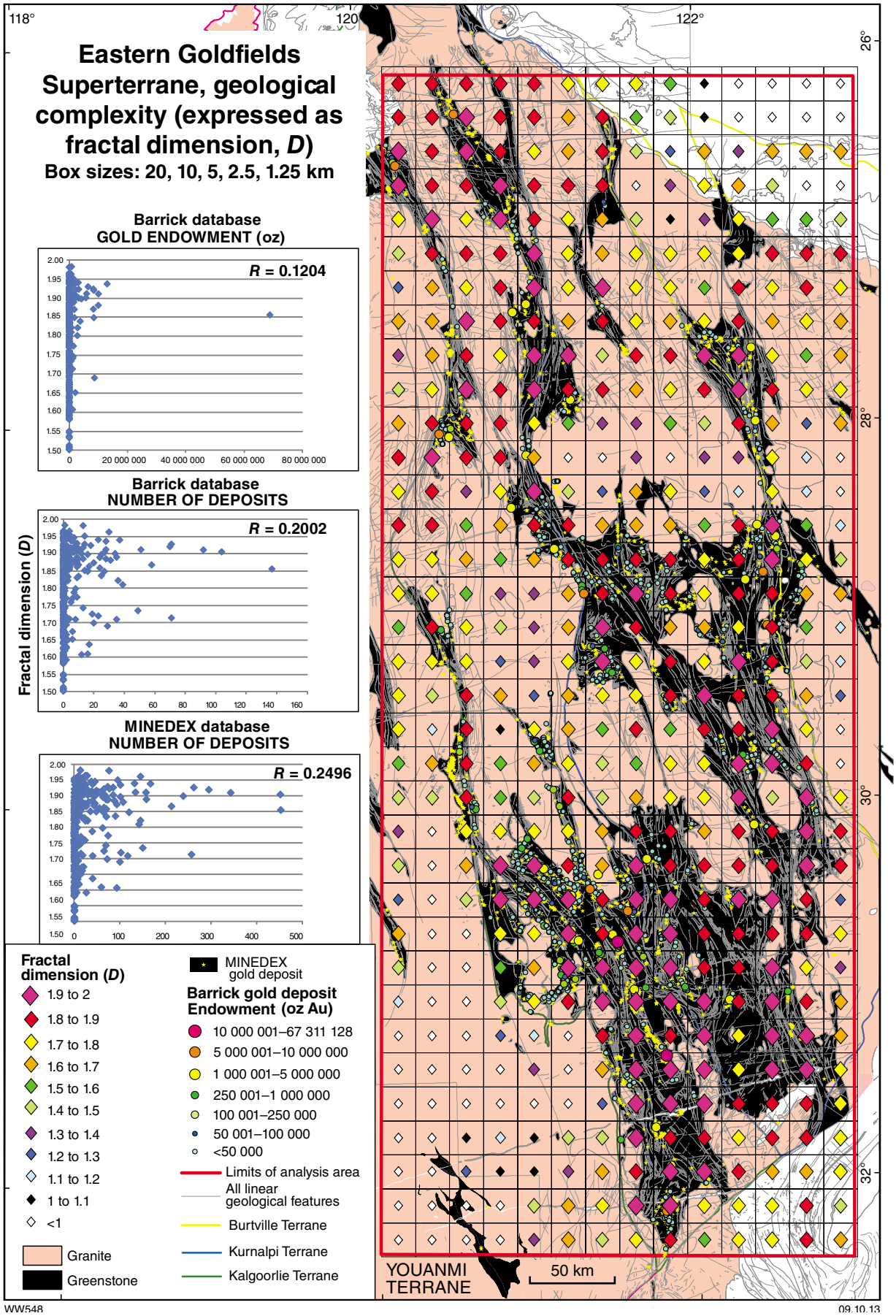

Figure 1.62. Distribution of gold deposits in the Eastern Goldfields Superterrane relative to geological complexity (expressed as fractal dimension *D*) (20, 10, 5, 2.5, and 1.25 km box sizes)

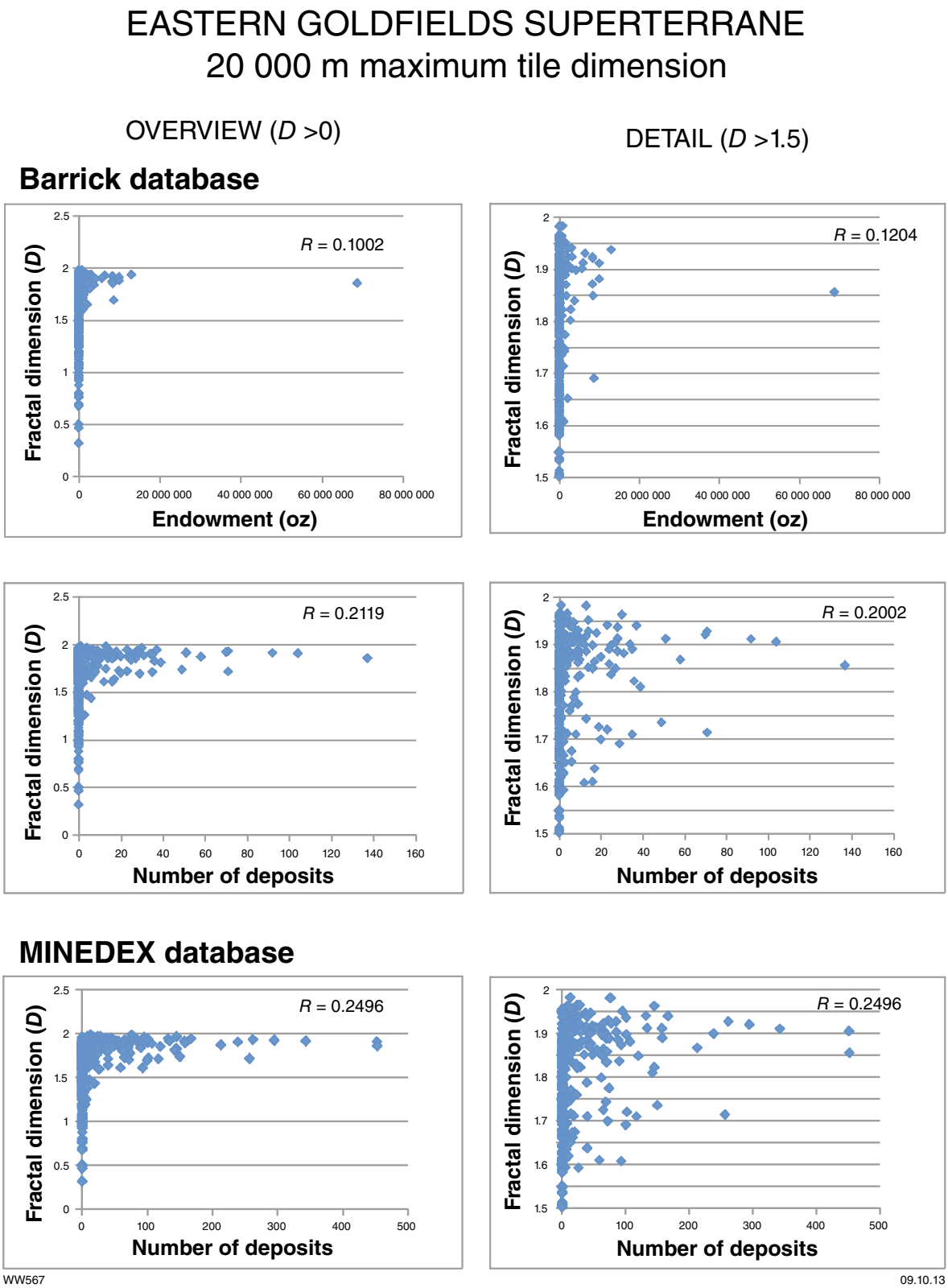

Figure 1.63. **Summary of correlations between gold deposits and fractal dimension (*D*) for the Eastern Goldfields Superterrane (20 km box size)**

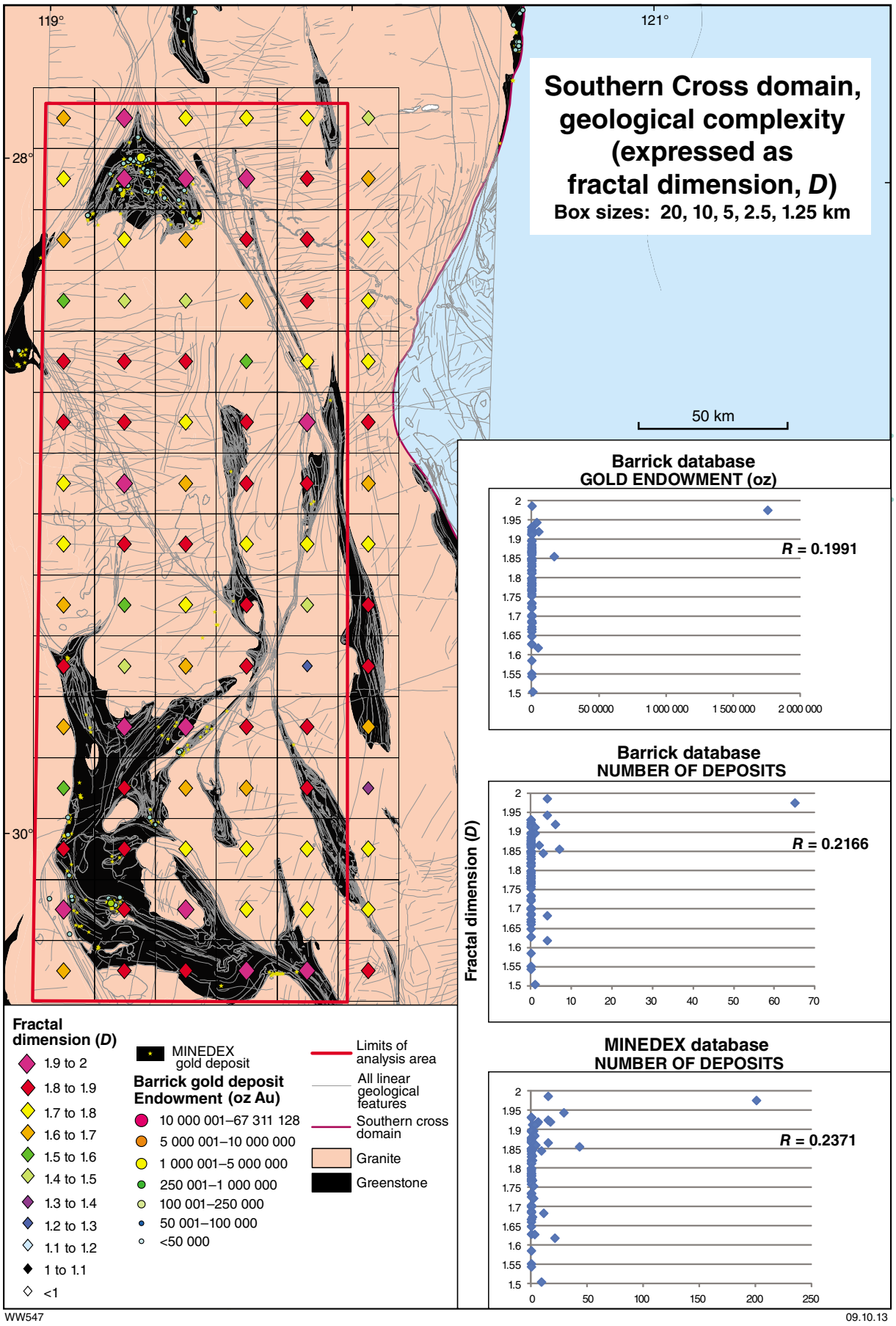

Figure 1.64. **Distribution of gold deposits in the northern Southern Cross domain relative to geological complexity (expressed as fractal dimension, *D*) to (20, 10, 5, 2.5, and 1.25 km box sizes)**

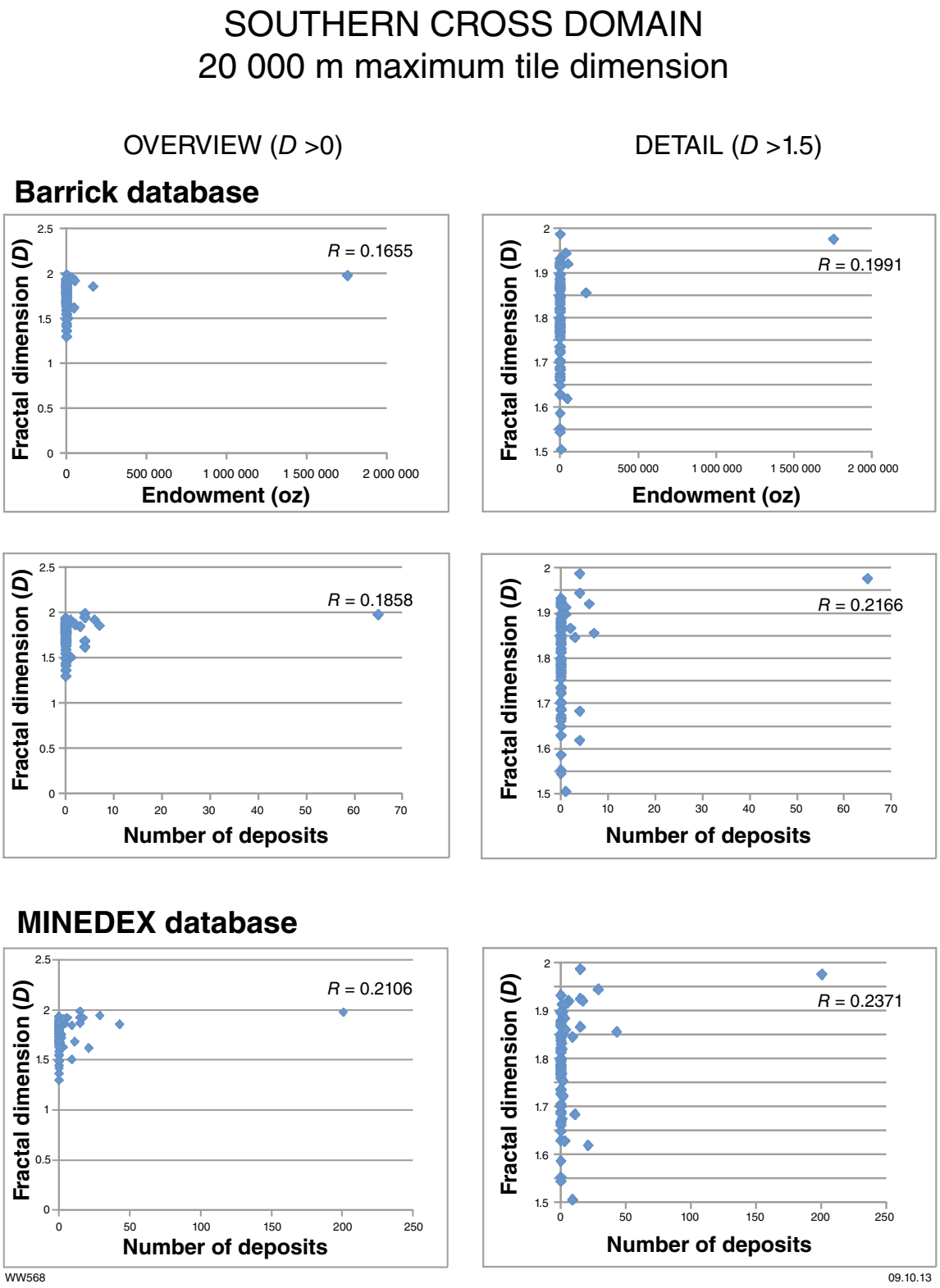

Figure 1.65. **Summary of correlations between gold deposits and fractal dimension (*D*) for the northern Southern Cross domain (20 km box size)**

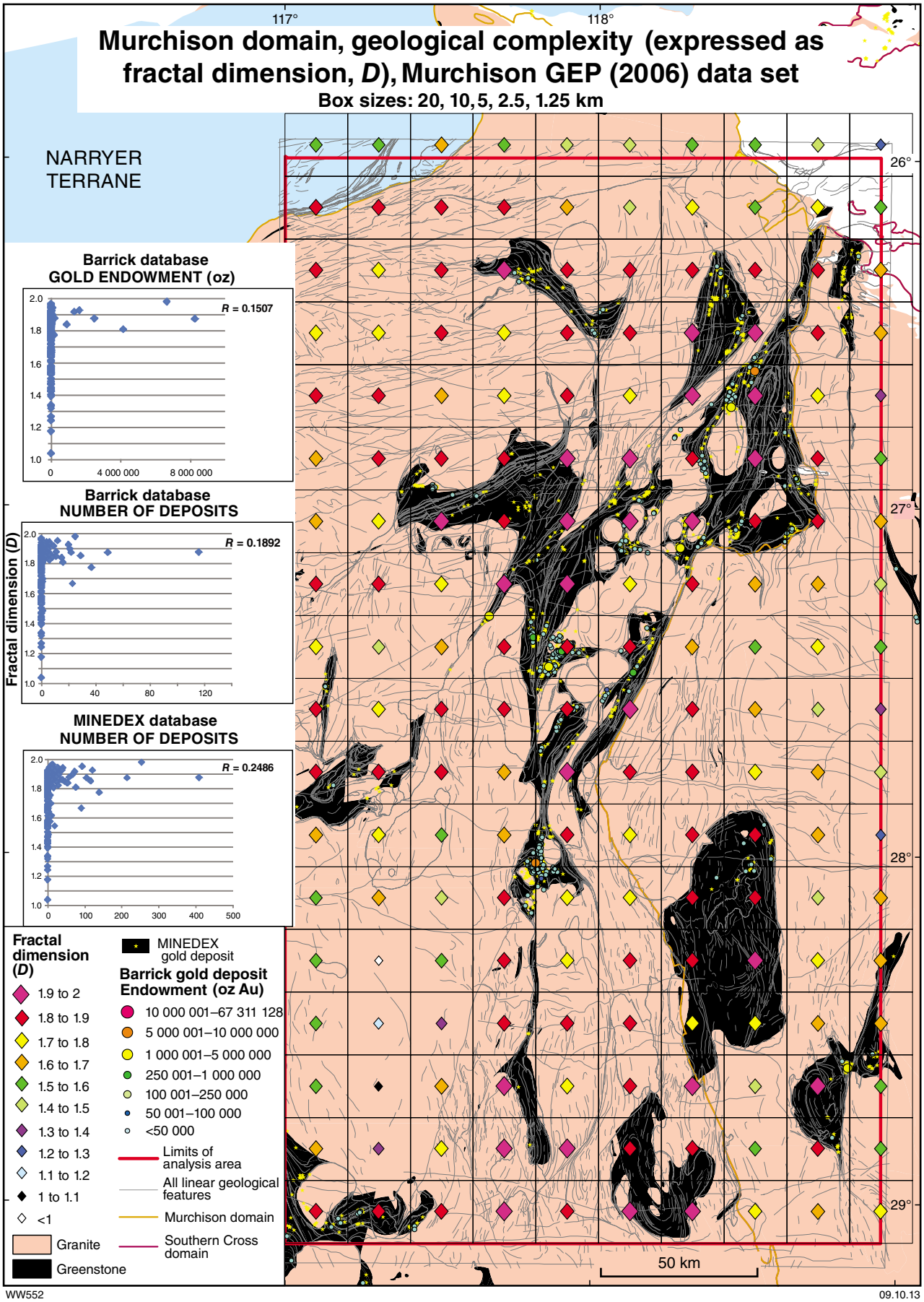

Figure 1.66. **Distribution of gold deposits in the northern Murchison domain relative to geological complexity (expressed as fractal dimension *D*) using GSWA GEP 2006 dataset (20, 10, 5, 2.5, and 1.25 km box sizes)**

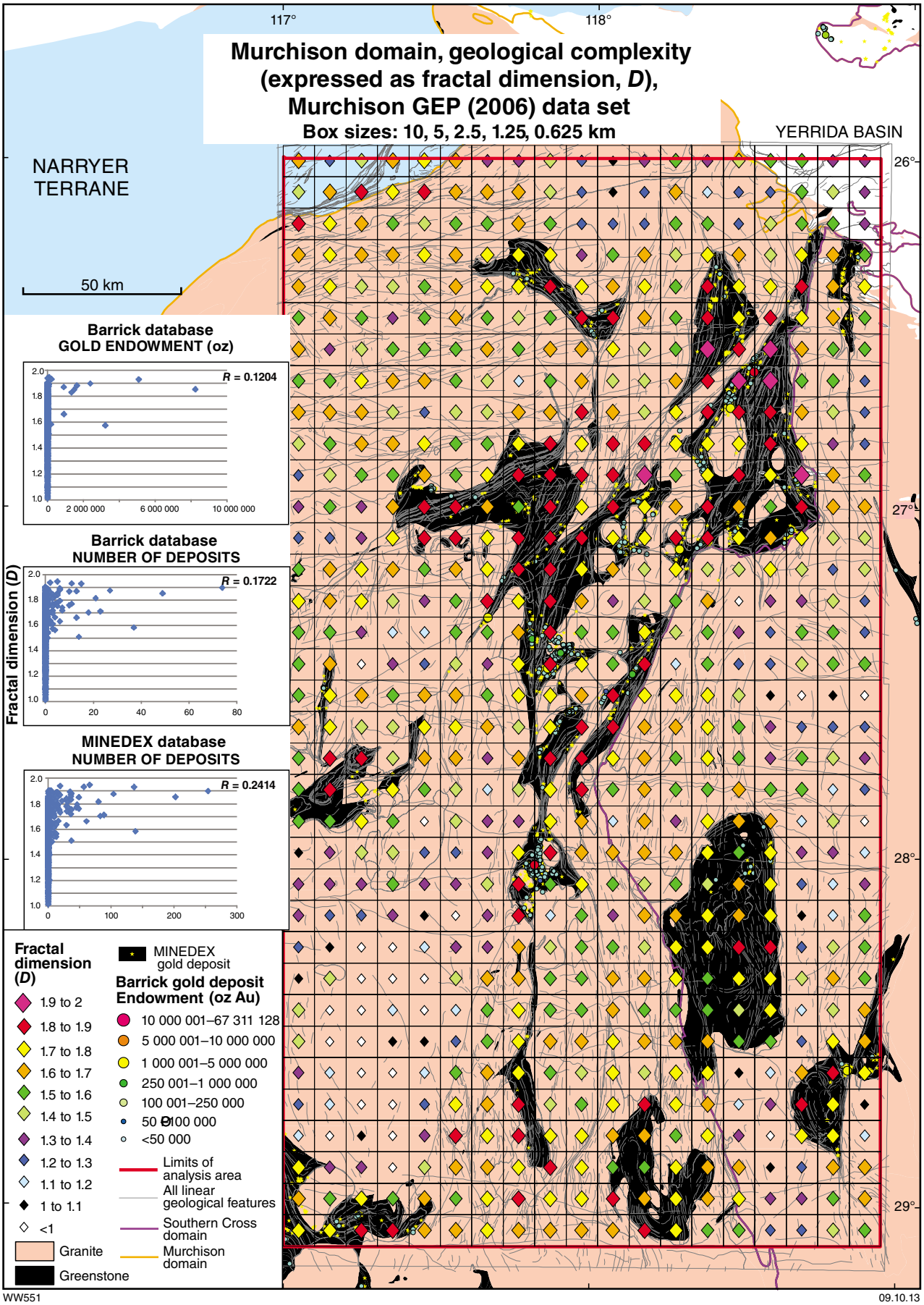

Figure 1.67. **Distribution of gold deposits in the northern Murchison domain relative to geological complexity (expressed as fractal dimension *D*) using GSWA GEP 2006 dataset (10, 5, 2.5, 1.25, and 0.625 km box sizes)**

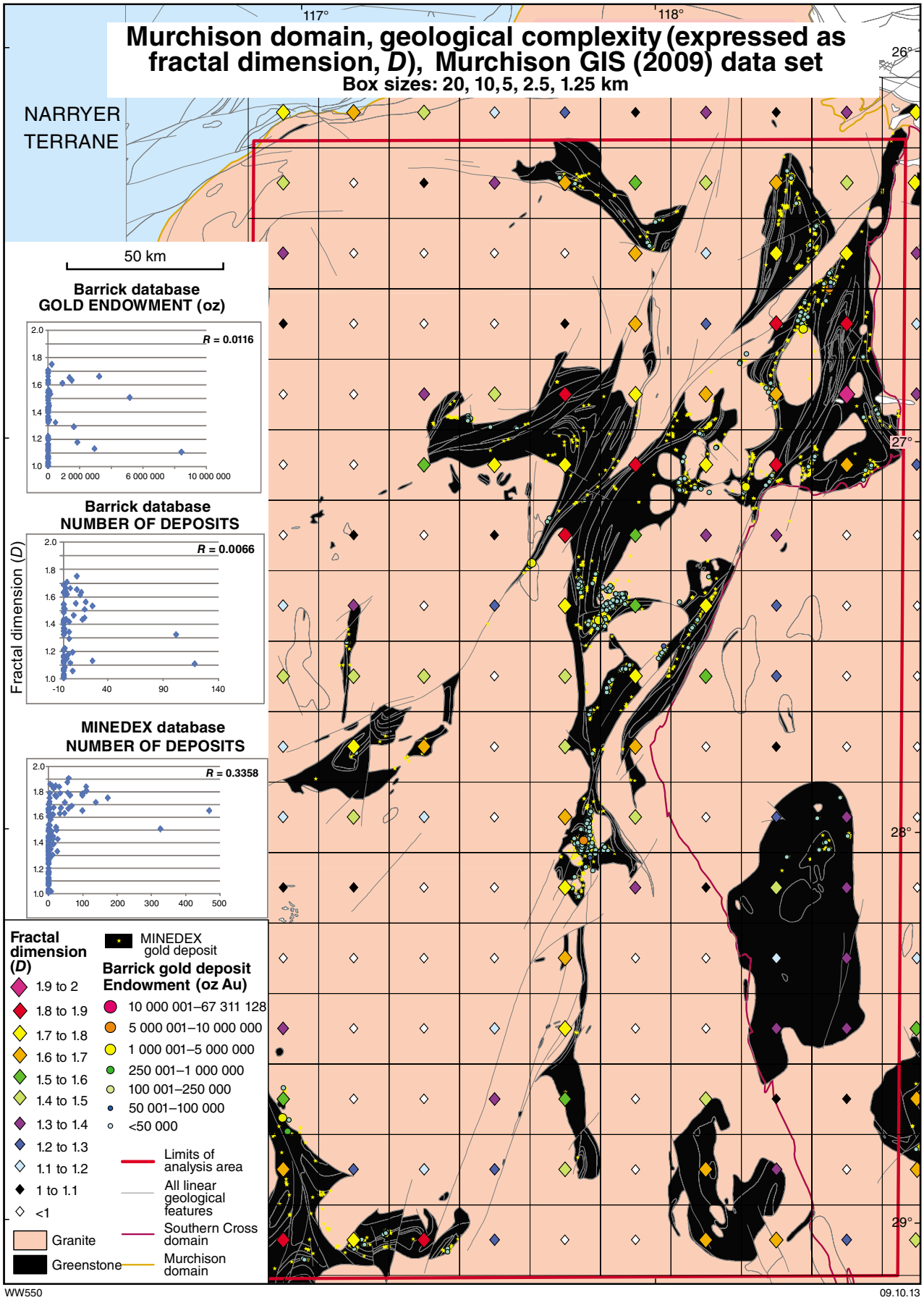

Figure 1.68. **Distribution of gold deposits in the northern Murchison domain relative to geological complexity (expressed as fractal dimension *D*) using GSWA GIS 2009 dataset (20, 10, 5, 2.5, and 1.25 km box sizes)**

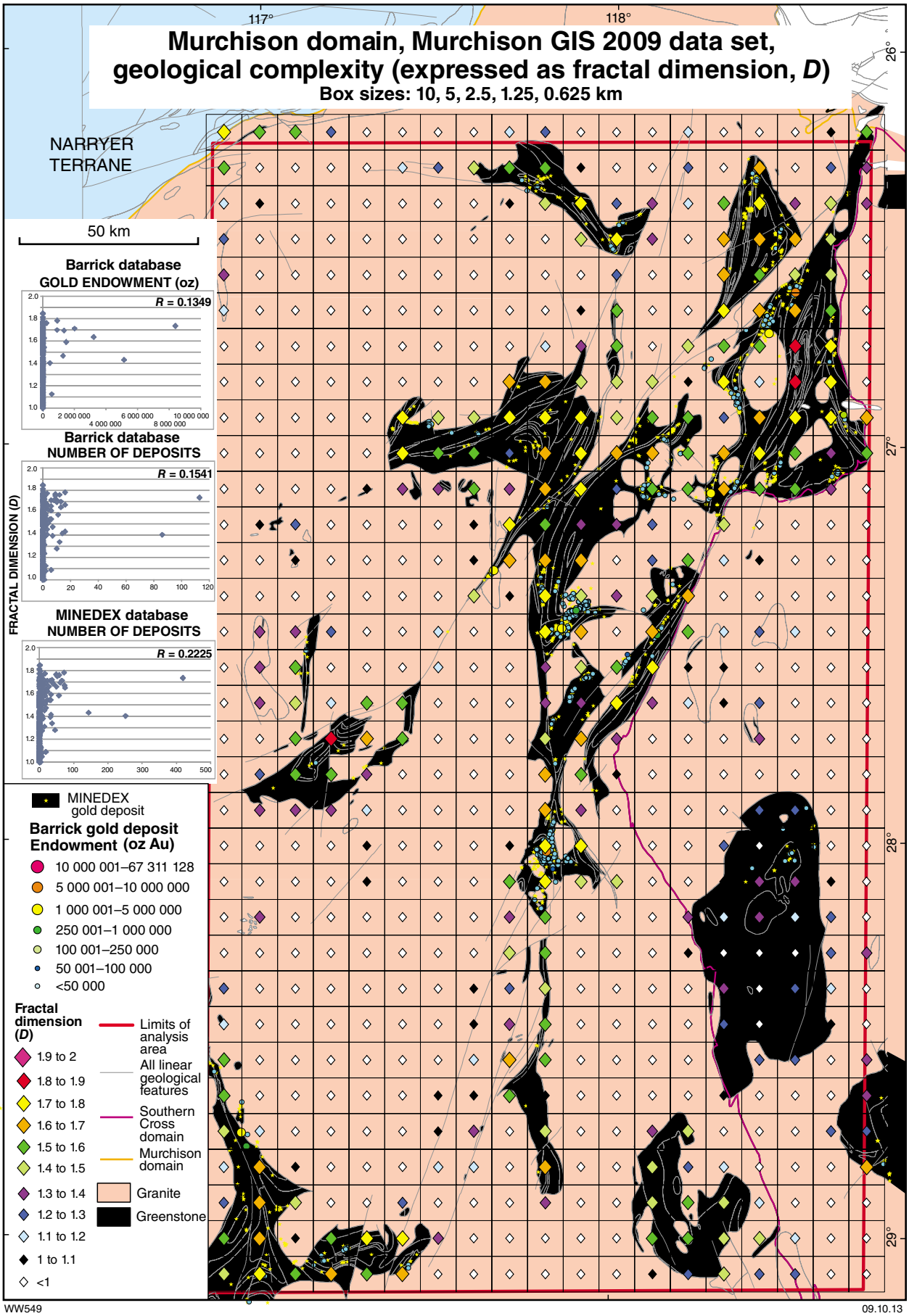

Figure 1.69. **Distribution of gold deposits in the northern Murchison domain relative to geological complexity (expressed as fractal dimension *D*) using GSWA GIS 2009 dataset (10, 5, 2.5, 1.25, and 0.625 km box sizes)**

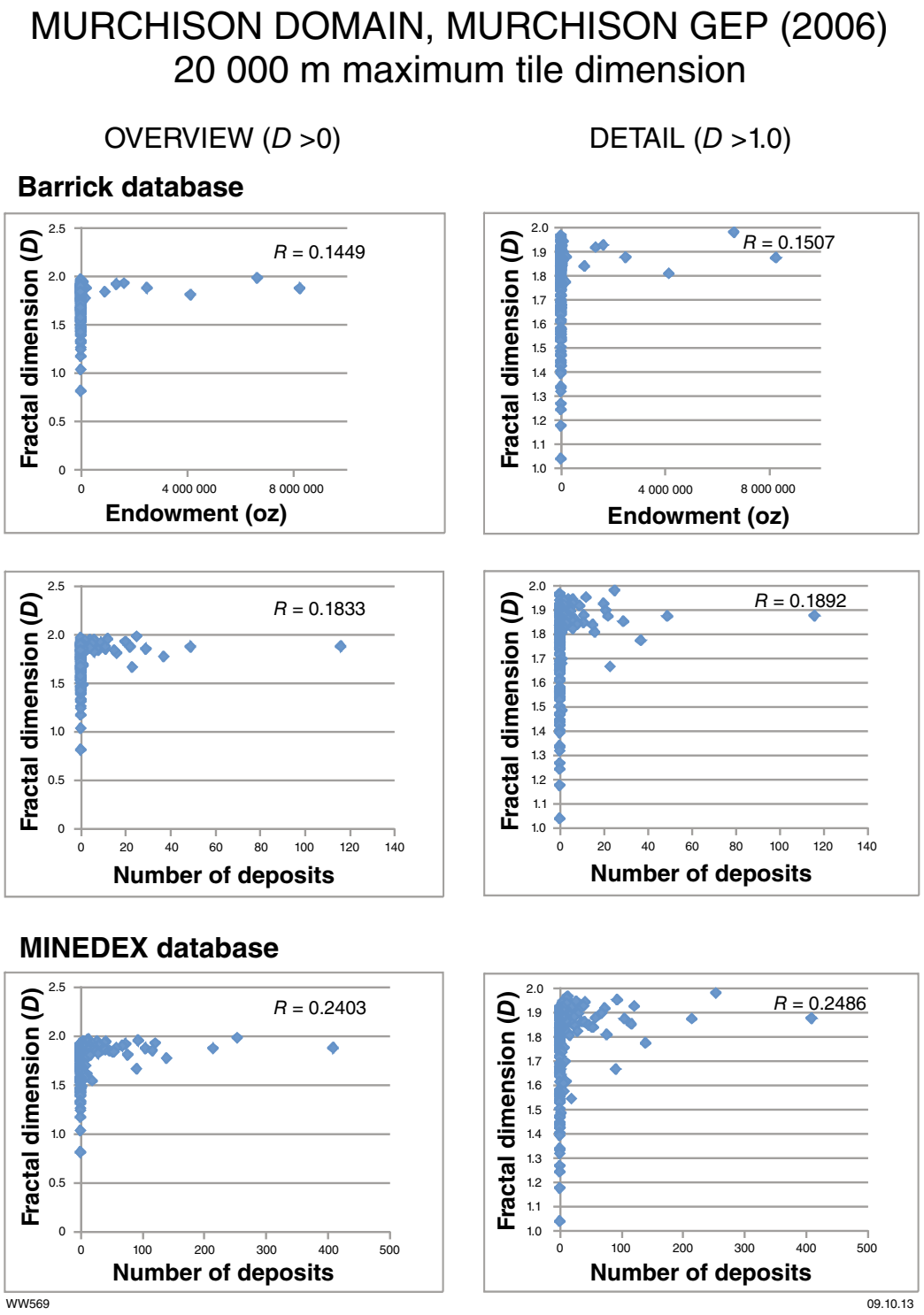

Figure 1.70. Summary of correlations between gold deposits and fractal dimension (*D*) for the northern Murchison domain (GSWA GEP 2006 dataset; 20, 10, 5, 2.5, and 1.25 km box sizes)

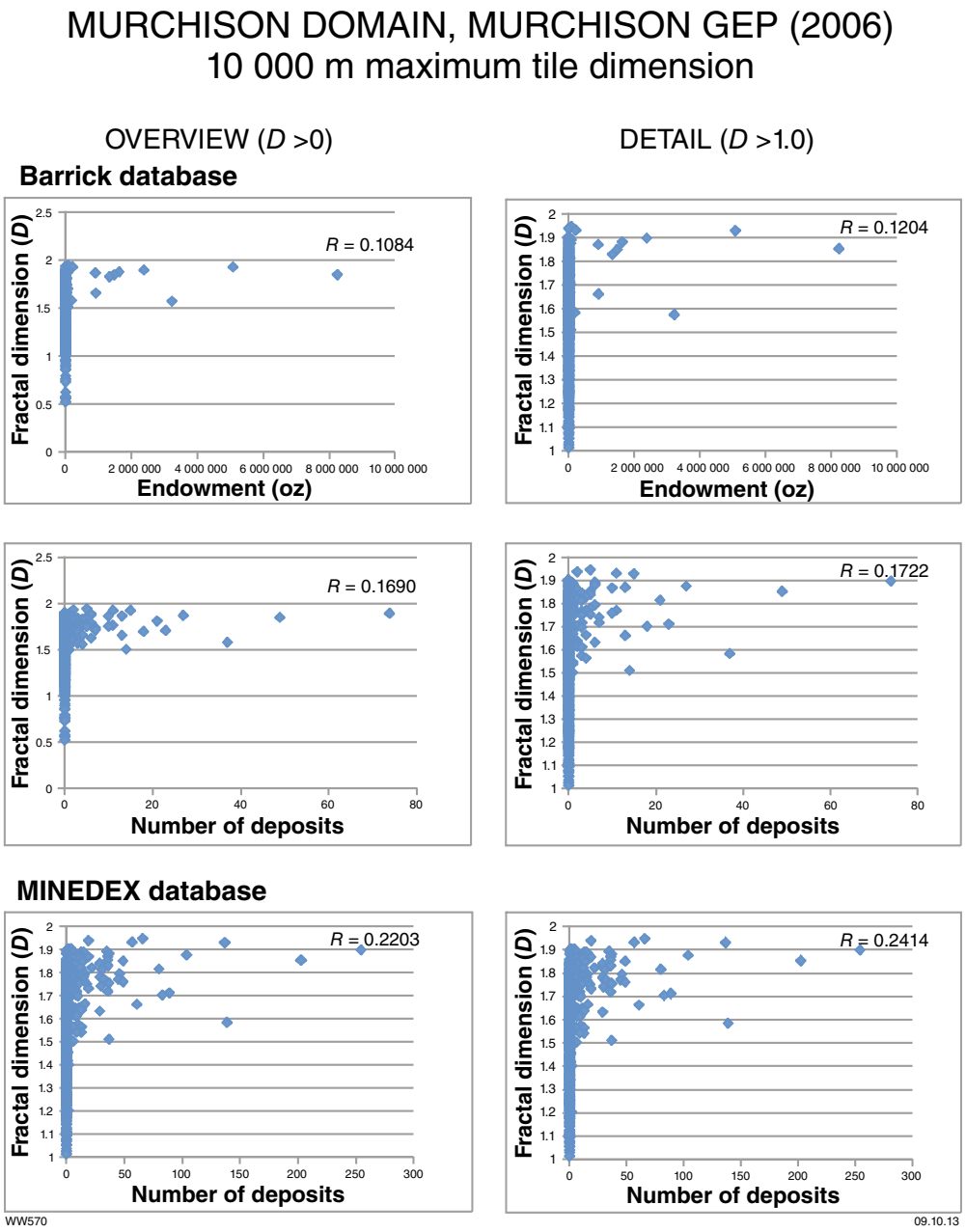

Figure 1.71. **Summary of correlations between gold deposits and fractal dimension (*D*) for the northern Murchison domain (GSWA GEP 2006 dataset; 10, 5, 2.5, 1.25, and 0.625 km box sizes)**

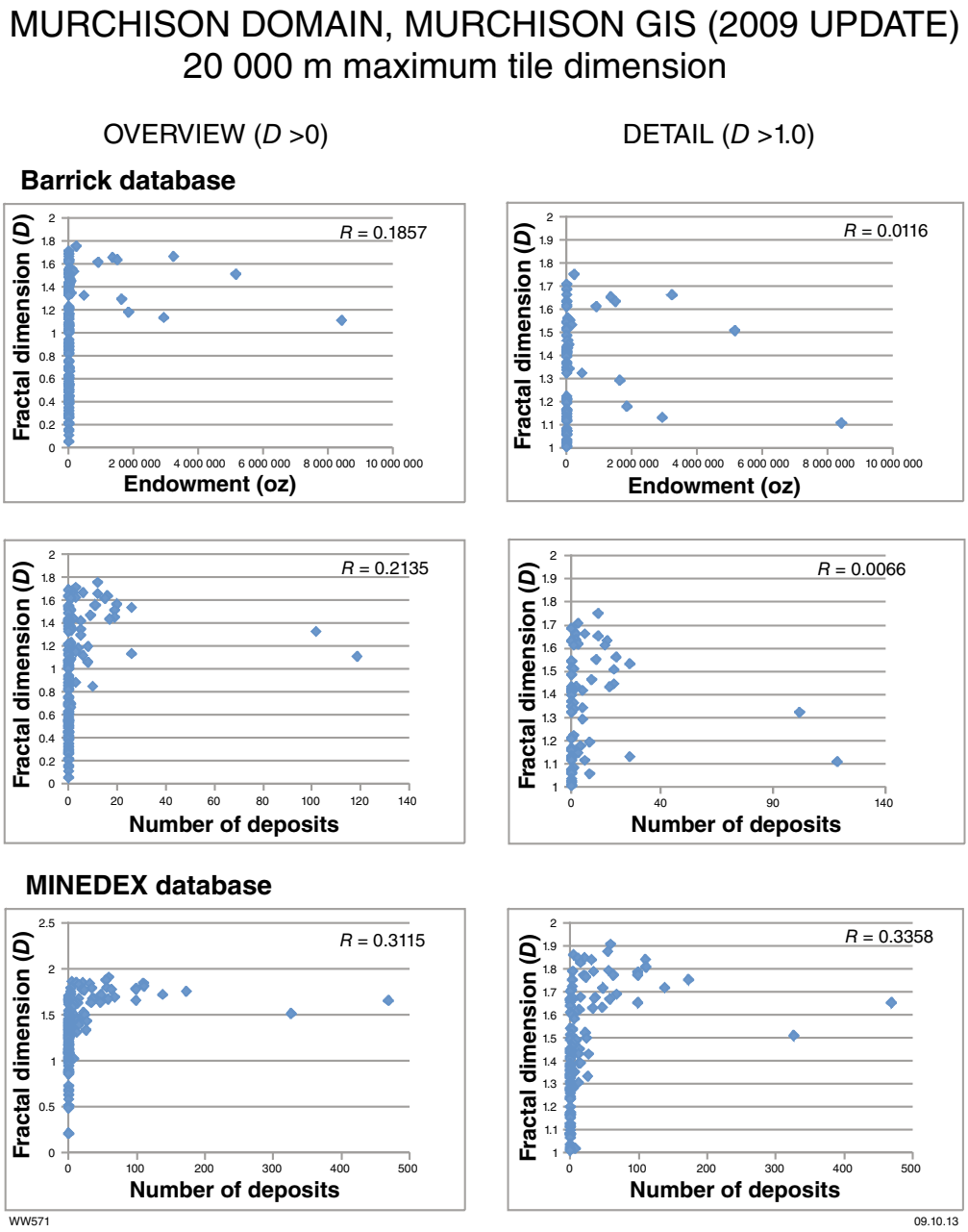

Figure 1.72. **Summary of correlations between gold deposits and fractal dimension (*D*) for the northern Murchison domain (GSWA GIS 2009 dataset; 20, 10, 5, 2.5, and 1.25 km box sizes)**

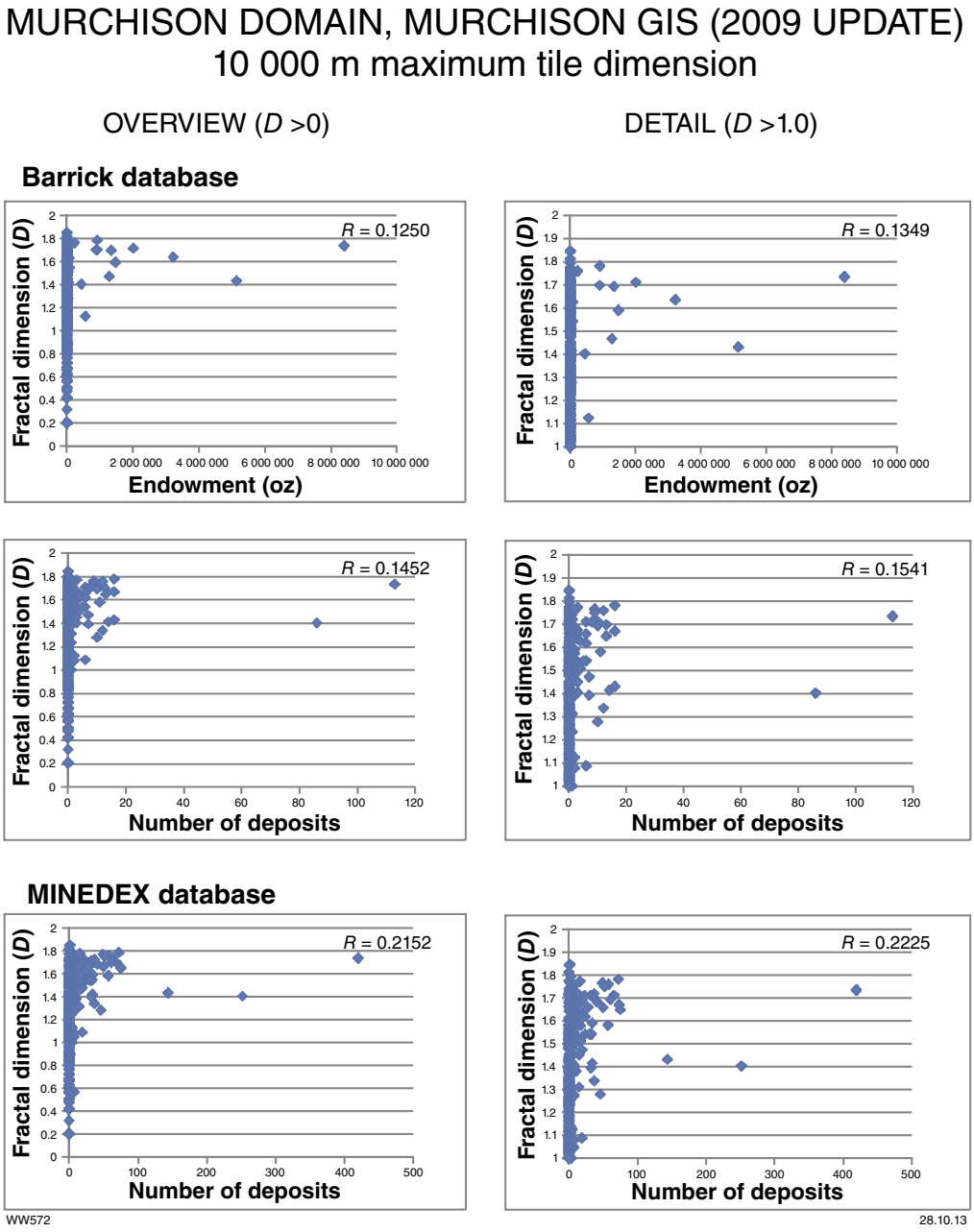

Figure 1.73. **Summary of correlations between gold deposits and fractal dimension (*D*) for the northern Murchison domain (GSWA GIS 2009 dataset; 10, 5, 2.5, 1.25, and 0.625 km box sizes)**

Application of regional-scale targeting results to produce gold prospectivity maps

Four of the more successful targeting criteria to emerge from the analyses presented above were used to produce regional-scale gold prospectivity maps of the Yilgarn Craton (Fig. 1.74) and Eastern Goldfield Superterrane (Fig. 1.75). The chosen criteria were:

1. Proximity to Mafic Group granite intrusions (Criterion 1.3)
2. Proximity to fault bends (Criterion 1.10)
3. Proximity to areas of high fault density (Criterion 1.8)
4. Within greenstone areas.

The fourth criterion listed above is not one of the 18 criteria discussed in detail in this Atlas, but is well known (e.g. Groves et al., 1989, 1998) and understood by exploration geologists. It is briefly discussed in the section of this Atlas headed Terranes and domains: Gold endowment (see Tables A1.3 and A1.4 for containment analyses for greenstone areas only).

In a separate exercise, two additional targeting criteria that yielded less-successful results (Criterion 1.13, within domes; Criterion 1.17, proximity to late-stage basins) were added to the analysis for the Eastern Goldfields Superterrane to determine to what extent their inclusion affected the results (Fig. 1.76).

The selected criteria were combined by using fuzzy logic (Bonham-Carter, 1995; Knox-Robinson, 2000) to generate spatial grids with the grid cells representing relative prospectivity for gold. The values assigned to each cell were then converted to a colour scale and used to produce prospectivity maps. Fuzzy logic is a knowledge-driven approach that uses expert opinion to determine critical input datasets and their associated fuzzy membership values. The results of the spatial analyses led to selection of the four targeting criteria listed above and also to the choice of %Endowment/%Area as the best parameter from which to determine fuzzy membership values, as doing so would better target large deposits.

The starting point for the fuzzy logic analysis was to determine the maximum %Endowment/%Area ratio for each of the selected targeting criteria. Then, critical thresholds for each were defined as the value at which the maximum value of %Endowment/%Area for that criterion was obtained. A particularly high maximum %Endowment/%Area ratio for the Yilgarn Craton (50.4) was obtained for the 1000 m buffer around Mafic granite intrusions. The fuzzy membership values for the other criteria were then obtained by normalizing their maximum %Endowment/%Area ratios to this value (50.4), thus obtaining fuzzy membership values in the range from zero to one (Bonham-Carter, 1995). Tables 1.4 and 1.5 summarize the fuzzy logic parameters used to produce the gold prospectivity maps of the Yilgarn Craton and Eastern Goldfields Superterrane.

Each targeting criterion represents an input data layer for the fuzzy logic analysis. The input layers were combined using a fuzzy gamma operator with a gamma value of 0.95 (Bonham-Carter, 1995). This operator determines prospectivity values at each grid point that include input from each of the data layers (criteria).

The regional gold prospectivity maps determined on the basis of fuzzy logic are presented in Figures 1.74 to 1.76, on which the distribution of deposits from both the Barrick gold deposits database (on which mapped prospectivity is based) and the MINEDEX database are shown for reference. Inevitably, there is a good correlation between the larger gold deposits and areas of high prospectivity. Many of the smaller deposits are in domains of low to moderate prospectivity. The maps also show several areas of relatively high prospectivity where there are few or no known gold deposits. These areas, which warrant further exploration scrutiny for gold, include (1) the central to northern parts of the Scotia–Kanowna dome, (2) the Depot Granodiorite, and (3) several areas at least partly coincident with Mafic Group granite intrusions in the Murchison domain (Fig. 1.74). Slightly less prospective are (4) several domains in the Southern Cross domain and (5) some small areas near the boundary between the Murchison domain and Narryer Terrane, and (6) between the Youanmi and the South West Terranes (Fig. 1.74).

Within the Eastern Goldfields Superterrane, several broad swathes of high prospectivity are identified (Fig. 1.75), based on the same targeting criteria as used for the Yilgarn Craton as a whole. Those that do not contain many known gold deposits and may thus be considered prospective for exploration include (1) the northwestern Yandal greenstone belt, (2) the belt of granite and greenstones linking the southern Yandal belt with the northern Agnew area, (3) the Pinjin greenstone belt to the south of the Laverton Tectonic Zone, (4) the Outcamp Tonalite and surrounding greenstones, (5) greenstones between the Kalpini and Binti Binti mining areas, and (6) greenstones west of the Norseman mining area (Fig. 1.75).

The addition of two extra targeting criteria for the Eastern Goldfields Superterrane analysis created finer divisions of prospectivity range but did not materially change the distribution of prospective areas (Fig. 1.76a). There are some small areas of moderate prospectivity that are obscured by mine symbols (compare red areas in Figs 1.76a and 1.76b). The limited influence of the two additional targeting criteria reflects the low fuzzy membership values assigned to these inputs, based on their relatively weak %Endowment/%Area ratios.

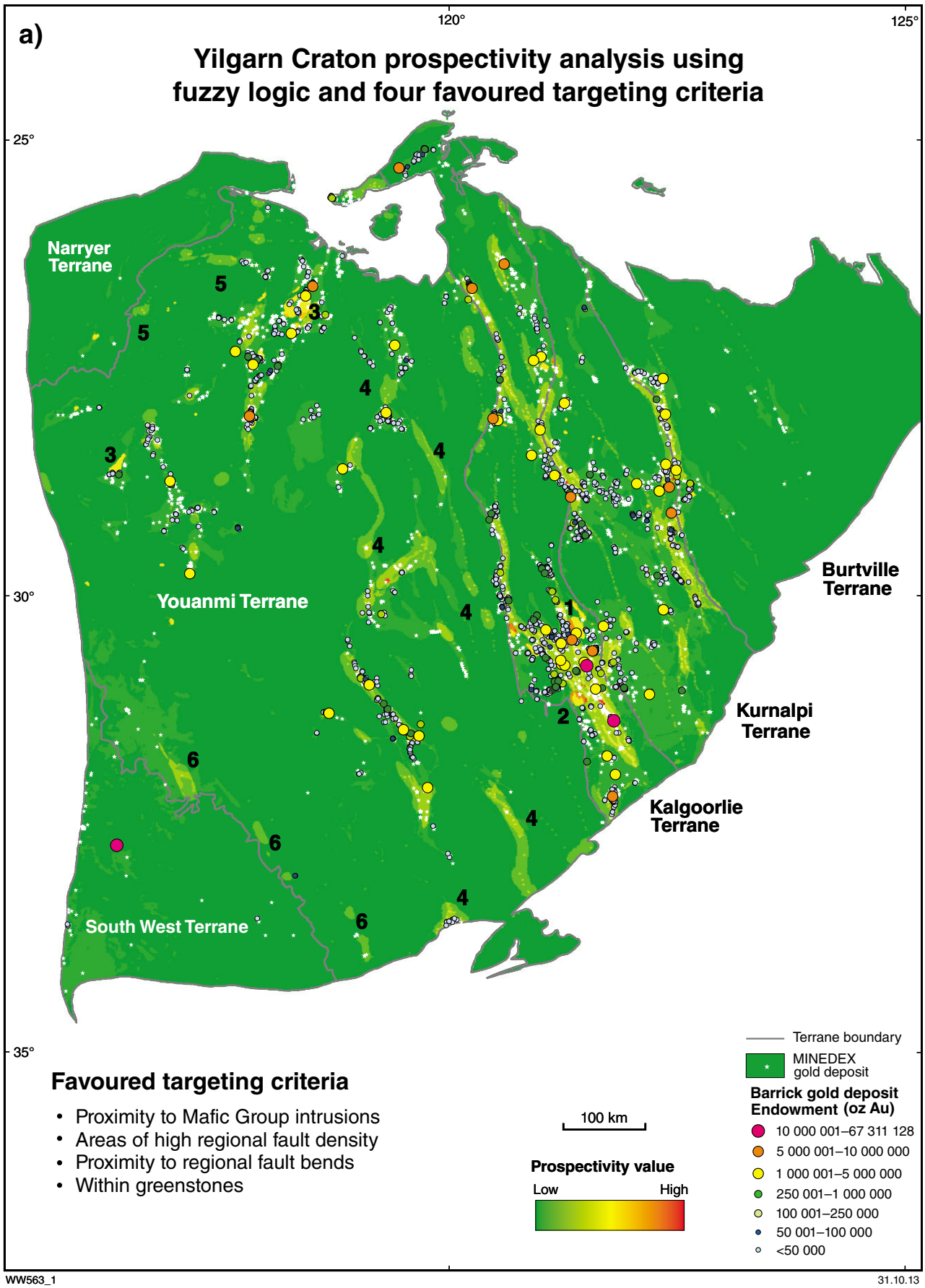

Figure 1.74. **Prospectivity maps of the Yilgarn Craton based on the four most-favoured targeting criteria: a) With gold deposits shown; b) without gold deposits. Numbers on maps indicate areas discussed in text that may warrant further exploration attention.**

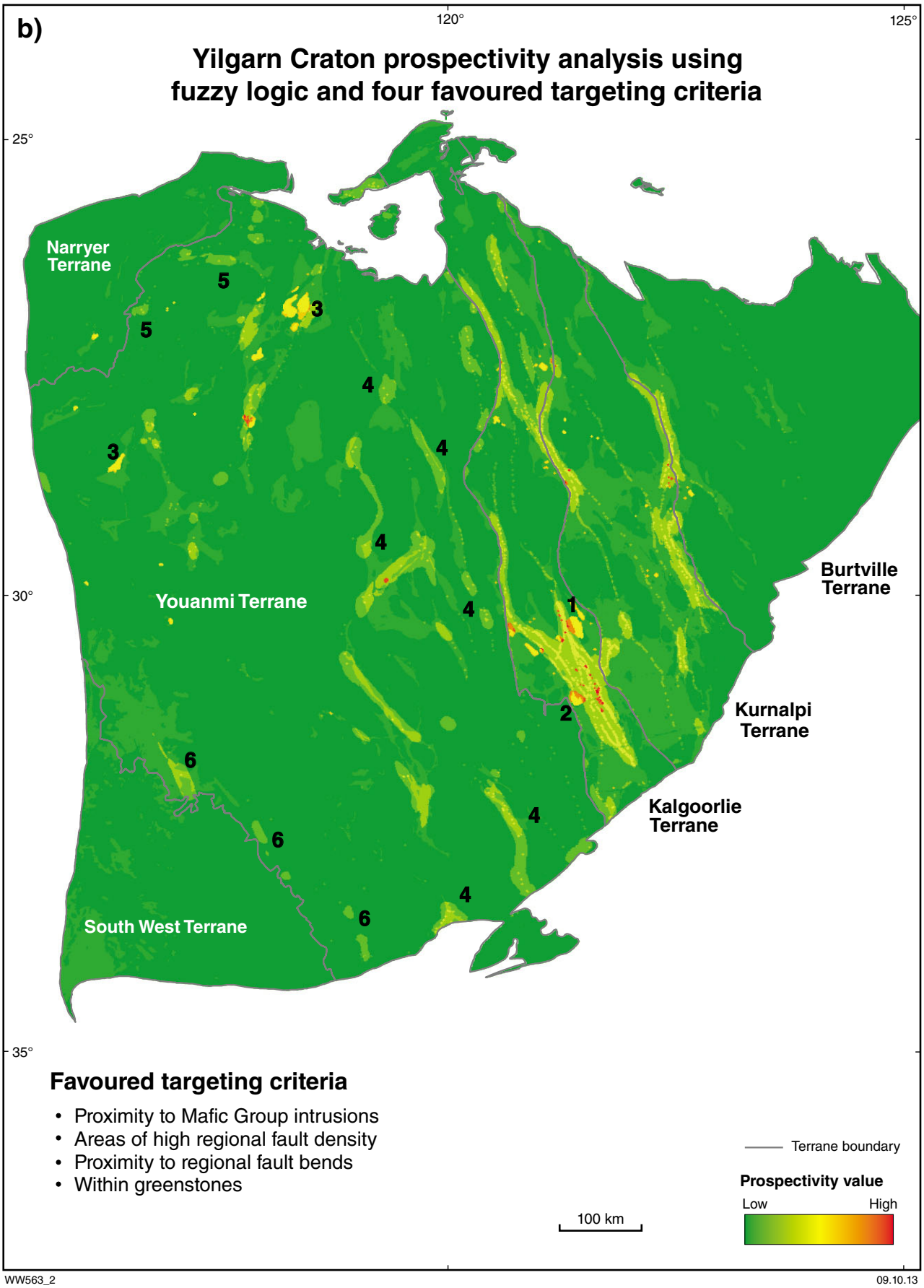
b)
120°
125°
Yilgarn Craton prospectivity analysis using
fuzzy logic and four favoured targeting criteria
25°
30°
35°
Narryer Terrane
Youanmi Terrane
South West Terrane
Burtville Terrane
Kurnalpi Terrane
Kalgoorlie Terrane
5
5
3
4
3
4
4
4
1
2
6
6
4
6
4
Favoured targeting criteria
• Proximity to Mafic Group intrusions
• Areas of high regional fault density
• Proximity to regional fault bends
• Within greenstones
Terrane boundary
Prospectivity value
Low
High
100 km
WW563_2
09.10.13

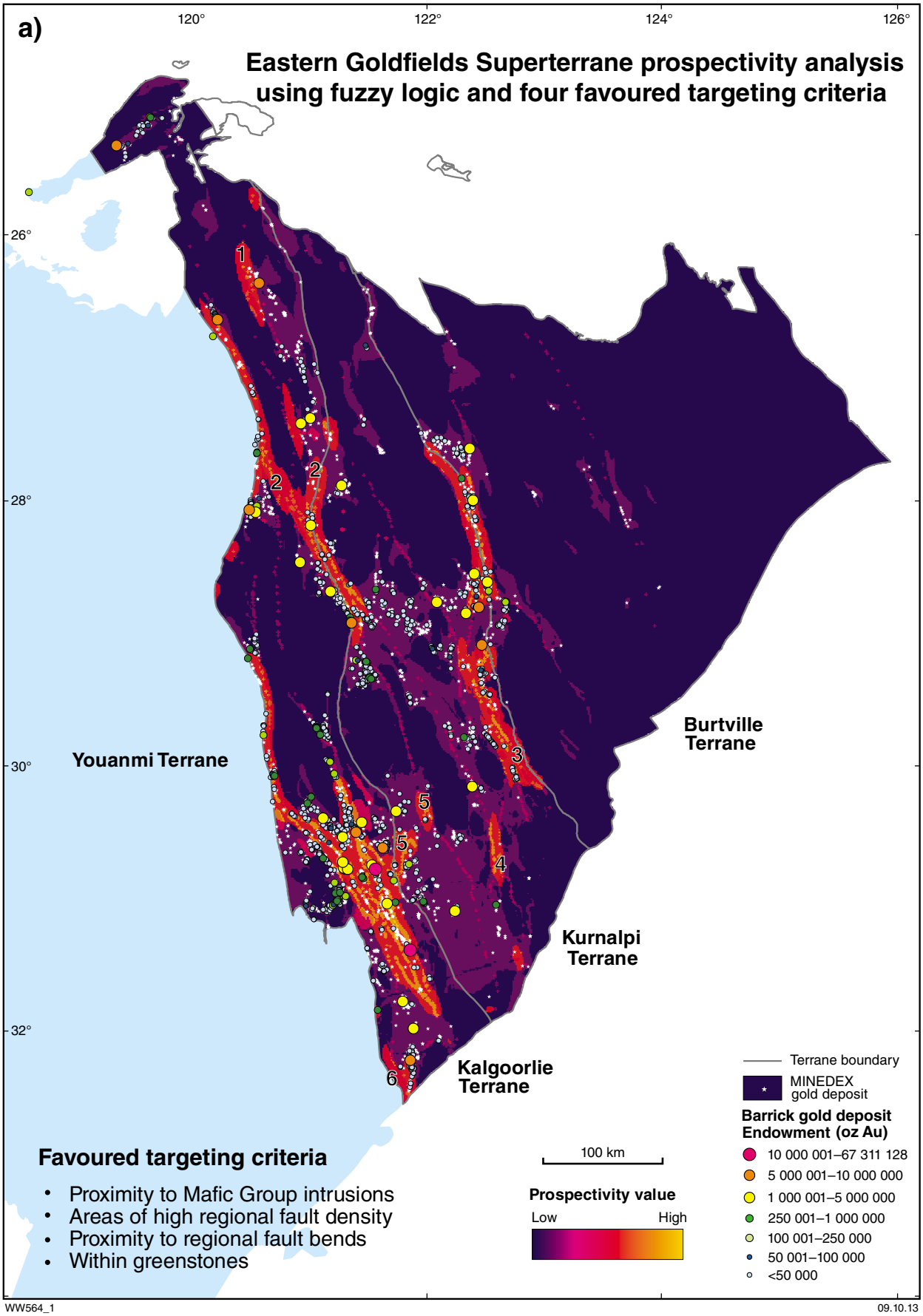

Figure 1.75. **Prospectivity maps of the Eastern Goldfields Superterrane based on the four most-favoured targeting criteria: a) With gold deposits shown; b) without gold deposits. Numbers on maps indicate areas discussed in text that may warrant further exploration attention.**

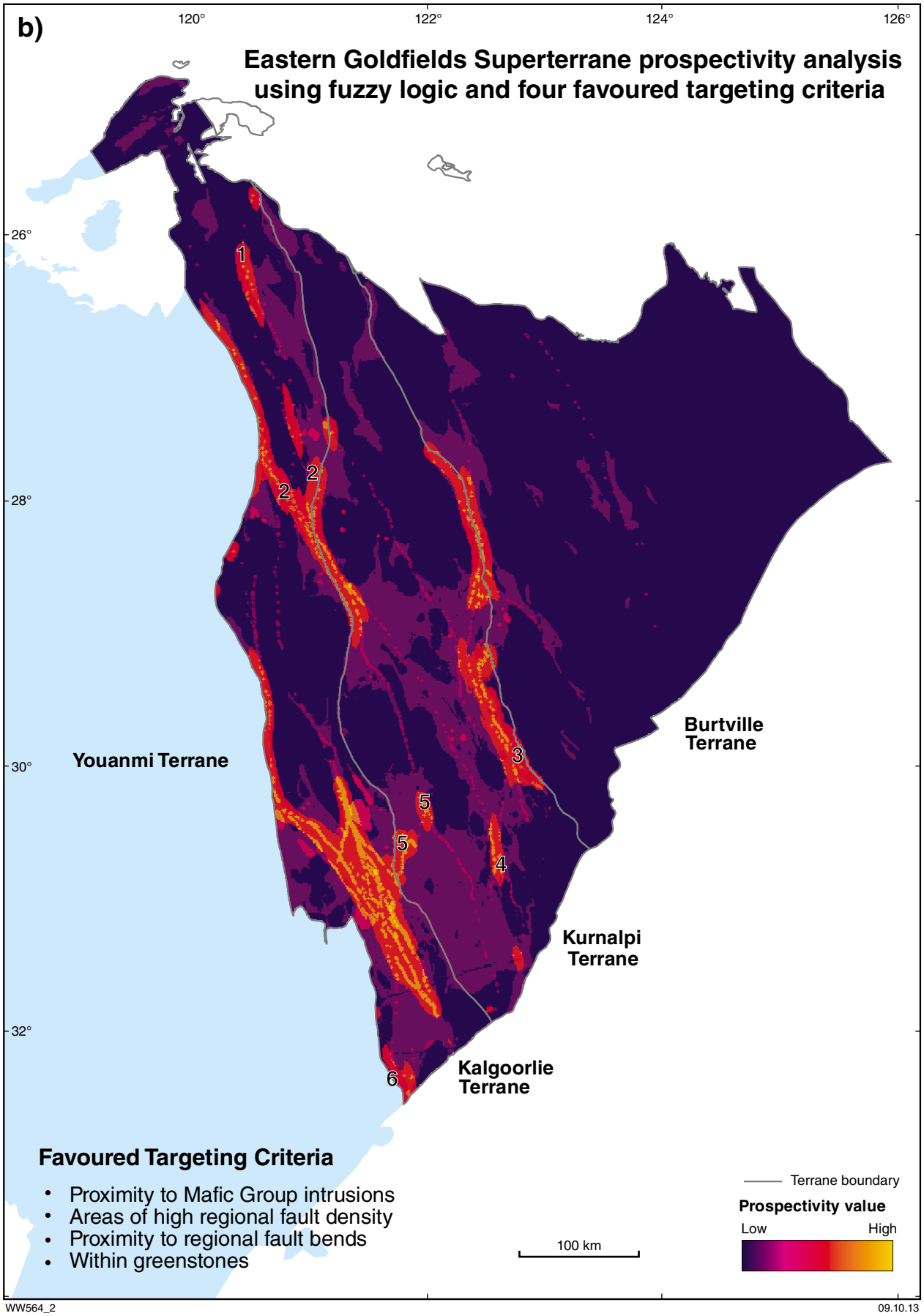
b)
Eastern Goldfields Superterrane prospectivity analysis
using fuzzy logic and four favoured targeting criteria
120°
122°
124°
126°
26°
28°
30°
32°
1
2
2
3
5
5
4
6
Youanmi Terrane
Burtville
Terrane
Kurnalpi
Terrane
Kalgoorlie
Terrane
Favoured Targeting Criteria
• Proximity to Mafic Group intrusions
• Areas of high regional fault density
• Proximity to regional fault bends
• Within greenstones
Terrane boundary
Prospectivity value
Low
High
100 km
WW564_2
09.10.13

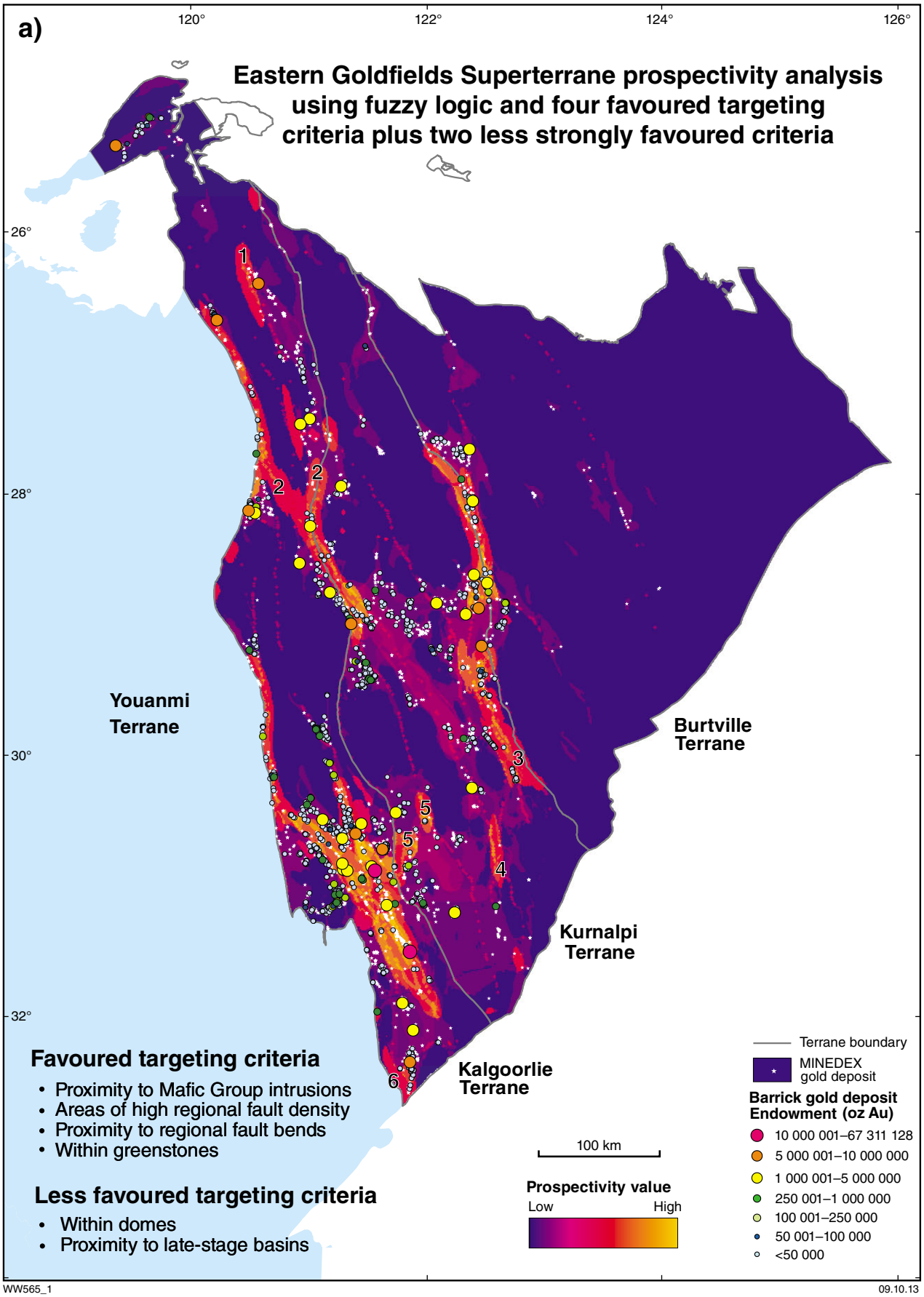

Figure 1.76. **Prospectivity maps of the Eastern Goldfields Superterrane based on the four most-favoured targeting criteria plus two less-favoured criteria: a) With gold deposits shown; b) without gold deposits. Numbers on maps indicate areas discussed in text that may warrant further exploration attention.**

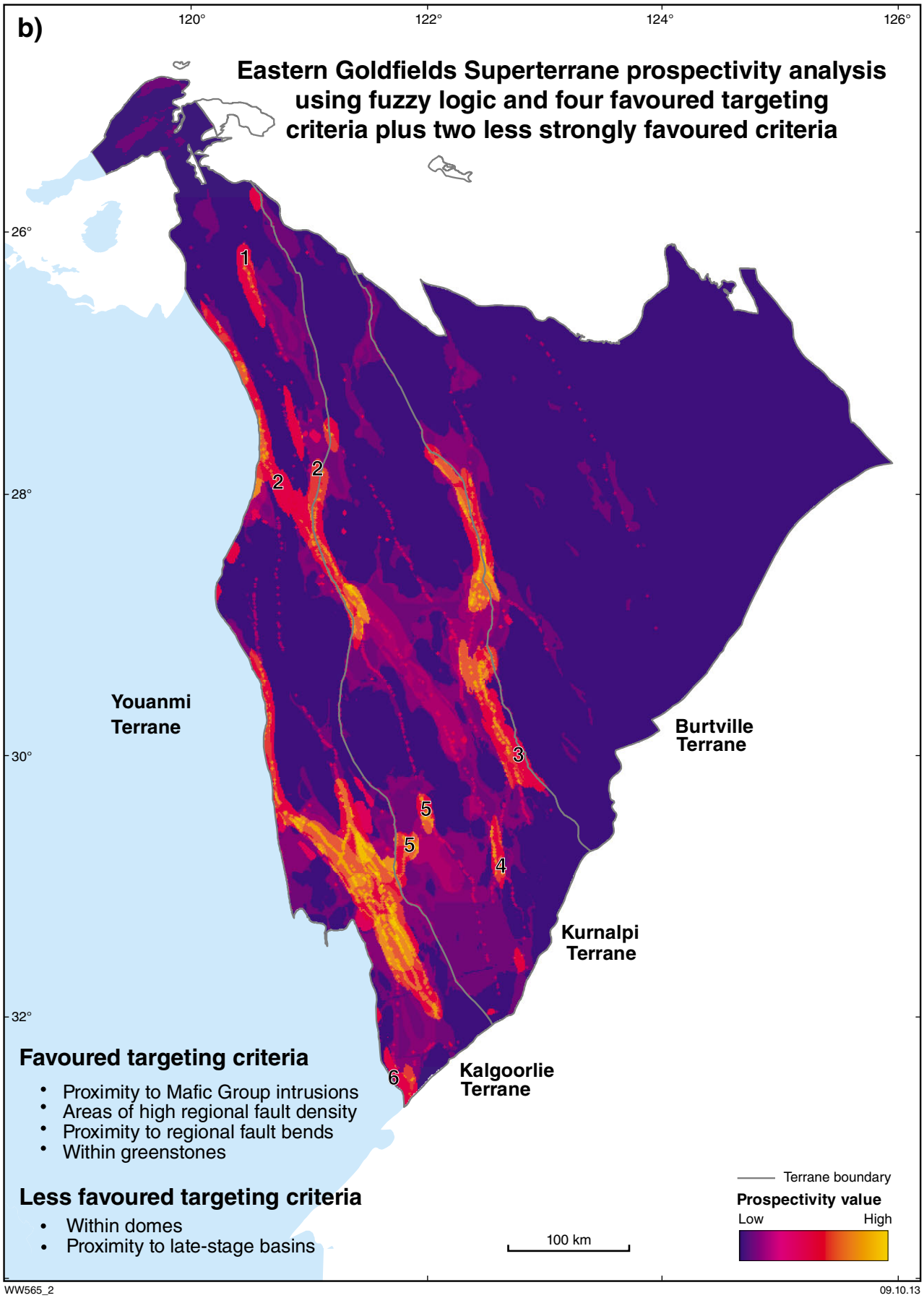
b)
120°
122°
124°
126°
Eastern Goldfields Superterrane prospectivity analysis using fuzzy logic and four favoured targeting criteria plus two less strongly favoured criteria
26°
28°
30°
32°
1
2
2
3
4
5
5
6
Youanmi Terrane
Burtville Terrane
Kurnalpi Terrane
Kalgoorlie Terrane
Favoured targeting criteria
• Proximity to Mafic Group intrusions
• Areas of high regional fault density
• Proximity to regional fault bends
• Within greenstones
Less favoured targeting criteria
• Within domes
• Proximity to late-stage basins
100 km
Terrane boundary
Prospectivity value
Low
High
WW565_2
09.10.13

Table 1.4. Critical thresholds, corresponding %Endowment/%Area values, and fuzzy membership values for four of the more successful regional targeting criteria for the Yilgarn Craton

Input layer	*Critical threshold*	*% Endowment%Area*	*Fuzzy membership value*
Fault density	>0.1 km/km^2	15	0.2976
Fault bends	1000 m buffer	11.9	0.2361
Mafic Group granites	1000 m buffer	50.4	1.0000
Greenstones	Containment	5.98	0.1186

Table 1.5. Critical thresholds, corresponding %Endowment/%Area values, and fuzzy membership values for six targeting criteria for the Eastern Goldfields Superterrane (comprising the same four criteria listed in Table 4, plus two of the less successful regional targeting criteria)

Input layer	*Critical threshold*	*%Endowment%Area*	*Fuzzy membership value*
Fault density	>0.1 km/km^2	108	1.0000
Fault bends	1000 m buffer	11.9	0.1102
Mafic Group granites	1000 m buffer	50.4	0.4667
Domes	Containment	2.39	0.0221
Late-stage basins	7500 m buffer	5.98	0.0554
Greenstones	Containment	3.71	0.0343

Relationship of calculated prospectivity to known gold deposits

A quantitative analysis of the spatial relationship between calculated prospectivity values and known gold deposits (Tables A1.97 to A1.102) shows poor correlations between calculated prospectivity value and both actual endowment (as a percentage of total endowment) and actual number of deposits (as a percentage of total number of deposits). When endowment and number of deposits are normalized by area, the correlation is much better. Using the Barrick gold deposits database for endowment and number of deposits, the correlation coefficient (R) was 0.44 between Prospectivity Value and %Endowment/%Area, and 0.75 for its correlation with %Deposits/%Area (Table A1.97). This is an interesting result, since the prospectivity map is predicated on %Endowment/%Area, not %Deposits/%Area. These results are replicated in data for the Eastern Goldfields Superterrane. Correlation coefficients for the Eastern Goldfields Superterrane prospectivity map are 0.38 for %Endowment/%Area and 0.49 for %Deposits/%Area (Table A1.98). As shown in Table A1.99, the addition of domes and late-stage basins (Criteria 1.13 and 1.17) to the analysis results in a deterioration of both correlation coefficients to R values of 0.03 (%Endowment/%Area) and 0.25 (%Deposits/%Area). These results suggest that the prospectivity map using the original four targeting criteria are more useful than those incorporating six criteria as input layers; the addition of domes and late-stage basins appears to compromise the usefulness of the maps.

As described above, the prospectivity maps are based on endowment rather than deposit density because fuzzy membership values were determined by %Endowment/%Area. Despite this foundation, the results indicate that domains with high prospectivity values will not only contain large deposits but also many small deposits. An independent assessment of this relationship was undertaken using the MINEDEX database (Tables A1.100 to A1.102). The resultant correlation coefficients between Prospectivity Value and %Deposits/%Area are 0.78 for the Yilgarn Craton (Table A1.100) and 0.53 for the Eastern Goldfields Superterrane (Table A1.101). As was the case for the results using endowment and deposit density from the Barrick gold deposits database, the addition of the two extra criteria (1.13 and 1.17) to the analysis for the Eastern Goldfields Superterrane resulted in a deterioration of the correlation coefficient from 0.53 to 0.28 (Table A1.102).

The results of the above analyses can be compared with those of Czarnota et al. (2010a), who published a prospectivity map for the Yilgarn Craton based on the principles of fuzzy logic. In that study, the input layers (targeting criteria) chosen were based on the subjective judgement of the authors, as were the weighting factors for each of the input layers. No robust spatial statistics were derived to determine quantitatively whether the input layer actually had a consistent and statistically significant relationship with gold mineralization, or the strength of any such relationship. Our approach, while also based on fuzzy logic, is based on the quantitative results of GIS spatial analysis relating known gold mineralization to a number of selected targeting criteria. Input layers contributing to the prospectivity maps included only those that showed a robust statistical relationship with known mineralization, and the weighting factor used was assigned in a semi-quantitative way by selecting one of the statistical measures (%Endowment/%Area) calculated as a result of the corresponding spatial analysis. Among the results of Czarnota et al. (2010a), a 5 km buffer around areas with a combined weighting factor of 15 captured 75% of the gold endowment in 5% of the area. A direct quantitative comparison of our results with those of Czarnota et al. (2010a) is not possible. Czarnota et al. (2010a) measured the success of their prospectivity map by quantifying the gold endowment within their buffer as a percentage of the total endowment in their analysis area, whereas we used the endowment data to determine the most effective targeting criteria.

Acknowledgements

Part 1 of the Yilgarn Gold Exploration Targeting Atlas makes use of a Yilgarn gold deposit database generously made available for the project by Barrick Gold Corporation. Matt Fallon and Antony Shepherd of Barrick are thanked for their support throughout the life of the YETA project. As manager of the project, Stephen Wyche provided solutions to many apparently insurmountable problems. Lee Hassan and Jyotindra Sapkota provided formal peer reviews of the document prior to submission for editing. Drafting of all maps was carried out by the patient and adaptive Joyce Peng. The final published version of Part 1 benefited from the experienced editorial hand of Alex Forbes.

References

Alibone, AH, McCuaig, TC, Harris, D, Etheridge, M, Munroe, S, Byrne, D, Amanor, J and Gyapong, W 2002, Structural controls on gold mineralisation at the Ashanti Deposit, Obuasi, Ghana: Society of Economic Geologists, Special Publication 9, p. 65–93.

Anand, RR and Butt, CRM 2010, A guide for mineral exploration through the regolith in the Yilgarn Craton, Western Australia: Australian Journal of Earth Sciences, v. 57, p. 1015–114.

Archibald NJ, Holden, D, Mason, R and Power, B 2001, There's a worm in my soup: wavelet based analysis for interpretation of crustal scale potential field data and implications for identification of giant gold deposits, *in* A Hydrothermal Odyssey *edited by* PJ Williams: James Cook University, Townsville, Australia, 2001, Abstracts. Economic Geology Research Unit Contribution 59, p. 5–7.

Barnett, CT and Williams, PM 2012, A radical approach to exploration: let the data speak for themselves: SEG Newsletter, v. 90, p. 1–17.

Bateman, R, Ayer, JA and Dubé, B 2008, The Timmins – Porcupine gold camp, Ontario: Anatomy of an Archean greenstone belt and ontogeny of gold mineralization: Economic Geology, v. 103, p. 1285–1308.

Bierlein, FP (editor) 2005, What are the fundamental characteristics of mineralised (trans-lithospheric) fault systems?: Final Report, Project A1, pmd*CRC, 24p.

Bierlein, FP, Murphy, FC, Weinberg, RF and Lees, T 2006, Distribution of orogenic gold deposits in relation to fault zones and gravity gradients: targeting tools applied to the Eastern Goldfields, Yilgarn craton, Western Australia: Mineralium Deposita, v. 41, p. 107–126.

Binns, RA, Gunthorpe, R and Groves, DI 1976, Metamorphic patterns and development of greenstone belts in the eastern Yilgarn Block, in The Early History of the Earth *edited by* BF Windley: New York, John Wiley and Sons, p. 303–316.

Blewett, RS, Cassidy, KF, Champion, DC, Henson, PA, Goleby, BR, Jones, L and Groenewald, PB 2004, The Wangkathaa Orogeny: an example of episodic regional "D2" in the late Archaean Eastern Goldfields Province, Western Australia: Precambrian Research, v. 130, p. 139–159.

Blewett, RS, Cassidy, KF, Henson, PA, Roy, IG, Champion, DC and Fomin, T 2008, Chapter 3.3, Question 2: Big systems – big signatures – anatomy of the Archaean Yilgarn Craton and implications for world-class gold mineral systems, *in* Concepts to targets: a scale-integrated mineral systems study of the eastern Yilgarn craton, *compiled by* Y4 Project Team: pmd*CRC Y4 Final Report, p. 83–112.

Blewett, RS, Czarnota, K and Henson, PA 2010a, Structural-event framework for the eastern Yilgarn Craton, Western Australia, and its implications for orogenic gold: Precambrian Research, v. 183, p. 203–229.

Blewett, RS, Henson, PA, Roy, IG, Champion, DC and Cassidy, KF 2010b, Scale-integrated architecture of a world-class gold mineral system: The Archaean eastern Yilgarn Craton, Western Australia: Precambrian Research, v. 183, p. 230–250.

Blewett, RS and Hitchman, AP (editors) 2006, Final Report – 3D Geological models of the eastern Yilgarn craton, Project Y2. Unpublished pmd*CRC report: Geoscience Australia, Record 2006/05, 276p.

Bloem, EJM, Dalstra, HJ, Groves, DI and Ridley, JR 1994, Metamorphic and structural setting of Archaean amphibolite-hosted gold deposits near Southern Cross, Yilgarn Block, Western Australia: Ore Geology Reviews, v. 9, p. 183–208.

Bonham-Carter, G.F., 1995, Geographic Information Systems for Geoscientists: Modelling with GIS: Computer Methods in the Geosciences 13. Pergamon Press, New York.

Cameron, EM and Hattori, K 1987, Archean gold mineralization and oxidised hydrothermal fluids: Economic Geology, v. 82, p. 1177–1191.

Cassidy, KF 2010, Gold systems in the eastern Yilgarn Craton: scale-integrated signatures and targeting criteria, *in* Yilgarn – Superior Workshop – Abstracts, Fifth International Archean Symposium, September, 2010, *compiled by* S Wyche: Geological Survey of Western Australia, Record 2010/20, p. 51–56.

Cassidy, KF, Champion, DC, Krapez, B, Barley, ME, Brown, SJA, Blewett, RS, Groenewald, PB and Tyler, IM 2006, A revised geological framework for the Yilgarn Craton: Geological Survey of Western Australia, Record 2006/8, 14p.

Cassidy, KF, Champion, DC, McNaughton, NJ, Fletcher, IR, Whitaker, AJ, Basttakova, IV and Budd, AR 2002, Characterisation and metallogenic significance of Archean granitoids of the Yilgarn craton, Western Australia: Minerals and Energy Research Institute of Western Australia (MERIWA), Report 222, 514p.

Cassidy, KF, Groves, DI and McNaughton, NJ 1998, Late-Archean granitoid-hosted lode-gold deposits, Yilgarn Craton, Western Australia: Deposit characteristics, crustal architecture and implications for ore genesis: Ore Geology Reviews, v. 13, p. 65–102.

Champion, DC and Cassidy, KF 2007, An overview of the Yilgarn Craton and its crustal evolution, *in* Proceedings of Geoconferences (WA) Inc Kalgoorlie '07 Conference *edited by* FP Bierlein and CM Knox-Robinson: Geoscience Australia Record 2007/14, p. 13–35.

Champion, DC and Sheraton, JW 1997, Geochemistry and Nd isotope systematics of Archaean granites of the Eastern Goldfields, Yilgarn Craton, Australia; implications for crustal growth processes: Precambrian Research, v. 83, p. 109–132.

Chen, SF, Witt, WK and Liu, S 2001a, Transpression and restraining jogs in the northeastern Yilgarn craton, Western Australia: Precambrian Research, v. 106, p. 309–328.

Chen, S, Libby, JW, Greenfield, JE, Wyche, S and Riganti, A 2001b, Geometry and kinematics of large arcuate structures formed by impingement of rigid granitoids into greenstone belts during progressive shortening: Geology, v. 29, p. 283–286.

Clark, DJ, Hensen, BJ and Kinney, PD 2000, Geochronological constraints for a two-stage history of the Albany-Fraser Orogen, Western Australia: Precambrian Research, v. 102, p. 155–183.

Colvine, AC, Andrews, AJ, Cherry, ME, Durocher, ME, Fyon, JA, Lavigne, MJ, Macdonald, AJ, Marmont, S, Poulsen, KH, Springer, JS and Troop, DG 1984, An integrated model for the origin of Archean lode gold deposits: Ontario Geological Survey Open-File Report 5524, 98p.

Cox SF, Braun, J and Knackstedt, MA 2001, Principles of structural control on permeability and fluid flow in hydrothermal systems: Reviews in Economic Geology v. 14, p. 1–24.

Cox, S. and Ruming, K 2004, The St Ives mesothermal gold system, Western Australia – a case of golden aftershocks?: Journal of Structural Geology, v. 26, p. 1109–1125.

Czarnota, K, Blewett, RS and Goscombe, B 2010a, Predictive mineral discovery in the eastern Yilgarn Craton, Western Australia: An example of district-scale targeting of an orogenic gold mineral system: Precambrian Research, v. 183, p. 356–377.

Czarnota, K, Champion, DC, Goscombe, B, Blewett, RS, Cassidy, KF, Henson, PA and Groenewald, PB 2010b, Geodynamics of the eastern Yilgarn Craton: Precambrian Research, v. 183, p. 175–202.

Davis, BK, Blewett, RS, Squire, R, Champion, DC and Henson, PA 2010, Granite-cored domes and gold mineralisation: Architectural and geodynamic controls around the Scotia-Kanowna Dome, Kalgoorlie terrane, Western Australia: Precambrian Research, v. 183, p. 316–337.

Dubé, B and Gosselin, P 2007, Greenstone-hosted quartz-carbonate vein deposits, *in* Mineral Deposits of Canada: A synthesis of major deposits types *edited by* WD Goodfellow: Geological Association of Canada, Mineral Deposits Division, Special Publication 5, p. 49–73.

Duuring, P, Hagemann, SG and Groves, DI 2000, Structural setting, hydrothermal alteration, and gold mineralisation at the Archaean syenite-hosted Jupiter deposit, Yilgarn craton, Western Australia: Mineralium Deposita, v. 35, p. 402–421.

Eisenlohr, BN, Groves, DI and Partington, GA 1989, Crustal-scale shear zones and their significance to Archaean gold mineralization in Western Australia: Mineralium Deposita, v. 24, p. 1–8.

Ewers, GR, Evans, N, Kilgour, B 2002a, MINLOC Mineral Localities Database (digital data set): Geoscience Australia, Canberra.

Ewers, GR, Evans, N, Hazell, M and Kilgour, B, 2002b, OZMIN Mineral Deposits Database (digital data set): Geoscience Australia, Canberra.

Fishwick, S and Rawlinson, N 2012, 3-D structure of the Australian lithosphere from evolving seismic datasets: Australian Journal of Earth Sciences: v. 59, p. 809–826.

Ford, A and McCuaig, TC 2010, The effect of map scale on geological complexity for computer-aided exploration targeting: Ore Geology Reviews, v. 38, p. 156–167.

Goldfarb, RJ, Baker, T, Dubé, B, Groves, DI, Hart, CJR and Gosselin, P 2005, Distribution, character, and genesis of gold deposits in metamorphic terranes: Economic Geology, 100th Anniversary Volume, p. 407–450.

Goleby, BR, Blewett, RS, Korsch, RJ, Champion, DC, Cassidy, KF, Jones, LEA, Groenewald, PB and Henson, PA 2004, Deep seismic reflection profiling in the Archaean northeastern Yilgarn Craton, Western Australia: implications for crustal architecture and mineral potential: Tectonophysics, v. 388, p. 119–133.

Goleby, BR, Blewett, RS and Reading, AM 2006, Chapter 4: tomographic studies of the Yilgarn lithosphere, *in* pmd*CRC Y2 Final Report, 3D geological models of the eastern Yilgarn craton *edited by* RS Blewett and AP Hitchman: Geoscience Australia, Record 2006/5, p. 108–127.

Goleby, BR, Korsch, RJ, Fomin, T, Bell, B, Nicoll, MG, Drummond, BJ and Owen, AJ 2002, Preliminary 3-D geological model of the Kalgoorlie region, Yilgarn Craton, Western Australia, based on seismic reflection and potential-field data: Australian Journal of Earth Sciences, v. 49, p. 917–933.

Goscombe, B, Blewett, RS, Czarnota, K, Groenewald, PB and Maas, R 2009, Metamorphic evolution and Integrated Terrane Analysis of the Eastern Yilgarn Craton: Rationale, methods, outcomes and interpretation: Geoscience Australia, Record 2009/23, 270p.

Gosselin, P and Dubé, B 2005, Gold deposits of Canada: distribution, geological parameters and gold content: Commission Geologique du Canada, Dossier public 4896, 205, 105p.

Grauch, VJS, Rodriguez, BD and Wooden, JL 2003, Geophysical and isotopic constraints on crustal structure related to mineral trends in north-central Nevada and implications for tectonic history: Economic Geology, v. 98, p. 260–286.

Griffin, TJ 2007, The exploration potential of the Yilgarn Craton: The obvious and not so obvious, *in* Proceedings of Geoconferences (WA) Inc Kalgoorlie '07 Conference *edited by* FP Bierlein and CM Knox-Robinson: Geoscience Australia Record 2007/14, p. 235–237.

Groves, DI, Barley, ME and Ho, SE 1989, Nature, genesis and tectonic setting of mesothermal gold mineralisation in the Yilgarn Block, Western Australia: Economic Geology, Monograph 6, p. 71–85.

Groves, DI, Goldfarb, RJ, Gebre-Mariam, M, Hagemann, SG and Robert, F 1998, Orogenic gold deposits: A proposed classification of in the context of their crustal distribution and relationship to other gold deposit types: Ore Geology Reviews, v. 13, p. 7–27.

Groves, DI, Goldfarb, RJ, Knox-Robinson, CM, Ojala, J, Gardoll, S, Yun, G and Holyland, P 2000, Late-kinematic timing of orogenic gold deposits and its significance for computer-based exploration techniques with emphasis on the Yilgarn Block, Western Australia: Ore Geology Reviews, v. 17, p. 1–38.

Groves, DI and Phillips, GN 1987, The genesis and tectonic controls on Archean lode gold deposits of the Western Australian shield: a metamorphic-replacement model: Ore Geology Reviews, v. 2, p. 287–322.

Groves, DI, Ridley, JR, Bloem, EMJ, Gebre-Mariam, M, Hagemann, SG, Hronsky, JMA, Knight, JT, McNaughton, NJ, Ojala, J, Vielreicher, RM, McCuaig, TC and Holyland, PW 1995, Lode gold deposits of the Yilgarn block: Products of late-Archean crustal-scale overpressured hydrothermal systems: Geological Society of London, Special Publication v. 95, p. 155–172.

Guj, P, Fallon, M, McCuaig, TC and Fagan, R 2011, A time-series audit of Zipf's Law as a measure of terrane endowment and maturity in mineral exploration: Economic Geology, v. 106, p. 241–259.

Hagemann, SG and Cassidy, KF 2000, Archean Orogenic Lode Gold Deposits: Reviews in Economic Geology, v. 13, p. 9–68.

Hall, C, 2006, The Mount Belches Formation – Black Flag Group, a late basin, or something else?: Geological Survey of Western Australia, Annual Review 2005–2006, p. 77–80.

Hall, G 1998, Autochthonous model for gold metallogenesis and exploration in the Yilgarn, *in* Geodynamics and Gold Exploration in the Yilgarn, Workshop Abstracts *edited by* SE Wood: Australian Geodynamics CRC, Nedlands, Perth, p. 32–35.

Hall, G 2007, Exploration success in the Yilgarn Craton: Insights from the Placer Dome experience – the need for integrated research, *in* Proceedings of Geoconferences (WA) Inc. Kalgoorlie '07 Conference *edited by* FP Bierlein and CM Knox-Robinson, September, 2007: Geoscience Australia, Record 2007/14, p. 199–202.

Hallberg, JA 1985, Geology and mineral deposits of the Leonora – Laverton area, northeastern Yilgarn Block, Western Australia: Hesperian Press, Perth, 140 p.

Halley, S 2007, Mineral mapping – how it can help us explore in the Yilgarn craton, *in* Proceedings of Geoconferences (WA) Inc Kalgoorlie '07 Conference *edited by* FP Bierlein and CM Knox-Robinson, September, 2007: Geoscience Australia, Record 2007/14, p. 143–144.

Harding, TP, Gregory, RF and Stephens, JH 1983, Wrench fault tectonics: Convergent wrench fault and positive flower structure, Ardmore Basin, Oklahoma: AAPG Special Volumes, Studies in Geology 15, Volume 3, p.13–17.

Henson, PA, Blewett, RS, Roy, IG, Miller, JMcL and Czarnota, K 2010, 4D architecture and tectonic evolution of the Laverton region, eastern Yilgarn Craton, Western Australia: Precambrian Research, v. 183, p. 338–355.

Hildenbrand, TG, Bereger, B, Jachens, RC and Ludington, S 2000, Regional crustal structures and their relationship to the distribution of ore deposits in the western United States, based on magnetic and gravity data: Economic Geology, v. 95, p. 1583–1603.

Hodkiewicz, PF, Weinberg, RF, Gardoll, SJ and Groves, DI 2005, Complexity gradients in the Yilgarn craton: fundamental controls on crustal-scale fluid flow and the formation of world-class orogenic-gold deposits: Australian Journal of Earth Sciences, v. 52, p. 831–841.

Hornby, P, Boschetti, F and Horowitz, F 1999, Analysis of potential field data in the wavelet domain: Geophysics Journal International, v. 137, p. 175–196.

Hronsky, JMA and Groves, DI 2008, Science of targeting: definition, strategies, targeting and performance measurement: Australian Journal of Earth Sciences, v. 55, p. 3–12.

Hronsky, JMA, Groves, DI, Loucks, RR and Begg, GC, 2012, A unified model for gold mineralisation in accretionary orogens and implications for regional-scale exploration targeting methods: Mineralium Deposita, v. 47, p. 339–358.

Isles, DJ, Harman, PG and Cunneen, JP 1989, The contribution of high resolution aeromagnetics to Archaean gold exploration in the Kalgoorlie region, Western Australia, *in* The Geology of Gold Deposits: The Perspective in 1988 *edited by* RR Keays, WRH Ramsay and DI Groves: Economic Geology Monograph 6, p. 389–397.

Knox-Robinson, CM., 2000, Vectorial fuzzy logic: a novel technique for enhanced mineral prospectivity mapping, with reference to the orogenic gold mineralisation potential of the Kalgoorlie Terrane, Western Australia: Australian Journal of Earth Sciences, v. 47, p. 929–941.

Kositcin, N, Brown, SJA, Barley, ME, Krapez, B, Cassidy, KF and Champion, DC 2008, SHRIMP U-Pb zircon age constraints on the Late Archaean tectonostratigraphic architecture of the Eastern Goldfields Superterrane, Yilgarn Craton, Western Australia: Precambrian Research, v. 161, p. 5–33.

Krapez, B, Brown, SJA, Hand, J, Barley, ME and Cas, RAF 2000, Age constraints on recycled crustal and supracrustal sources of Archaean metasedimentary sequences, Eastern Goldfields Province, Western Australia: evidence from SHRIMP zircon dating: Tectonophysics, v. 322, p. 89–133.

Krapez, B and Pickard, AL 2010, Detrital zircon age spectra for late Archaean synorogenic basins of the Eastern Goldfields Superterrane, Western Australia: Precambrian Research, v. 178, p. 91–118.

Krapez, B, Standing, JG, Brown, SJA and Barley, ME 2008, Late Archaean synorogenic basins of the Eastern Goldfields Superterrane, Yilgarn Craton, Western Australia Part II. Kurnalpi Terrane: Precambrian Research, v. 161, p. 154–182.

McCuaig, TM, Beresford, S and Hronsky, J 2010, Translating the mineral systems approach into an effective exploration targeting system: Ore Geology Reviews, v. 38, p. 128–138.

Micklethwaite, S and Cox, SF 2004, Fault segment rupture, aftershock-zone fluid flow, and mineralization: Geology, v. 32, p. 813–816.

Miller, J., 2007, New structural insights into the world-class Archean Wallaby gold deposit, Laverton, Western Australia, *in* Proceedings of Geoconferences (WA) Inc Kalgoorlie '07 Conference *edited by* FP Bierlein and CM Knox-Robinson: Geoscience Australia, Record 2007/14, p. 246.

Miller, J, Blewett, R, Tunjic, J and Connors, K, 2010, The role of early formed structures on the development of the world class St Ives goldfield, WA: Precambrian Research, v. 183, p. 292–315.

Mueller, AG 2007, Copper-gold endoskarns and high-Mg monzodiorite-tonalite intrusions at Mt Shea, Kalgoorlie, Australia: implications for the origin of gold-pyrite-tennantite mineralization in the Golden Mile: Mineralium Deposita, v. 42, p. 737–769.

Mueller, AG, Campbell, IH, Schiotte, L, Sevigny, JH and Layer, PW 2008, Constraints on the age of granitoid emplacement, metamorphism, gold mineralization, and subsequent cooling of the Archean greenstone terrane at Big Bell, Western Australia. Economic Geology, v. 91, p. 896–915.

Myers, JS 1995, The generation and assembly of an Archaean supercontinent: evidence from the Yilgarn craton, Western Australia: Geological Society of London, Special Publication 95, p. 143–154.

Nguyen, PT, Cox, SF, Harris, LB and Powell, CMcA 1998, Fault valve behaviour in optimally oriented shear zones: an example at the Revenge gold mine, Kambalda, Western Australia: Journal of Structural Geology, v. 20, p. 1625–1640.

O'Driscoll, EST 1968, Notes on the structure of the Broken Hill lode and its tectonic setting, in Broken Hill Mines – 1968, edited by M Radmanovich and JT Woodcock: Australasian Institute of Mining and Metallurgy, Monograph 3, p. 87–102.

O'Driscoll, EST 1990, Lineament tectonics of Australian ore deposits, in Geology and Mineral Deposits of Australia and Papua New Guinea, edited by E Hughes: Australasian Institute of Mining and Metallurgy, Monograph 6, p. 33–41.

Ojala, VJ, Ridley, JR, Groves, DI and Hall, GC 1993, The Granny Smith gold deposit: the role of heterogeneous stress distribution at an irregular granitoid contact in a greenschist facies terrane: Mineralium Deposita, v. 28, p. 409–419.

Oliver, NHS, Ord, A, Valenta, RK and Upton, P 2001, Deformation, fluid flow and ore genesis in heterogeneous rocks, with examples and numerical models from the Mount Isa district, Australia: Reviews in Economic Geology, v. 14, p. 51–74.

Oliver, NHS, Valenta, RK and Wall, VJ 1990, The effect of heterogeneous stress and strain on metamorphic fluid flow, Mary Kathleen, Australia, and a model for large-scale fluid circulation: Journal of Metamorphic Geology, v. 8, p. 311–331.

Penczak, RS and Mason, R 1997, Metamorphosed Archean epithermal Au-As-Sb-Zn-(Hg) vein mineralization at the Campbell mine, northwestern Ontario: Economic Geology, v. 92, p. 696–719.

Phillips, GN and De Nooy, D 1988, High-grade metamorphic processes which influence Archean gold deposits with particular reference to Big Bell, Australia: Journal of Metamorphic Geology, v. 6, p. 95–114.

Phillips, GN and Groves, DI 1983, The nature of Archaean gold-bearing fluids as deduced from gold deposits of Western Australia: Journal of the Geological Society of Australia, v. 30, p. 25–39.

Phillips, GN and Powell, R 2010, Formation of gold deposits: a metamorphic devolatilization model: Journal of Metamorphic Geology, v. 28, p. 689–718.

Powell, R, Will, TM and Phillips, GN 1991, Metamorphism in Archaean greenstone belts; calculated fluid compositions and implications for gold mineralization: Journal of Metamorphic Geology, v. 9, p. 141–150.

Reading, AM, Kennett, BL and Dentith, MC 2003, Seismic structure of the Yilgarn Craton, Western Australia: Australian Journal of Earth Sciences, v. 50, p. 427–438.

Ridley, JR 1993, The relations between mean rock stress and fluid flow in the crust: with reference to vein- and lode-style deposits: Ore Geology Reviews, v. 8, p. 23–37.

Robert, F, Poulsen, KH, Cassidy, KF and Hodgson, CJ 2005, Gold Metallogeny of the Superior and Yilgarn Cratons: Economic Geology 100th Anniversary Volume, p. 1001–1033.

Rock, NMS and Groves, DI 1988, Can lamprophyres resolve the genetic controversy over mesothermal gold deposits?: Geology, v. 16, p. 538–541.

Rock, NMS, Groves, DI, Perring, CS and Golding, SD 1989, Gold, lamprophyres, and porphyries: What does their association mean?: Economic Geology, Monograph 6, p. 609–625.

Salier, BP, Groves, DI, McNaughton, NJ and Fletcher, IR 2004, The world-class Wallaby gold deposit, Laverton, Western Australia: An orogenic-style overprint on a magmatic-hydrothermal magnetite-calcite alteration pipe: Mineralium Deposita, v. 39, p. 473–494.

Salier, BP, Groves, DI, McNaughton, NJ and Fletcher, IR 2005, Geochronological and stable isotope evidence for widespread orogenic gold mineralization from a deep-seated fluid source at ca 2.65 Ga in the Laverton gold province, Western Australia: Economic Geology, v. 100, p. 1363–1388.

Sheldon, HA and Micklethwaite, S 2007, Damage and permeability around faults: Implications for mineralization: Geology, v. 35, p. 903–906.

Sheldon, HA and Ord, A 2004, Coupled processes in faulted environments, *in* Predictive Mineral Discovery CRC, June 2004 Conference *edited by* AC Barnicoat and RJ Korsch: Geoscience Australia, Extended Abstracts p. 199–202.

Sheppard, S and Taylor, WR 1992, Barium- and LREE-rich, olivine-mica-lamprophyres with affinities to lamproites, Mt Bundy, Northern territory, Australia: Earth and Planetary Science Letters, v. 28, p. 303–325.

Smithies, RH and Champion, DC 1999, Geochemistry of felsic igneous alkaline rocks in the Eastern Goldfields, Yilgarn craton, Western Australia: a result of lower crustal delamination? – implications for late Archaean tectonic evolution: Journal of the Geological Society of London, v. 156, p. 561–576.

Sofoulis, J 1963, Norseman, WA Sheet SI51-2: Geological Survey of Western Australia, 1:250 000 Geological Series Explanatory Notes.

Sofoulis, J 1966, Widgiemooltha, WA Sheet SH51-14: Geological Survey of Western Australia, 1:250 000 Geological Series Explanatory Notes.

Spaggiari, CV, Kirkland, CL, Pawley, MJ, Smithies, RH, Wingate, MTD, Doyle, MG, Blenkinsop, TG, Clark, C, Oorschot, CW, Fox, LJ and Savage, J 2012, The geology of the east Albany–Fraser Orogen – A field guide: Geological Survey of Western Australia, Record 2011/23, 95p.

Spooner, ETC 1993, Magmatic sulphide/volatile interaction as a mechanism for producing chalcophile element enriched, Archean Au-quartz, epithermal Au-Ag and Au skarn hydrothermal ore fluids: Ore Geology Reviews, v. 7, p. 359–379.

Standing, JG 2008, Terrane amalgamation in the Eastern Goldfields Superterrane, Yilgarn craton: evidence from tectonostratigraphic studies of the Laverton greenstone belt: Precambrian Research, v. 161, p. 114–134.

Swager, CP 1997, Tectono-stratigraphy of late Archaean greenstone terranes in the southern Eastern Goldfields, Western Australia: Precambrian Research, v. 83, p. 11–42.

Swager, CP, Goleby, BR, Drummond, BJ, Rattenbury, MS and Williams, PR 1997, Crustal structure of granite–greenstone terranes in the Eastern Goldfields, Yilgarn Craton, as revealed by seismic reflection profiling: Precambrian Research, v. 83, p. 43–56.

Tripp, GI 2013, Stratigraphy and structure in the Late Archaean of the Kalgoorlie district, Australia: Critical controls on greenstone-hosted gold deposits: James Cook University of North Queensland, PhD thesis (unpublished).

Tripp, GI, Cassidy, KF, Rogers, J, Sircombe, K and Wilson, M 2007, Stratigraphy and structural geology of the Kalgoorlie greenstones: key criteria for gold exploration, *in* Proceedings of Geoconferences (WA) Inc Kalgoorlie '07 Conference *edited by* FP Bierlein and CM Knox-Robinson: Geoscience Australia, Record 2007/14, p. 203–208.

Van Kranendonk, MJ and Ivanic, TJ 2009, A new stratigraphic scheme for the northeastern Murchison Domain, Yilgarn Craton: Geological Survey of Western Australia, Annual Review 2007–2008, p. 34–47.

Walshe, JL, Neumayr, P, Cleverley, J, Petersen, K, Andrew, A, Whitford, D, Carr, GR, Kendrick, M, Young, C and Halley, S 2008, Chapter 3.4, Question 3: Multiple fluid reservoirs in Eastern Yilgarn gold systems, in Concepts to targets: a scale-integrated mineral systems study of the eastern Yilgarn craton: pmd*CRC Y4 Final Report, *compiled by* Y4 Project Team, p. 113–153.

Walshe, J, Neumayr, P and Petersen, K 2006, Scale-integrated, architectural and geodynamic controls on alteration and geochemistry of gold systems in the Eastern Goldfields Province, Yilgarn craton: MERIWA Report 256 (project M358), 290p.

Weinberg, RF, Hodkiewicz, PF and Groves, DI 2004, What controls gold distribution in Archean terranes?: Geology, v. 32, p. 545–548.

Wilkins, C 1993, A post-deformational, post-peak metamorphic timing for mineralization at the Archaean Big Bell gold deposit, Western Australia: Ore Geology Reviews, v. 7, p. 439–483.

Williams, PR and Whitaker, AJ 1993, Gneiss domes and extensional deformation in the highly mineralised Archaean Eastern Goldfields province, Western Australia: Ore Geology Reviews, v. 8, p. 141–162.

Witt, WK 1990, Geology of the Bardoc 1:100 000 sheet: Geological Survey of Western Australia, Record 1990/14, 50p.

Witt, WK 1991, Regional metamorphic controls on alteration associated with gold mineralization in the Eastern Goldfields province, Western Australia: Implications for the timing and origin of Archean lode-gold deposits: Geology, v. 19, p. 982–985.

Witt, WK, 1992, Porphyry intrusions and albitites in the Bardoc–Kalgoorlie area, Western Australia, and their role in Archean epigenetic gold mineralization: Canadian Journal of Earth Sciences, v. 29, p. 1609–1622.

Witt, WK 1993, Gold mineralization in the Menzies–Kambalda region, Eastern Goldfields, Western Australia: Geological Survey of Western Australia, Report 39, 166p.

Witt, WK and Davy, R 1997, Geology and geochemistry of granitoid rocks in the southwest Eastern Goldfields Province: Geological Survey of Western Australia, Report 49, 137p.

Witt, WK and Hagemann, SG 2013, Intrusion-related hydrothermal alteration in the Yilgarn. Part 2 of a hydrothermal history of the Yilgarn greenstones: CET Newsletter, 23, p. 1–15 and 24, p. 1–14.

Witt, WK, Hagemann, SG and Miller, JM 2012a, Tectonic and structural controls on lode-gold deposits: Continental- to Deposit-scale: AIG Structural Geology and Resources Conference, Kalgoorlie, September 2012, Abstracts, p. 176–179.

Witt, WK, Ford, A and Hanrahan, W 2012b, Regional targeting criteria for gold in the Yilgarn Craton: which ones work and how well?: Geological Survey of Western Australia, Record 2012/2, p. 10–13.

Witt, WK, Knight, TJ and Mikucki, EJ 1997, A synmetamorphic lateral fluid flow model for gold mineralization in the Archean southern Kalgoorlie and Norseman Terranes, Western Australia: Economic Geology, v. 92, p. 407–437.

Witt, WK, Mason, DR., Hammond, DP 2009, Archean Karari gold deposit, Eastern Goldfields Province, Western Australia: a monzonite-associated disseminated gold deposit: Australian Journal of Earth Sciences, v. 56, p. 1061–1086.

Witt, WK and Vanderhor, F 1998, Diversity within a unified model for Archaean gold mineralization in the Yilgarn Craton of Western Australia: An overview of the late-orogenic, structurally-controlled gold deposits: Ore Geology Reviews, v. 13, p. 29–64.

Woodall, R 1994, Empiricism and concept in successful mineral exploration: Australian Journal of Earth Sciences, v. 41, p. 1–10.

Wyche, S, Fiorentini, M, Miller, JL and McCuaig, TC 2012, Geology and controls on mineralisation in the Eastern Goldfields region, Yilgarn Craton, Western Australia: Episodes v. 35, p. 273–282.

Wyman, D and Kerrich, R 1988, Alkaline magmatism, major structures, and gold deposits: implications for greenstone belt gold metallogeny: Economic Geology, v. 83, p. 454–461.

Y4 Project Team 2008, Concepts to Targets: a scale-integrated mineral systems study of the Eastern Yilgarn Craton: pmd*CRC Project Y4 Final Report (unpublished), 162p. plus DVDs.

Zibra, I, Gessner, K, Korsch, R, Blewett, RS, Jones, T, Milligan, P, Jones, LEA, Wyche, S, Doublier, MP, Hall, CE, Chen, SF, Romano, SS, Ivanic, TJ, Pawley, MJ, Patison, N, Kennett, BLN and Van Kranendonk, MJ 2013, Preliminary interpretation of deep seismic lines 10GA-YU3 and the southeastern part of 10GA-YU1: Murchison domain of the Youanmi Terrane, *in* Youanmi and Southern Carnarvon Seismic and Magnetotelluric (MT) Workshop, Preliminary edition, *compiled by* S Wyche, TJ Ivanic and I Zibra: Geological Survey of Western Australia, Record 2013/6, 109-117.

Appendix

Tabulated results of GIS spatial analyses

(provided as Excel spreadsheets)

	Tables
Terranes and domains: Gold endowment	A1.1 to A1.4
Targeting Criterion 1.1: Seismic tomography and tomographic edges	A1.5
Targeting Criterion 1.2: Sm-Nd isotope basement domains and gradients	A1.6 to A1.7
Targeting Criterion 1.3: Granite Groups	A1.8 to A1.18
Targeting Criterion 1.4: Regional gravity lineaments	A1.19 to A1.39
Targeting Criterion 1.5: Aeromagnetic discontinuities	A1.40 to A1.53
Targeting Criterion 1.6: Greenstone thickness	A1.54 to A1.55
Targeting Criterion 1.7: Regional faults	A1.56 to A1.58
Targeting Criterion 1.8: Regional fault density	A1.59 to A1.61
Targeting Criterion 1.9: Regional fault intersections	A1.62 to A1.64
Targeting Criterion 1.10: Regional fault bends	A1.65 to A1.69
Targeting Criterion 1.11: Fault vergence anomalies	A1.70 to A1.71
Targeting Criterion 1.12: Constriction zones	A1.72 to A1.74
Targeting Criterion 1.13: Domes	A1.75 to A1.76
Targeting Criterion 1.14: Granite–greenstone contacts	A1.77 to A1.79
Targeting Criterion 1.15: Regional metamorphic domains and regional strain	A1.80 to A1.85
Targeting Criterion 1.16: Regional strain partitioning	A1.86 to A1.88
Targeting Criterion 1.17: Late-stage basins	A1.89 to A1.90
Targeting Criterion 1.18: Geological complexity	A1.91 to A1.96
Relationship of calculated prospectivity to known gold deposits	A1.97 to A1.102

The Yilgarn Gold Exploration Targeting Atlas, a collaborative project involving the Geological Survey of Western Australia, the Centre for Exploration Targeting at the University of Western Australia, and several industry groups, is a three-part document of which this is the first. Part 1 provides quantitative analyses and assessments of eighteen regional targeting criteria for gold exploration in the Yilgarn Craton as a whole, and at superterrane, terrane, and domain level. The targeting criteria range from well-established targeting techniques (e.g. proximity to regional faults and fault intersections) to relatively new concepts (e.g. proximity to fault vergence anomalies, domes, and late-stage basins). Spatial analyses were based on GSWA's 1:500 000-scale shape files, legacy shape files from the Predictive Mineral Discovery Cooperative Research Centre, GSWA's MINEDEX database, and a gold deposit database compiled by Barrick Gold Corporation. Systematic examination of the eighteen regional-scale targeting criteria has produced robust spatial statistics for application in gold exploration in the Yilgarn Craton, but also with potential application to orogenic gold provinces elsewhere. This study of the Yilgarn Craton has established strong associations of gold with greenstone belts, Mafic Group granite and porphyry intrusions, regional faults, regional fault density, regional fault bends and intersections, and areas of lower greenschist low-pressure metamorphism. Some other targeting criteria were shown to provide an advantage compared to random exploration, but are less effective than the aforementioned most-successful criteria.

Further details of geological products and maps produced by the Geological Survey of Western Australia are available from:

Information Centre
Department of Mines and Petroleum
100 Plain Street
EAST PERTH WA 6004
Phone: (08) 9222 3459 Fax: (08) 9222 3444

www.dmp.wa.gov.au/GSWApublications

WITT et al.

REGIONAL-SCALE TARGETING FOR GOLD IN THE YILGARN CRATON: PART 1 OF THE YILGARN GOLD EXPLORATION TARGETING ATLAS

REPORT 125